Terms and Conditions of Use of Digitised Theses from Trinity College Library Dublin

Copyright statement

All material supplied by Trinity College Library is protected by copyright (under the Copyright and Related Rights Act, 2000 as amended) and other relevant Intellectual Property Rights. By accessing and using a Digitised Thesis from Trinity College Library you acknowledge that all Intellectual Property Rights in any Works supplied are the sole and exclusive property of the copyright and/or other IPR holder. Specific copyright holders may not be explicitly identified. Use of materials from other sources within a thesis should not be construed as a claim over them.

A non-exclusive, non-transferable licence is hereby granted to those using or reproducing, in whole or in part, the material for valid purposes, providing the copyright owners are acknowledged using the normal conventions. Where specific permission to use material is required, this is identified and such permission must be sought from the copyright holder or agency cited.

Liability statement

By using a Digitised Thesis, I accept that Trinity College Dublin bears no legal responsibility for the accuracy, legality or comprehensiveness of materials contained within the thesis, and that Trinity College Dublin accepts no liability for indirect, consequential, or incidental, damages or losses arising from use of the thesis for whatever reason. Information located in a thesis may be subject to specific use constraints, details of which may not be explicitly described. It is the responsibility of potential and actual users to be aware of such constraints and to abide by them. By making use of material from a digitised thesis, you accept these copyright and disclaimer provisions. Where it is brought to the attention of Trinity College Library that there may be a breach of copyright or other restraint, it is the policy to withdraw or take down access to a thesis while the issue is being resolved.

Access Agreement

By using a Digitised Thesis from Trinity College Library you are bound by the following Terms & Conditions. Please read them carefully.

I have read and I understand the following statement: All material supplied via a Digitised Thesis from Trinity College Library is protected by copyright and other intellectual property rights, and duplication or sale of all or part of any of a thesis is not permitted, except that material may be duplicated by you for your research use or for educational purposes in electronic or print form providing the copyright owners are acknowledged using the normal conventions. You must obtain permission for any other use. Electronic or print copies may not be offered, whether for sale or otherwise to anyone. This copy has been supplied on the understanding that it is copyright material and that no quotation from the thesis may be published without proper acknowledgement.

Novel Macrocyclic and Acyclic Ligands for Metal Ion Coordination - Design, Synthesis and Physical Evaluation

Claire Nolan B.Sc.

A Thesis Submitted for the Degree of Doctor of Philosophy

Dept. of Chemistry, University of Dublin, Trinity College

October 2002

Abstract:

Supramolecular chemistry is a relatively young discipline dating back to the late 1960s and early 1970s and, as such, is a highly diverse and dynamic field incorporating organic, inorganic and physical chemistry. Much of the inspiration and origins of supramolecular chemistry comes from the chemistry found in living biological systems. The overlap of disciplines helps us understand and mimic the biological processes in nature using synthetic means with the emphasis on the recognition and targeting of physiologically important species. Chapter one will detail the history and development of supramolecular chemistry with the main focus being on lanthanide luminescence.

The main focus of this thesis is the development of novel lanthanide complexes for potential biological applications in immunoassays, as catalysts for RNA cleavage, sensors, NMR chiral shift reagents and as contrast agents for MRI. Chapter two will discuss the synthesis of lanthanide luminescence compounds, a three-membered pyridine macrocycle **86** which was previously synthesised by Miyahara *et al* and two Schiff-base macrocycles **100** and **101** using a variety of lanthanide ions as template ions. These compounds were designed incorporating the efficient energy transfer of bipy compounds to lanthanide ions but with additional flexibility to allow the lanthanide ion to be fully encapsulated removing quenching solvent molecules. The advantage of these lanthanide complexes is their long excitation state lifetimes and long wavelength emission, which makes them suitable for *in vivo* measuring. **86** was attempted to be prepared in two sections via a five-step reaction scheme involving standard organic procedures in the literature with modifications, to increase the yield, using commercially available reagents. After numerous attempts **86** was synthesised in 5 mg. Scale-up of the reaction was attempted but was proved to be unsuccessful. A different approach to cyclisation, namely lanthanide-templated Schiff base synthesis, was also evaluated. **100** and **101** were synthesized using this procedure. The characterisation of these complexes was difficult to achieve because of solubility problems. Comparison of the UV spectra of the starting materials *vs.* the complexes showed a red shift. CHN data were inconclusive about the nature of the complexes formed. It is unsure if the macrocyclic complexes were synthesised but experimental data suggests that perhaps a polymer type materials were synthesised instead. Luminescent data was obtained for the Eu(III) and Tb(III) complexes and these showed some luminescent intensity.

An intermediate **96** in the development of **86** was found to have an interesting box-like structure when analysed by X-ray crystallography. **96** was complexed with a number of

transition metals, Cu(II), Zn(II), Ni(II), Co(II), Fe(II) and crystals were grown and examined by X-ray crystallography. All the complexes were found to be monomeric structures except the Cu(II) complex, which was a dimer. These complexes were then investigated as possible catalysts for RNA cleavage using UV kinetic spectroscopy. It was found that the Cu(II) complex was the best cleaver of HPNP (a model for RNA) with the Zn(II) complex coming a close second. The UV and fluorescence properties of these complexes were examined in a variety of solvents. **96** was found to be an efficient chemosensor for Zn(II). In comparison, Cu(II) quenched fluorescence because of efficient metal-to-ligand electron transfer. ^{1}H NMR titrations of the ligand with Cu(I) and Zn(II) in MeCN and DMSO-d_6 showed a significant shift in the methylene groups and hydroxy groups with a corresponding loss of splitting on the addition of 0 to 10 equivalents of the metal ion. These results provided further proof of the solution-state processes occurring in the complexes.

A novel PET sensor **181** for lithium was synthesized. Lithium is used to treat manic-depressives and is currently detected using ion-selective electrodes. A sensor was developed composed of a diaza-9-crown-3-ether receptor, with an amide functionality to aid lithium recognition, which is connected to a naphthalene fluorophore via a chiral methylene spacer group. pH studies showed the sensor had a pKa of 7.2. Unfortunately this limits its use in biological systems at a physiological pH of 7.4. The fluorescence properties of the sensor were extensively studied in a variety of solvents and at a variety of pHs using different lithium salts. The sensor was selective and specific for lithium in MeCN and to a lesser extent in MeOH compared to sodium, potassium, calcium and magnesium. ^{1}H NMR studies of the sensor with 0 to 15 equivalents of lithium showed changes in shift and splitting up on coordination with lithium.

Following from this work, novel acyclic and cyclic compounds were developed and synthesized. Pseudopeptides were synthesized from simple, commercially available diamines and L-alanine or L-proline using standard peptide methodologies. These were synthesized in good yields and complexed to Pt(II) and were evaluated as therapeutic drugs in St. James Hospital. They showed EC_{50} values between 65 and 100 which were poor results and suggest that further functionalisation of the complexes is required. The addition of Bromo-n-alkene (where n = 3-5) group to the N-position of the pseudopeptide and the O-position of **96** was carried out with the intention of forming novel macrocyclic ligands. The cyclisation was carried out via ring-closing metathesis using Grubbs catalyst. It was hoped that the introduction of Cu(II) to the derivatives of **96** would form a dimer complex which could form

a catenane structure when cyclised via ring-closing metathesis. The pseudopeptide derivatives were synthesised but could not be isolated from the starting materials. The derivatives of **96** were isolated but could not be cyclised.

This thesis has discussed a vast range of fields and it was necessary to include a brief introduction into each field. Although a number of good results were obtained in each chapter, a number of inconclusive results were also obtained. Suggested outcomes and further work was discussed in the conclusion section at the end of each chapter.

This Thesis has not been submitted as an exercise for a degree at any other university. Except where otherwise indicated, the work described herein has been carried out by the author alone.

I give permission for the Library to lend or copy this thesis upon request.

Claire Nolan

October 2002

Acknowledgements:

There are a ton of people, both family, friends and colleagues, I have to thank for being around and helping out during the course of this thesis.

Firstly I would like to thank everyone in Trinity; especially Patsy, Martin, Fred, Ed, Seamus, Peggy, Kieron, Brendan, Theresa, Brendan M., Paul and John Kelly for all there help in sourcing equipment, glassware etc. especially towards the end when it everything was required ASAP. For all the help with the NMR work I would like to thank Dr. John O'Brien. Thank you to the lecturers who were willing to give their time when it was asked for and the Head of Department, Prof. Sean Corish. A special thank you to the secretaries for solving all minor crisis smoothly and without fuss.

Next a big thank you to my supervisor, Dr. Thorrfinnur Gunnlaugsson, who inspired us all with his enthusiasm. Thank you to all the members, past and present, of Thorris group, which has grown a little since I first started there with Caroline and Mark. To these two, I want give a big group hug, here's to Thorris originals, we finally made it! Caroline, it must be my turn to pay for the posh coffee!! To Joe, Celine and Aoife I'd like to thank to you for your help with accurate mass and all the other stuff you did! To Tom, thanks for looking out for me when I was working late. I also want to thank my fellow members of the Werner Chemical society 1999-2000 committee, Caroline, Rob, Brian, Gar, Tom, Yvonne and Aoife,

For financial support of this thesis I would like to thank: financially the HEA, National Pharmaceutical Biotechnology centre – Bioresearch Ireland and the Department of Chemistry for the Krieble Scholarship.

I would also like to thank the following for their insights into the work performed in this thesis, Prof. Clive Williams and Prof. A.P. de Silva.

Dr. Mark Nieuwenhausen performed all crystallography work and all anti-tumour activity work was performed by Dr. Tony McElliott. A huge thank you to both of them.

To all my friends, especially Tracy, Lillian, Ann-Marie, Eva and Claire, I would like to say that I finally did it and that I'm in about as much shock as them about it too.

Last but not least I would like to thank my parents and sisters, Marie, Joanne and Laura, for putting up with me for the last twenty *ahem* years when I seem to torment myself and them by doing these things that put me into such a tizzy.

I would like to dedicate this thesis to my parents, Rita and Fran, for all their help, support and especially their love. Cheers!

For my parents, Rita and Fran

Advice
By Langston Hughes

Folks, I'm telling you,
Birthing is hard
And dying is mean –
So get yourself
A little loving
In between

The Silver Swan
By Orlando Gibbons

The Silver Swan, who living had no note,
When death approached unlocked her silent throat;
Leaning her breast against the reedy shore,
Thus sung her first and last, and sung no more:
Farewell, all joys; O death, come close mine eyes;
More geese than swans nmow live, more fools than wise.

Abbreviations

BET	Back Energy Transfer
Bipy	2,2'Bispyridyl
$CHCl_3$	Chloroform
DCM	Dichloromethane
DMF	Dimethyl Foramide
EC_{50}	Effective Concentration at which 50% of cells are killed
EtOAc	Ethyl Acetate
EtOH	Ethanol
ET	Energy Transfer
HOBt	
HOMO	Highest Occupied Molecular Orbital
HPNP	2-Hydroxypropyl-*p*-Nitrophenol Phosphate
IC	Interconversion
ISC	Intersystem Crossing
KI	Potassium Iodide
LUMO	Lowest Unoccupied Molecular Orbital
LMCT	Ligand to Metal charge Transfer
MeCN	Acetonitrile
MeOH	Methanol
MLCT	Metal to Ligand Charge Transfer
MRI	Magnetic Resonance Imaging
$NaBH_4$	Sodium Borohydride
PET	Photoinduced Electron Transfer
Φ	Quantum Yield
RCM	Ring Closing Metathesis
Tosyl	*p*-Toluene sulphonyl
TFA	Trifluoroacetic acid
THF	Tetrahydrofuran

Table of Contents

Chapter 1

Introduction to Supramolecular Chemistry

1.1: Review Of Supramolecular Chemistry

This project is concerned with the study of supramolecular chemistry. Supramolecular chemistry is the study of the interactions of large host molecules with smaller guests such as anions, cations and small organic molecules. With the death of Donald J Cram (1919-2001) in the past year, it is perhaps time to carry out a quick review of his achievements and those of his fellow Nobel Prize winners in the development of the field of supramolecular chemistry; Charles Pederson and Jean-Marie Lehn. This chapter will briefly describe the inspiration in the development of supramolecular chemistry, the different processes involved, some examples of supramolecular compounds and some applications. The chapter will then go on to describe fully the processes involved in lanthanide luminescence detailing the applications and describing some lanthanide complexes.

Much of the inspiration and origins of supramolecular chemistry comes from the chemistry found in living biological systems. Nature has evolved an enormous amount of highly specific, selective and cooperative chemistry that enables living systems to maintain themselves in their environment[1]. Examples of this include valinomycin **1** and nonactin **2**. These molecules are examples of naturally occurring macrocyclic antibodies. They transport metal ions through the lipophilic cell membrane *via* the carrier mechanism. This involves a carrier ligand (ionophore) that is able to both bind selectively to the metal cation and shield it from the lipophilic region of the cell membrane.

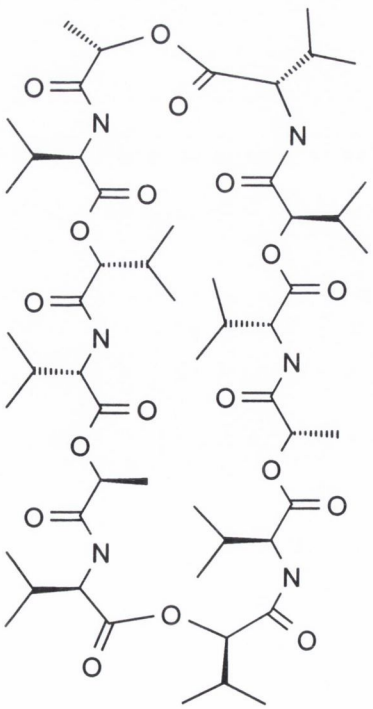

1

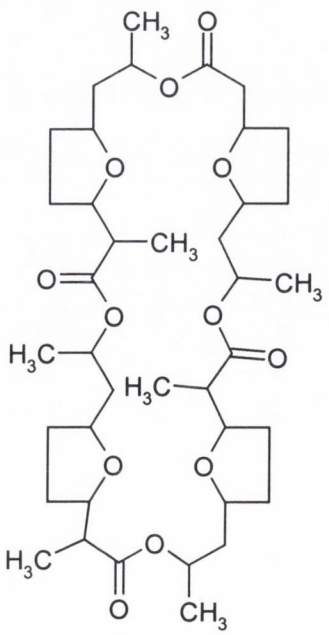

2

Valinomycin **1** is natural phase transfer agent. It is an antibiotic, which operates by selectively transporting potassium cation through the lipophilic cell membrane. The crystal structure of **1** with potassium ion is shown in Figure 1.1. Valinomycin **1** can be isolated from the bacterium *Steptomyces Fulvissimus* and catalyses the exchange of K^+ and H^+ across the mitochondria membrane without affecting Na^+ concentration. The molecule consists of a threefold repetition of four amino acid residues and forms an octahedral complex with potassium through electrostatic interactions between potassium and the ester carbonyl oxygens. **1** can therefore be described as a selective receptor for potassium ions because sodium ion uptake is extremely poor.

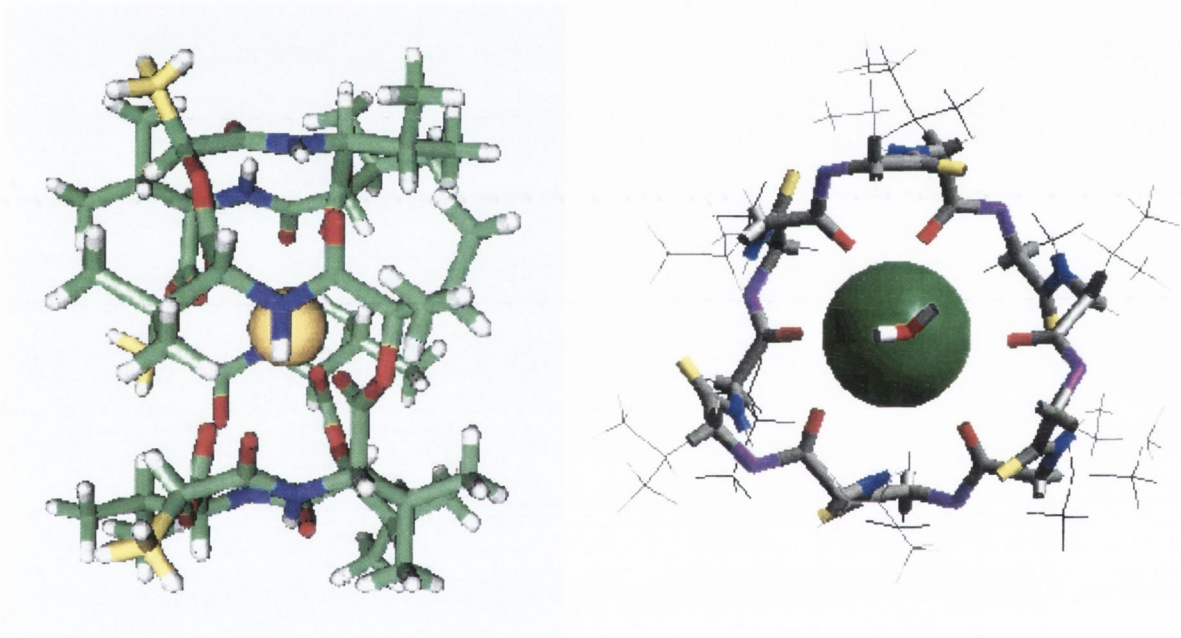

Figure 1.1: These pictures show the molecular structure of valinomycin when bound to a potassium ion via the carbonyl oxygens.

Organisation in biological systems is often the result of molecular association based on non-covalent intermolecular forces[2]. Enzymes, genes, antibodies, ionophores and other biological systems possess receptor sites that can selectively bind suitable substrates giving rise to highly specific molecular recognition. Natural receptors are extremely complicated molecules but by developing artificial, synthetically accessible receptors in the laboratory, molecular recognition can be achieved. Supramolecular chemistry describes the interaction of matter, *i.e.* the guest, with an artificial receptor/host[1,3] bound to one another in a definable structural relationship by intermolecular forces[4]. Supramolecular photochemistry exploits such structure-specific interactions which play a key role in determining the photochemical or photophysical properties of the host on complexation with the guest[2]. Molecular recognition

in the supramolecular complex, formed by host-guest binding, rests on the principle of molecular complementarily[5]. That is, to form a supramolecular complex the host must have multiple binding sites, which attract binding sites of guest molecules without generating strong non-bonding repulsions. The contacts between the host and guest depend on the complementary placement of binding sites on the receptor. Some recognition factors include steric complimentary, good interaction sites, large contact sites, multiple interaction sites and strong overall binding. Design principles must be applied to the receptor to achieve the desired intermolecular interactions[13] for guest recognition. Steric similarities with respect to the size and shape of the receptor compared to the guest. Good multiple interaction sites are necessary for maximum electrostatic and binding interactions and also large contact sites. The application of design principles to supramolecular species achieves the desired intermolecular interactions to suggest the use of heteroatoms in the receptor is required to achieve optimum dipole and electrostatic interactions. Also, the presence of aromatic groups can give rise to π-π interactions. In this context, macrocyclic molecules are generally preferred to acyclic molecules because of their increased thermodynamic stability. They are also less heavily solvated, kinetically more inert and less flexible which means less loss of disorder on complexation. This is known as the "macrocyclic effect"[6]. This preorganisation of the host for binding with low solvation leads to more stable complexes.

Recognition occurs *via* intermolecular interactions between the receptor and the guest. These interactions include electrostatic forces such as ion-ion, ion-dipole and dipole-dipole, hydrogen bonding, π-π stacking, van der Waals forces, π-acid to π-base interactions, metal to ligand binding and solvent reorganisation. These bonds are typically weaker than covalent bonds, of *ca.* 350 $kJmol^{-1}$ for carbon-to-carbon single bonds compared to 5-20 $kJmol^{-1}$ for hydrogen bonds. These low bonding energies suggest that reversibility of recognition in the complex is feasible. However, such binding molecules can often lead to highly stable supramolecular species. The properties of these systems, therefore, depend on the controlled number and efficient use of weak intermolecular forces.

Host-Solvent + Guest-Solvent ⇌ **Host-Guest-Solvent + Solvent-Solvent**

Example 1.1: Equation showing the interaction of the solvent with the host and guest.

In solution state chemistry, the role of solvents on complexation is an important factor[4]. The binding forces between the solvent-host and solvent-guest are frequently of the same type as those between the host and guest suggesting the solvent must be displaced before complexation. The solvent competes with both the host and guest for occupancy of binding sites. The presence of the solvent affects the equilibrium desolvation energy due to unfavourable enthalpy and favourable entropy effects. It must be noted that if the Solvent-Solvent term has strong interactions, a strong Host-Guest complex is formed and the equilibrium goes to the right hand side of example 1.1. The more highly polar the solvent is, the less strong the Host-Guest complex. This is due to an efficient interaction between the host and solvent, which means the equilibrium goes to the left hand side. The solvent plays an important role in recognition processes especially if it effectively solvates the host, guest or host-guest complex. It effects equilibrium because desolvation gives unfavourable enthalpy due to the energy required to break the solvent bonds and favourable entropy because of an increase of disorder on solvent release. There are a number of effects: The hydrophobic effect describes the poor solvation power of water with the apolar surface of the host-guest complex. The binding energy is increased because of the entropic advantage of water liberation and the forming of enthalpically favourable solvent-solvent hydrogen bonds. Electrostatic interactions control the binding strength. The dielectric constant of solvation measures bulk polarity and reflects the dipole moment of the solvent molecule. Those solvents with high dipole moment interact better with charged species and shield these species thus decreasing the strength of host-guest interaction. The donor acceptor ability of the solvent is another effect. A good donor solvent can solvate the guest (*i.e.* a cation) and can thus compete with the host for binding. The solvent, especially polar solvents, can also affect absorption or emission properties of the host-guest complex.

1.2 Types of Hosts and their Complexes with Guests

The serendipitous discovery by CJ Pederson of crown ethers[5] was the catalyst in the development of supramolecular chemistry. The general structure of crown ether consists of ether oxygens linked by ethylene groups, some examples of which are shown in Figure 1.1. These molecules were found to complex alkali metals, especially sodium and potassium, in their cavity. This effective metal binding ability is due to the chelate and macrocyclic effect. The chelate effect is described as the effect of having a number of heterocyclic atoms in the ligand, which can bind to the metal ion. The cation sits in the cavity and is held together by ion-dipole electrostatic interactions. There is a strong relationship between the cavity size, the cation radius and the stability of the complex as seen in Table 1.1.

BINDING CONSTANT			
CROWN ETHER	**Sodium**	**Potassium**	**Cesium**
[18]Crown-6	4.32	6.1	4.62
[21]Crown-7	-----	4.32	5.02

Table 1.1: Table showing variety of binding constants for some crown ethers with a various alkali metals

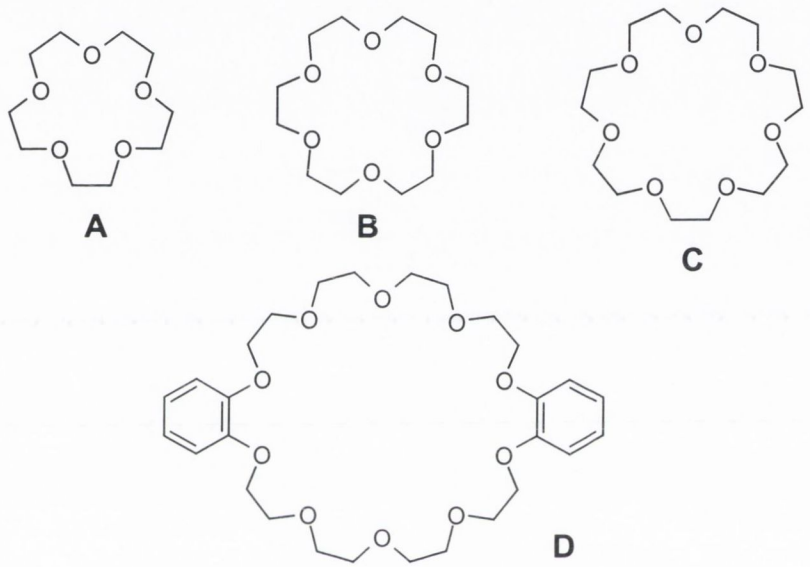

Figure 1.2: Variety of crown ethers. A: [15]Crown-5-Ether, B: [18]Crown-6-Ether, C: [21]Crown-7-Ether and D: Dibenzo[30]Crown-10-Ether.

The oxygen atoms can be replaced by other heteroatoms such as nitrogen and sulphur. Cyclen (1,4,7,10-tetraaza[12]crown-4-ether) **3** is an example of an aza-crown ether where all the oxygens are replaced by nitrogens. With the addition of the nitrogen atoms into the crown ether, the crown ether can be further functionalised with pendant arms. These give an extra coordination group and are known as lariat crown ethers, for example **4** and **5**. This group of compounds combine higher rigidity and preorganisation with additional stability and flexibility.

Concurrently with this work, Jean-Marie Lehn[1,6,13] investigated the use of cryptands with possible use in biological applications. Cryptands are 3-D analogues of crown ethers. They are cage like bicyclic molecules enabling spherical recognition of metal ions. It was anticipated that the metal ion could be encapsulated entirely within a crown-like host with

subsequent gains in cation selectively and enhancement of ionophore–like transport properties. The cryptand **6** is selective for potassium.

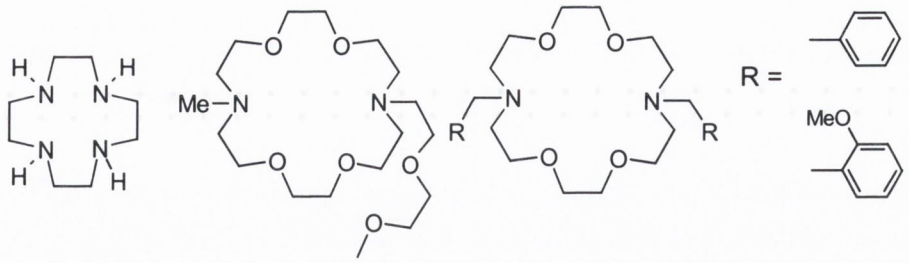

3 **4** **5**

The key to dramatically enhanced metal ion binding ability of cryptands compared to the crown ethers is the 3-D nature of the cavity, which enables recognition of the metal ion to take place. The cryptands have high stability and selectivity, slow exchange rates with other cations and efficient shielding of the cation from the solvent environment. Spherands were designed and developed by Donald J. Cram[5,6]. They are rigid macrocyclic systems that contain enforced cavities fully organised for recognition during synthesis rather than during complexation. The molecule below, **7**[5], is selective for the lithium ion where binding occurs through electrostatic interactions *via* the oxygen atoms. These compounds have strong binding ability and are selective for the lithium ion guest. The cavity size can be selected based on the ionic radii of the ion of interest. Following from this hemispherands and cryptospherands were developed. These are hosts where cavities are at least half organised for binding[4]. This means that half the cavity is rigid with the binding sites facing into the cavity. The rest of the molecule is flexible.

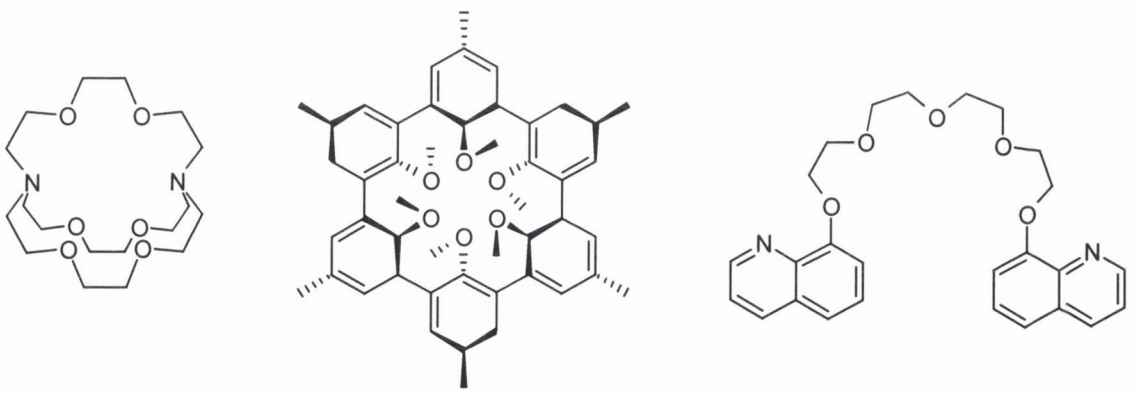

6 **7** **8**

Vögtle, Weber and co-workers developed molecules called podands, which are examples of non-cyclic hosts[1]. They have less cation affinity but the extra flexibility allows them to

engage in multiple bridging and helical binding modes, which is unknown for the less flexible crown ethers. In molecule **8**, the addition of a rigid functional group at the end of the podand enhanced binding by an extra degree of organisation. From these early developments there has been an explosion in the variety and types of hosts developed and their applications. The rest of this chapter is concerned with the applications of supramolecular compounds.

1.3 Applications of Supramolecular Compounds

This section has briefly highlighted the many applications of supramolecular chemistry. It is a diverse field to review and because of this, the rest of this introduction is devoted to an overview of lanthanide luminescence complexes and their uses, which is relevant to the work discussed in this thesis.

There are many applications for supramolecular compounds, some of which are discussed here. They have found use in medicine as therapeutic drugs and diagnostic devices, as sensors, MRI imaging agents, molecular devices, phase transfer agents and sequestering agents[2,7,13]. They have also found use in synthetic chemistry such as phase transfer agents, which help solubilise inorganic salts in non-polar solvents. Examples of such systems include crown ethers. The separation of mixtures is of prime importance in the pharmaceutical industry and in environmental chemistry. For example, the removal of a pollutant such as a heavy metal from aqueous solutions is environmentally important[1,13]. To this end supramolecular substrates have been developed where the receptor can be attached to a solid support, which can be used to remove a particular substance from the environment. Izatt, Bradshaw and Christensen[8,9] have produced a number of examples of such materials that are designed to selectively remove or concentrate metal ions in solution. These separations are achieved due to the differences in the binding constants of the various substrates with the receptor bound to the stationary phase, which is a direct consequence of their design. This method is being further developed to remove radioactive metal residues[9]. Chiral chromatographic separation materials have been developed by Cram[4] and co-workers using macromolecules to separate amino acid enantiomers. This is of benefit to the pharmaceutical industry, which often has to resolve enantiomers of chiral drugs that possess different activities.

Of particular interest to the rest of this thesis is the development of sensing systems such as chemosensors. A sensor[2,3,13] is compound containing a receptor and a reporter unit that can report the presence of a guest by some physical means such as changes in the

absorption or fluorescence spectrum or electrochemical change for example Figure 1.3. The sensor is selective for the guest of interest and allows the monitoring of any concentration changes giving real-time, on-time information.

Fig. 1.3: Example of the structure of a sensor, in this case a PET sensor (discussed fully in chapter 4)

There are two important strategies towards sensor production. Firstly, the sensor can be incorporated into a modified material such as an electrode. This modified electrode shows a selective response to the presence of the guest of interest allowing quantitative analysis of the guest. Secondly, the sensor can incorporate both a reporter group that shows changes in the photophysical properties of the receptor upon recognition. The reporter group is either a chromophore or fluorophore. This will be discussed fully in chapter five.

The pharmaceutical industry has successfully applied the principles of supramolecular compounds[10,11,13] for instance magnetic resonance imaging (MRI) contrast agents[10,11] and anti-tumour agents[13] have been developed based on supramolecular assemblies. The current crops of MRI contrast agents are based on paramagnetic lanthanide complexes an example of which is the Gd^{3+} complex of DOTA **9** shown below. These compounds are designed to accumulate in a particular part of the body and enhance visibility in magnetic resonance imaging (MRI) scans due to the high paramagnetism of the lanthanide ion, usually Gd^{3+}, enhancing water proton relaxation thus allowing any abnormalities to be seen.

These compounds are designed to be kinetically and thermodynamically inert so no "toxic" lanthanide ions are released into the body prior to excretion through the kidneys. As an example of therapeutic drugs based on supramolecules, the lutetium complex **10** has been shown to have therapeutic properties as a photodynamic-therapy agent for destroying tumours[7].

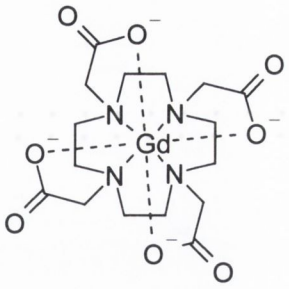

9

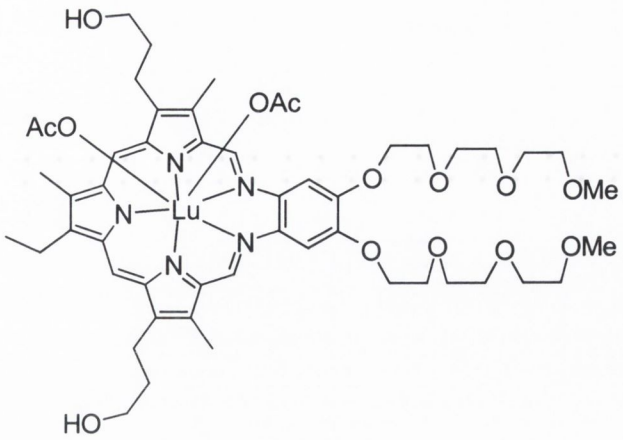

10

10 accumulates in tumour cells and is exposed to UV light, which promotes it to a short-lived excited singlet state that may form a long-lived triplet state. This triplet state converts normal triplet oxygen to singlet oxygen, which is known to kill cancerous tumours. This section has shown the many applications of supramolecular complexes especially lanthanide luminescence complexes, which will be fully discussed in the next sections.

1.4 Lanthanide Luminescent Complexes and their Applications

As discussed above the use of lanthanide complexes is well established in medicine in particular as MRI contrast agents. However other properties of the lanthanides, particularly the ability of many of them to emit upon irradiation has recently attracted the attention of researchers. This thesis will try to address this by developing novel macrocyclic hosts for lanthanide ions that can be used as luminescent devices. Supramolecular complexes may interact with light in a number of ways leading to a branch of chemistry called supramolecular photochemistry[2,13]. This area has led to the development of supramolecular photochemical devices that can be used as light-converting systems, sensors, energy processing storage devices and photosensitive supramolecular catalysts, which activate a reaction upon light absorption[12,13]. Amongst other things supramolecular photochemistry can offer the opportunity to examine stable lanthanide complexes, which are capable of becoming molecular device. The complexation of ions to receptors can often affect the receptors photophysical or photochemical properties in many ways thus changing photophysical properties such as luminescent intensities and changes in absorption, of luminescence or emission wavelength and excited state lifetimes[12]. The design of complexes of lanthanide ions with encapsulating ligands is an important theme in the field of supramolecular

photochemistry because it offers the possibility of obtaining stable luminescent complexes[2]. A relevant aspect of this research is the possibility of optimising the luminescent properties of the metal ion by suitable choice of ligand. The following is a review of lanthanide complexes that have been developed as photochemical supramolecular devices. There is an increasing interest in the application of lanthanides in the investigation of properties and function of biochemical systems and in the determination of biologically active substances[12].

1.4.1 Properties Of Lanthanide Luminescence

Lanthanide luminescence offers many advantages over the more common fluorescence techniques in biological applications. Although they are both non-invasive and highly sensitive techniques (10^{-12}–10^{-11}M), the long-lived luminescence lifetime of the lanthanide complexes overcomes the problems of autofluorescence from other biological fluorescent compounds, such as proteins and nucleic acids, and light scattering problems in biological media. Detection of many lanthanide ions occurs at long wavelengths for example the major emission wavelengths occur in the green (545 nm) for Tb^{3+} and red (612 nm) for Eu^{3+} region

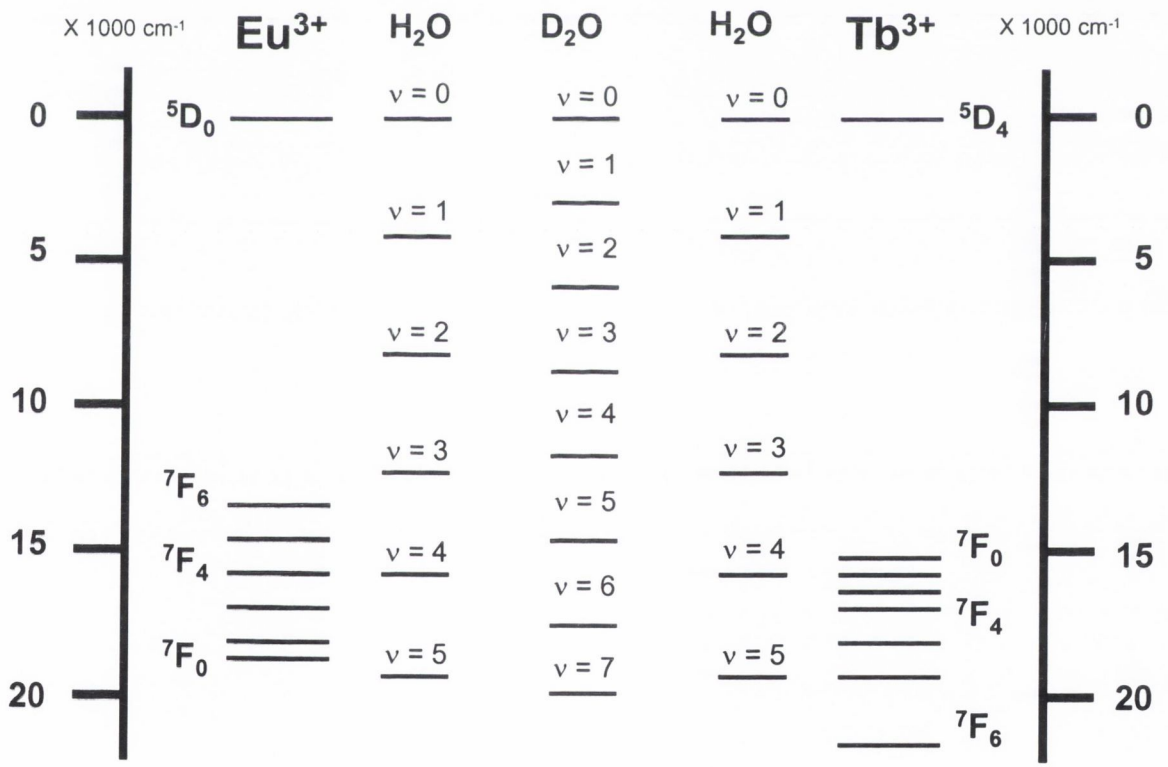

Fig. 1.4: Diagram showing the energy levels for Eu^{3+} and Tb^{3+} and highlighting the deactivating effect of water and D_2O

of the electromagnetic spectrum. The body inefficiently absorbs these wavelengths, in particular red colours, which is important from a diagnostic point of view. Lanthanide ions prefer negatively charged donor groups of the order O>N>S. They have variable coordination numbers ranging from six to twelve with eight or nine being the most common[15]. For an efficient luminescent device, the ligand must fully encapsulate the lanthanide ion because the coordination of water molecules quenches luminescence as discussed previously. The lanthanide ions are also thought to be toxic in the body but once in a strongly coordinating ligand they are relatively safe and kinetically inert. The lanthanide complex must thus be kinetically stable when other inorganic cations and phosphates are present especially in biological media. Lanthanides can form complexes with many biological substances including donor groups, such as COO^-, amide or phosphate groups, as ligands (in amino acids and nucleotides). Binding can also occur as a consequence of lanthanide ion coordination to oxygen on carbonyl or hydroxyl groups *e.g.* in sugars or nucleosides. Lanthanide luminescence occurs from electronically excited lanthanide ions[1,6,13]. In the absence of strongly absorbing ligands, lanthanide luminescence, such as Eu^{3+} and Tb^{3+} the most commonly used ions, is very weak because transitions between states of f^n configuration are strictly parity forbidden by the La Porte Rule of Parity[2] and the probability of such transitions are so low that the molar absorption co-efficients are of the order of 1 (compared to 10 000 for fluorescent organic compounds). In complexes of lanthanide (III) ions, specifically Eu^{3+} and Tb^{3+}, with an encapsulating ligand, an intense luminescence is obtained *via* the "antenna effect"[2,14] where energy is absorbed by the ligand and transferred to the lanthanide ion leading to emission. This has been defined as a light conversion process *via* an *Absorption-Electron Energy Transfer-Emission* sequence.

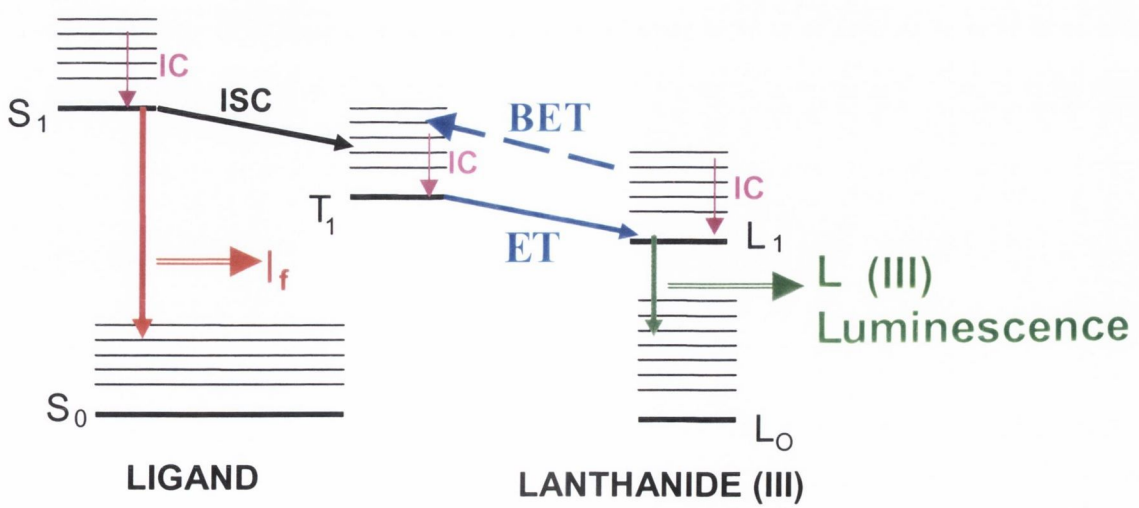

Figure 1.5: The diagram shows the *Absorption-Energy Transfer-Emission* sequence. IC is interconversion, ISC is intersystem crossing ET is energy transfer and BET is back-energy transfer.

It must be noted that distinct absorbing (ligand) and emitting (lanthanide (III) ion) components are present. The efficiency of this luminescence is affected by the intensity of the ligand absorption, efficiency of the ligand to metal energy transfer *i.e.* the distance between the ligand and the metal which tails off by $1/r^6$ (where r is the intermolecular radius between the sensitising ligand and the metal centre) and the efficiency of the metal luminescence. Figure 1.5 describes the typical energy level diagrams for lanthanide luminescence with an antenna moiety. When using this energy transfer process from the ligand to the lanthanide (III) ion, the ligand is irradiated at an appropriate wavelength and an electron is promoted to its excited state. The electron can either lose its energy *via* fluorescence or non-radiation deactivation to its ground state or undergo intersystem crossing to the triplet state. This energy can be passed to the lanthanide-excited state from the triplet state of the ligand. The energy is then "lost" *via* lanthanide luminescence. The energy level of the excited state of the lanthanide ion must be lower in energy than the triplet state of the ligand to ensure energy transfer.

$$q = A(1/\tau_{H2O} - 1/\tau_{D2O}) - X$$

Equation 1.2: Equation to determine the hydration state around the lanthanide complex q where X is the correction factor for the oscillators, τ is the lifetime of the complex in solution and A is the experimental parameter

The energy transfer from the triplet state of the ligand to the excited state of the lanthanide ion is the rate-determining step. The importance of the luminescence of lanthanide ions is related to its unique characteristics such as long lifetimes (milliseconds compared to nanoseconds for many fluorescent compounds such as anthracene and pyrene), line like emissions of a few nm bandwidth and emission at long wavelengths will give rise to large Stokes' shifts (150nm-300nm). This makes these ions unique among the species that are known to luminese. These characteristics occur because the emitting excited state and ground state have the same f^n electronic configuration and these same f orbitals are shielded from the environment by the outer s and p orbitals. The ground electronic state if the ^7F_J state for the lanthanides with the first excited state being $^5D_4$ for Tb^{3+} and $^5D_0$ for Eu^{3+} as highlighted in Figure 1.4. The coordination environment (solvent) affects the luminescence intensity and lifetime due to the presence of solvent molecules coordinated to lanthanide (III) ions and low-lying, short-lived excited states of the water molecules as highlighted in Figure 1.4, which can deactivate the excited state through vibrational energy loss. This is in particular due to the presence of the N-H and O-H oscillators[15]. The hydration state around the lanthanide ion is described by **q** and

the equation is seen in Equation 1.2[67]. By careful choice of the coordination environment, non-radiative losses can be controlled or reduced substantially. Water and hydroxyl anions are strongly coordinating ligands and can quench the lanthanide luminescence through O-H vibrations. The non-radiative relaxation between various vibrational states may occur *via* interaction of the electronic levels of the lanthanide ion with suitable vibrational modes of the solvent environment. The efficiency of these processes depends on the energy gap between the ground and excited states and the vibrational energy of the oscillators (*e.g.* solvent molecules). When solvents containing O-H groups are co-ordinated to lanthanide ions, efficient non-radiative deactivations take place *via* vibronic coupling with the vibrational states of the O-H oscillators as highlighted in Figure 1.4. This suggests that the coordination environment affects the luminescence intensity and lifetime *via* the presence of solvent molecules coordinated to the metal ion. It also suggests that the presence of a highly coordinating ligand containing at least eight coordination sites to prevent solvent coordination as it is known that lanthanide ions have coordination numbers between seven to twelve with eight and nine being the most favourable.

In summary, to populate the lanthanide ion excited state it is suggested that a number of properties must be present to obtain optimum energy transfer to the lanthanide ion. These properties are:

- high kinetic and thermodynamic stability in aqueous solvent and biological media
- very high coordination number for the lanthanide ion *ca* eight or nine
- high quantum yield[§] for lanthanide emission
- high emission wavelengths
- fully encapsulating to prevent quenching water molecules coordinating
- good emission lifetime of approximately 0.4-0.8ms
- kinetically stable in the presence of other inorganic ions (*i.e.* metal ion exchange)
- high absorption coefficient in the near UV to visible region ($\lambda > 360$ nm)

1.4.2 Lanthanides as Luminescent Probes

One of the first uses of lanthanide luminescence was as probes to determine the structure of biological molecules[16,17] including the determination of discrete equilibrium structure, the distribution of structure types in homogenous systems and biomolecule-solvent interaction by direct radiation of the lanthanides $4f^n$ electrons using direct excitation by laser. Prior to the work of Richardson *et al*[17] there had been little use made of metal ion

luminescence to study biomolecular structures because none of the metal ions essential to biological structure are known to emit under biological conditions. The exceptions to this are the lanthanide ions especially Eu^{3+} and Tb^{3+} (not normally found in biology), which are luminescent in aqueous solution and retain their luminescence when bound to complex ligand systems. The lanthanide ions also exhibit multiple emissions where relative intensities and line splitting patterns that are sensitive to the detailed nature of the ligand environment around the lanthanide ion. It must be noted that there is no "directionality" associated with lanthanide-ligand interactions suggesting that the geometry and primary coordination are determined only by the ligand characteristics. For structure determination with lanthanide ions, the binding site must effectively remove water molecules from the lanthanide ion. The size and geometry of the binding site must be compatible with donor atom preference of lanthanide ions. Most importantly there must be no major perturbation to the ligand once the lanthanide ion is bound. The lanthanide ions have coordination properties, which are similar to those of divalent alkali earth metals and are useful as substitutional probes for calcium. Biological activity is often retained suggesting isomorphous replacement.

Lanthanide ions especially Eu^{3+} and Tb^{3+} are introduced into a system and employed as luminescent probes that are sensitive to the influence of the environment[18]. The emission spectrum identifies the donor groups in the ligand and lanthanide ion binding sites. The changes in intensity of the lanthanide emission bands or ligand luminescence quenching provide information on the interaction between the ligand donor group and the lanthanide ion and the complex stoichiometry. The measurement of emission lifetimes of Tb^{3+} and Eu^{3+} in water and D_2O provides information on the number of water molecules in the inner coordination sphere of the lanthanide ion. From the ratio of the intensity and structure of the lanthanide emission bands conclusions can be made about the symmetry of the bonds and the conformational properties of the ligand at the metal binding sites. The advantage of the lanthanide luminescence probes provides high sensitivity with respect to structural and analytical probes. This permits detection of very small changes in the structure of the studied compounds and allows the detection limit of the determined substances to be lowered. Below, the use of lanthanide ions in biological systems will be briefly discussed. Horrocks and co-workers[16] used lanthanide ions to replace calcium in proteins specifically Thermolysin. The lanthanide substitution was found to have no effect on the enzymatic ability of the protein. The other coordination effects discussed above are applicable here. It was also noted that the additional charge on the lanthanide (III) ion compared to calcium (II) caused no problem during replacement because most biological macromolecules contain charged groups and

counterions, which counteract this effect. In fact, the only discernible chemical difference is slower ligand exchange rates and greater binding constants for lanthanide ions. These techniques are sensitive, non-destructive and applicable to a wide variety of biological macromolecules.

Calcium and magnesium are the most abundant metals in biological systems but the investigation of their binding and transport properties are hindered by their lack of spectral characteristics, which are required for structure elucidation. The antibiotic Lasalocid A **11** is a known ionophore for both monovalent and divalent cations. **11** was studied in MeOH and MeOH:H_2O with Eu^{3+} and Tb^{3+} by Richardson and co-workers using circular polarised luminescence (CPL)[19], which is a technique, used to study the effect of stereochemistry upon emission. It is a sensitive indicator of binding and is used as a probe for site symmetry and stereochemistry in chiral systems. Lanthanide optical activity is generally observable only when a chiral ligand is bound directly to the Ln^{3+} and is strong only when there is some Ln^{3+}:ligand multidentate chelation.

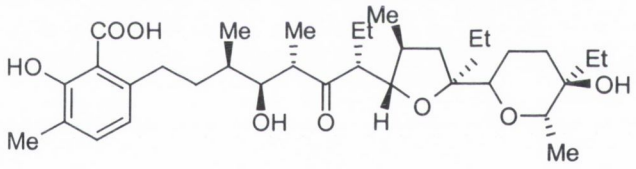

11

The strongest ligating group was found to be the COOH group of the salicylic acid moiety. When Tb^{3+} is bound to this group there is an enhancement in the Tb^{3+} emission but not of the optical activity in the $^5D_4$ to ^7F_J emission because the chiral centres are too far removed from the ion. Under solution conditions, the ligand wraps around the metal and binds *via* the five donor oxygen atoms in the non-salicyclate moiety. Strong Tb^{3+} emission optical activity is now observed proving that a 6 coordinate chelate is formed with the nine chiral centres in close proximity to Tb^{3+}.

High resolution, laser excitation and emission spectroscopy allows the following to be detected in proteins. The number of chemically different sites in the material, the total formal charge of the ligating group directly bound to the lanthanide ion and the symmetry of these sites. The amino acid in the protein is usually monitored. Bünzli and co-workers[20] used Eu^{3+}

as a replacement probe for Ca^{2+} to study metal sites of bovine α-lactal bumine. This is a protein with a molecular weight of approximately 14,200 $gmol^{-1}$. Luminescent titrations prove that there are more than two lanthanide ion-binding sites per protein molecule. High-resolution excitation spectra show population of three metal ion sites, two of which are relatively defined within the protein. The third site is less defined and its population is pH dependant suggesting the metal ion is fixed on the outskirts of the protein. Laser excitation of Eu^{3+} was used for the identification of metal ion binding sites in bovine α-lactal bumin. Two binding sites contained four negatively charged groups and were related to the Ca^{2+} binding site. The third type of chemical environment is a non-specific metal binding site taken by Eu^{3+} after saturation of the other binding sites.

Analytical probes can be used to determine the presence of organic analytes (such as tetracycline) using lanthanide luminescence[21]. Novel heptadentate chelating agents with Eu^{3+} form stable complexes. These are used as luminescent labels in capillary electrophoresis separation of a variety of samples of biological interest for example amino acids, peptides and proteins. Yb^{3+} complexes with porphyrin are used as fluorescent labels of malignant tumours in mice *in vivo*[22]. These complexes emit in the 900-1050 nm range thus eliminating autofluorescence and enhancing the luminescence contrast value of the tumour[21]. These complexes are not phototoxic which is very important with respect to diagnostic applications. Lanthanide luminescence can also be used as analytical probes to monitor the chemical modification of guanine residues in nucleic acid[21]. The interaction of Tb^{3+} with phosphate moieties of single-strand nucleic acids results in enhanced lanthanide luminescence. The excitation spectra is characteristic for the base moiety bound and the emission spectra is characteristic for the lanthanide ion. Although in double-stranded nucleic acid the lanthanide is more tightly bound, there is a quenching of lanthanide luminescence due to the alteration of the energy of T_1 levels for the base. This characteristic enhancement of Tb^{3+} luminescence is used to monitor the chemical modification of guanine residues in nucleic acids occurring during their biological functions or by their attack from carcinogens[21].

1.4.3 Lanthanide Luminescence Complexes as Fluorescent Labels

As briefly shown in the previous section, there is a considerable interest in using the unique spectroscopic properties of some of the lanthanide ions, specifically Eu^{3+} and Tb^{3+}, when they are chelated with appropriate organic ligands. The unique properties of some of the lanthanide complexes prompted the development of fluorescence labels in the area of clinical chemistry and molecular biology as alternative tools to radioactive labelling[21]. The most

important applications are labels for time-resolved fluoroimmunoassays, nucleic acid hybridisation, metal ion coordination in proteins, structural studies of biomacromolecular materials and sensors. From the interest in lanthanide ions as probes for biomolecules came the use of lanthanide ion complexes as homogenous immunoassays. Immunoassays make use of a long-range energy transfer between luminescent lanthanide ion complexes (usually Eu^{3+} and Tb^{3+}) and an acceptor[13,22] *i.e.* the indirect irradiation of the lanthanide ion by an antenna molecule. All immunoassays must be highly sensitive and specific[23]. Radioimmunoassays provide these important properties but are problematic because of their associated radioactivity. These fluorescence labels work *via* the *Absorption-Energy Transfer–Emission* processes as described in Figure 1.5.

Time-resolved fluoroimmunoassays[18,24] are a developing area of interest where the luminescent property of lanthanide ions is successfully used for the analysis of biological substances by immunological methods. The sensitivity and specificity of this technique ensures it advantage over other fluoroimmunoassays methods. Immunoassays are based on the process of binding an antigen with an appropriate antibody. This specific reaction forms an immunological complex. An antibody is an antigen-binding immunoglobin that functions as the effector in an immune response. An antigen is a foreign macromolecule *i.e.* from a virus, bacteria, pollen or transplant tissue that does not belong to the host organism and elicits an immune response. Diagnostically the process usually occurs on plastic surfaces to which the antibody is covalently attached. To determine the amount of analyte, the label is introduced to one of the substrates of immunological reaction. The label must be easy to detect and identify. In radioimmunoassays the label is the radioactive isotope and in fluoroimmunoassays the label is the fluorescent emission compound. The advantage of this method is safer, more sensitive, faster and simpler measurement. The chelates of Eu^{3+}, Tb^{3+}, Dy^{3+} and Sm^{3+} are used as labels of antigens or antibodies[21]. The measurement of laser excitation luminescence of lanthanide complex is performed by time-resolved methods, *i.e.* delay of 200-400 ms after excitation, therefore only lanthanide emission is measured as explained above. The lanthanide chelates must be water soluble, have functional groups capable of forming a covalent bond to immunoactive compounds (*i.e.* antigen or antibody), be characterised by a high stability constant and high yield of energy transfer from the ligand and lanthanide. There are two types of commercially available immunological assays[26]. Dissociation-Enhanced Lanthanide Fluoroimmunoassays (DELFIA) is a two-stage process of measurement with the participation of two different lanthanide complexes. The first stage involves the immunological reaction between a lanthanide ion, usually Eu^{3+}, in a complex

with an isothiocynate derivative of EDTA. This forms a stable bond with the immunoactive agent *via* the formation of a covalent bond between the thiocyanate with the free amine group of the antibody. The second stage involves an antigen-antibody conjugation with the lanthanide complex label treated with an enhancement solution (2-naphtoyltrifluoracetone), detergent and synergistic agent (TOP). This solution is at low pH allowing the lanthanide ion to be dissociated from the primary compound forming a chelate with 2-naphtoyltrifluoracetone and emitting an intense luminescence. The measurement of the luminescent content of Eu^{3+} in the solution is determined within 5 x 10^{-4} to 1 x 10^{-8} M. Cyberfluor is a more modern method where a sensitising Eu^{3+} chealator is introduced into the immunoactive agent and an excess of Eu^{3+} is used to form the fluorescent complex[26]. The Eu^{3+} chelate with 4,7-bis(chlorosulphophenyl)1,10-phenanthroline-2,9-dicarboxylcic acid (BCPDA) acts as the label with a detection limit of 3 x 10^{-3} M. The two chlorosulphonyl groups form a covalent bond with the amino groups of the antibody. This method has been employed to determine the α-fetoprotein present in serum, prolactin, thyrotropin and growth hormones[21].

The potential usefulness of lanthanides as labels for histochemical techniques and immunoassays has focused attention on the development of novel macrocyclic ligands having functionalised peripheral substituents suitable for attachment to the biosubstrate[25]. Here the lanthanide ions are in a ligand cage and protected from the solvent. These form stable, water-soluble compounds and emit intense luminescence. Their use is expected to simplify the procedure and increase the sensitivity of flouroimmunoassays. The development of novel lanthanide ion complexes is described below. Of particular interest is the use of pyridine-based ligands for lanthanide complexes.

1.4.4 Novel Lanthanide Luminescence Complexes

Lanthanide ions do not exhibit strong coordinating ability towards conventional ligands especially in aqueous solution as discussed on section 1.4.1[14]. The pioneering work in creating suitable ligands for the lanthanides was preformed by Lehn and co-workers[2,12,13,23]. These ligands were based on the use of 2,2'-bipyridine (bipy) and 1,10-phenanthroline (phen) moieties which act as a combined coordinator and antenna ligand, incorporated into a macrocyclic cage-like structures. These are essentially rigid molecules with a cavity suitable for lanthanide ions. Although nitrogen is a poor donor ligand that binds weakly to lanthanide ions, entrapment of the ions in a cage can greatly enhance the properties even in the absence of stronger donor such as ether oxygen or carboxylate groups. In initial experiments,

macrocycles were studied with Eu^{3+} and Tb^{3+}. The strong $^5D \rightarrow {}^7F$ emission of lanthanide ions was enhanced by the triplet state of the ligand *via* the antenna effect as described in Figure 1.4 and 1.5. It was found that cryptates with three bipy groups[2,13] **12** now known as the Lehn cryptand were the most promising labels because of the high absorption coefficients, luminescent lifetimes and increased quantum yields of emission.

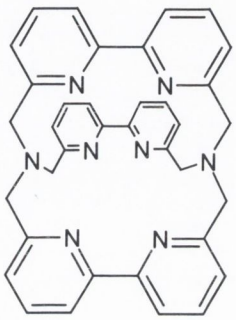

12

The presence of other species in the coordinating environment may affect luminescence explaining why a fully encapsulating ligand is required. When the acyclic ligands **13** and **14** below were studied it was found that they were only stable in MeOH as a gradual decomposition of the complex occurred in water. The acyclic ligand **15** was studied by Mukhala[26,27] and co-workers as possible lanthanide chelates for immunoassays. The carboxylic groups aided lanthanide ion binding giving it overall eight coordination. The substituents were found to have significant effects on the luminescent properties.

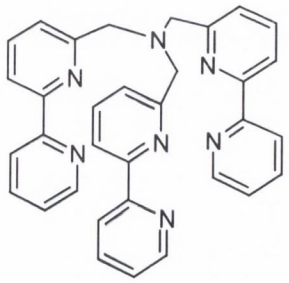

13

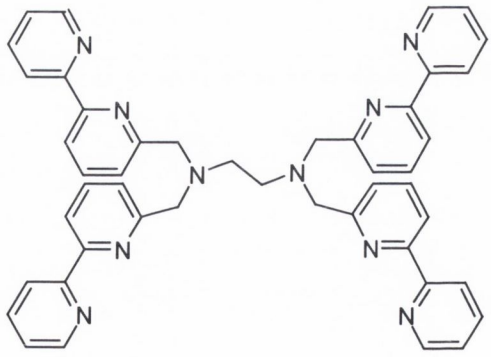

14

Continuing on from the basic architecture of **15**, acyclic ligand **16** was found to be the best ligand for increasing the chelating effect, shielding the lanthanide ion from water and the coordinating environment. It was found that the more electro-donating the X group is, the

better the energy transfer from the ligand to the lanthanide ion is. This gave quantum yields comparable to those of macrocycle **17**, which contains a ring composed of two bipy moieties with two other bipy moieties as pendant arms and provides a competitive alternative to **12**.

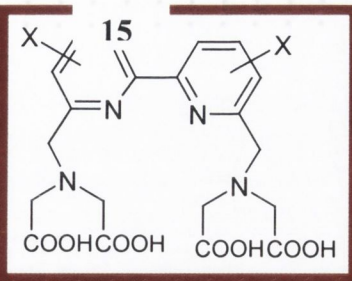

Substituent (X)	Relative Intensity	
	Eu3+	Tb3+
4,4'-dimethyl	5.61	5.51
Unsubstituted	5.5	5.51
4,4'-dinitro	4.14	weak
4,4'-diphenyl	5.52	5.18

Table 1.2: Table showing the intensity of binding of lanthanide ions by changing a number of substituents.

17 incorporated one more bipy group than **12** to provide no extra degree of flexibility leading to more favourable coordination of the ligand around the lanthanide ion. Furthermore this led to more efficient orbital overlapping of the ligand giving rise to more efficient energy transfer to the lanthanide ion and better shielding.

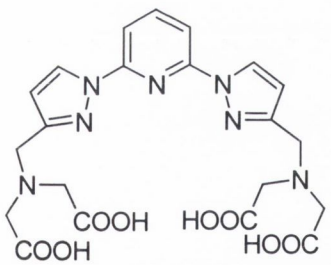

16

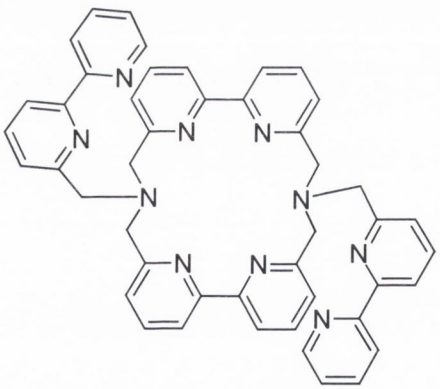

17

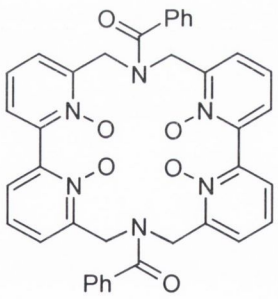

18

Other related examples included the development of N-oxide macrocyclic complexes[28], because the lanthanide ions are known to prefer negative ions in the order O>N>S. One of the initial compounds produced was **18** having four N-oxides. This gave a good quantum yield with a luminescence emission fingerprint at around at 614nm, which is ideal for practical applications. The complex was very stable in water and efficiently shielded the lanthanide ion from the coordination environment. A range of other compounds **19** and **20** were also developed. The acyclic complex **19** with Eu^{3+} in a 3:1 ligand to metal stoichiometry showed exceptional luminescence in acetonitrile with long lifetime and good quantum yields but

unfortunately was not stable in water. In contrast, the Eu^{3+} complex of **20** had shorter lifetimes and decreased quantum yield in comparison to **18** but was stable in water

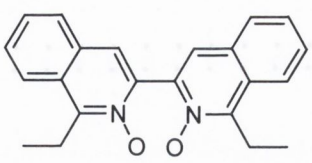

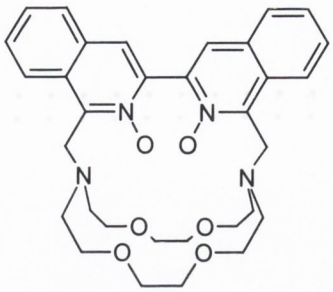

19 **20**

Comparing the emission spectrum and the number of solvent molecules of **21** and **22** to **12** demonstrated that the ligands containing two N-oxides with three bipy groups gave comparable intensity in water and D_2O with more effective shielding of the lanthanide ion. These experiments suggest that the inclusion of the N-oxide group in the ligand provides better luminescent properties with greater stability in water.

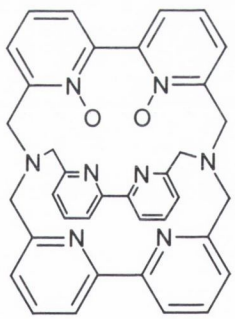

21 **22**

Putting three N-oxide bipy-type groups into the macrocyclic complexes **23** to **26** did not give any increased emission properties. This implies that the nature of the counterion should be accounted for when designing a ligand for luminescent probes provided that the lanthanide ion is not completely shielded from the solvent environment.

To recap, the initial lanthanide luminescent ligands were mostly based on heteroaromatic moieties (*e.g.* Bipy and Phen). These were found to be efficient antennas but give imperfect encapsulation leading to quenching of luminescence by water molecules. The addition of N-oxides into the ligand gave far superior encapsulation with better shielding of

the lanthanide ion from the solvent environment. The N-oxide ligands are also more efficient donor groups because of the high electron density on the oxygen atoms thus leading to stronger binding ligands *i.e.* the best ligands are cyclic with a cavity for encapsulation but with some degree of flexibility and as many photoactive groups as possible.

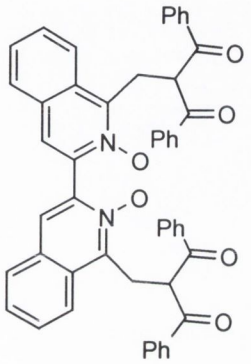

23

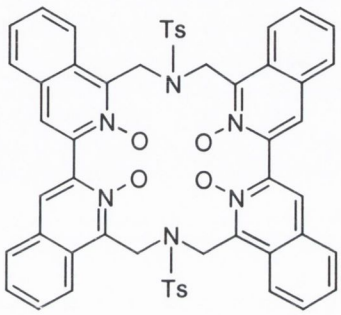

24

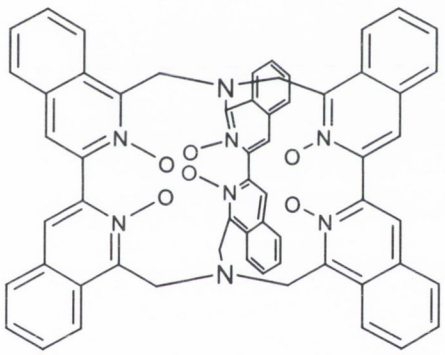

25

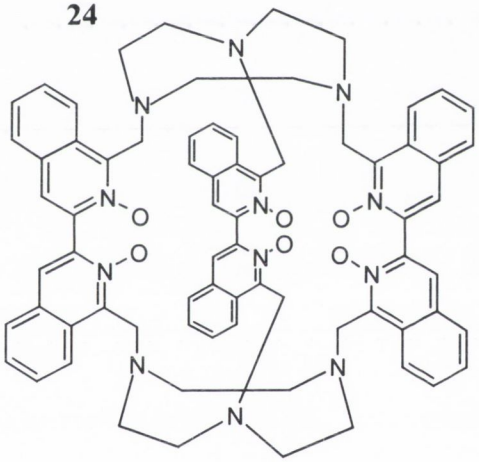

26

Moving away from the bipy-type ligands, Shinkai[26,29] and co-workers developed lipophilic phenyl phosphates ligands **27** and **28**. These ligands had high luminescent quantum yield with Eu^{3+} and Tb^{3+} in water. The lanthanide ion is bound *via* the phosphate moieties in a stoichiometric ratio of 3:1 [ligand to lanthanide ion] leading to full, effective encapsulation of the lanthanide ion. The bifunctional ligand **28** is an especially good sensitizer.

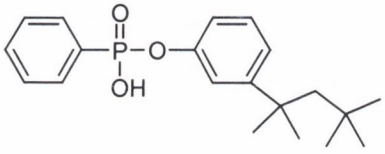

27

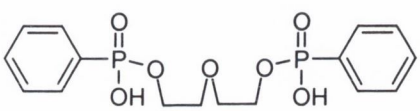

28

It seems, therefore, that either the lanthanide complexes of acyclic or macrobicyclic ligands incorporating sensitising units can be taken into account as potential markers for time-resolved fluoroimmunoassays provided that the complexes are inert enough to avoid loss of the lanthanide ion either *via* precipitation or cation exchange.

Verhoeven and Reinhoudt *et al* have reported the use of triphenylene[30] **29** as a good sensitiser for both Eu^{3+} and Tb^{3+} when encapsulated in calix[4]arene receptors. Although **29** has a high triplet state generated with high efficiency and long lifetimes, there were some disadvantages. The molar extinction coefficient is quite low and **29** was devoid of any lanthanide ion binding sites.

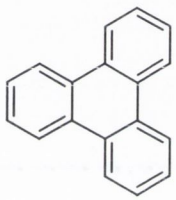

29

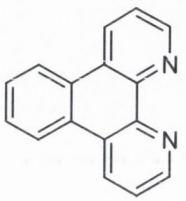

30

To overcome this problem, two heteroatoms were introduced into the triphenylene moiety to produce diazatriphenylene[31] **30**, which combines the superior photophysical properties of **29** with the strong complexing ability of the nitrogen atoms used by Lehn in their 2,2'-bipyridine cryptates. This moiety binds to lanthanide ions in 2:1 ligand:metal stoichiometry in MeCN. It was found that **30** was able to sensitise both Eu^{3+} and Tb^{3+} with extremely high efficiency. This is determined using the quantum yield Φ, which is determined using the equation photons emitted, divided by the photons absorbed. The efficiency was found to be Φ=0.41 and Φ=0.55 for **29** and **30** respectively in MeCN. The high molar extinction coefficient of **30** with a λ_{max} >330 nm makes this a promising molecule for applications in time-resolved fluoroimmunoassays. Verhoeven and Reinhoudt *et al* continued developing a series of tetraazatriphenylene[32] derivatives (**31** to **37**) with structural variations to vary absorption characteristics and to determine the effect of the functional groups on the photophysical properties in non-hydroxylic solvents. All these ligands form 2:1 complexes with lanthanide ions in MeCN. The substituents either improve the photophysical properties or else contain a reactive group, which can be used for attachment to the biological material of interest. The addition of two further nitrogens to **30**, forming the ligand, **31**, enhances the absorption characteristics in the important wavelength region above 330 nm. It was found that compounds **35** to **37** obtained quantum yields significantly lower than those for **30** to **33**,

which was related to a slow energy transfer. **34** was sterically not able to sensitise Eu^{3+} or Tb^{3+} probably due to the presence of the chloride moieties. All these compounds, especially **30** to **33**, formed strong luminescent complexes with efficient energy transfer (quantum yields close to unity). Any inefficiency in energy transfer to Tb^{3+} can be related to lack of sufficient triplet energy, whereas inefficiency towards Eu^{3+} was attributed to electron-transfer quenching by LMCT.

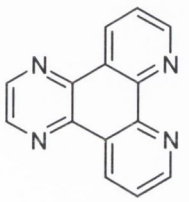

31

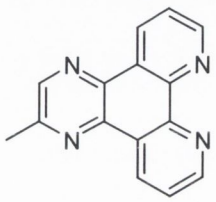

32

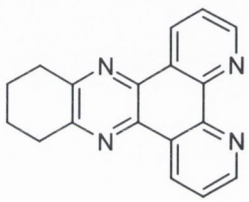

33

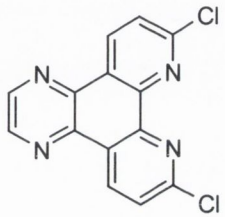

34

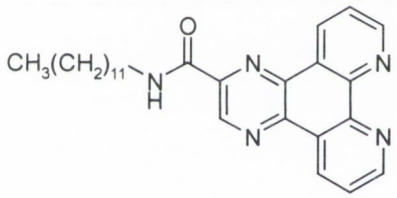

35

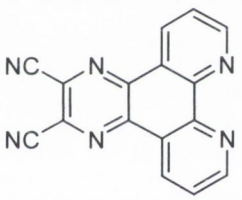

36

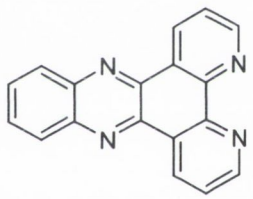

37

These compounds combined high triplet energy with a strong resistance to quenching by oxygen, which is quite advantageous. It must be remembered that the actual efficiency of a luminescent label, for example in bioassays, cannot be deduced from the quantum yield alone. The extinction coefficient at the excitation wavelength also plays a role.

Verhoeven *et al* expanded the azatriphenylenes from sensitisation in non-hydroxylic solvents to aqueous solutions by the addition of anionic moieties[33]. These formed water soluble, stable complexes. Compounds **38** to **40** were able to sensitise lanthanide ions but had lower quantum yields in aqueous solution compared to compounds **31** to **37** in non-hydroxylic solvents due to the protonation of the nitrogens on the far phenyl ring thus quenching the excited state.

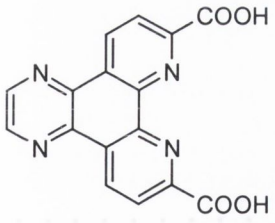

38

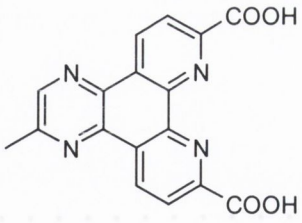

39

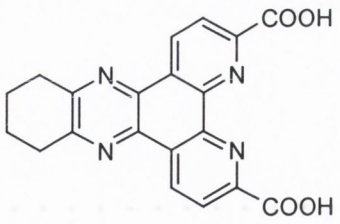

40

The development of **41** based on triphenylene with the addition of two carboxylic groups did not improve the shielding of the lanthanide ion compared to **38** to **40** and it was suggested by the authors that the presence of the carboxylic and amino moieties acted as oscillators facilitating the quenching of lanthanide luminescence.

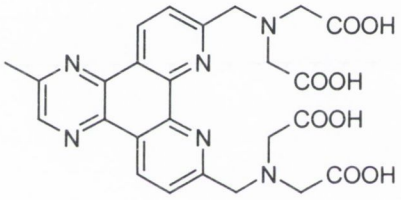

41

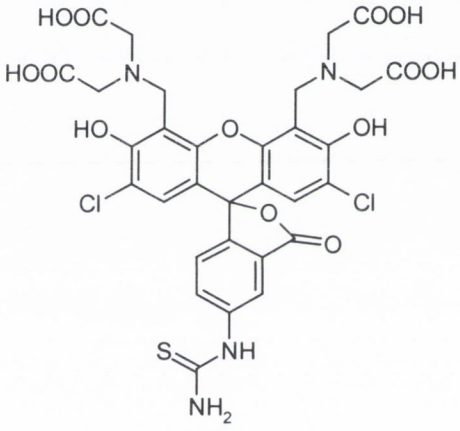

42

Verhoeven then developed luminescent labels based on a fluorescein type ligand[34,35] **42** using Yb^{3+}. The ligand **42** contains a thiocynate moiety that was able to covalently attach to proteins, with the lanthanide ion binding *via* the carboxylic moieties in a 1:1 stoichiometry. The protein conjugates of the [Yb^{3+}.**42**] complex retained similar photophysical characteristics compared to the ligand without the thiocynate moiety and can be used as model medicinal diagnostic tests. The long-lived luminescence counteracts any autofluorescence and light scattering effects from biological media. While these are an attractive new class of luminescent labels in aqueous media, the overall luminescent quantum yields need to be improved by suppressing non-radiative deactivation of the luminescent states and overcoming the problem of quenching by the solvent water molecules.

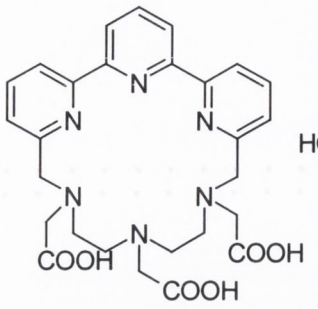

43

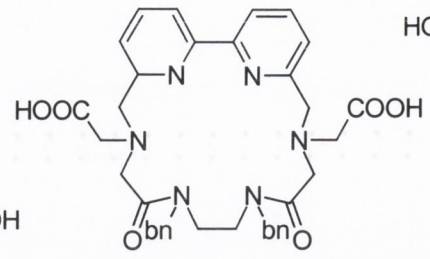

44a

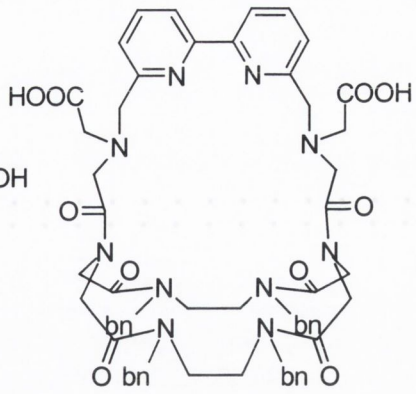

44b

Picard and co-workers developed novel lanthanide ligands for luminescence studies. One of the first ligands developed was a ligand based on the terpy moiety **43**[36]. The carboxylic groups allow the formation of a strong neutral complex with electrostatic interactions and increased solubility in water. The terpy moiety is a suitable sensitiser for energy transfer and **43** contained nine possible coordination sites. The molecule **43** showed high luminescence properties and was stable in aqueous solution displaying **43**'s usefulness as a luminescent biolabel for time-resolved fluoroimmunoassays. Following from this work, Picard *et al* prepared photoreactive ligands **44a** and **44b**[37,38,39] composed of a bipy macrocyclic framework with aminocarboxylic groups. They found[38] that the two carboxylic units aided solubility and stability in aqueous solution. The compounds had efficient energy transfer in aqueous solution compared to the other bipy cryptates discussed above, especially ligand **44**, which was prepared in four steps.

Bunzli *et al* developed a crown ether based ligand,[40] **45**. **45a** was not found to be a good sensitiser for lanthanide ions because of the presence of the lone pair of electrons of the N-H group, which deactivates the lanthanide luminescence. This is similar to that observed upon protonation of the nitrogens in **31**.

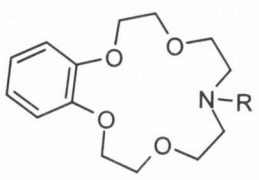

R = (a) H
(b) COCOPh
(c) CH_2COOH

45

The presence of the conjugated COCOPh group in **45b** enhances Eu^{3+} luminescence but not Tb^{3+}. The addition of the CH_2COOH group in **45c** enhances the sensitising power of Tb^{3+} but with weak Eu^{3+} luminescence. These results demonstrate that this ligand provides a good framework for the fine-tuning of the photophysical properties of the lanthanide ion complexes by functionalising the amine groups with a suitable substituent.

This section has served to highlight some of the luminescent lanthanide complexes available as possible time-resolved fluoroimmunoassays. In the next section the use of Schiff-base ligands for lanthanide ion coordination will be discussed.

1.4.5 Schiff Base Ligands

The design and synthesis of macrocyclic lanthanide complexes is currently attracting considerable attention as a route to supramolecular devices, sensors and efficient RNA cleavage catalysts[41]. Luminescent complexes are also useful in immunoassays provided they contain functional groups for covalent linking to biosubstrates as discussed in section 1.4.3. Also the complexes of Gd^{3+} have high relaxitivity and are useful as contrast agents in MRI provided their tolerance is enhanced by appropriate functional groups in the complex as per section 1.3. This suggests that the functionalisation of the ligand is required for theses bio-medical applications. The lanthanide metal-templated cyclic Schiff-base condensation reactions provide a means of easy access to otherwise difficult to acquire complexes, directing cyclisation and preventing polmerisation, with the ability to further functionalise. The template effect is where the metal ion directs and controls the formation of a macrocyclic compound from acyclic starting materials as demonstrated in Figure 1.6.

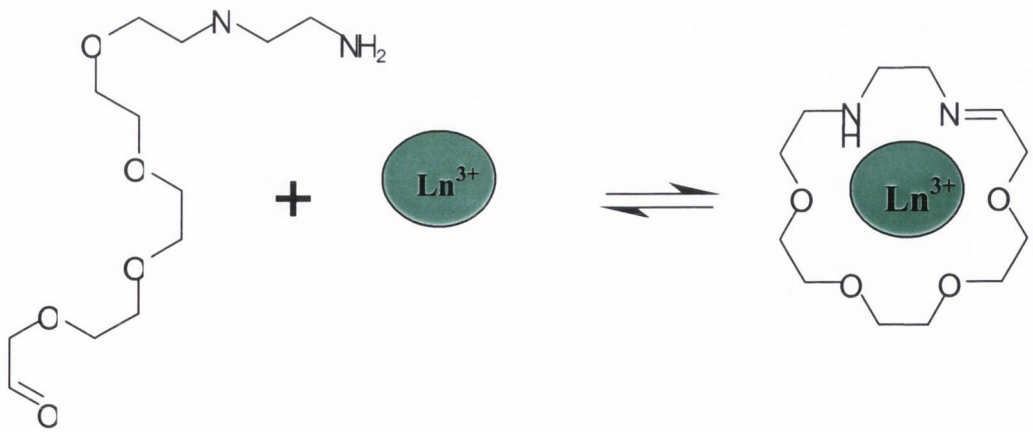

Fig. 1.6: Diagram showing the formation of a macrocyclic complex by metal templated synthesis.

The ability of the lanthanide ions to promote Schiff-base condensation of appropriate diamine and dicarbonyl precursors, resulting in the formation of lanthanide complexes of otherwise inaccessible macrocyclic ligands, is by now well established and reviewed[41,42,43]. The main focus of research has studied identical macrocyclic frameworks with all the lanthanide ions (except Pm^{3+} which is radioactive). This is for two reasons. Firstly, to study the influence of structure and dynamics of the ligand framework on the physiochemical properties on the lanthanide ion in order to identify the ligand design feature required to form robust lanthanidecomplexes. The second is to design flexible macrocyclic compounds that can adapt to the geometric requirements of the lanthanide ion of varying sizes. These complexes may form 1+1, 2+2, 3+3 or 4+4 macrocycles, as shown in Figure 1.7, without the presence of the lanthanide but more usually form 1+1 or 2+2 macrocycles depending on the chain length of the diamine, the lanthanide ion radius, the preferred geometry of the complex and the electronic nature of the lanthanide ion. The Schiff-base macrocyclic complexes are typically inert to metal dissociation.

One of the first types of Schiff-base ligands for transition metal ions was **46,** which was synthesised using 2,6-diacetylpyridine with hydrazine in the presence of Fe(II) or Co(II) forming a conjugated macrocyclic ligand[41].

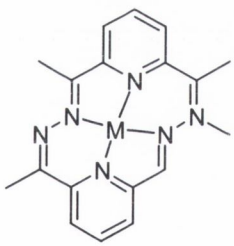

46

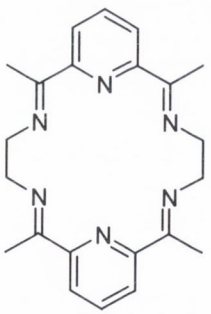

47

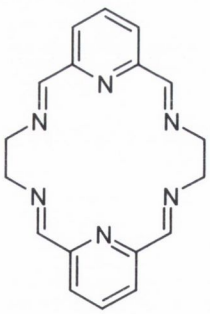

48

This macrocycle was also isolated when Tb^{3+}, Dy^{3+}, Ho^{3+}, Er^{3+}, Tm^{3+}, Yb^{3+}, Lu^{3+} ions were used. From this, Hart *et al* developed **47** from the condensation of 2,6-diacetylpyridine and 1,2-diaminoethane with various lanthanide ions[44] and **48** synthesised from 2,6-diformylpyridine with 1,2-diaminoethane[45,46,47]. These are inert toward metal release in solution, even under conditions that would result in the immediate decomposition of most other lanthanide complexes such as high temperatures and strong acids.

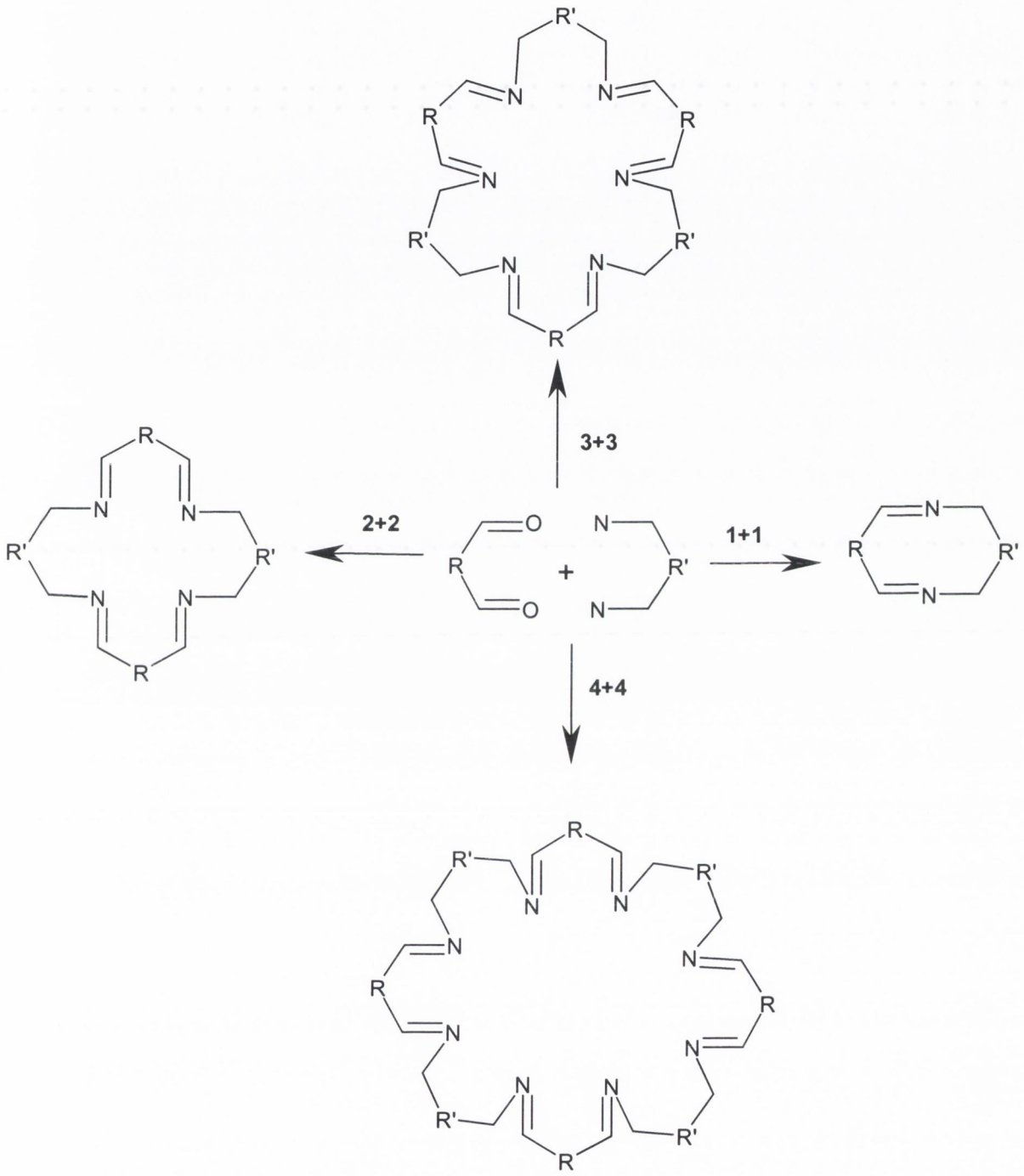

Figure 1.7: The diagram shows the possible ring structures available when no metal is used. R is usually a dicarbonyl aromatic head unit. R' may be an aliphatic chain or aromatic unit containing an amino end-group. Note: The lanthanide ion has been omitted for clarity

Vallerino and co-workers developed complex **47** as a mixture of constitutional and stereoisomers from (R)-, (S)- and (R,S)-1,2-diaminopropane in an attempt to answer three questions[48]: (1) Are constitutional isomers formed in the lanthanide-templated macrocycle synthesis and are they distinguishable? (2) Can synthetic conditions provide some degree of isomer selectivity? (3) Can isomers be separated and identified structurally? They did this by looking at the complex of **47** with La^{3+}. When La(III)acetate was used constitutional isomers were formed which were distinguished by ^1H NMR. The temperature of the reaction provided a degree of isomer selectivity. The constitutional isomers had different solubilities and could be separated, in minimal yields, by ^1H NMR-monitored fractional crystallisation. Reports have been published investigating the chiral properties of these and other complexes[49].

Alexander and co-workers investigated a number of similar complexes[42] with the aim of preparing symmetric [2+2] macrocyles incorporating aromatic rings in lateral and/or head units that exhibit moderate flexibility and form more stable complexes than those of very flexible macrocycles. The reaction of 2,6-diacetalpyridine with 1,2-diaminopropane or 1,3-diaminopropane in the presence of lanthanide ions produced 2+2 lanthanide complexes **49** and **50** respectively.

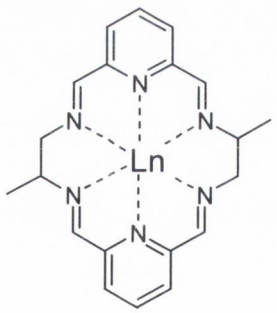

49

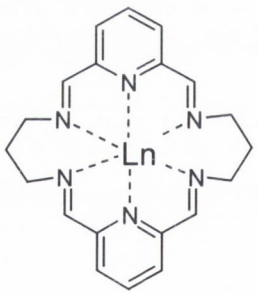

50

These formed complexes with all the lanthanide ions with varying degrees of water molecule coordination. This method is used to generate a wide variety of 2+2 complexes with a pyridine head unit with lateral aliphatic chains by appropriate combination of counterions and experimental conditions. The ease and yield of the metal-templated synthesis was found to depend on the choice of counterions, for example the acetate anion has more good donor oxygens than the perchlorate anion. The coordination numbers of the ligands tend to decrease along the group because of the subsequent decrease in ionic radius of the lanthanide ions[42]. The template synthesis of the lanthanide ions in assembly of these macrocycles is due to the

adaptability of the macrocycles to fold due to the steric and geometric demands of the lanthanide ion.

The Alexander group went on to study 2+2 complexes containing 2,6-dicarbonylpyridines and aromatic and cyclic lateral units such as **51** and **52** below. **51** was found to be suitable to study lanthanide ion chiral optical properties[42,50]. **52** was only formed with the lower atomic mass lanthanide ions from La^{3+} to Dy^{3+}, excluding Ce^{3+}, in 75-80% yield[51]. They were also formed in varying stoichiometries depending on the geometrical requirements of the lanthanide ion[52]. To increase the binding ability of the macrocycle, the pyridine head units in **50** were replaced with phenol moieties to yield **53**[53]. This provided a macrocycle with nitrogen and oxygen donors, with hard and soft base characteristics, forming more stable complexes. **53** is an 18-membered dioxa-tetraaza ligand, which showed different geometry depending on the position of the lanthanide ion in the group. Although the yield of the synthesis usually decreases along the lanthanide ion series for other macrocycles, for **53** they increase because of the match of the larger lanthanide ions to the size of the cavity. The presence of hydroxy groups and other complexing agents caused **53** to decompose.

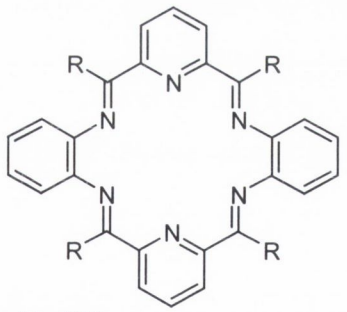

R = H, CH_3

51

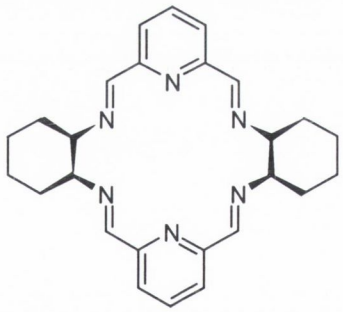

52

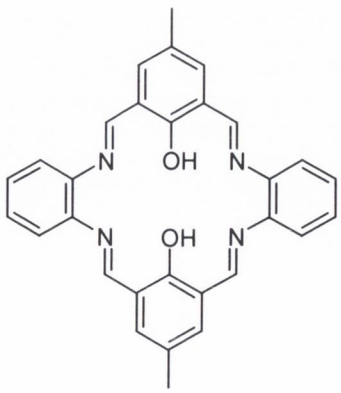

53

The addition of peripheral substituents to the four position of phenol in **53** was also investigated by the Alexander group for tethering to biological substrates[54]. This yielded **54**, which was formed with all the lanthanide ions except La^{3+} and Ce^{3+}. While these substituents did not prevent the formation of the Schiff-base macrocycle they did lower the overall yields[55]. The size of the lanthanide ion was not thought to affect the yield of the synthesis of these complexes because the macrocycle was able to fold accordingly around the lanthanide ion. The Alexander group then went on to study homodinuclear lanthanide ion complexes, which could be used to study lanthanide ion distances[56] *e.g.* **55** and **56**. The presence of the aliphatic lateral units in **55** increases the flexibility and adaptability of the macrocycles towards the lanthanide ions because of the stoichiometry of the complexes formed.

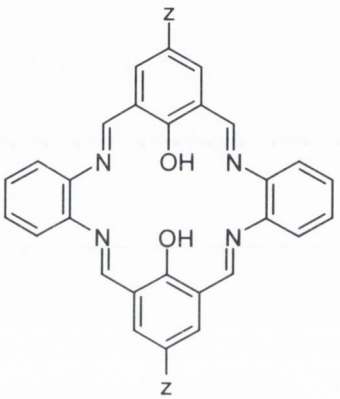

Z = Cl. Br

54

Furthermore the dinuclear Eu^{3+} complex of **55** showed ligand sensitised Eu^{3+} emission upon irradiation of the phenolate moiety. In related work, Vigato and co-workers studied the asymmetric compartmental 1+1 Schiff base macrocyles **57** to **61**[57,58]. These homonuclear compounds were synthesised in good yield and were found to be very stable to metal dissociation. Heterodinuclear complexes of **59** with barium and lanthanum salts have been synthesised and are currently being studied for their magnetic properties.

Fenton and co-workers developed novel 1+1 complexes using 2,6-dicarbonylpyridine with 1,5-bis(2aminophenoxy)-3-oxapentane or 1,2-bis(2-aminophenoxy)ethane to yield **62** and **63**, respectively, which are mixed nitrogen and oxygen macrocycles[59,60]. The effect of changing the aliphatic bridge length and the counter ion (ClO_4 and NO_3) on the chemical selectivity and complex syntheses was investigated[59]. For **62** the yields were low, *ca.* 23%, and complexes formed with the nitrates of La^{3+}, Ce^{3+}, Pr^{3+}, Sm^{3+}, Eu^{3+}, Gd^{3+}, Tb^{3+} and Dy^{3+}

and with the perchlorates of La^{3+} and Ce^{3+}. The complexes of **63b** were formed with the perchlorate salts of La^{3+}, Ce^{3+}, Pr^{3+}, Nd^{3+}, Gd^{3+}, Ho^{3+} and Er^{3+}.

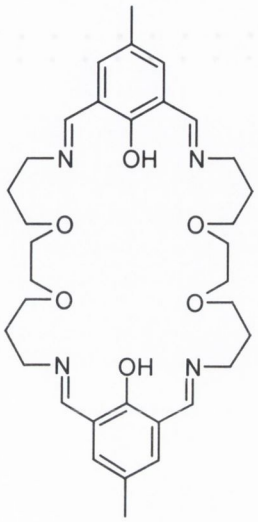

55

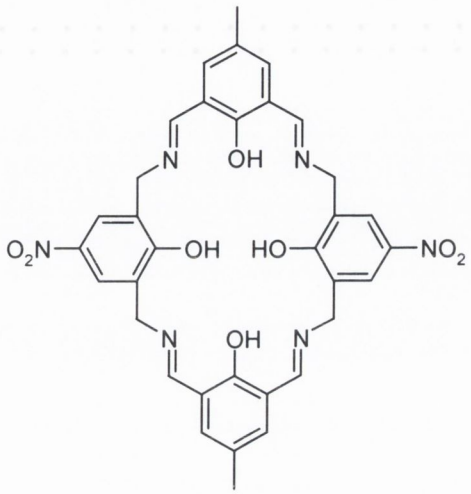

56

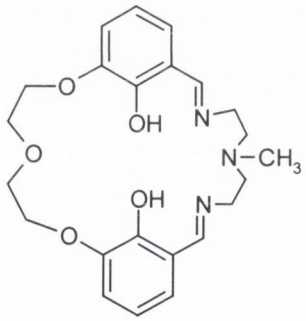

57

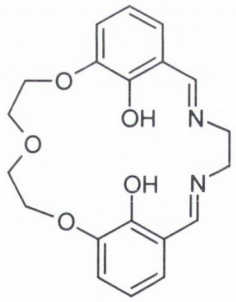

58

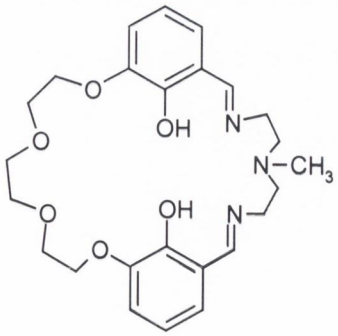

59

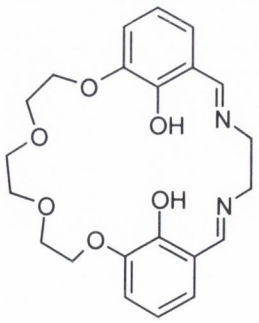

60

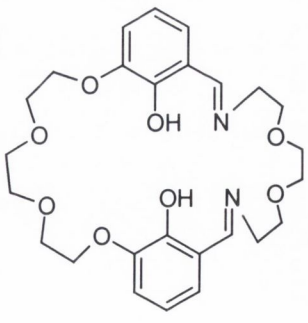

61

These complexes have decreased stability compared to **62** because of the lower length of bridged aliphatic units increasing ring strain. For **63a** the yield of complexation was between 30-70% of the perchlorate salts of Ce^{3+}, Pr^{3+}, Nd^{3+}, Gd^{3+}, Tb^{3+}, Ho^{3+} and Er^{3+}. The complexes showed a range of complexed water molecules from three for the Pr^{3+} complex to fourteen for the Ho^{3+} complex. The Fenton group went on to prepare the metal-free reduced macrocycles **64** and **65** *via* the reduction of **62** and **63** to compare the effect of these modifications on ligand flexibility and coordinating ability with lanthanides[61].

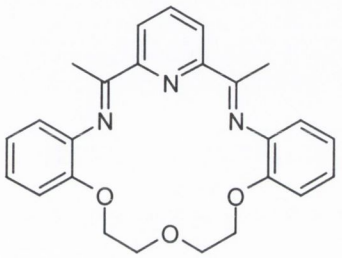

62

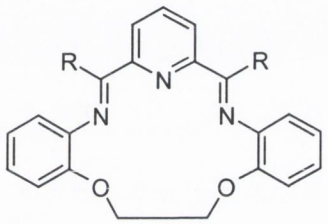

63

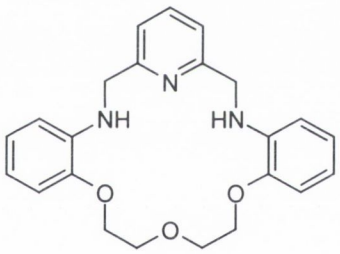

64

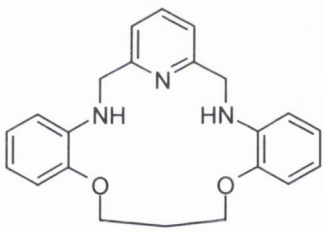

65

The introduction of aromatic units to replace the aliphatic units led to mixed nitrogen and oxygen macrocyclic ligands. Fenton and co-workers prepared **66** from **67,** which had been made using template synthesis by reduction of **66** using $NaBH_4$ in MeOH[62]. **66** was synthesised in good yield with the perchlorate salts of La^{3+} to Er^{3+} with the formula [Ln.**66**][ClO_4]$_3$.xH_2O (where x equals the number of bound water molecules) and the less soluble complexes of the nitrate salts of La^{3+} to Lu^{3+} with the formula [Ln.**66**][NO_3]$_3$. In general the yields decrease with decreasing ionic radii of the lanthanide ions. In continuation of these studies, the Fenton group prepared novel 26-membered N_3O_5-donor macrocyclic ligands **68** which was reduced using $NaBH_4$ to give **69**[63]. **68** was formed with the lanthanide nitrate salts of La^{3+} to Lu^{3+} except Pm^{3+} and Dy^{3+} with the formula [Ln.**63**][NO_3]$_3$.xH_2O.yEt_2O (where x equals the number of bound water molecules and y equals the number of bound diethyl ether molecules).

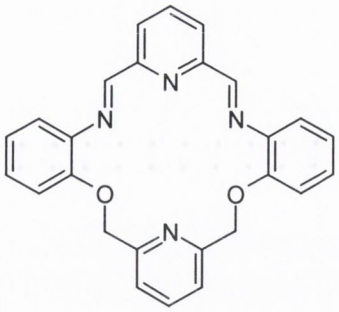

66

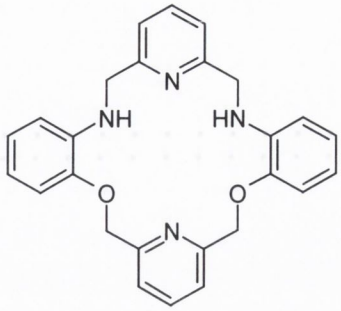

67

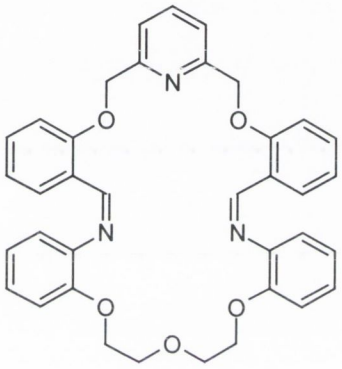

68

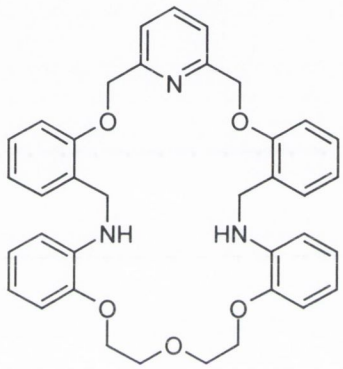

69

The complex was also formed with the perchlorate salts of La^{3+}, Ce^{3+}, Pr^{3+}, Nd^{3+}, Sm^{3+}, Tb^{3+}, Dy^{3+}, Ho^{3+} and Er^{3+} in varying yields. For the preparation of **69** only complexes with La^{3+} and Lu^{3+} nitrate salts and La^{3+}, Ce^{3+} and Pr^{3+} perchlorate salts were synthesised. The aromatic pyridine groups were replaced by aliphatic units to yield **70,** which were characterised as complexes of the form [Ln.**70**][NO_3]$_3$.xH2O) with lanthanide ions La^{3+} to Yb^{3+} except Dy^{3+} and [Ln.**70**][ClO_4].xH_2O with lanthanide ions[64] La^{3+}, Ce^{3+}, Pr^{3+}, Sm^{3+}, Gd^{3+} and Er^{3+}. The macrocyclic ligand **71** was synthesised *via* the reduction of **70** to increase the flexibility towards lanthanide ions. When the heavier lanthanide ions (Gd^{3+}, Er^{3+} and Lu^{3+}) were complexed to **71**, it was found that dinuclear complexes were formed but only mononuclear complexes had been formed with **70**. Vallarino and co-workers also took up the search for novel Schiff-base macrocyclic ligands for lanthanide ions. At first they investigated the chiral properties of established ligands[48,50] but then they developed novel ligands such as **72**[65] having functionalised peripheral substituents suitable for tethering to biosubstrates.

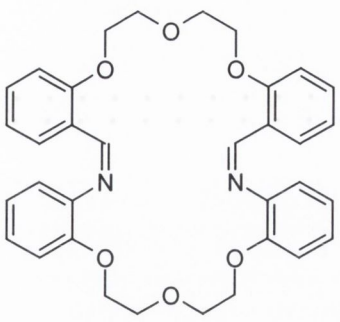

70

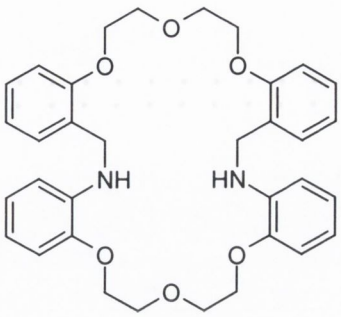

71

This complex can exist as stereoisomers and constitutional isomers depending on the chirality of the carbon bearing the aromatic substituent. La^{3+} acetate salts were used because they gave high yields with better solubility in MeOH. Again, the reaction temperature offered some degree of isomer selectivity. Reactions at the X position were achieved without detrimental effect to the lanthanide ion complex.

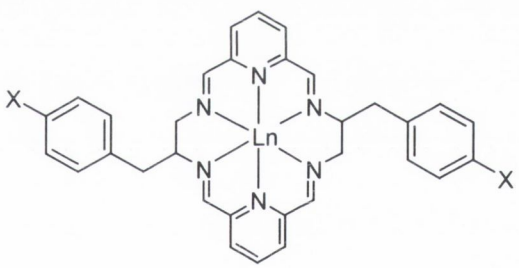

X= H, OH, NH_2

72

The Morrow group prepared a number of Schiff-base molecules for use as potential catalysts for the cleavage of RNA. The Schiff base ligand **48** was complexed to La(III) and Eu(III) were efficient in the hydrolysis of RNA mimics[66]. The hydrolysis of RNA mimics by lanthanide complexes but especially transition metal complexes will be discussed fully in chapter 3.

This section on metal-templated Schiff-base synthesis has served to highlight an efficient and versatile approach to obtaining otherwise unobtainable lanthanide macrocyclic complexes for use as time-resolved fluoroimmunoassays, lanthanide luminescent devices and catalysts for RNA cleavage.

1.4.6 Lanthanide Luminescent Devices

While the previous sections discussed lanthanide luminescence and some of the lanthanide complexes developed, this section will give a brief example/overview of some of the applications of lanthanide luminescence for future use as luminescent devices for biological and industrial use.

The Parker group has extensively studied lanthanide luminescence using complexes based on cyclen [1,4,7,10-tetraazacyclododecane] with sensitising derivatives at the N-position such as in **73, 74**[67] and **75**[68] shown below. These compounds were reasonable sensitisers for lanthanide ions under physiological conditions *i.e.* in water at pH7.4 and in the presence of high ionic strengths.

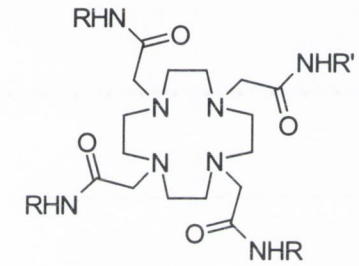

73 R = Me, R' =

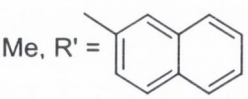

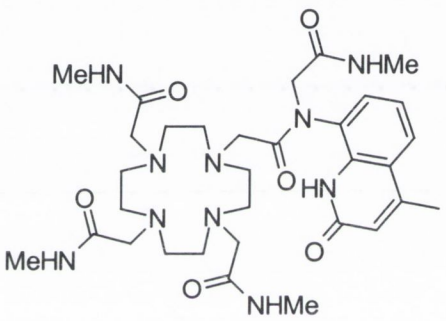

75

74 R =R'

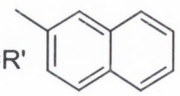

The Parker group has further developed these molecules into luminescent sensors for physiological important species. Luminescent chemosensors offer an attractive method for the detection of various physiological ions and molecules. Delayed lanthanide luminescence (discussed in section 1.4.1) affords an attractive means of overcoming autofluorescence and light scattering effects from the biological media. With this in mind **76** was complexed to Eu^{3+} and Tb^{3+} and investigated as pH sensors[69,70]. At neutral pH the absorption spectrum of the phenanthroline ligand shows four distinct bands in water, which changes significantly at pH 1.5 revealing only two distinct bands with a notable increase in intensity. When excited at *ca.* 375nm, pH dependence was observed in the lanthanide ion emission. At pH 6.8 a weak emission for the Eu^{3+} complex of **76** was observed, which was greatly enhanced on addition of H^+ with a corresponding luminescence enhancement factor of 500. pKa studies of this

complex show a pKa of around 4 corresponding to the protonation of the nitrogen moiety on the phenanthroline unit. The addition of a methyl group at the N position of the phenanthroline unit (quaternisation) **77** changes the selectivity of the sensor to OH^- with a maximum at pH 10.6 for the Eu^{3+} complex and pH 11.2 for the Tb^{3+} complex. The detection of chloride in the body is important because it is essential for maintaining a proper water distribution and in regulating both the normal anion/cation balance and the osmotic pressure. The fluorescence of the Eu^{3+} complex of **78** was selectively quenched in the presence of chloride ions but less so in the Tb^{3+} complex[69,70]. The emission intensity of the Tb^{3+} complex of **77** and **79** was measured as a function of O_2 concentration. The Tb^{3+} emission lifetimes were used to characterise the pO_2 dependence independent of pH and insensitive to the presence of anions.

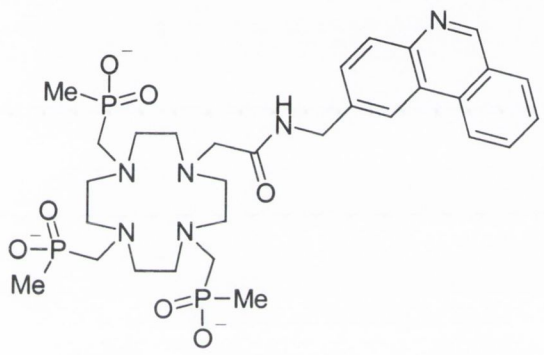

76

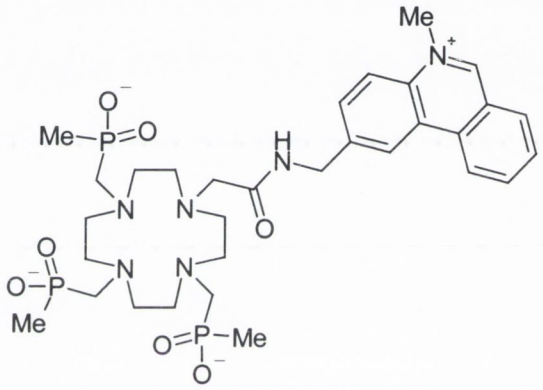

77

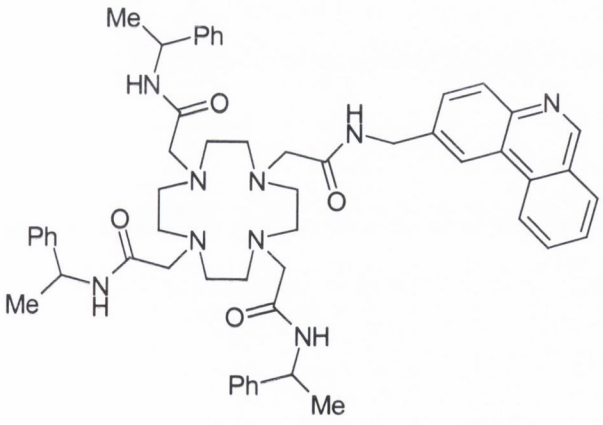

78

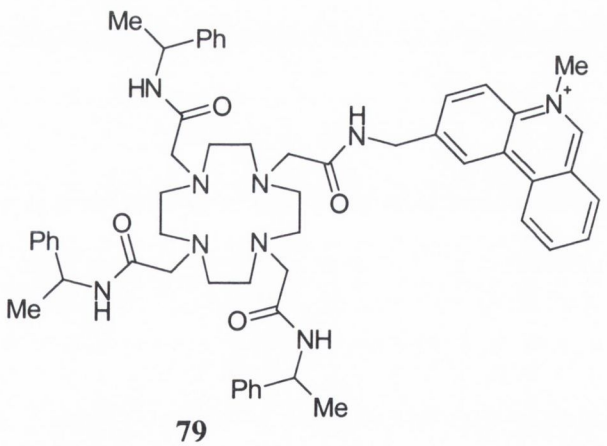

79

Gunnlaugsson and co-workers have developed several types of lanthanide luminescent sensors such as **80** and **81** for H^+ based on cyclen derivatives[71,72,73]. The absorption spectra in water of **80** and **81** showed a pH dependant bathochromic shift, with the formation of a new band at 261nm on addition of H^+. The fluorescence emission spectra increased in intensity in alkaline solution. The largest and most significant pH dependence was observed in the

delayed Eu^{3+} emission between pH 3-7. The luminescent enhancement for **81** was at least 250 with a lesser value of 30 for **80**. Gunnlaugsson[74] developed a novel Eu^{3+} luminescent chemosensor based on cyclen derivatives **82** for determining pH in highly acidic environments. The emission spectra of **82** showed increase in intensity from pH 6 to 1.5 upon addition of acid. It was noticed that **82** displayed dual luminescence behaviour; the fluorescence emission of the ligand is "*switched on*" between pH 3.3 and 5.5; whereas the Eu^{3+} emission is "*switched on*" between pH 1.8 and 3.5.

Bencini and co-workers[75] have also developed a novel pH dependant lanthanide luminescent complex **83** using a bipy-type cryptate. The insertion of the flexible polyamine group allows increased kinetic stability to the lanthanide ion. At neutral pH, the Eu^{3+} complex of **83** displayed a maximum of luminescence, which decreased in the presence of H^+.

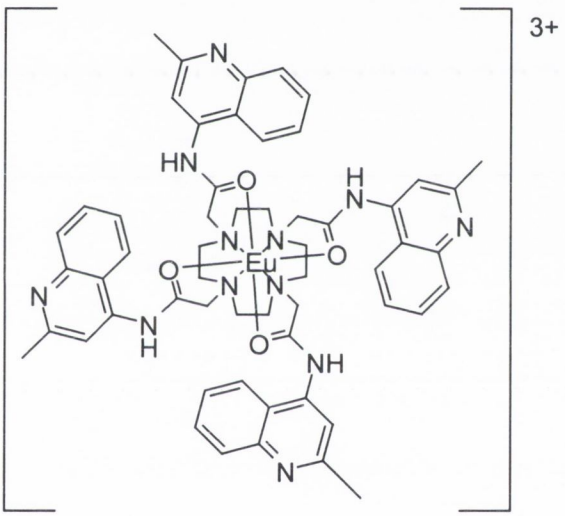

80

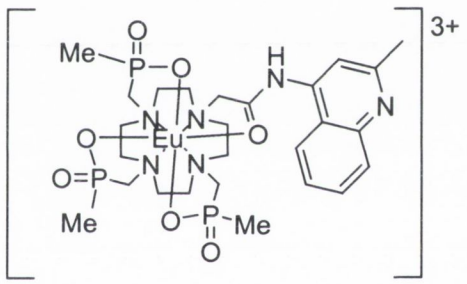

81

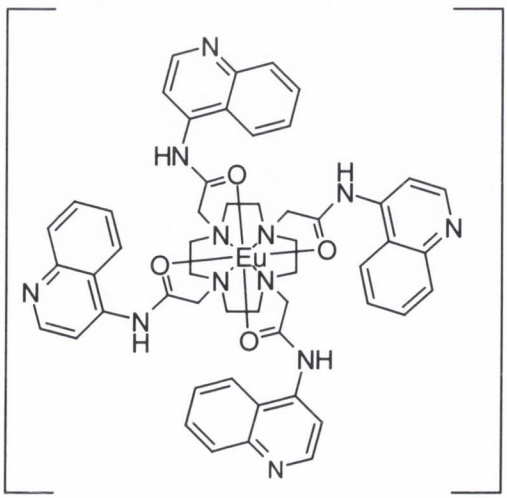

82

The Faulkner group used the Lehn cryptand **12** to show that Yb(III) and Nd(III) were also luminescent in the near-IR region of the electromagnetic spectrum[76,77]. The long lifetime of the Nd(III) complex due to the C-H oscillators suggest the possibility for the synthesis of effective luminescent Nd(III) complexes could be achieved ensuring C-H oscillators are removed form the ligand environment.

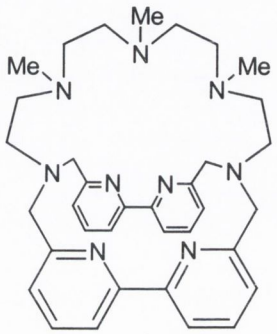

83

The detection of Zn^{2+}, using delayed lanthanide luminescence, was achieved by Parker and co-workers *via* the addition of a known Zn^{2+} receptor site to cyclen derivatives **84** and **85**[78,79]. The addition of $ZnCl_2$ was monitored *via* changes in the absorbance, fluorescence and lanthanide emission at pH 7.4. The Tb^{3+} complex of **84** was found to be the most promising Zn^{2+} selective sensor. The absorbance spectrum of the Tb^{3+} complex of **84** showed a small blue-shift, in the fluorescence spectrum a small shift was seen from 440 to 430nm on metal binding with a corresponding reduction in intensity. A band at 365nm increased in intensity. No significant changes were seen with Ca^{2+} and Mg^{2+}. These changes were observed even in a simulated extracellular environment in the presence of $MgCl_2$, $CaCl_2$, NaCl, and KCL. While the Tb^{3+} complex of **84** was selective and sensitive for Zn^{2+} over other physiologically important ions, practicable analysis is not easy because the system needs longer wavelength excitation ($\gtrsim$350 nm).

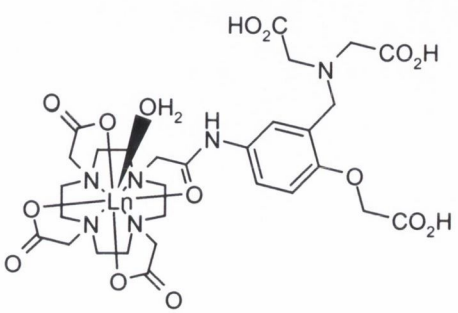

84

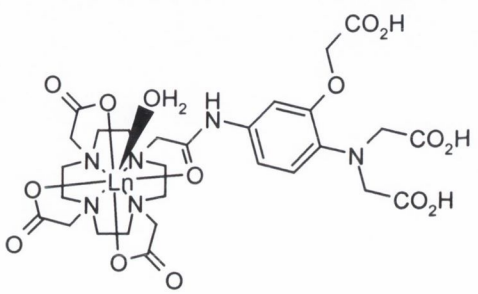

85

Ln = Eu. Tb

1.5 Conclusion

This introductory chapter has given an overview of the development and current status of supramolecular chemistry of the lanthanide ions particularly the use of lanthanide luminescence. Supramolecular chemistry is a relatively young discipline and, as such, is a highly diverse and dynamic field. This chapter has highlighted the many varieties of supramolecular complexes available and their industrial and biological applications. The lanthanide complexes have many desirable features for medical and industrial applications including: time-resolved fluoroimmunoassays, catalysts for RNA cleavage, sensors, as probes for determining biomolecular structure and contrast agents for MRI. The development of luminescent devices for the sensing of physiologically important ions was reviewed in section 1.4.6. A number of lanthanide complexes have been developed as "antenna" groups for efficient energy transfer to the lanthanide ion and these are discussed. A simple and versatile approach to synthesising normally inaccessible macrocyclic ligands using lanthanide metal templated Schiff base synthesis was discussed.

The main focus of this thesis will be the synthesis of novel lanthanide complexes using macrocyclic synthesis and lanthanide metal-templated Schiff base synthesis. Their photophysical properties will be evaluated and discussed. A precursor to these lanthanide complexes was complexed to transition metals. The photophysical properties were evaluated as well as the ability to catalyse RNA cleavage. Novel peptide based acyclic and cyclic ligands were synthesised. The acyclic Ligands were complexed to platinum and their therapeutic value was studied. A novel photoinduced electron transfer (PET) sensor for lithium was designed. The sensors ability to be selective and specific for lithium at the therapeutic range (0.5–1.5 mM) over other physiological important ions was investigated.

Chapter 2

Novel Lanthanide Complexes

2.1 Introduction

In chapter 1, the importance of lanthanide luminescence and the number of antenna ligands available to coordinate to the lanthanide ion was discussed. The design and synthesis of macrocyclic lanthanide complexes is currently attracting considerable attention as a route to supramolecular devices, sensors and efficient RNA cleavage catalysts. This chapter will discuss the synthesis of a three-membered pyridine ring, **86**, for lanthanide ion coordination. The synthesis of this molecule has been previously reported by Miyahara *et al*[82]. Until now, no further work on **86** has been reported. This chapter will discuss the synthesis of **86** and the obstacles encountered on the way. Due to the difficulties encountered in the synthesis of **86**, novel Schiff-base complexes **100** and **101** were prepared using a number of lanthanide ions as templates. Due to solubility problems, these complexes could not be fully characterised but lanthanide luminescence measurements on the Eu(III) and Tb(III) salts showed some luminescent intensity suggesting the Schiff-base ligand was transferring energy to the lanthanide ion.

As discussed in chapter 1, for indirect excitation of the lanthanide ion to occur it is necessary for the ligand to possess light absorbing moieties which can pass this energy to the lanthanide ion as shown in Figure 1.5. The efficiency of this luminescence is affected by the intensity of the ligand absorption of the ligand and efficiency of the ligand to metal energy transfer *i.e.* the distance between the ligand and the metal. It was therefore felt that the presence of the pyridine groups would be sufficient to transfer energy from the ligand to the lanthanide ion. These pyridine-based macrocyclic compounds were chosen for lanthanide ion complexation because it was felt that the presence of the lone pair of electrons on the pyridine nitrogens would increase the number of binding sites on the molecule for lanthanide ion complexation to lanthanide ion. The further functionalisation of these complexes would also increase the number of binding sites available to the lanthanide ion at the amine position. The four-pyridine Schiff-base complexes were synthesised from two intermediates in the synthesis of **86**. Lehn *et al* has previously discussed the synthesis of the free amine **102**, which was synthesised by conventional synthetic methods. No further development of this ligand has been reported in the literature. Schiff-base synthesis provides an efficient and versatile approach to obtaining otherwise unobtainable lanthanide macrocyclic complexes for use as time-resolved fluoroimmunoassays, lanthanide luminescent devices and catalysts for RNA cleavage.

2.2 Design, Synthesis and Characterisation of 2,11,20-Triaza[3.3.3](2,6)Pyridinophane

2,11,20-Triaza[3.3.3](2,6)pyridinophane **86** has previously been synthesised in 2% yield in a one-pot synthesis by Kaptein *et al*[80] and in a number of steps in 67% yield on gram scale by Miyahara *et al*[81,82]. In so far as it has been determined by extensive literature searches, neither groups have gone on to develop **86** in any way. Upon discovering the molecule **86** in the literature with a multistep synthesis on gram scale[82], it was decided to utilise **86** as a ligand for lanthanide ions and to determine the corresponding lanthanide complex's luminescent properties. **86** contains three pyridine rings and three amino moieties. The lone pairs of electrons on the nitrogen atoms provide six coordination positions with a further three positions available if functionalisation was to occur at the amine positions to produce, for example, **86 b** → **e**. This provides the potential for at least nine coordination sites. The high number of coordination sites makes functionalisation of **86** ideal for complexing to lanthanide ions which prefer at least eight coordination sites as discussed in chapter 1.

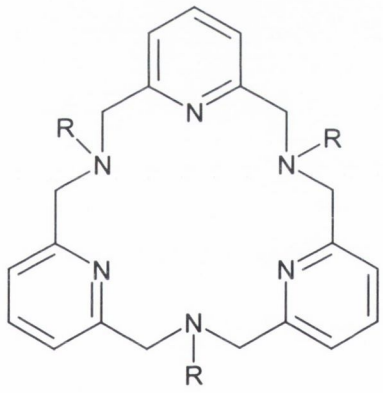

86

a: H

b:

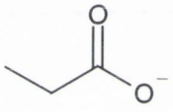

c:

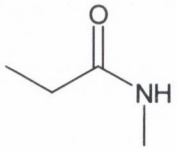

d:

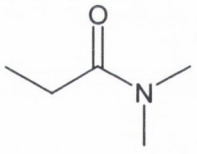

e:

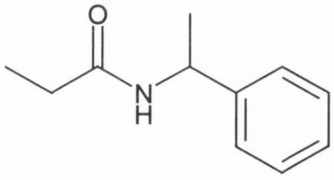

The pyridine groups are chromophores, which absorb energy and transfer it to the lanthanide ion for luminescence to take place. The functionalisation at the amine positions suggest that moieties could be added to the macrocycle for tethering to biological substrates so the luminescent ability of the lanthanide complex could be utilised, for example as sensors or switches.

2.2.1 Synthesis of 2,11,20-Triaza[3.3.3](2,6)Pyridinophane

The paper by Miyahara *et al* suggested that **86** could be easily synthesised in a number steps in good yield[82]. This was attempted. The first step was to prepare 2,6-methyl pyridine dicarboxylate **87** from 2,6-pyridine dicarboxylic acid **88** as shown in Scheme 2.1[83].

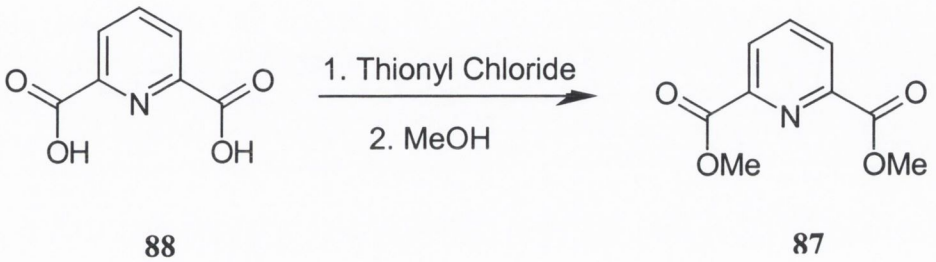

88 **87**

Scheme 2.1: Synthesis of 2,6-methyl pyridine dicarboxylate 87 from 2,6-pyridine dicarboxylic acid 88

This was prepared from the refluxing of **88** in thionyl chloride to yield the corresponding bis-acid chloride, which was not isolated. By refluxing the acid chloride in methanol, **87** was isolated by filtration to produce white crystals in 87% yield. The ^{1}H NMR spectra showed a singlet at 4.05 ppm representing the methyl ester groups, a triplet at 8.06 ppm representing the hydrogen in the *para* position to nitrogen in the pyridine ring and a doublet at 8.34 ppm representing the hydrogen in the *meta* position to the nitrogen of the pyridine ring. The synthesis was easily scaled up to 50 g scale. The second step in the synthesis of **86** involved the reduction of the ester **87** using $NaBH_4$ in ethanol to yield 2,6-bis(hydroxymethyl)pyridine **89** in 65% yield as shown in Scheme 2.2[83]. This reaction proceeded well with the use of continuous extraction to isolate **89** from aqueous solution. The ^{1}H NMR spectra showed a singlet peak at 4.80 ppm representing the CH_2 group adjacent to the hydroxy group, a doublet at 7.23 ppm representing the hydrogens *meta* to the nitrogen of pyridine and a triplet at 7.74 ppm representing the hydrogen *para* to the nitrogen of pyridine.

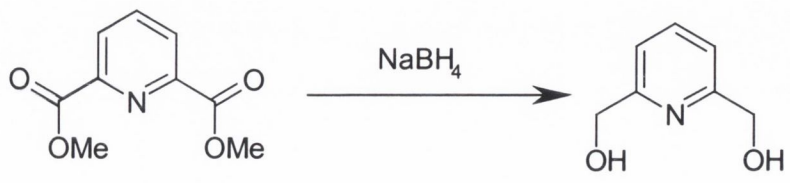

87 **89**

Scheme 2.2: Synthesis of 2,6-bis(hydroxymethyl)pyridine 89 from the reaction of 2,6-pyridine dicarboxylic acid 88 with $NaBH_4$ in ethanol

89 was then used to synthesise 2,6-bis(bromomethyl)pyridine **90** and 2-hydroxymethyl-6-bromomethylpyridine **91**. The first method was to synthesise **90** from 2,6-lutidene **92** and N-bromosuccinimide in benzene according to Rabjohn *et al,* as shown in Scheme 2.3[84]. Unfortunately this gave a number of products as shown by ^{1}H NMR with **90** being present in about 5% yield. **90** could only have been isolated with numerous chromatography procedures and this was not attempted.

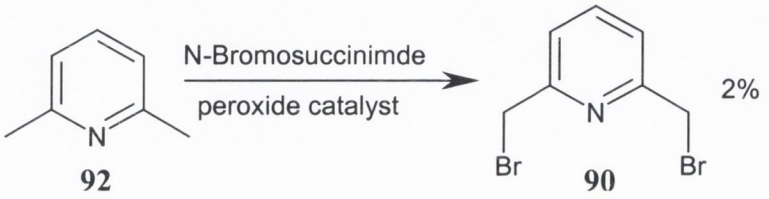

Scheme 2.3: Synthesis of 2,6-bis(bromomethyl)pyridine 90 from the reaction of 2,6-lutidiene with *N*-bromosuccinimide

Instead **90** and **91** were synthesised by refluxing **89** in 48% hydrobromic acid with subsequent neutralisation with 40% NaOH(aq) as shown in Scheme 2.4 giving a pink precipitate upon cooling to 0°C[83]. The precipitate was shown by ^{1}H NMR to contain both **90** and **91** and the bis bromo product **90** was isolated by flash silica chromatography using 100% DCM eluent in 27% yield. The ^{1}H NMR spectra of **90** showed a singlet at 4.56 ppm representing the CH_2 group adjacent to bromine group, a doublet at 7.06 ppm representing the hydrogen *meta* to the nitrogen of pyridine and a triplet at 7.75 ppm representing the hydrogen *para* to the nitrogen of the pyridine group. When the column was then eluted with DCM and 2% methanol, **91** was recovered in 41% yield. The ^{1}H NMR spectra of **91** showed two singlets at 4.59 and 4.79 ppm representing the CH_2 groups adjacent to the hydroxy and bromine groups respectively, two doublets at 7.22 and 7.40 ppm representing both hydrogens in the *meta* position to the nitrogen of pyridine and a triplet at 7.75 ppm representing the hydrogen *para* to the nitrogen of pyridine. Attempts to increase the yield of one product over the other were achieved by reducing the amount of HBr to give an increase in the yield of **91** and *vice versa* to give **90**. This was the best method to isolate **91** in good yield. However the yield of **90** was increased by using phosphorus tribromide (PBr_3) instead of hydrobromic acid as the brominating agent resulting in a yield of 87% as shown in Scheme 2.4[82]. This was achieved by stirring **89** in DCM at 0°C to which an excess of PBr_3 in DCM was added dropwise. The resulting mixture was left to stir at room temperature overnight, followed by neutralisation with 40% NaOH. By carefully monitoring the addition of PBr_3, a crude precipitate containing both **90** and **91** could also be formed and isolated by the same chromatography method as described above with

similar yields as the 48% HBr method. The two products, **90** and **91**, were further reacted to make more intermediates in the synthesis of **86**.

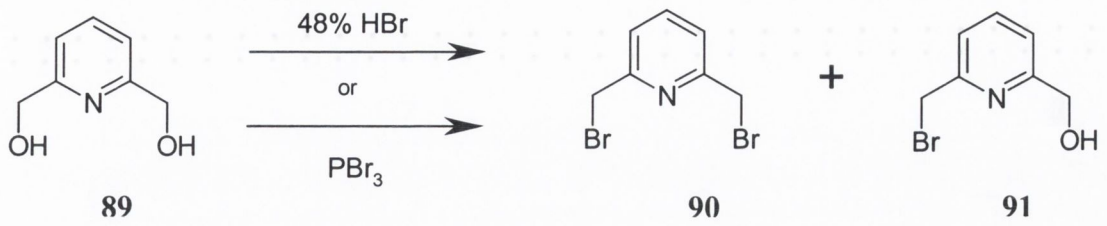

89 **90** **91**

Scheme 2.4: The synthesis of 90 and 91 from 2,6-bis(hydroxymethyl)pyridine using either 48% HBr or PBr_3

90 was refluxed with potassium phthalimide and K_2CO_3 to produce 2,6-bis(phthalimdemethyl)pyridine **93** in the Gabriel synthesis as shown in Scheme 2.5 in 78% yield. The reaction proceeded well with side products present. To increase the yield of the reaction KI was added in a 10% catalytic amount to replace the bromine atom with iodine, which is a better leaving group than bromine. The ^{1}H NMR spectra showed a singlet at 4.93 ppm representing the CH_2 groups adjacent to the pyridine group, a doublet at 7.15 ppm and a triplet at 7.61 ppm both representing the hydrogens *para* and *meta* to the nitrogen of pyridine respectively and a multiplet at 7.78 ppm representing the aromatic peaks of the phthalimide moiety.

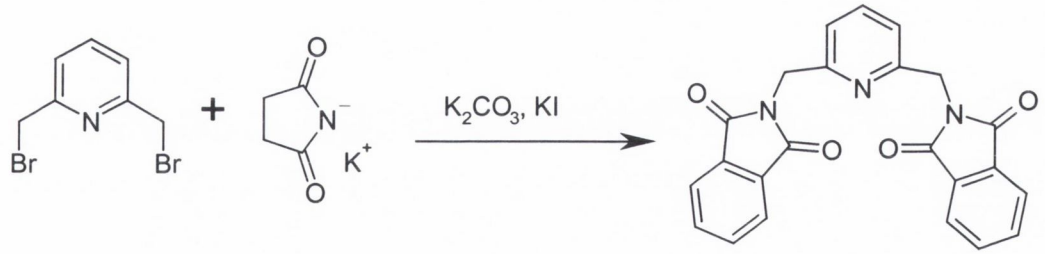

90 **Potassium Phthalimide** **93**

Scheme 2.5: The synthesis of 2,6-bis(phthalimidemethyl)pyridine from 2,6-bis(bromomethyl)pyridine and potassium phthalimide

The addition of hydrazine monohydrate in refluxing ethanol removed the phthalimide group yielding 2,6-bis(aminomethyl)pyridine dichloride **94** in 92% yield, Scheme 2.6. It was found that a hot filtration was required to gain the maximum yield of **94**. The ^{1}H NMR spectra of **94** displayed a singlet at 4.37 ppm representing the CH_2 group adjacent to the amino group, a

doublet 7.43 ppm and a triplet at 7.91 ppm representing the hydrogens on pyridine *meta* and *para* to the nitrogen respectively. Attempts were made to isolate the free amine of **94**. Firstly **94** was dissolved in water and brought to pH 14. This was then extracted with either chloroform, toluene or ethyl acetate all realising the free amine of **94** as a clear oil in low yield (*ca* 12%). A search of the literature found a method by Vöglte *et al* that describes the synthesis of the free amine of **94** in good yield[85]. Instead of isolating **94** by reducing the solvent under vacuum, the solvent was brought to pH 14 and continuously extracted with benzene. This was attempted but the free amine of **94** was once again only obtained as a colourless oil in 5 % yield. Another attempt was pursued using an ion exchange column to remove the HCl group[80]. This gave the free amine of **94** but only in 10% yield as a colourless oil. Because of these difficulties it was decided to use **94** as its HCl salt instead of the free amine in the next stage of the synthesis.

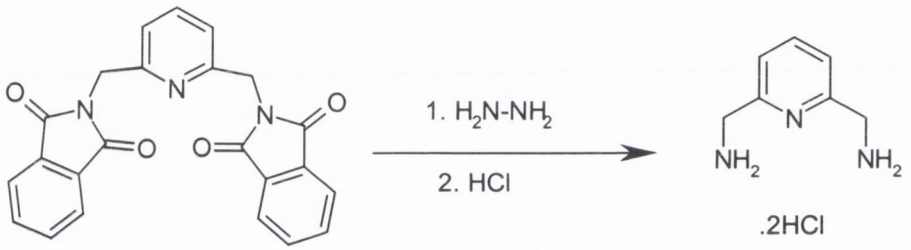

93 **94**

Scheme 2.6: Synthesis of 2,6-bis(aminomethyl)pyridine 94 from its corresponding bis-phthalimide 93

The next sequence in the synthesis was the addition of a *p*-toluenesulphonyl group (tosyl) to the amine moiety of **94**, which acts as a protecting group whilst also activating the nitrogen for a nucleophilic attack[86], to produce 2,6-bis[(amino-*p*-tosyl)methyl]pyridine **95**[82]. Miyahara *et al* suggested that the tosyl group could be added by reacting **94** in dioxane with *p*-toluene sulphonyl chloride in the presence of KOH in water as shown in Scheme 2.7. A mixture of **94** and *p*-tosyl chloride in dioxane was stirred for two hours, KOH in water was added dropwise and the reaction was allowed stir overnight. This gave colourless crystals after an aqueous work-up. When analysed by ^{1}H NMR and ES-MS it was found that these crystal were only the starting material *p*-toluenesulphonyl chloride. Analysis of the aqueous layer showed only the presence of **94**.

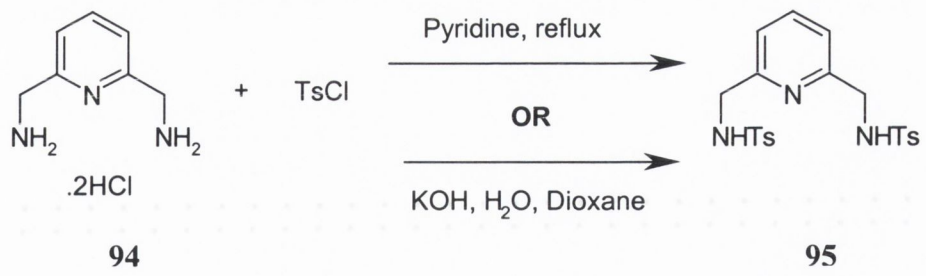

Scheme 2.7: Attempted synthesis of 2,6-bis[(amino-*p*-tosyl)methyl]pyridine 95 from the reaction of 2,6-bis(aminomethyl)pyridine 94 with *p*-toluenesulphonylchloride

Further examination of the reaction conditions described by Miyahara *et al* was conducted and found that one molar equivalent of base was not adequate to sufficiently deprotonate the amine to induce its nucleophilicity. The above reaction was then repeated using six equivalents of base. Furthermore, the reaction was also repeated under reflux. Whereas no reaction was shown to have taken place at room temperature, continuous monitoring showed the formation of a new product with a corresponding decrease in the presence of *p*-tosyl chloride. When the mixture was heated, the reaction required four days to reflux to completion. Unfortunately ^{1}H NMR spectra and ES-MS analysis showed the presence of numerous other products as well as the presence the starting materials. Attempts were made to triturate **95** from the obtained oily residue using EtOH or a chloroform:petroleum ether mixture, which is known to crystallise *p*-tosyl chloride from solution[86], but these attempts proved to be unsuccessful. From these results it became apparent that an alternative method for the formation of **95** was required. A search of the literature found a number of papers by Lehn *et al* describing the synthesis of the analogous four pyridine-membered macrocycles where **95** played a part as an intermediate[87]. Unfortunately none of these papers described the synthesis of **95** and instead referred back to a Ph.D. dissertation, which was not obtainable. Another approach was to react **90** with *p*-toluenesulphonyl amide using Na_2CO_3 as reported in a similar reaction by Che *et al*[88]. *p*-Tosyl amide and 10% Na_2CO_3 aqueous solution were refluxed overnight in toluene to which **90** was added dropwise over one hour. This gave a precipitate upon cooling that was collected by filtration. ^{1}H NMR analysis showed the precipitate was only *p*-tosyl amide. The filtrate was then concentrated giving pale pink crystals. ^{1}H NMR analysis showed these crystals were the starting material **90**. Adapting this procedure Na_2CO_3 was replaced with K_2CO_3 and KI and the reaction carried out in refluxing acetone. Again analysis of the precipitate and filtrate showed that **95** had not been formed.

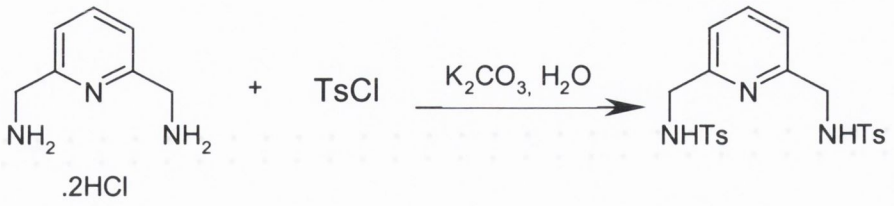

94 **95**

Scheme 2.8: Synthesis of 2,6-bis[(amino-*p*-tosyl)methyl]pyridine 95 from the reaction of 2,6-bis(aminomethyl)pyridine.2HCl 94 and *p*-tosyl chloride

Another approach was to reflux **94** and *p*-tosyl chloride in pyridine as shown in Scheme 2.7. The reaction was quenched by pouring the resulting mixture over ice. The resulting precipitate was collected by filtration but once again the precipitate contained a mixture of the two starting materials, **94** and *p*-tosyl amide. In the synthesis of cyclen type compounds, for example **3**, the intermediate amines are protected by the addition of a tosyl group as discussed in chapter 5[86]. It was decided to try this method to synthesise **95** as shown in Scheme 2.8. The synthesis involved the reflux of **94** with K_2CO_3 and *p*-tosyl chloride in water. After twelve hours reflux, a black precipitate was seen that was collected by filtration and washed with water, methanol and diethyl ether. The resulting grey precipitate was dried under vacuum. Analysis by ^{1}H NMR and ES-MS showed that **95** was synthesised cleanly in approximately 55% yield. The ^{1}H NMR of **95** showed a singlet at 2.4 ppm representing the CH_3 group of the tosyl moiety, a singlet at 4.20 ppm representing a CH_2 adjacent to the amine moiety and a singlet at 5.80 ppm representing the amide proton and signals representing the aromatic region. Although **95** was only obtained in average yield, it was decided that this was acceptable since reaction could be easily scaled-up.

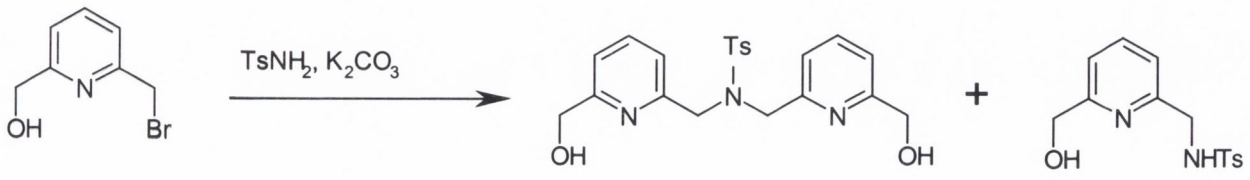

91 **96** **97**

Scheme 2.9: Condensation of 2-bromomethyl-6-hydroxymethylpyridine 91 with *p*-tosylamide resulting in *N,N*-bis[(6-hydroxymethyl)pyridin-2-yl]-*p*-tosylamide 96

The second stage in the synthesis was to make *N,N*-bis[(6-hydroxymethyl)pyridin-2-yl]-*p*-tosylamide **96** from the condensation of **91** and *p*-tosylamide in the presence of K_2CO_3 and acetone as shown in Scheme 2.9. After refluxing for four days the reaction was cooled to room temperature and the precipitate removed by filtration. The filtrate was collected and the solvent was removed leaving a brown oil, which crystallised upon standing overnight. The only side product obtained was **97** which could be isolated by column chromatography. The ^{1}H NMR spectra of **96** showed the presence of a singlet a 2.46 ppm representing the methyl group on the *p*-tosyl moiety and two singlets at 4.57 and 4.60 ppm for the CH_2 groups adjacent to the hydroxy and amine moieties respectively. The aromatic region of the spectrum showed three doublet peaks at 7.24, 7.33 and 7.76 ppm corresponding to the hydrogens on the pyridine moiety and a doublet and triplet at 7.04 and 7.54 ppm respectively corresponding to hydrogens on the benzyl ring in the tosyl moiety. In the original report by Miyahara *et al* the use of 5:1 chloroform:ethyl acetate as an eluent to isolate **96** was described. However, it was found that this was not an ideal eluent. Instead the use of 98:2 DCM:Methanol gave better yield of **96** of 21% for the 5:1 chloroform:ethyl acetate eluent compared to 62% yield for 98:2 DCM:Methanol eluent. Attempts were made by Miyahara to utilise other solvents instead of acetone such as DMF in the reaction but these caused by-products to be formed[81]. With the aim of improving the yield of **96**, the reaction was carried out in MeCN. Unfortunately it was found that the reaction did not proceed at all even after six days at reflux.

With the aim of converting the two methyl alcohols to their corresponding bromides, **96** was reacted with PBr_3 in the presence of DCM for twelve hours to form **98** as shown in Scheme 2.10. The reaction was neutralised with 40% NaOH and the organic layer collected. The solvent was removed leaving pink crystals in 97% yield, which were found by ^{1}H NMR and ES-MS to be **98**. The ^{1}H NMR spectra of **98** showed a singlet at 2.45 ppm representing the CH_3 group of the tosyl moiety and two singlets at 4.37 and 4.59 ppm representing the CH_2 peaks adjacent to the amine and bromine group respectively. The aromatic region of the spectrum showed a multiplet at 7.27 ppm representing the aromatic hydrogens on the pyridine moieties, a triplet at 7.58 ppm and a doublet at 7.75 ppm representing the aromatic hydrogens on the benzyl ring of the tosyl moiety.

The penultimate step in the synthesis of **86** was the formation of the *p*-tosyl-protected macrocycle *N,N',N''*-tri-*p*-tosyl-2,11,20-triaza[3.3.3](2,6)pyridinophane **99** formed by the reaction of **98** with **95** as shown in Scheme 2.11. Miyahara *et al* suggested that **99** could be synthesised using phase transfer conditions where **99** was added dropwise over five hours to a

solution of *n*-butylammonium iodide and **95** stirring vigorously under reflux in DCM and 25 % KOH (aq).

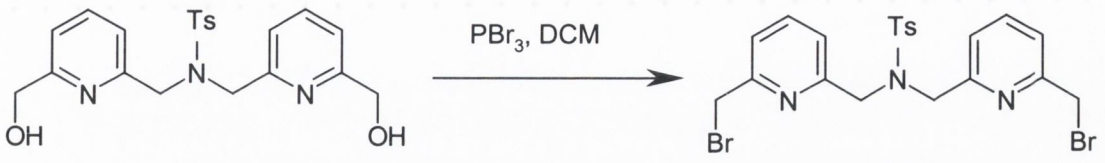

96 **98**

Scheme 2.10: Synthesis of *N,N*-bis[(6-bromomethyl)pyridin-2-yl]-*p*-tosylamide 96 form the bromination of *N,N*-bis[(6-hydroxymethyl)pyridin-2-yl]-*p*-tosylamide 96 in PBr_3

This approach was not followed due to the problems encountered in other synthesis of the intermediates as discussed above. Instead the synthetic method employed was that used by Parker *et al* in the synthesis of the azacrown ethers[86]. **99** was synthesised by adding **98** in MeCN to a stirring solution containing **95**, Cs_2CO_3 and KI in MeCN over twenty minutes. This solution was stirred for two days under inert atmosphere and then refluxed for a further twelve hours. The precipitate formed was removed by filtration and the solvent removed under vacuum. The residue was taken up in chloroform and washed with 10 % K_2CO_3 and the product was obtained in 59% yield after recrystallisation from chloroform:diethyl ether. The ^1H NMR spectra of the highly symmetrical molecule **99** shows a singlet at 2.44 ppm for the methyl group of the tosyl moiety, a singlet at 4.30 ppm representing the CH_2 group, a doublet and multiplet at 7.68 ppm and 7.29 ppm respectively representing the aromatic hydrogens on the tosyl group and a doublet and triplet at 7.14 and 7.44 ppm for the hydrogens on the pyridine moiety.

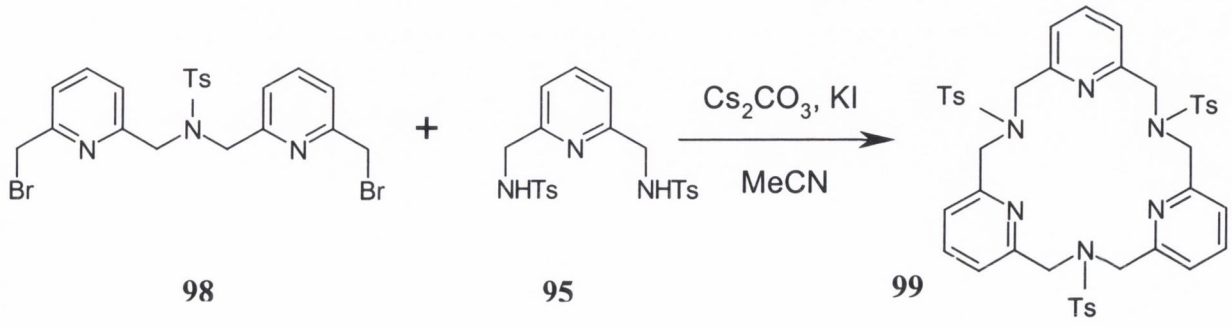

98 **95** **99**

Scheme 2.11: Synthesis of the *p*-tosyl protected macrocycleby reaction of *N,N*-bis[(6-bromomethyl)pyridin-2-yl]-*p*-tosylamide with 2,6-bis[(amino-*p*-tosyl)methyl]pyridine

99 was finally refluxed in concentrated H_2SO_4 to remove the three *p*-tosyl groups in the final step of the synthesis resulting in the 3-pyridine membered macrocycle **86** as seen in Scheme 2.12[82,86]. The reaction was quenched by adding the reaction mixture to ice and the pH brought to 14 using 40% NaOH. **86** was then extracted into diethyl ether. The solvent was removed under reduced pressure resulting in a clear oil, which was found to be pure by ^{1}H NMR and ES-MS analysis in 89% yield. However only 5 mg of **86** was isolated. **86** is a highly symmetrical molecule with only three signals expected to be seen. The ^{1}H NMR is shown in Figure 2.1 and shows three signals, an aromatic doublet at 7.12 ppm, an aromatic triplet at 7.57 ppm, a singlet at 3.97 ppm corresponding to the methylene group and a broad singlet at 2.01 ppm representing the amine moiety. ES-MS shows one peak at 361.4.

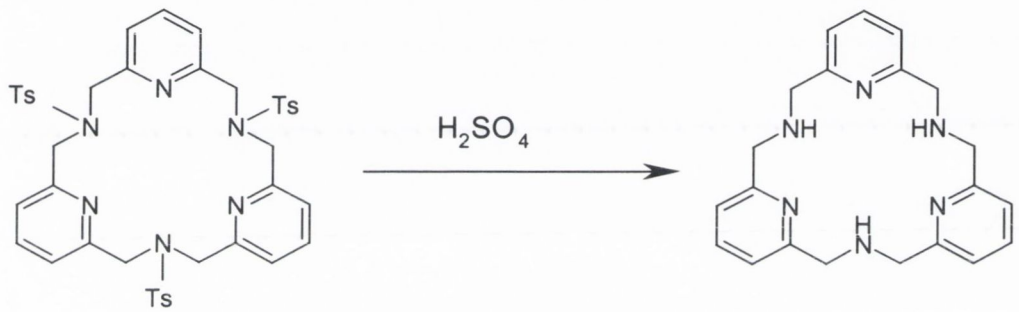

99 **86**

Scheme 2.12: Removal of the *p*-tosyl groups from 99 to yield the free macrocycle 86

When the reaction to form **99** was repeated on a bigger scale it was impossible to isolate the product even by using recrystallisation and chromatography methods. The sample was found to contain **95** and **99**, no matter what isolation method was employed. It was decided to just use this crude material to synthesise **86** using the same conditions above. Unfortunately the ^{1}H NMR showed a mixture of the impurity **95** and the product **86,** which could not be isolated. After all the problems described above in the synthesis of **86** it was exciting to finally isolate **86**. Unfortunately the amount of **86** isolated was insufficient to do any further work such as functionalisation at the amine positions or complexing to lanthanide ions. After all the effort in the synthesis of **86** it was disappointing not to do any further work with the macrocycle **86**.

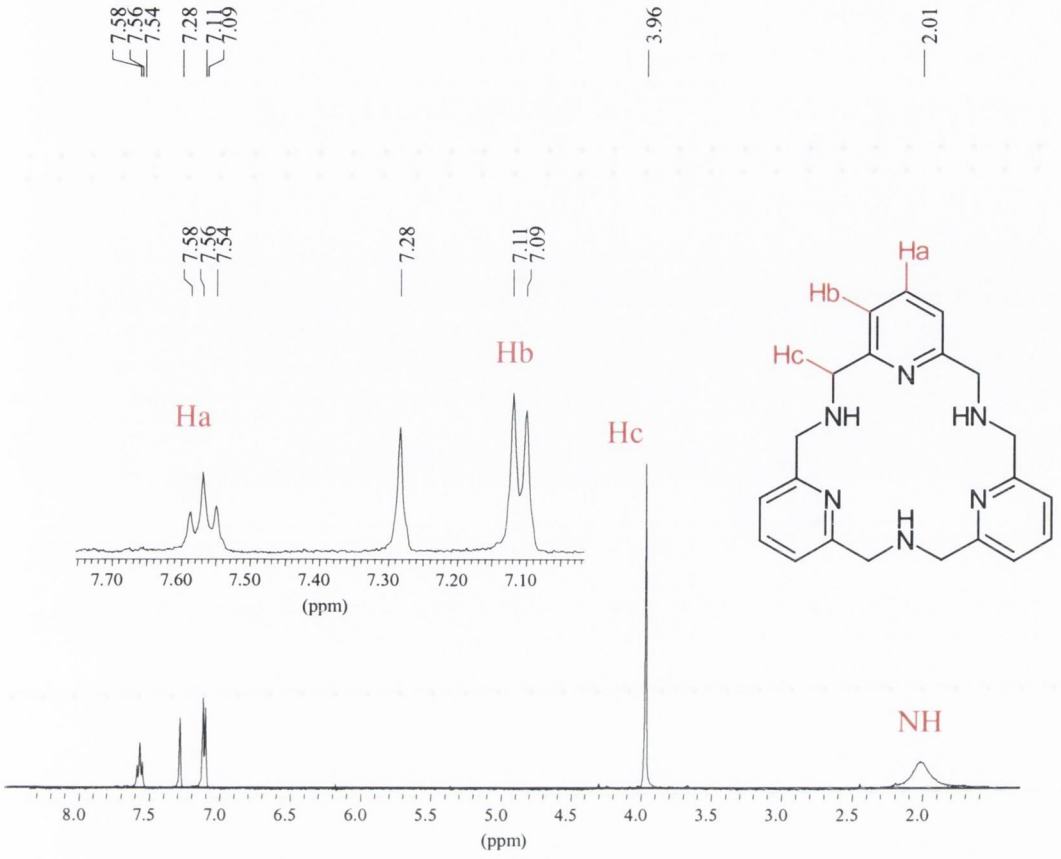

Fig. 2.1: ^{1}H NMR of the macrocycle 86. The symmetrical nature of 86 makes the ^{1}H NMR spectra very simple

2.3: Design, Synthesis and Photophysical Evaluation of Novel Schiff-Base Complexes:

Chapter 1 described in detail the development and history of lanthanide Schiff-base complexes. The lanthanide-templated synthesis of these molecules provides a quick and easy route to the synthesis of otherwise inaccessible macrocyclic ligands. This section will describe the synthesis and attempted characterisation of novel Schiff-base complexes. The lanthanide luminescence studies will also be discussed.

In chapter 1, section 1.4.5 dealt with the development of lanthanide-templated Schiff-base synthesis and highlighted the efficient and versatile approach to obtaining otherwise unobtainable lanthanide macrocyclic complexes for applications as time-resolved fluoroimmunoassays, lanthanide luminescent devices and catalysts for RNA cleavage. A number of lanthanide complexes have been developed as "antenna" groups for efficient energy transfer to the lanthanide ion and Schiff-base synthesis provides a simple approach to

synthesising normally inaccessible macrocyclic ligands using lanthanide templated Schiff-base synthesis.

The ability of the lanthanide ions to promote Schiff-base condensation of appropriate diamine and dicarbonyl precursors, resulting in the formation of lanthanide complexes of otherwise inaccessible macrocyclic ligands, is by now well established and reviewed[89,90,91]. The lanthanide metal-templated cyclic Schiff-base condensation reactions provide a means of easy access to otherwise difficult to acquire complexes with the ability to further functionalise at the amine position. It was hoped that the synthesis of the lanthanide complexed macrocycles **100** and **101** could be achieved and by the reduction of these would lead to the removal of the lanthanide ion resulting in the corresponding free amines, **102** and **103**. These free amines could be further functionalised and complexed to lanthanide ions to create lanthanide luminescent devices.

2.3.1: Synthesis of Novel Schiff-Base Complexes **100**:

Novel Schiff-base complexes were synthesised from 2,6-pyridine dicarbaldehyde **104** and 2,6-bis(aminomethyl)pyridine hydrochloride **94** using a variety of lanthanide ions to yield **100**. A thorough search of the literature has found that these four-membered Schiff-base molecules have never been synthesised although the corresponding free amine **102** has previously been prepared by Lehn *et al* using conventional synthetic methods[87]. It was hoped that these Schiff-base complexes would provide an alternative to the three-pyridine macrocycle **86** discussed above and be effective "antenna" moieties for modulating lanthanide luminescence because of the larger cavity size.

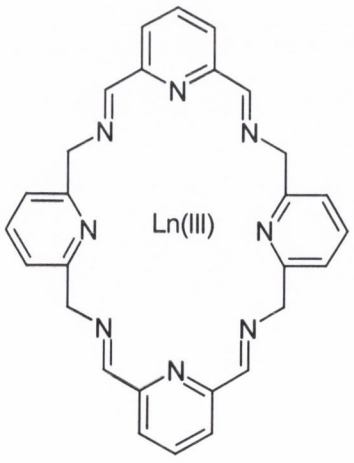

100

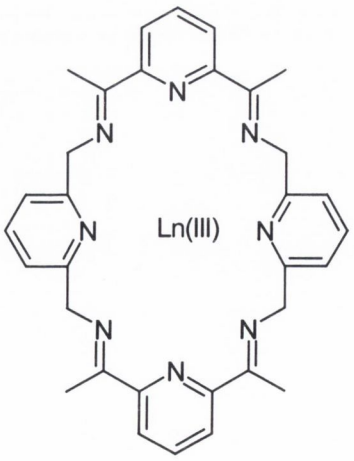

101

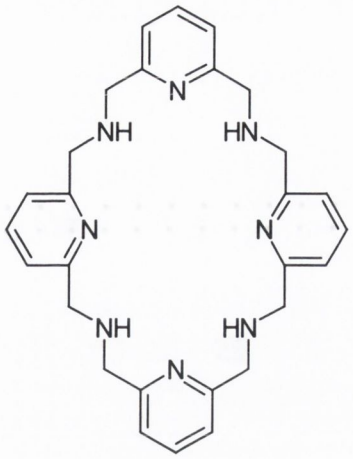

102

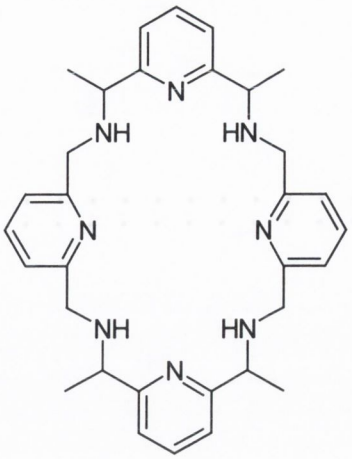

103

As discussed in chapter 1, lanthanide Schiff-base complexes are synthesised by the lanthanide ion acting as a template in the condensation reaction between an aldehyde with an amine. Other ions such as Ba^{2+}, Cu(II) and Ni(II) have been used as template ions but they are not relevant to this thesis[89]. The amine used was 2,6-bis(aminomethyl)pyridine hydrochloride **94**, an intermediate in the synthesis of **86**. For the lanthanide complex **100** the aldehyde used was 2,6-pyridine dicarbaldehyde **104**. This was synthesised by the oxidation of 2,6-bis(hydroxymethyl)pyridine **89** using selenium oxide refluxing in dioxane in 80% yield[92]. The synthesis of **104** was attempted using manganese dioxide as the oxidising agent[93]. Although the reaction conditions were milder than using selenium oxide, the reaction proceeded in only 2% yield. Also approximately 10 equivalents of manganese dioxide were required to drive the reaction, which caused problems when the reaction was done on a large scale.

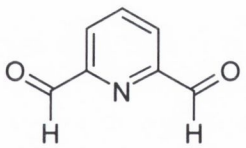

104

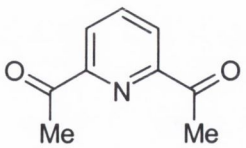

105

Figure 1.6 in chapter one shows the method of synthesis of the Schiff-base complexes. The lanthanide ion acts as a template bringing together the amine and the aldehyde moieties, which react with each other to form the complex. To investigate this synthesis, the first complex made was the Sm(III) complex of **48,** [**48.**$Sm(NO_3)$], which has been previously

been synthesised by the Nelson and Fenton groups[94,95,96]. [**48**.Sm(NO_3)] was synthesised by adding Sm(NO_3)$_3$ to a stirring solution of **104** and diaminoethane in MeOH and refluxing the resulting mixture for four hours under inert atmosphere. The reaction was cooled and the pale yellow precipitate formed was collected by filtration. Previous crystal structure and IR data show that [**48**.Sm(NO_3)] is composed of Sm(**48**)(OH)(NO_3)$_2$.H_2O[94,97]. The Sm(III) ion is complexed to the macrocycle and is coordinated to the four imine nitrogen atoms and two pyridine nitrogens as well as a bidentate nitrate anion, a water molecule and a hydroxide ion[97]. Like these papers suggest, only IR and CHN data could be obtained for [**48**.Sm(NO_3)]. Lack of solubility of the complexes is a major stumbling block to fully characterising the Schiff-base complexes. The IR data for [**48**.Sm(NO_3)] compared favourably to the literature. Fenton and co-workers observed a sharp peak in the IR spectrum at 3220 cm^{-1} for complexes using the lanthanides from Nd(III) to Lu(III) (except Pm(III) and Eu(III)), which they attributed to a secondary amine[98]. The IR spectra of [**48**.Sm(NO_3)] showed a strong peak at 3381 cm^{-1} but nothing was observed at 3220 cm^{-1} as suggested by Fenton *et al.* Importantly a peak was seen at 1659 cm^{-1} corresponding to C=N, furthermore no C=O peak (for the starting material) at 1759 cm^{-1} was observed. Other peaks were seen in the spectrum corresponding to NO_3 (1384 cm^{-1}) and pyridine moieties (1591 cm^{-1}). The ^{1}H NMR spectrum in d_6-DMSO in which [**48**.Sm(NO_3)] was partially soluble, showed two singlet resonances at 2.70 and 3.50 ppm respectively peaks seen in the aromatic region with two singlet peaks at 7.3 and 7.7 ppm with a doublet doublet at 8.31 ppm. This information tells little of the nature of [**48**.Sm(NO_3)] and it is not completely certain what complex was synthesised.

With the information gleaned from the synthesis of [**48**.Sm(NO_3)], **100** was synthesised from **102** and **94** using a variety of lanthanide (III) salts such as nitrates, acetates and triflates. The characterisation results are shown in Table 2.1. The first reaction was carried out by the addition of two equivalents of **94** to a stirring solution of two equivalents of **104** and one equivalent of Sm(NO_3)$_3$ in methanol under inert atmosphere under reflux to produce [**100**.Sm(NO_3)]. The brown precipitate observed was collected by filtration and washed with diethyl ether. Attempts to characterise the Sm(III) complex of **100** [**100**.Sm(NO_3)] proved fruitless as the complex was not soluble in MeOH, MeCN, H_2O, DMF, chloroform, acetone and DMSO. A ^{1}H NMR in DMSO-d_6 was recorded in which [**100**.Sm(NO_3)] was partially soluble but this showed no signals. The filtrate was also reduced down and analysed. The ^{1}H NMR spectra of the filtrate in DMSO-d_6 showed no signals. The IR spectra showed peaks at 1645 cm^{-1} and 1452 cm^{-1} corresponding to imine and NO_3 moieties respectively. Again no peaks corresponding to the aldehyde (1725 cm^{-1}) and amine

(*ca.* 3300 cm^{-1}) starting materials were present suggesting that some form of a Schiff-base complex [**100**.$Sm(NO_3)$] was formed although the exact nature of the complex could not be proven. The experiment proved inconclusive for the presence of the macrocyclic ligand and suggests that the polymer complex may have been prepared instead. This experiment was run again using the same lanthanide ion salt but by adding excess molar equivalents of sodium borohydride at the end of the reaction with the aim of reducing the imine of [**100**.$Sm(NO_3)$] *in situ* to give the free amine macrocycle **102** as suggested by the Fenton group[99]. This molecule has previously been synthesised by the Lehn group using macrocyclic synthetic methods in a number of synthetic steps[100]. Hence using the Schiff-base synthesis, **102** could be prepared in one easy synthetic step, which would be a great advantage over the Lehn method. This was done by stirring a solution of **104** and $Sm(NO_3)_3$ in methanol in the presence of **94** under reflux for four hours under inert atmosphere. The red-brown solution was cooled to 0°C and sodium borohydride was added slowly to avoid exothermic conditions and stirred overnight at room temperature. The cloudy yellow solution was concentrated and the resulting yellow residue was taken up in $CHCl_3$ and washed with 10% K_2CO_3(aq). The ^{1}H NMR spectrum in DMSO-d_6, in which the solid material was partially soluble, showed a multiplet at 1.25 ppm, a triplet at 7.05 ppm and a broad multiplet at 8.05 ppm. This information told little about the nature of the product of this reaction as the ^{1}H NMR characterisation data of **104** by Lehn *et al* showed a singlet at 4.35 ppm, a doublet at 7.52 ppm and a triplet at 7.98 ppm. Attempts to isolate **104** by acid-base extraction and recrystallisation in ammonia-saturated MeOH proved fruitless. The original Lehn paper did not contain any IR data. Comparing the IR of the yellow solid observed in the above reaction to the IR of [**100**.$Sm(NO_3)$] showed no difference in the spectra suggesting that imine was not reduced and the yellow solid was probably [**100**.$Sm(NO_3)$]. The CHN data obtained, C 47.62 %, H 4.04 %, N 19.00 %, did not agree with the theoretical data for [**100**.$Sm(NO_3)_3$] (C 41.01 %, H 4.30 %, N 18.79 %). Addition of solvent or counterion molecules did not reconcile the theoretical data with the actual CHN data. It is hard to determine the structure of [**100**.$Sm(NO_3)$] but it can be said that the Schiff-base complex was probably formed from the IR data and not **104**.

Two other Schiff-base complexes of **100** were prepared using NO_3 as the counterion, [**100**.$Gd(NO_3)$] and [**100**.$Pr(NO_3)$] using the same synthesis as that of [**100**.$Sm(NO_3)$] described above. Again solubility problems prevented analytical data on the structure of [**100**.$Gd(NO_3)$] and [**100**.$Pr(NO_3)$] to be determined. The ^{1}H NMR spectrum of [**100**.$Pr(NO_3)$] run in DMSO-d_6 was recorded in which the complex was partially soluble and showed two singlets at 3.2 and 4.2 ppm and three singlets in the aromatic region at 7.2, 7.9 and 8.6 ppm.

The IR spectrum displayed peaks at 3370 cm^{-1} indicating the presence of coordinated and lattice water. A peak at 1620 cm^{-1} indicating the presence of an imine group and peaks around 1458 cm^{-1} indicative of nitrate counterions. The IR data obtained for [**100**.Gd(NO_3)] were similar to that of [**100**.Pr(NO_3)]. The IR spectrum displayed resonances indicative of coordinated water, imine groups, pyridine moieties and nitrate moieties. The Schiff-base complexes, [**100**.Pr(trif)] and [**100**.Gd(trif)] were prepared by adding **94** to a stirring solution of **104** and the appropriate lanthanide triflate. It was interesting to see if the counterion played a role in increasing the yield and/or the solubility of the Schiff-base complex. [**100**.Pr(trif)] was synthesised in similar yield as [**100**.Pr(NO_3)]. The ^1H NMR and IR spectra of [**100**.Pr(trif)] was slightly different to [**100**.Pr(NO_3)] as the data in Table 2.1 shows. The Schiff-base complex [**100**.Gd(trif)] was characterised using ^1H NMR and IR methods and the data is shown in Table 2.1. The ^1H NMR data of [**100**.Gd(NO_3)] compared to [**100**.Gd(trif)] was significantly different with only one multiplet peak seen at 8.4 ppm for [**100**.Gd(NO_3)] whereas [**100**.Gd(trif)] shows a variety of singlet peaks. The IR data gives much the same information showing coordinated and lattice water peaks, imine peak, pyridine peaks and peaks representing the triflate counterions. [**100**.Pr(trif)] and [**100**.Gd(trif)] were not any more or less soluble in a variety of solvents as [**100**.Pr(NO_3)] and [**100**.Gd(NO_3)] suggesting that for Gd(III) and Pr(III) the counterion plays a minor role in the solubility of the Schiff-base complexes.

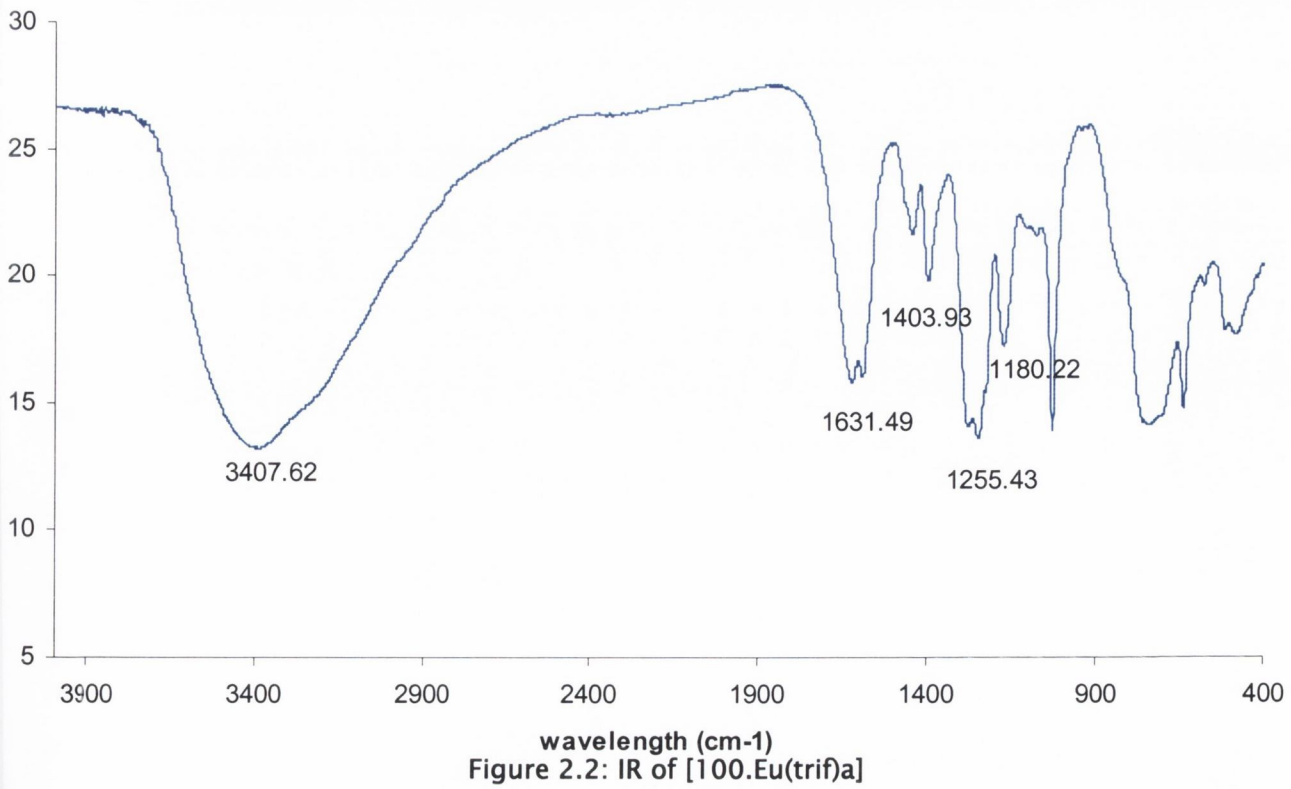

Figure 2.2: IR of [100.Eu(trif)a]

Yb(III) and La(III) ion triflate salts were used to synthesise the Schiff-base complexes [**100**.Yb(trif)] and [**100**.La(trif)]. These lanthanide ions were chosen because they represented both ends of the lanthanide series in the periodic table and would tell us if the size of the lanthanide ion would also affect the synthesis of the Schiff-base complex. Both complexes, [**100**.Yb(trif)] and [**100**.La(trif)], were synthesised in the same way as described above by adding **104** to a stirring solution of **94** and the appropriate lanthanide salt in MeCN and then refluxing for four hours. [**100**.Yb(trif)] produced a brown solid in good yield. The ^{1}H NMR spectrum in DMSO-d_6 showed two singlets at 3.9 and 4.3 ppm and three singlets in the aromatic region of the spectrum at 7.5, 7.9 and 8.5 ppm. Again the IR spectrum provides information on the functional groups present in the complex. The peak at 3390 cm^{-1} represents coordinated and lattice water molecules, 1635 cm^{-1} suggests the presence of imine groups, 1592 and 1457 cm^{-1} indicate the presence of pyridine moieties and the triflate counterions are identified by peaks at 1250 and 1169 cm^{-1}. The [**100**.La(trif)] complex was prepared in the same way as [**100**.Yb(trif)] producing brown solid in good yield. The ^{1}H NMR of [**100**.La(trif)] yielded little information with peaks seen at 2.1 ppm (singlet), 2.9 ppm (doublet) and a singlet at 4.2 ppm. The aromatic region shows a triplet at 7.2 ppm and singlets at 7.5, 7.9 and 8.5 ppm. The IR spectrum provided more information about the functional groups present in the complex. Coordinated and lattice water molecules are seen at 3067 cm^{-1}, 1618 cm^{-1} indicates an imine group, 1459 cm^{-1} indicates the presence of pyridine moieties and peaks at 1277 and 1163 cm^{-1} suggest the presence of triflate molecules. Considering the difference in ionic radii of La(III) and Yb(III), both [**100**.La(trif)] and [**100**.Yb(trif)] were synthesised in similar yield with similar IR and ^{1}H NMR spectra. These results suggest that the size of the ionic radii of the lanthanide plays no role in the synthesis of these Schiff-base complexes of **100**.

Four Schiff-base complexes were synthesised, [**100**.Eu(trif)], [**100**.Tb(trif)], [**100**.Eu(CH_3COO^-)] and [**100**.Tb(CH_3COO^-)]. The Schiff-base complexes containing acetate as the counter ion, [**100**.Eu(CH_3COO^-)] and [**100**.Tb(CH_3COO^-)], were synthesised by adding **94** to a stirring solution containing **104** and the appropriate lanthanide acetate salt in methanol as before and the precipitate formed was collected by filtration and washed with diethyl ether. Both [**100**.Eu(CH_3COO^-)] and [**100**.Tb(CH_3COO^-)] were synthesised in good yields as yellow solids. The ^{1}H NMR data for [**100**.Eu(CH_3COO^-)], when recorded in DMSO-d_6, showed a triplet peak at 7.2 ppm thus providing little information about the structure of [**100**.Eu(CH_3COO^-)]. The IR data of [**100**.Eu(CH_3COO^-)] showed peaks at 3395 cm^{-1} corresponding to coordinated and lattice water, 1620 cm^{-1} suggesting the presence of an imine

group, 1459 cm^{-1} indicative of pyridine moieties. The peaks at 1566 cm^{-1} and 1402 cm^{-1} show the presence of acetate molecules, with the difference between the two peaks being 164 cm^{-1} indicating that the acetate molecules are ionic in nature and are not involved in bidentate coordination[101]. Once again the ^1H NMR of complex [**100**.Tb(CH_3COO^-)] provided no information about the structure of the complex because the molecule was insoluble in most solvents and only partially soluble in DMSO-d6. Only a triplet peak at 7.2 ppm was seen in the ^1H NMR spectrum of [**100**.Tb(CH_3COO^-)]. The IR spectra was similar to that of the Eu(III) complex. Again the acetate moieties had peaks at 1560 and 1441 cm^{-1}, with the difference between the two, 119 cm^{-1}, suggesting that the acetate molecules are coordinated to the lanthanide ion in a bidentate manner[101]. The triflate Schiff-base complexes, [**100**.Tb(trif)] and [**100**.Eu(trif)], were synthesised in the same way as [**100**.Tb(CH_3COO^-)] and [**100**.Eu(CH_3COO^-)] in reasonable yield as above except the reaction solvent was MeCN producing brown solid. Again solubility problems prevented much characterisation data from being collected with the complexes being only partially soluble in DMSO-d_6 for NMR analysis. The ^1H NMR for [**100**.Tb(trif)] gave little information about the structure of [**100**.Tb(trif)] with only a multiplet signal seen at 4.7 ppm with another broad multiplet peak in the aromatic region of the spectra at 8.9 ppm. The IR spectra for both complexes were similar to those before and are shown in Table 2.1. The peaks representing the imine, pyridine and triflate moieties are seen.

It was thought that because the hydrochloride salt of **94** was used in the synthesis of the Schiff-base complexes, that that HCl group might be affecting the synthesis or the solubility of the complexes. The free amine, 2,6-bis(aminomethyl)pyridine **106**, was difficult to obtain as discussed above but the product obtained from the ion exchange column approximately in 10 % yield was used in the synthesis of [**100**.Eu(trif)a]. The synthesis was followed as above yielding a green solid in low yield by precipitation using diethyl ether. As before [**100**.Eu(trif)a] was not soluble in most solvents and only very partially soluble in DMSO-d_6 and because of this the ^1H NMR was not conclusive. The IR spectra had slightly different shifts to those seen for [**100**.Eu(trif)] suggesting that the complexes had slightly different composition as observed in Table 2.1. Comparison of the IR data for [**100**.Eu(trif)] and [**100**.Eu(trif)a] show, for example, the imine peak for [**100**.Eu(trif)] compared to [**100**.Eu(trif)a] have shifted from 1618 cm^{-1} to 1623 cm^{-1}.

As discussed above, the only information obtained about the nature of the complexes was through IR spectroscopy. It is difficult to determine if the complexes had in fact been

synthesised although evidence in the literature suggest that Schiff-base complexes are readily synthesised in this manner.

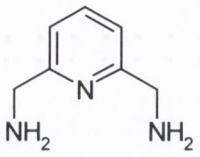

106

The Schiff-base lanthanide complexes of **100** are heavily conjugated and it would be expected that their UV-Vis spectrum would be considerably different to that of their starting materials **104** and **94**. All the Schiff-base complexes were dissolved in DMSO (as much as possible) and their UV-Vis spectrum compared to that of the starting materials. Figure 2.3 displays a number of UV-Vis spectra showing the differences between the UV of the starting material and that of the Schiff-base complexes for [**100**.Tb(CH_3COO^-)] and [**100**.Gd(NO_3)]. The UV spectra of the starting materials shows maximum absorption at 270 and 305 nm for **104** and 275 nm for **94** as shown in Table 2.1. For [**100**.Tb(CH_3COO^-)] a red shift to 330 nm is seen and for [**100**.Gd(NO_3)] a red shift to 330 nm is also seen. These shifts in may be due to charge-transfer bands between the metal ion and the ligands but is more likely due to the formation of an imine bond, which makes the complex more, conjugated.

2.3.2: Synthesis of Novel Schiff-Base Complexes **101**:

The solubility of the complexes of **100** was a limitation in the characterisation to find the true nature of the complexes. To overcome this four Schiff-base complexes of **101,** [**101**.Eu(trif)], [**101**.Tb(trif)], [**101**.Yb(trif)] and [**101**.La(trif)], were prepared from the lanthanide template synthesis of **94** with 2,6-diacetyl pyridine **105**, which was commercially available (Aldrich), to evaluate the presence of the methyl substituent in aiding the solubility of the complexes. These complexes were all synthesised as above. The triflate salts, [**101**.Eu(trif)] and [**101**.Tb(trif)], were synthesised in good yields resulting in yellow solids.

The presence of the methyl substituent did not aid solubility as both complexes had similar solubility to [**100**.Eu(trif)] and [**100**.Tb(trif)]. Once more, ^{1}H NMR spectra were recorded on these complexes in DMSO-d_6 in which the complexes were partially soluble. [**101**.Eu(trif)] showed a singlet at 4.2 ppm. The aromatic region of the spectrum displayed a triplet at 7.2 ppm, two singlets at 7.5 and 7.9 ppm with another singlet at 8.6 ppm.

Complex	Ln(III)	Counterion	Yield	Colour	^{1}H NMR (ppm)	IR (cm^{-1})	CHN (C; H; N)	UV-Vis (nm)
[48.Sm(NO_3)]	Sm(III)	Nitrate	0.036 g	yellow	8.6 (d,d); 7.7 (s), 7.3 (s); 3.5 (s); 2.7 (s)	3380, 1659, 1591, 1384		
[100.Sm(NO_3)]	Sm(III)	Nitrate	0.012 g	brown	no signals seen	3386, 1645, 1452,	51.56; 4.21; 23.37	310
[100.Sm(NO_3)]	Sm(III)	Nitrate	0.024 g	yellow	8.1 (b,m); 7.1 (t); 1.3 (s)	3396, 1569, 1452, 1342	47.62; 4.04; 19.00	310
[100.Pr(NO_3)]	Pr(III)	Nitrate	0.228 g	orange	8.6 (s); 7.9 (s); 7.2 (s); 4.2 (s); 3.2 (s)	3370, 1707, 1620, 1458	36.50; 3.27; 14.17	320
[100.Gd(NO_3)]	Gd(III)	Nitrate	0.24 g	brown	8.4 (m)	3385, 1706,1618, 1560, 1457	38.42; 3.24, 13.99	330
[100.Gd(trif)]	Gd(III)	Triflate	0.27 g	orange	9.3 (s); 8.6 (s); 8.1 (s); 5.6 (s); 4.9 (s)	3380, 1740, 1618, 1463, 1277, 1164	28.19; 3.21; 12.05	330, 370
[100.Pr(trif)]	Pr(III)	Triflate	0.26 g	brown	8.6 (s); 7.5 (s); 7.3 (s); 4.2 (s); 4.0 (s,b)	3124, 1738, 1617, 1454, 1276, 1164	28.15; 2.81; 12.89	325, 380
[100.La(trif)]	La(III)	Triflate	0.38 g	brown	8.6 (s); 7.9 (s) 7.5 (s); 7.2 (t); 4.2 (s); 2.9 (d); 2.1 (s)	3067, 1618, 1459, 1277, 1163	28.48; 2.73; 9.65	325
[100.Yb(trif)]	Yb(III)	Triflate	0.26 g	brown	8.5 (s); 7.9 (s) 7.5 (s); 4.3 (s); 3.9 (s,b)	3390, 1742, 1631, 1457, 1250, 1169	25.88; 2.64; 12.17	325
[100.Tb(trif)]	Tb(III)	Triflate	0.13 g	brown	8.9 (m, b); 4.7 (m)	3334, 1635, 1592, 1457, 1246, 1166	25.33; 2.46; 10.13	330, 400
[100.Eu(trif)]	Eu(III)	Triflate	0.15 g	brown	8.6 (s); 7.9 (m)	3367, 1618, 1458, 1243, 1165	26.66; 2.75; 11.98	325
[100.Eu(trif)a]	Eu(III)	Triflate	0.021 g	green	no signals seen	3398, 1623, 1446, 1280, 1174	--------	330
[100.Eu(CH_3COO^-)]	Eu(III)	Acetate	0.068 g	yellow	7.2 (t)	3395, 1620, 1566, 1459, 1402	44.40; 3.90; 18.88	325
[100.Tb(CH_3COO^-)]	Tb(III)	Acetate	0.074 g	yellow	7.2 (t)	3406, 1618, 1560, 1459, 1441	40.52; 3.21; 16.96	330
[101.Eu(trif)]	Eu(III)	Triflate	0.22 g	yellow	8.6 (s); 7.9 (s); 7.5 (s); 7.2 (t); 4.2(s)	3369, 1617, 1461, 1246, 1164	26.70; 3.28; 10.63	325
[101.Tb(trif)]	Tb(III)	Triflate	0.19 g	yellow	9.41 (s); 8.7 (m); 4.9 (s)	3376, 1617, 1463, 1277, 1162	27.73; 3.63; 12.26	325, 400
[101.Yb(trif)]	Yb(III)	Triflate	0.30 g	brown	-19.4; -13.6; -5.8; -3.7; 3.4; 24.2; 37.2; 42.6; 65.6; 91.0	3375, 1616, 1462, 1272, 1169	26.67; 2.84; 13.13	310, 400
[101.La(trif)]	La(III)	Triflate	0.33 g	brown	8.7 (s); 7.9 (s); 7.4 (s); 7.3 (d); 4.2 (s,b)	3371, 1618, 1461, 1277, 1163	25.71; 3.01, 12.97	325, 400

Table 2.1: Characterisation data for all the Schiff-based complexes formed

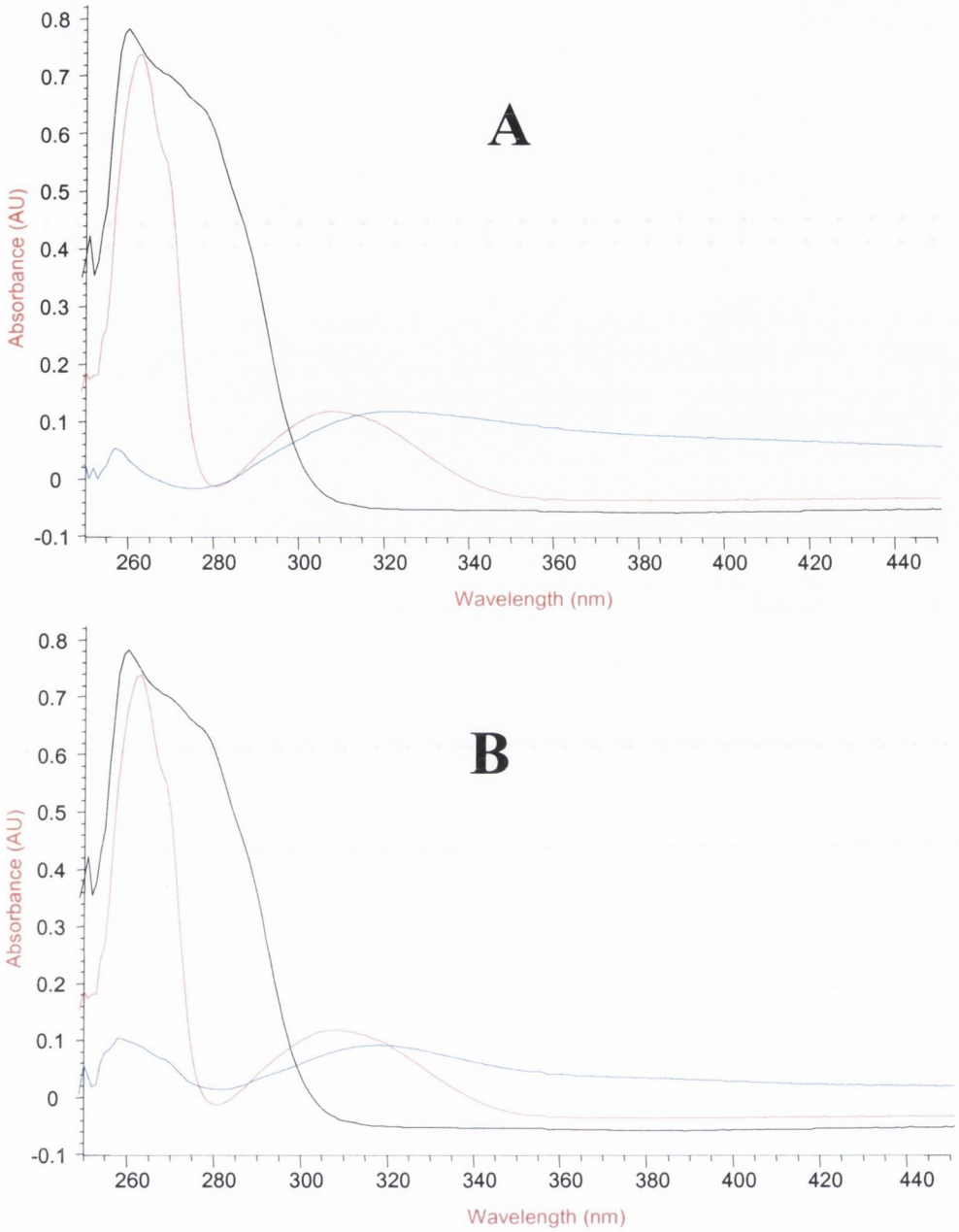

Fig. 2.3: UV Spectra comparing the starting materials 94 (black line) and 104 (red line) and the complex (blue line) for A: [100.Tb(CH_3COO^-)] and B: [100.Gd(NO_3)]

The IR data demonstrated the presence of a number of indicative functional groups for Schiff-bases, with coordinated and lattice water appearing at 3369 cm^{-1}, the imine group appearing at 1617 cm^{-1}, pyridine moieties occurring at 1461 cm^{-1} and the triflate counterions appearing at 1246 and 1164 cm^{-1}. The [**101**.Tb(trif)] complex displayed a different ^1H NMR spectrum to [**101**.Eu(trif)] with a singlet peak at 4.9 ppm and two peaks in the aromatic region , a multiplet at 8.7 ppm and a singlet at 9.41 ppm. Again the IR spectrum displayed the characteristic peaks of these Schiff-base complexes with coordinated and lattice water occurring at 3376 cm^{-1}, the imine functional group at 1617 cm^{-1}, pyridine moieties at 1463

cm^{-1} and the triflate counterions appearing at 1277 and 1162 cm^{-1}. The complexes [**101**.La(trif)] and [**101**.Yb(trif)] were also synthesised as these lanthanide ions surface at either end of the lanthanide series. Both complexes were synthesised as discussed above yielding brown solids in good yield.

Once again solubility problems prevents characterisation of these complexes from occurring. Both complexes were only partially soluble in DMSO-d_6. It was the ^1H NMR spectrum of [**101**.Yb(trif)] which provided interesting results displaying a number of singlet peaks in a range from –19.4 ppm to 91.0 ppm. It is not unexpected to find peaks of the lanthanide ligands within this region. Unfortunately the ^1H NMR spectrum again gives little information about the nature of [**101**.Yb(trif)] and only the IR spectrum, discussed above, gives any information about the functional groups present in the complex as shown in Table

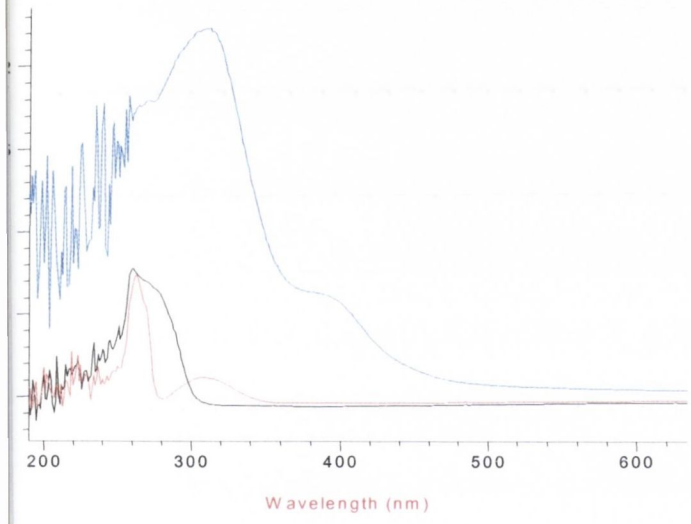

Fig. 2.4: UV Spectra comparing the starting materials 94 (black line) and 105 (red line) and the complex (blue line) for [101.Yb(Trif)] in DMSO

2.1. Comparison of the UV spectra of the complexes of **101** to the starting materials, **94** and **105**, again show a red shift in the UV-Vis spectrum as shown in Table 2.1. For example [**101**.Yb(trif)] shows a maximum absorption at 330 and 400 nm, a considerable shift upfield compared to the starting materials, as shown in Figure 2.3, providing tangible evidence that the lanthanide Schiff-base complexes may have been synthesised.

2.3.3: Luminescence Studies on the Eu(III) and Tb(III) Schiff-Base Complexes:

The intended use of the Schiff-base macrocycles was to provide a quick and simple method for synthesising novel lanthanide complexes as potential building blocks for luminescent sensors and switches. As discussed in chapter 1, the direct excitation of the

lanthanide ions, specifically Eu(III) and Tb(III), can only be achieved using a laser light source at the appropriate wavelength. Ligand molecules are used as "antennas" by absorbing energy and transferring this energy to the lanthanide ion where an electron is promoted to the first excited state. The energy released as light when the electron deactivates to its ground state is the lanthanide luminescence as shown in Figure 1.5. Therefore any luminescence data obtained during luminescence measurements when excited at the appropriate wavelength would help prove that the Schiff-base complexes were synthesised.

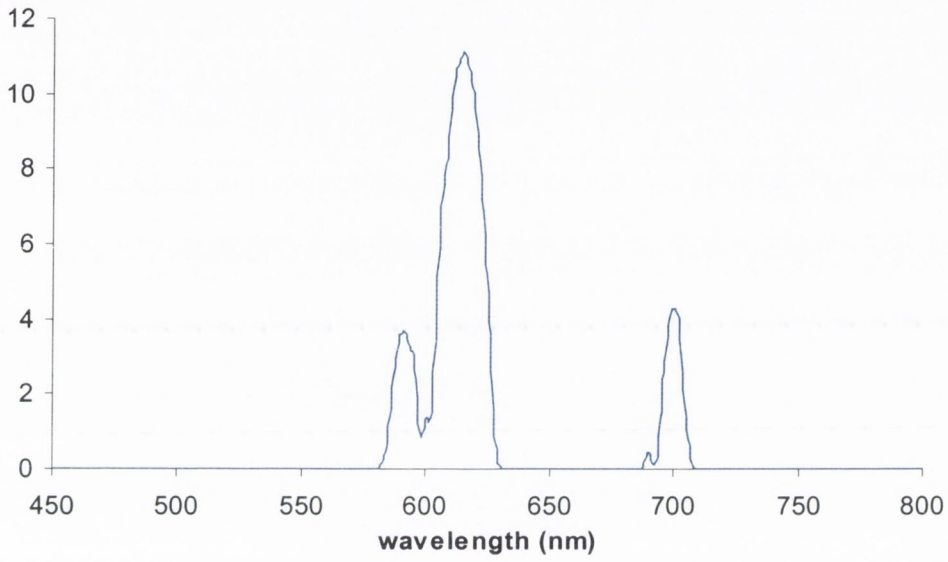

Fig. 2.4: Lanthanide luminescence of [100.Eu(trif)].

The Eu(III) and Tb(III) Schiff-base complexes of **100** and **101** were investigated for their ability to undergo lanthanide luminescence. The complexes had an optical density of 0.1, were excited at 300 nm or at the longest wavelength and luminescence were observed in the region 450 to 800 nm. The optical density could not be determined because of solubility problems. Table 2.2 shows the luminescent data for all the Eu(III) and Tb(III) complexes.

COMPLEX	*UV-Vis λ (nm)*	*Excitation λ (nm)*	*Emission λ (nm)*
[100.Eu(CH_3COO^-)]	325	330	625
[100.Tb(CH_3COO^-)]	330	330	495, 50, 600, 625
[100.Eu(trif)]	325	330	595, 610, 700
[100.Eu(trif)a]	330	330	595, 610, 700
[100.Tb(trif)]	330, 400	330	495, 550, 580, 625
[101.Eu(trif)]	325	330	No luminescence
[101.Tb(trif)]	325, 400	330	No luminescence

Table 2.2: Luminescent data for all the Eu(III) and Tb(III). All measurements run in DMSO

The luminescence spectra of [**100**.Eu(CH_3COO^-)] shows a single peak at approximately 617 nm with only a few nm bandwidth a characteristic property of lanthanide luminescence. The quantum yields could not be determined due to problems with solubility. The presence of the Schiff-base ligand increases the lanthanide luminescence of Eu(III) from an intensity of 28 to 50. The luminescence spectra of [**100**.Eu(trif)] as seen in Figure 2.4 shows a similar increase in intensity but with three peaks at 590, 605 and 700 nm, each a few nm bandwidth. This suggests the counterion did not effect the luminescent ability of [**100**.Eu(trif)] and [**100**.Eu(CH_3COO^-)]. When luminescent studies were run on [**100**.Eu(trif)a], the complex synthesised using the free amine **106**, there was a dramatic increase in luminescence ability as seen in Figure 2.5. There were three intensity peaks at 595, 605 and 700 nm as for [**100**.Eu(trif)a] with the maximum intensity of 640 at 605 nm. This suggests that the presence of coordinating Cl^- ions in [**100**.Eu(CH_3COO^-)] and [**100**.Eu(trif)] plays a role in the quenching of the lanthanide luminescence of Eu(III), although IR, ^1H NMR data and solubility studies suggest there is no advantage in utilising the free amine **106** in the synthesis. The presence of the methyl substituents on [**101**.Eu(trif)] did not improve the lanthanide intensity of Eu(III), in fact no luminescence was observed for [**101**.Eu(trif)].

The lanthanide luminescent spectrum of [**100**.Tb(trif)] showed three peaks at 550, 595 and 645 nm with a corresponding minimal increase in intensity spectra of 12 to 16 at 550 nm. The lanthanide luminescence spectrum of [**100**.Tb(CH_3COO^-)] showed a dramatic lanthanide luminescent intensity as seen in Figure 2.6.

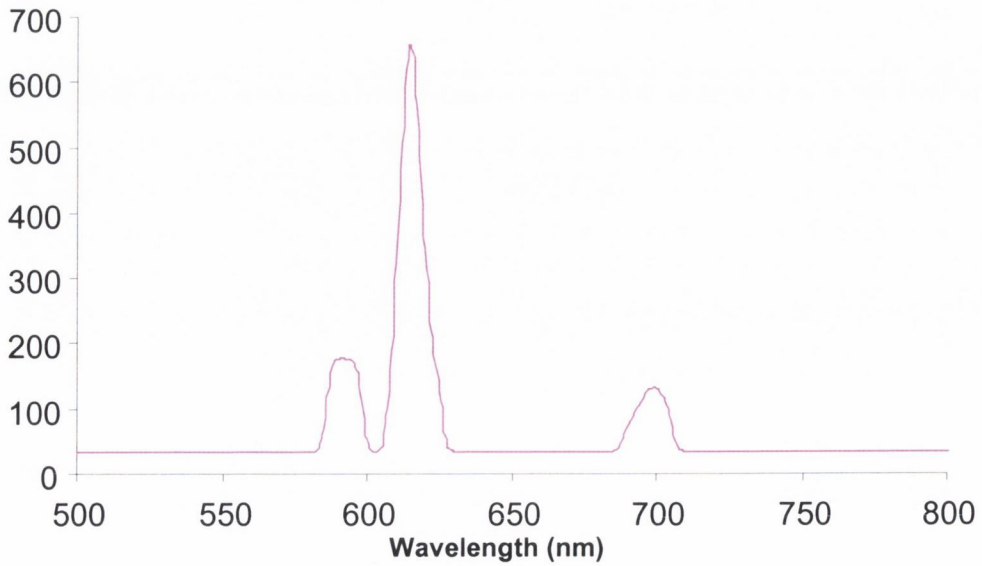

Fig. 2.5: Lanthanide luminescence spectrum for [100.Eu(trif)a]

There were four peaks seen at 495, 550, 595 and 604 nm in the spectrum. The peak at 550 nm showed the maximum intensity of 110. This data suggests that the counterion had an effect on the luminescence of Tb(III). The lanthanide luminescence of the complex [**101**.Tb(trif)] was also investigated to determine the effect of the methyl group on Tb(III) luminescence. It was found that there was no luminescence when the complex was excited at 330 nm. There may be a number of reasons for this such as the choice of solvent used or the effect of the counterion which could deactivate luminescence.

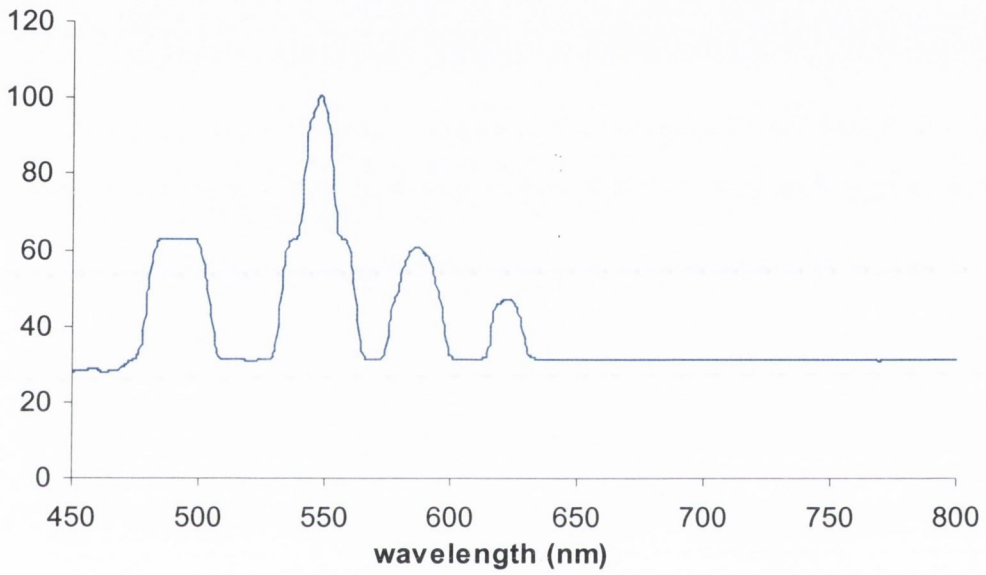

Fig 2.6: Lanthanide luminescence spectrum of [100.Tb(CH_3COO^-)]

2.3.4: Possible Structure of the Schiff-Base Complexes:

The CHN data for all the complexes, shown in Table 2.1 proved inconclusive and it is hard to determine the true nature of the complexes because of the problem with solubility. The actual CHN data could not be reconciled with their theoretical values even when a number of solvent and counterion molecules were included in the analysis. A number of possible structures for these complexes have been postulated and are shown below Figure 2.6 along with their corresponding theoretical CHN values. A comparison of this data with the actual CHN data in Table 2.1 shows that these structures do not correspond. All that can be said about the Schiff-base complexes produced is that the IR data show the presence of the imine peak and the loss of the carbonyl peak. UV-Vis data show the complexes are red shifted compared to the starting materials and are therefore more conjugated. Luminescence data show some lanthanide luminescence when excited at 330 nm suggesting that the complex is

transferring energy to the lanthanide ion. This suggests that perhaps polymeric complexes were formed which would explain the solubility and characterisation difficulties.

2.4: Conclusion:

This chapter has described the synthesis of a three-pyridine macrocyclic ligand **86**, which it was hoped could be further functionalised but due to scale-up problems could not be easily achieved. A substantial effort was invested to optimise the yield of the reaction at each stage of the synthesis to finally achieve **86.**

The Schiff-base macrocycles were synthesised using lanthanide template synthesis. Solubility problems prevented a number of characterisation methods to be run thus it is hard to determine the true nature of these macrocycles. IR data proved the presence of the imine moieties and the counterions and no evidence was seen of the characteristic peaks of the starting materials such as aldehyde carbonyl peak or an amine peak. ^{1}H NMR spectra were run but provided little information. Unfortunately CHN data proved inconclusive suggesting that the complexes were surrounded by water molecules either coordinated to the lanthanide ion or within the crystal lattice. UV-Vis analysis comparing the UV spectra of the starting materials, **94, 104** and **105**, to the complexes provided some evidence that the complexes were being formed as in all cases there was a significant red shift in wavelength indicating that they were more conjugated. Lanthanide luminescence spectra of all Eu(III) and Tb(III) showed lanthanide luminescence in most case suggesting that the ligand is transferring energy to the lanthanide ion, which was the goal of this section. It is possible that polymer complexes were formed. Further work is currently being undertaken using high resolution MS to determine the exact nature of these complexes. Although not all goals and objectives were achieved in this chapter, interesting results were achieved.

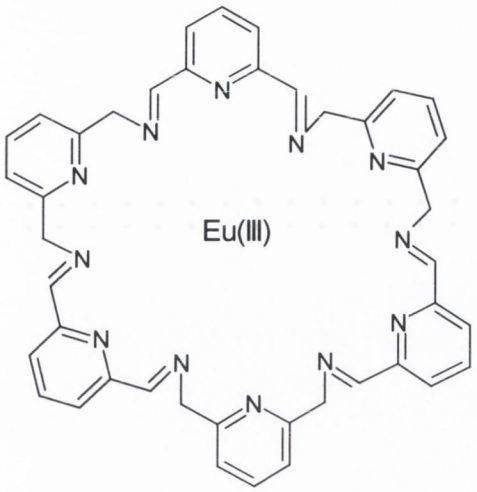

C 58.20% H 4.88% Eu 17.53% N19.39%

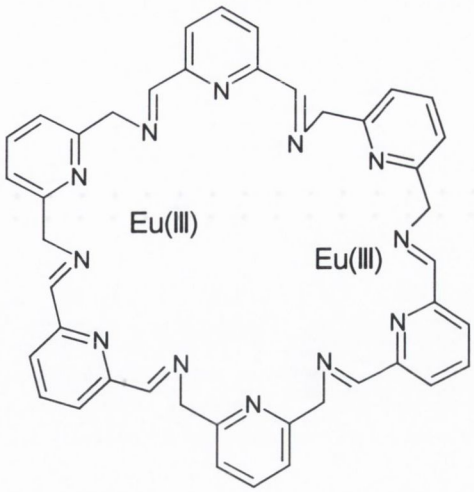

C 49.52% H 4.16% Eu 29.83% N16.50%

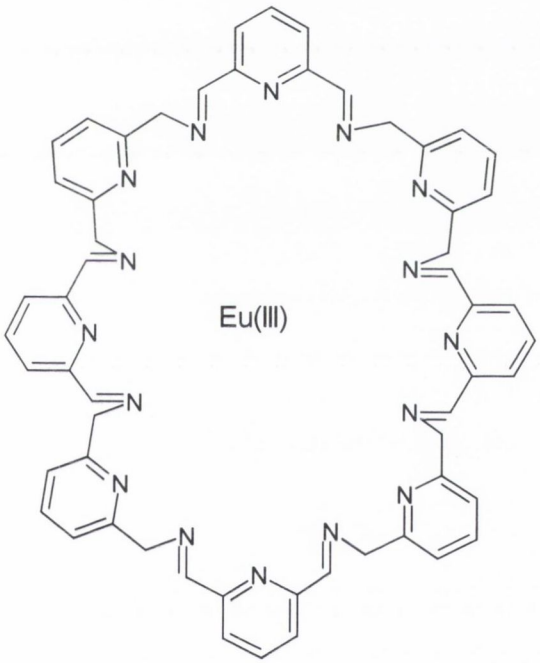

C 61.14% H 4.67% Eu 13.81% N 20.37%

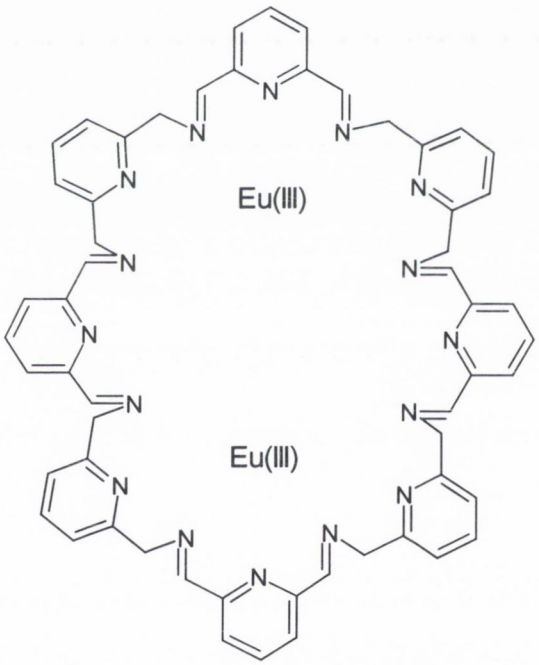

C 53.59% H 4.34% Eu 24.22% N17.86%

Fig. 2.6: A number of possible structures for these complexes with Eu(III)

Chapter 3

RNA Cleavage using Transition metal Complexes

3.1 Introduction to the Hydrolysis of RNA

The aim of the work in this chapter was to develop and evaluate a novel ligand for transition metals [Cu(II), Ni(II), Zn(II), Co(II), Fe(II)] as potential catalysts for the hydrolysis of the RNA mimic HPNP (2-hydroxypropyl *p*-nitrophenyl phosphate)[102]. Concurrently with this work, the ground and excited states of the complexes were investigated. The phosphodiester cleavage of RNA using organic-metal complexes as catalysts is of current interest due to their potential as therapeutic agents for cancer and viral diseases and as tools for molecular diseases. There are three major types of RNA. Ribosomal RNA (rRNA) serves

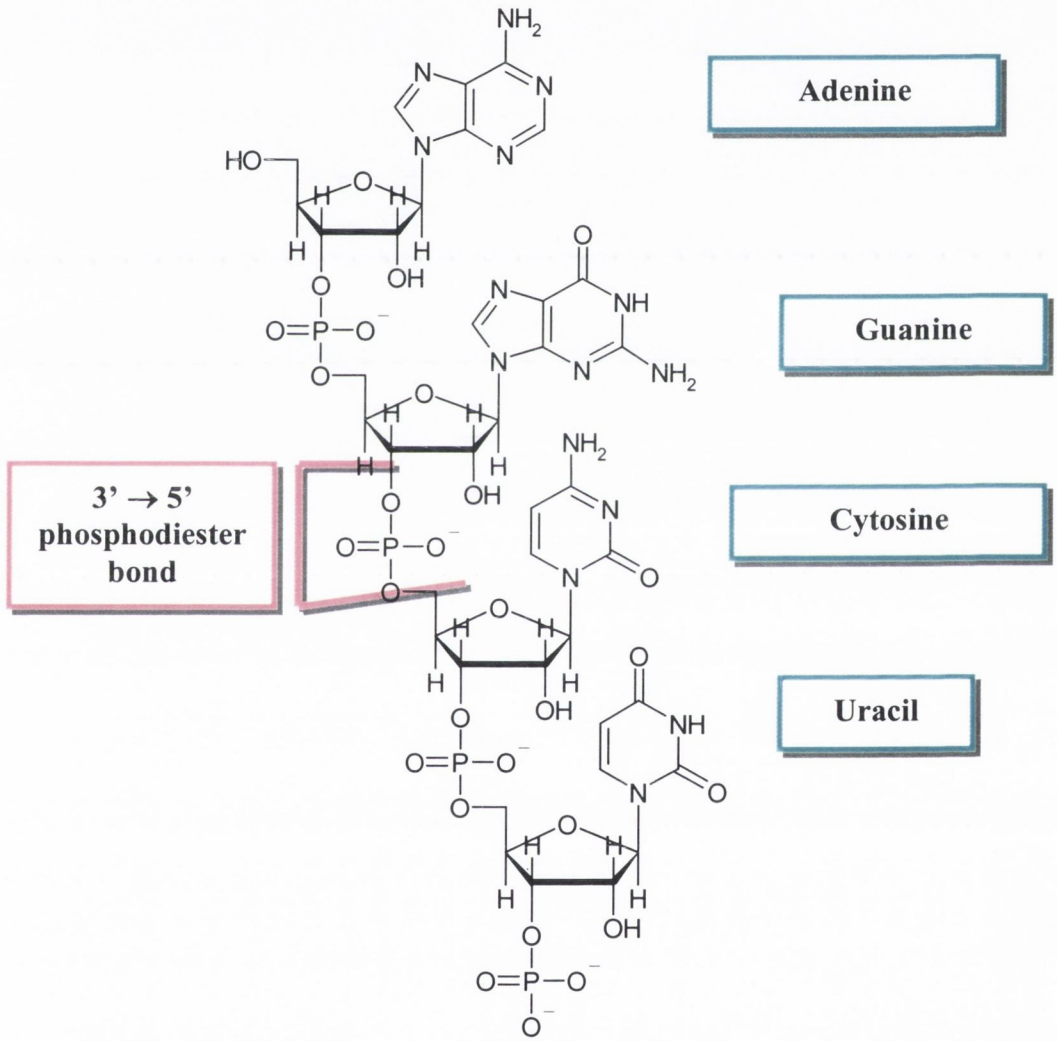

Fig. 3.1: Structure of RNA showing the bases and the 3'-5' phosphodiester bond.

as a site for protein synthesis. Transfer RNA (tRNA) is an "adaptor" molecule that carries specific amino acids to the site of protein synthesis whereas messenger RNA (mRNA) carries the genetic information from DNA to the site of protein synthesis and once there is used as a template for protein synthesis. RNA is different to DNA due to the presence of a 2'-hydroxy

function on the ribose and the use of uracil instead of thymine in the nucleotide base. The structure is shown in Figure 3.1. The phosphodiesters have been chosen by nature as the connecting links between the sugars and bases of DNA and RNA because of their ability to remain stable in aqueous and lipophilic media for a long time[103]. Nature has developed both ribozymes and ribonucleases to achieve rapid, site-specific cleavage of RNA under physiological conditions. A ribozyme is an RNA molecule, which adopts a three-dimensional structure that allows it to catalyse a reaction, usually with the participation of one or more metal ions[104]. The 2'-hydroxy function on RNA ribose has been found to increase hydrolysis of the phosphodiester bond faster than in DNA, which lacks this functionality[105]. It must be noted that whereas the half-life of DNA is *ca* four billion years, for RNA it is *ca* 110 years with the 2'-OH group providing 10^9-fold rate acceleration[106].

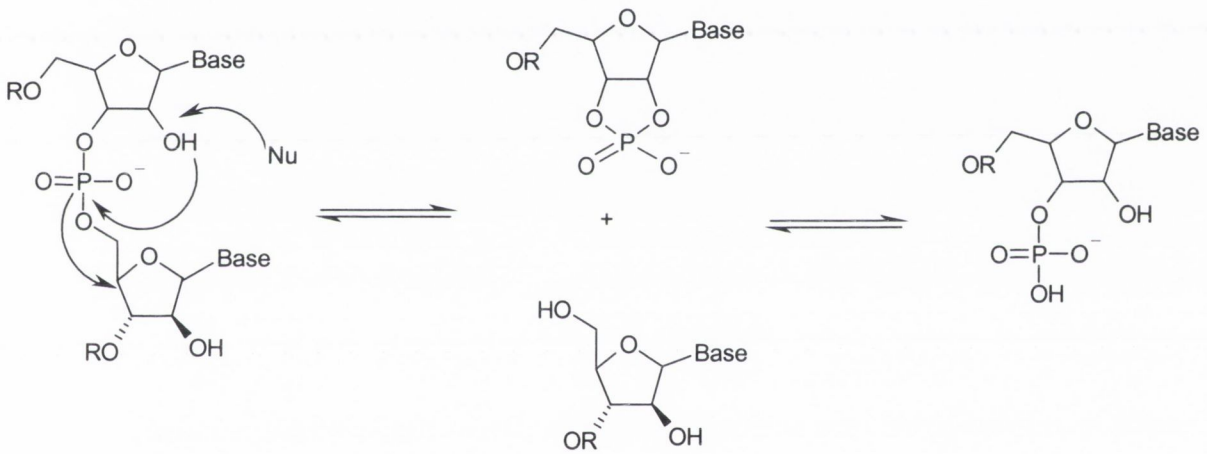

Fig. 3.2: Hydrolytic cleavage of RNA. *Step 1.* Cleavage-transesterfication. *Step 2.* Hydrolysis of the cyclic phosphodiester. Both the 2' and 3' monophosphate (shown) products can be formed. 'Nu' represents a nucleophile or another activating agents such as Lewis acid metal centre or a metal-bound water molecule (or hydroxide).

Ribonucleases and ribozymes all hydrolyse phosphodiester bonds with the direct participation of one or more metal ion centres, such as Mg^{2+}, Zn(II) or Co(III). In many of these, one or more water molecules are directly bound to the metal ions. For enzymes that carry out RNA hydrolysis,[107] the ions participate in the hydrolytic process by either direct (inner sphere) or indirect (outer sphere) activations modes of the 2'-hydroxy function. In the former, the metal can stabilize the phosphodiester by so-called Lewis acid activation, *e.g.* by direct metal coordination, and by stabilising the leaving groups upon its expulsion. This is however, thought to be of lesser importance than the role of the metal ion in the nucleophilic

activation process of the 2'-hydroxy group of the ribose (figure 3.2), which takes place through metal bound water molecules (or hydroxy groups depending on pH) that deprotonate the 2'-hydroxy group which consequently makes it more nucleophilic[108]. These steps are all pH dependant. The first step involves cleavage-transesterification where the nucleophile attacks the 2'-OH on the ribose yielding the phosphorane intermediate. The next stage involves the hydrolysis of the cyclic phosphodiester with the expulsion of a leaving group[108]. Because of this, there has been great interest in making synthetic analogues of such biocatalysts for use as potential drugs for treating genetically based diseases, by interfering with protein expression at the mRNA level. Several mono-, di- and tri-nuclear transition metal compounds have been designed as enzyme mimics and their catalytic ability investigated by employing phosphodiester models and RNA. A few of these transition metal complexes have been incorporated into oligonucleotide conjugates as potential antisense agents. However, many of these metalloenzyme mimics have been made *in situ*, yielding complexes that are difficult to analyse and often have poor water solubility. Furthermore, free metal ions in solution can give rise to *non-specific* phosphodiester hydrolysis. Additionally, these enzyme mimics often suffer from rather low catalytic turnover. All these setbacks render their use for *in vivo* applications limited.

Metal complexes form the basis for the most effective artificial systems that have been created in efforts to reproduce enzyme-like reactivity[106,109]. The ligands surrounding the metal are the only means to control the modes of action and activity, which are important to understand the relationship between activity and ligand structure. There are five mechanisms through which a metal ion can promote the rate of hydrolysis of the phosphodiester[110] (Figure 3.3). The first method (A) is by Lewis acid activation of the phosphate oxygen by the metal. The second method (B) occurs if a nucleophile, such as a hydroxy moiety, is coordinated to the metal resulting in nucleophilic activation. The third method (C) occurs when the metal coordinates to the leaving group causing leaving group activation. These are all direct or inner sphere activation methods. There are also outer sphere activation methods. Methods (D) and (E) occur when a coordinated water molecule acts as a general acid or base catalyst.

Synthetic ribozyme mimics have many advantages over natural ribozymes[111], including lower molecular weight, which offer an advantage in drug delivery. Natural ribozymes have complex tertiary structures that rely on incorporation into natural RNA residues, whereas in ribozyme mimics stability can be optimised.

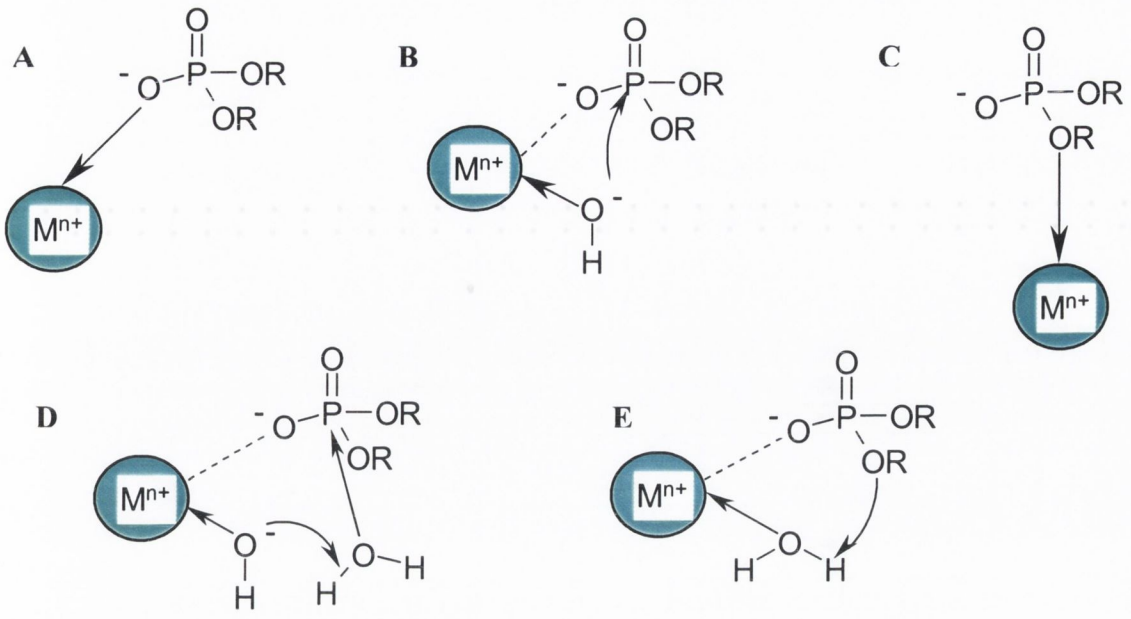

Fig. 3.3: The five mechanisms through which a metal ion can promote the rate of hydrolysis of the phosphodiester. A: Lewis acid activation by M^{n+}. B: Nucleophilic activation. C: Leaving group activation. D and E: Acting as general acid/base activation. This is fully explained in

Over the past ten years attempts have been made to synthesise compounds, which promote RNA cleavage, and to attach these to oligonucleotides to form artificial ribozymes or ribonucleases where both recognition and cleavage can be individually tuned and optimised. One of the first RNA ribonucleases developed used imidazole **107** because it was known that *bovine pancreatic ribonuclease* hydrolysed RNA using an imidazole group as a general base and an imidazolium group as a general acid[112]. The authors also showed that mounting two imidazole groups onto the primary face of a β-cyclodextrin produced a catalyst. This catalyst

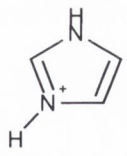

107

could hydrolyse a cyclic phosphate ester of 4-*t*-butylcatechol. The authors developed this further to use imidazole buffers to determine the mechanism of catalysis by ribonucleases[113,114] as shown in Figure 3.3. This was able to hydrolyse 4-*t*-butylcatechol cyclic phosphodiester showing that the rate depended on the concentration of catalyst and protonation states of the buffer[112,113,114].

While the earlier work by the Bashkin and Breslow groups used non-metal catalysts for the hydrolysis of RNA[115,112], this thesis is mainly concerned with the use of metal bound catalysts for the hydrolysis of RNA. It is known that DNA and RNA are susceptible to hydrolysis by metal ions[116]. The Butzlow group noted that polynucleotides degraded at high temperatures in the presence of Zn(II). They also noted the difference in susceptibility of RNA compared to DNA by the competitive effect of Zn(II) hydrolysis on polynucleotides compared to calf thymus DNA. They stated that the rate of hydrolysis for RNA was 4,000 times greater than DNA at pH 7 in the presence of Zn(II) [116]. Continuing from their investigations into the ability of imidazoles to hydrolyse phosphodiesters Breslow and co-workers studied the effect of incorporating Zn(II)[117,118]. The rate of catalysis by imidazole was more effective with Zn(II) and the mechanism involves Lewis acid/base catalysis. It was found that the presence of Zn(II) can accelerate cleavage by a factor of 150.

Chin and co-workers looked at the ability of Co(III) coordinated to an organic ligand to hydrolyse phosphodiesters[119,120,121]. The complex **108** incorporated a cyclen ligand with Co(III). This complex hydrolysed an inactivated phosphodiester, which is used to mimic DNA[119]. The complex **109** was then developed to catalyse inactivated phosphodiesters[120,121]. This gave reasonable rates of cleavage and helped to develop the mechanism of cleavage as described in Figure 3.3.

The Komiyama group investigated the use of **109** as a catalyst for the selective cleavage of RNA which mimics the ribonucleoside dimers adenylyl(3'-5')adenosine (ApA) and uridyl(3'-5')uridine (UpU)[122]. At pH 7 and 50°C the cleavage of ApA by **109** was 15 x 10^{-3} hr^{-1} giving a 10^5-fold rate acceleration. The metal-bound water molecules promoted the departure of the hydroxy ion at the 5' position by general acid catalysis.

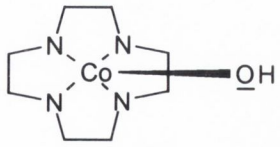

108

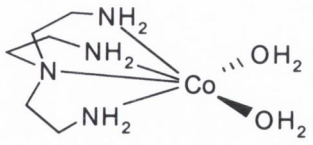

109

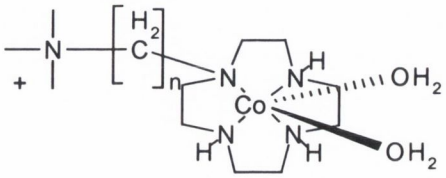

n = 3, 4, 5, 6

110

Schneider *et al* also investigated the use of Co(III) with cyclen derivatives **110** as catalysts for the cleavage of the DNA mimic bis(nitrophenyl)phosphate (BNPP)[123]. These complexes all have an enforced *cis* configuration which helps stabilise the transition state. They found these complexes gave dramatic, enzyme-like rate of 30-fold enhancement for the hydrolysis of BNPP.

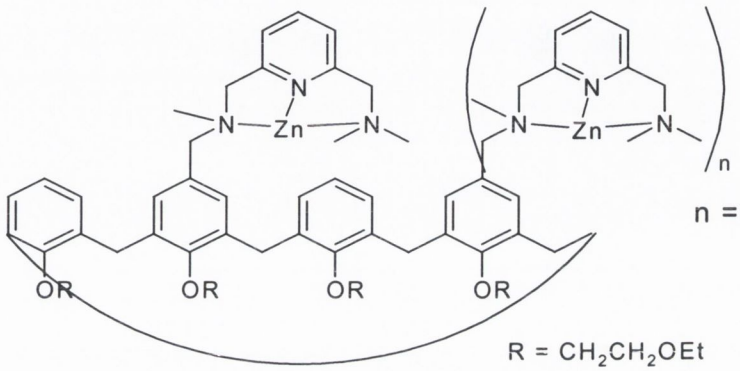

111

In 1997 Reinhoudt and co-workers used dinuclear Zn(II) calixarene derivatives as catalysts for RNA cleavage in a DMSO:H_2O mixture[124,125]. They stated that the dinuclear metal centres in ribonucleases were usually separated by 3-5 Å. The metal centres function as Lewis acids generating a reactive nucleophile and stabilising the transition state and leaving group. By designing dinuclear complexes on rigid molecular scaffolds which orient the metal in such a way that the metal to metal distance matches the distance required for selective recognition and binding of the transitional state. They used calixarenes to provide this rigid scaffold. The calixarenes derivatives **111**, where n = 1 (dinuclear), was not as effective. The calixarene was not involved in any part of the hydrolysis. Replacing the Zn(II) with Co(II), Ni(II) and Cu(II) gave no increase in the rate of catalysis[124]. The Reinhoudt group then investigated dinuclear Cu(II) complexes again based on the calixarene scaffold using **112** [125]. The dinuclear complex was a more effective RNA-mimic than the mononuclear complex because of the efficiency of the synergistic action of the two Cu(II) centres which are well preorganised on the calixarene scaffold.

112

The complex showed an increase in rate enhancement of 23000 fold at pH 7 and 25°C for the cleavage of HPNP. **112a** has a low pKa with a rate of hydrolysis of 1.0 x 10^4 hr^{-1}. The addition of the hydroxymethyl and amino methyl groups, **112b** and **112c** respectively gave more information on the ability of the calixarene to act as a rigid scaffold[126]. The amino methyl group on **112c** was chosen to mimic the ammonium group of the lysine residue on

RNAase A, which activates the phosphoryl group while two histidine molecules cooperate in the deprotonation of the nucleophile and in the protonation of the leaving group.

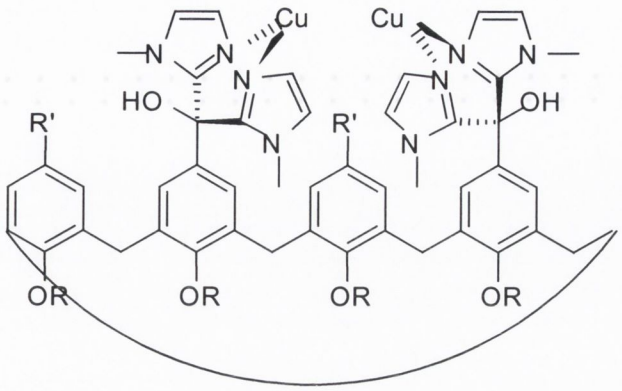

a : R = CH_2CH_2OEt, R' = H
b : R = CH_2CH_2OEt, R' = CH_2OH
c : R = CH_2CH_2OEt, R' = CH_2NH_2

112

Phosphodiester Type	*PSEUDO FIRST ORRDER RATE CONSTANT ($K_{OBS}/10^5 S^{-1}$)*				
	113 - Zn_3	**113 – Zn_2Cu**	**113 – Cu_3**	**111 – Dinuclear**	**111 - mononuclear**
GpG	7.2	88	28	0.45	-----
UpU	8.5	13	1.2	0.45	0.56
GpA	4.6	5.9	-----	-----	-----
ApA7.2	0.44	0.46	0.47	0.28	0.31

Table 3.1: Showing the rate of hydrolysis of a number of catalysts.

The presence of these groups gave good rates of cleavage at different pHs. **112b** gave the best rate at pH 6.2 but it was not especially active even at this pH. **112c** gave the best rate of cleavage at pH 7.4. These results were still not comparable to the cleavage by enzymes. More importantly the addition of these groups can be used for further functionalisation for example to oligonucleotides for antisense procedures.

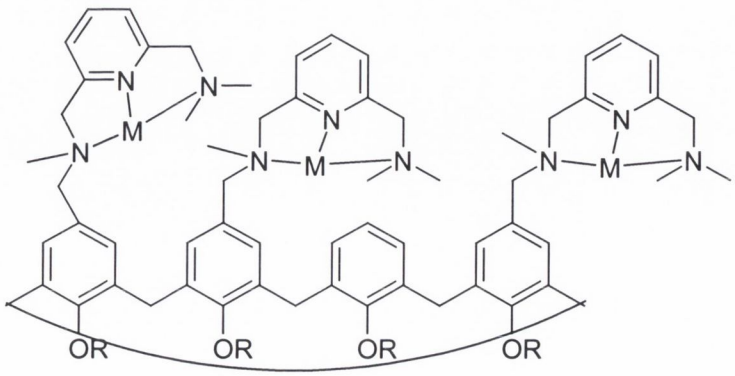

R = CH_2CH_2OEt

113

When three metal centres were incorporated into the calixarene **113** there was a high rate enhancement with significant nucleobase specificity[127]. From Table 3.1 it can be seen that all the complexes were specific for GpG compared to UpU. This may be due to a better fit because of the different size of the nucleosides. The two Zn(II) activate the phosphoryl group and the third Zn(II) is bound to the nucleoside[128].

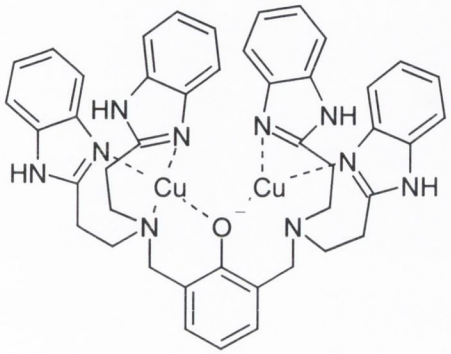

114

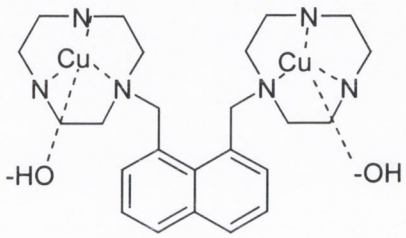

115

The Chin group was one of the first groups to report on the high catalytic ability of Cu(II) complexes[128,129,130]. The dinuclear Cu(II) complex **114** incorporates a bridging phenoxide unit[129]. Both the Cu(II) ions cooperate in the cleavage of HPNP with a rate acceleration of 2 $x10^4$. Unfortunately this catalytic ability could not be repeated on the dinucleotides probably due to steric hindrance. To continue from this work the complex **115** was developed using a bridging naphthalene unit[130]. At pH 6 **115** was 300-500 times more reactive than its mononuclear analogue for the cleavage of ApA. It is suggested that the Cu(II) both binds the phosphoryl group by double Lewis acid coordination and the metal bound hydroxide ion acts as a nucleophile.

The Hamilton group developed a number of terpy-based molecules to complex Cu(II) **116-121**[131,132,133]. They designed these complexes to be selective for the different nucleotide bases, especially adenine-containing substrates, and to contain at least one metal bound water molecule. These complexes were all found to give good rates of catalysis with acceptable selectivity. Whereas **116** was regioselective because it is able to bind to the bases **117** was

COMPOUND	K_{obs} (s^{-1})
116	5.74×10^{-6}
117	6.96×10^{-7}
118	1.53×10^{-5}
119	3.89×10^{-5}

Table 3.2: The rate of cleavage of ApA by compounds 116 to 119

base selective because of π-π stacking[131]. **118** was selective for the hydrolysis of the RNA mimic ApA compared to CpC with a substantial difference in the pseudo-first order rate of 152 x 10^6 s^{-1} compared to 13.2 x 10^6 s^{-1} for ApA and CpC respectively[133]. The nucleobase and regioselectivities do not correlate with the size and shape of the nucleobases. The selectivities may be due to specific interactions of the nucleobases with the ligands such as hydrogen binding or π-π stacking. The complex **118** proved that the metal-bound water molecule was essential for catalysis but this molecule was protonated at neutral pH. The addition of tertiary amino groups in **119** to **121** overcame this problem with complexes **120** and **121** being especially effective as shown in Table 3.2.

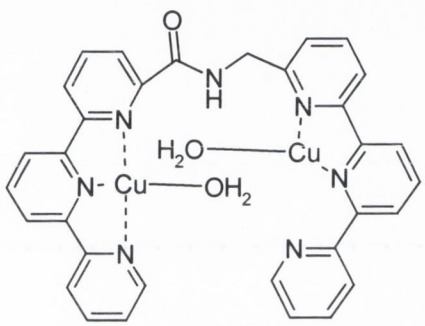

116

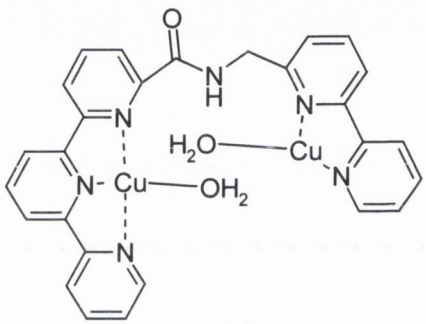

117

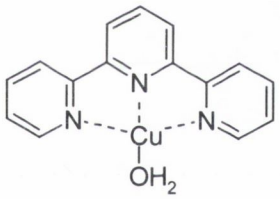

118

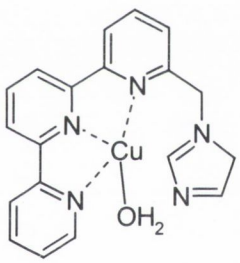

119

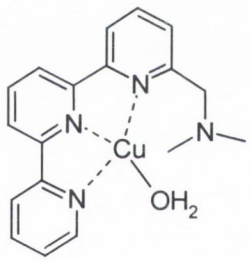

120

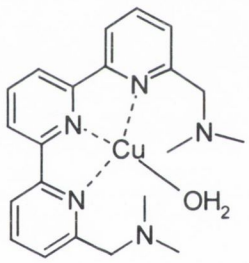

121

Komiyama *et al* developed more transition metal complexes for RNA hydrolysis[134,135,136,137,138]. A dinuclear Zn(II) complex **122** was developed containing binding pyridine groups and two bound metal ions to mimic the enzyme active site[134]. **122** efficiently hydrolysed ApA at pH 7 and 50°C and is deemed a good artificial ribonuclease. From this basic skeleton a trinuclear Zn(II) complex **123** was synthesised[137]. It was known that three metal centres are commonly found in natural ribonucleases. **123** was highly efficient for the hydrolysis of ApA. The Komiyama group developed a novel Zn(II) complex **124** for the photoregulation of the hydrolysis of RNA. They showed that the hydrolysis of RNA could be reversibly photo-controlled using this complex **124**.

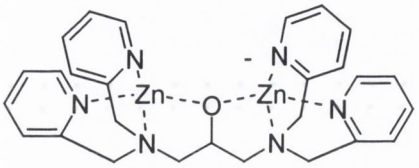

122

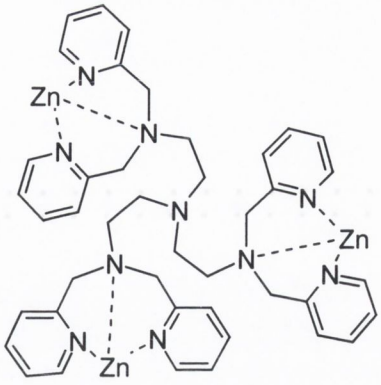

123

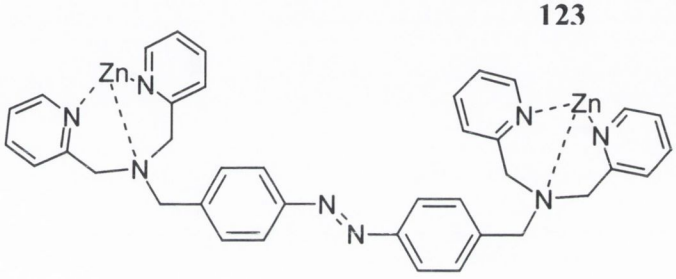

124

More recent research by the Planalp group[139,140] in 2001 showed copper complexes based on diaminocyclohexane **125** were efficient for the hydrolysis of RNA. The variations in the R groups give different properties and cleavage ability. When R=Me the cleavage ability was good, especially for DNA cleavage. The Clifford group developed large macrocyclic ligands to incorporate two metal centres[141]. The dinuclear Cu(II) complex **126** efficiently cleaved the DNA mimic DNPDEP. **126** has optimum cleavage at around pH 6 but when two water molecules are coordinated to the metal the optimum cleavage is at pH 11.

The Schneider group developed novel aromatic containing ligands to determine the effect of aromatic stacking on RNA catalysis[142]. The mononuclear Cu(II) complexes based on **127** showed that the presence of the aromatic groups acted as a cofactor in the catalytic Cu(II) complexes, which could be similar to the natural metal-based enzymes in increasing the catalytic ability using the RNA mimic BNPP. The copper complexes only gained catalytic ability with the introduction of a suitable ligand but it must be remembered that there must be free coordination sites on the metal to aid catalytic ability.

Stable lanthanide complexes have been successfully applied as RNA cleavers. Lanthanides were chosen for a number of reasons including their high ionic potential, high coordination number and good substitution lability. While the free lanthanide ions are

effective cleavers of RNA, their toxicity requires them to be fully encapsulated by an appropriate ligand.

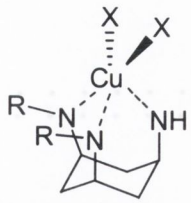

125

R	***X***
Me	Cl
Et	Cl
n-propyl	Cl
CH_2-Thienyl	Cl
CH_2-Furanyl	Cl
Et	Br
Et	H_20

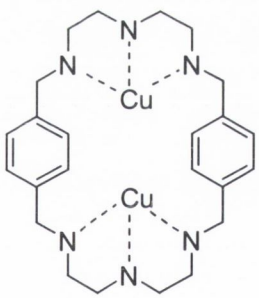

126

This ligand should also aid the catalytic ability of the complex. One of the first types of lanthanide complexes used for RNA hydrolysis was developed by Morrow and co-workers using cyclen derivatives as ligands for lanthanide ions[143,144]. Only the eight coordinate La(III) complex **128** efficiently hydrolyses RNA[143]. The complex is kinetically inert and remains intact *in vivo* at 37°C and at pH 6. According to the Morrow group, generally the later lanthanide ions are better cleavers of RNA because they are better Lewis acids[143]. The lanthanide complexes that do not have coordination sites for direct binding of phosphate ester substrates are relatively inefficient at promoting transesterification[144].

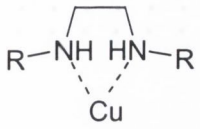

127

a: R = H

b: R =

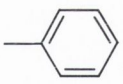

c: R =

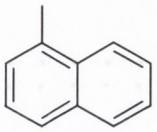

d: R =

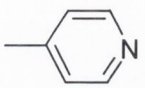

e: R =

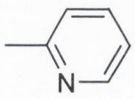

f: R = CH_3

1.27	**kobs(10^{-6} s^{-1})**
a	0.75
b	13.8
c	75.2
d	10.6
e	0.21
f	4.6

The Eu(III) complex of **128** was not an effective cleaver because there are no available coordination sites whereas the La(III) complex of **128** was because it had a free coordination position, which could bind to the diethyl phosphate. As has been stated before[106], the metal ion promotes the hydrolysis of phosphate esters and generally proceeds by the coordination of the phosphate ester to the metal and then intramolecular attack by coordinated water and hydroxy molecules. The Morrow group developed the cyclen derivative **129**, which contains hydroxy groups within the ligand[145]. The presence of the hydroxy groups help increase the efficiency of catalysis. The Schiff base ligand **130** was complexed to La(III) and Eu(III), and both these complexes were efficient in the hydrolysis of RNA mimics[144].

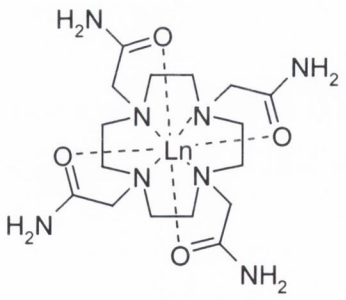

128

In 1992 Komiyama and co-workers used Ce(IV) clusters to catalyse the hydrolysis of RNA[146, 147,148]. A number of Schiff-base ligands were chosen to encapsulate the lanthanide ion to create novel lanthanide ion complexes. The La(III), Ce(III) and Eu(III) complexes of **132** and the La(III) and Ce(III) complexes of **132** were tested for the hydrolysis of tRNA[149]. These complexes are more selective than the free lanthanide ions.

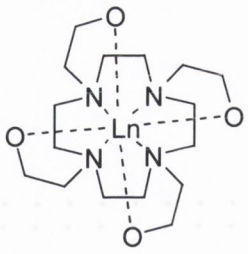

129

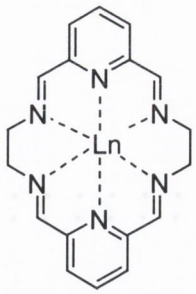

130

The site-selectivity and specificity depends on the ligand structure. Schneider and co-workers looked at a range of known, commercially available ligands complexed to Eu(III) for the cleavage of DNA[150]. They stated that the catalytic lanthanide ion must be within kinetically stable complexes. This immobilisation of the lanthanide ions can raise the affinity of the lanthanide ion for selective DNA cleavage. The ligands **133** to **136** were complexed to Eu(III) and the ratio of rate constants is shown in Table 3.3 . The Table shows these complexes can hydrolyse DNA with catalytic turnover comparable to ribonucleases using stable readily available ligands for lanthanide ion complexes. The catalytic ability of the lanthanide ion is retained even when it is complexed within kinetically and thermodynamically stable complexes. Importantly the ligands can be further modified to increase their effectiveness and selectivity[150].

Expanding on these results, Schneider and co-workers developed binuclear lanthanide complexes using Eu(III) and Pr(III)[151,152]. Complexes **139** to **141** were synthesised but the small metal-to-metal distance made them moderate cleavers of RNA mimics. The Eu(III) complex of **142** was more effective because the metal-to-metal bond distance was *ca.* 3Å. When EDTA was added there was no cleavage observed suggesting that the complexes were not stable to ligand exchange on binding to the metal complex[151].

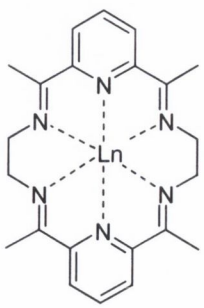

131

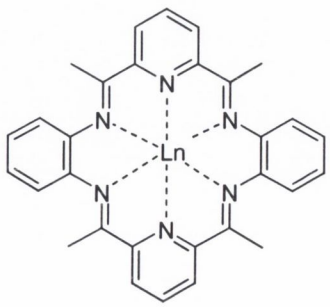

132

Compound	Ratio of Rate Constants
137	0.38
138	0.92
133	0.13
134	0.17
135	0.62
136	0.49

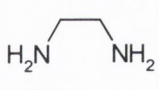

133

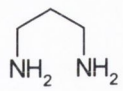

134

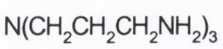

135

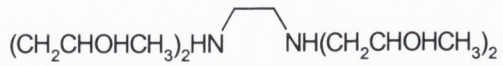

136

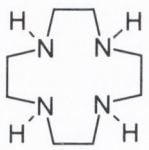

137

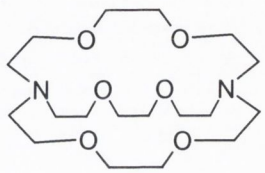

138

The Park group used cryptates to encapsulate lanthanide ions[153,154,155,156]. Ligand **143** was complexed to La(III), Ce(III) and Eu(III). These lanthanide ion complexes were good catalysts and the experiments showed the complex acted as a nucleophile[154]. No pH dependence on rate was observed due to the size of the lanthanide ions[153]. Studies on the dissociation kinetics found that the dissociation depended on the concentration of the complex[155] and on the concentration of the buffer[156]. The Häner group developed lanthanide complexes that could be covalently attached to oligoribonucleotides to cleave a partially complimentary RNA in a sequence specific manner[157]. The complexes they chose were the Schiff-base macrocycles **144** and **145**. These could be attached to the oligionucleotide *via* the amino group on **145** and the carboxylic acid group on **144**.

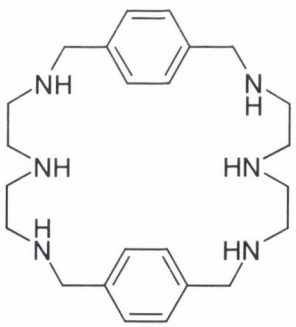

139

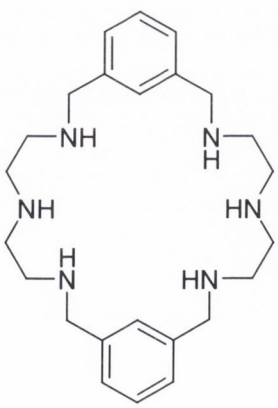

140

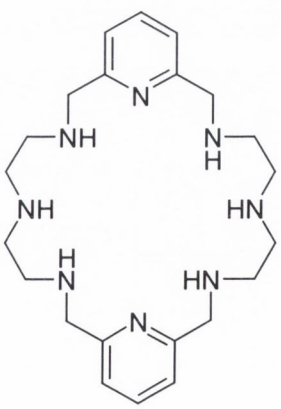

141

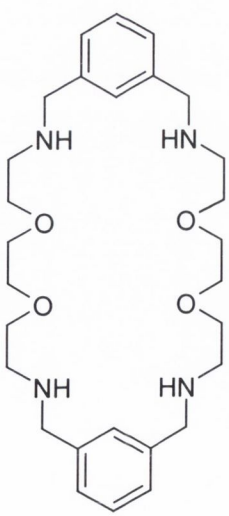

142

Further investigations into these complexes showed that the lanthanide ion had two bound water molecules, which were replaced by the phosphate ester during cleavage[158]. This chapter will now discuss the synthesis and evaluation of a bispyridyl acyclic ligand **L** for transition metals for efficient hydrolysis of the RNA-mimic HPNP.

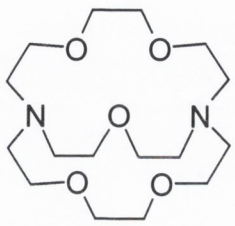

143

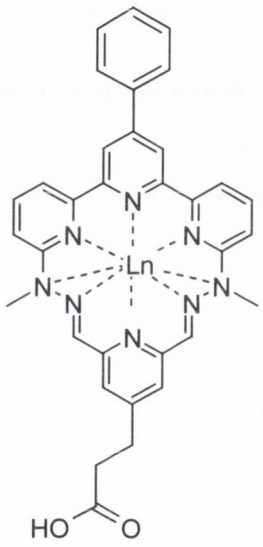

144

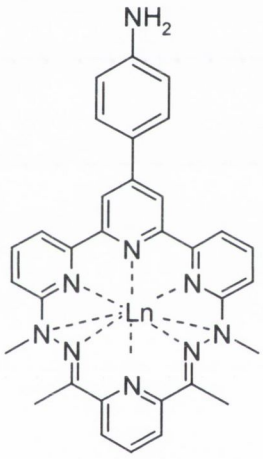

145

3.2 Design of a Catalyst for RNA Hydrolysis

As discussed above it is important that the ligand contain coordination sites for strong binding with the presence of a metal-bound water molecule being an advantage in the complex. The previous work by Chin, Morrow, Reinhoudt *etc* has shown that the ligand must

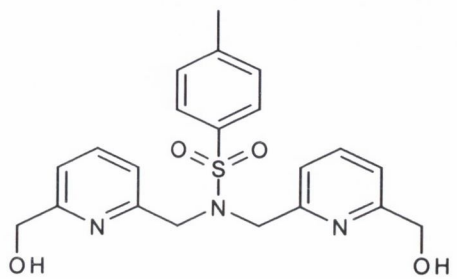

L

also contain a metal bound water molecule or a hydroxy group to achieve efficient RNA hydrolysis. To this end a ligand **96** N-bis[[6-(hydroxymethyl)pyrid-2-yl[methyl]-*p*-tosylamide (hereon known as **L**), an intermediate in the synthesis of the pyridinophane **86** as discussed in chapter 2, was chosen to be ligand for the complexation of transition metal ions. The presence of the hydroxy groups is also advantageous for the hydrolysis of RNA. It contains many chelating groups for the complexation of transition metal ions. A crystal structure of **L**, Figure 3.4, was obtained showing interesting properties. **L** was found that the ligand had a box-like shape with the pyridine moieties parallel to each other but not undergoing intramolecular π–π stacking. The hydroxymethyl groups were constrained by hydrogen bonding to water molecules. This is discussed fully in section 3.4. The crystal structure showed that **L** had the potential to complex transition metals because it is an open molecule with many of the chelating groups available for complexation. The introduction section above discussed many types of metal complexes used as RNA catalysts, which highlighted the main requirements for ligands to be potential RNA catalysts principally, they are to contain hydroxy groups, have strong binding ability and also leave free coordination sites on the metal ion to aid catalytic ability. It was decided to complex **L** to transition metal ions, Cu(II), Zn(II), Ni(II), Fe(II) and Co(II), because transition metal complexes have been found to be useful catalysts for the hydrolysis of RNA as discussed above[131,135,142].

3.3: Synthesis of the Catalyst for RNA Hydrolysis:

Developing from these basic ideas, a ligand **L** (*N,N*-bis[[6-(hydroxymethyl)pyrid-2-yl[methyl]-*p*-tosylamide) **96**, an intermediate in the synthesis of the pyridinophanes in Chapter 2, was chosen as a potential ligand for transition metal ion complexes for the catalytic cleaving of model RNA moieties. The molecule **L** was synthesised according to a modified procedure by Miyahara[159] *et al* according to scheme 2.9 in chapter 2. The transition metal complexes of **L.Fe(II)**, **L.Cu(II)**, **L.Co(II)**, **L.Zn(II)** and **L.Ni(II)** were all prepared by dissolving **L** in dry CH_3CN and adding one equivalent of the corresponding anhydrous perchlorate metal salt and recrystallising in a diethyl ether atmosphere. For **L.Cu(II)**, the complex was formed from the $Cu(ClO_4)_4MeCN$ salt and subsequent oxidation in air yielded the **L.Cu(II)** complex as green crystals. The **L.Zn(II)** complex was formed from the zinc perchlorate salt yielding colourless crystals. The **L.Fe(II)** complex was formed from the iron perchlorate salt yielding brown crystals. The **L.Ni(II)** complex was formed from the nickel perchlorate salt yielding pale blue crystals. The **L.Co(II)** complex was formed from the cobalt perchlorate salt yielding pink crystals. All complexes were fully characterised by CHN,

ESMS and IR, UV and fluorescence. Spectroscopy. **L.Cu(I)** and **L.Zn(II)** were also analysed by ^{1}H and ^{13}C NMR.

3.4 Crystal Structures Of The Catalysts

Crystals of **L**, **L.Cu(II)**, **L.Fe(II)**, **L.Ni(II)**, **L.Co(II)** and **L.Zn(II)** were grown, which were suitable for single crystal X-ray crystallographic determination. Data were collected on a Brücker SMART diffracter at *ca.* 153K by Dr. Mark Nieuwenhuyzen from Queens University, Belfast. The first crystal structure determined was of **L** (fig. 3.4). The asymmetric unit of **L** contains **L** with two water molecules. There are no intramolecular π-π stacking interactions between the pyridine moieties because they are not perpendicular to one another. The hydroxymethyl interactions are influenced by hydrogen-bond interactions. The molecule is further constrained by water-OH and water-N hydrogen bonds.

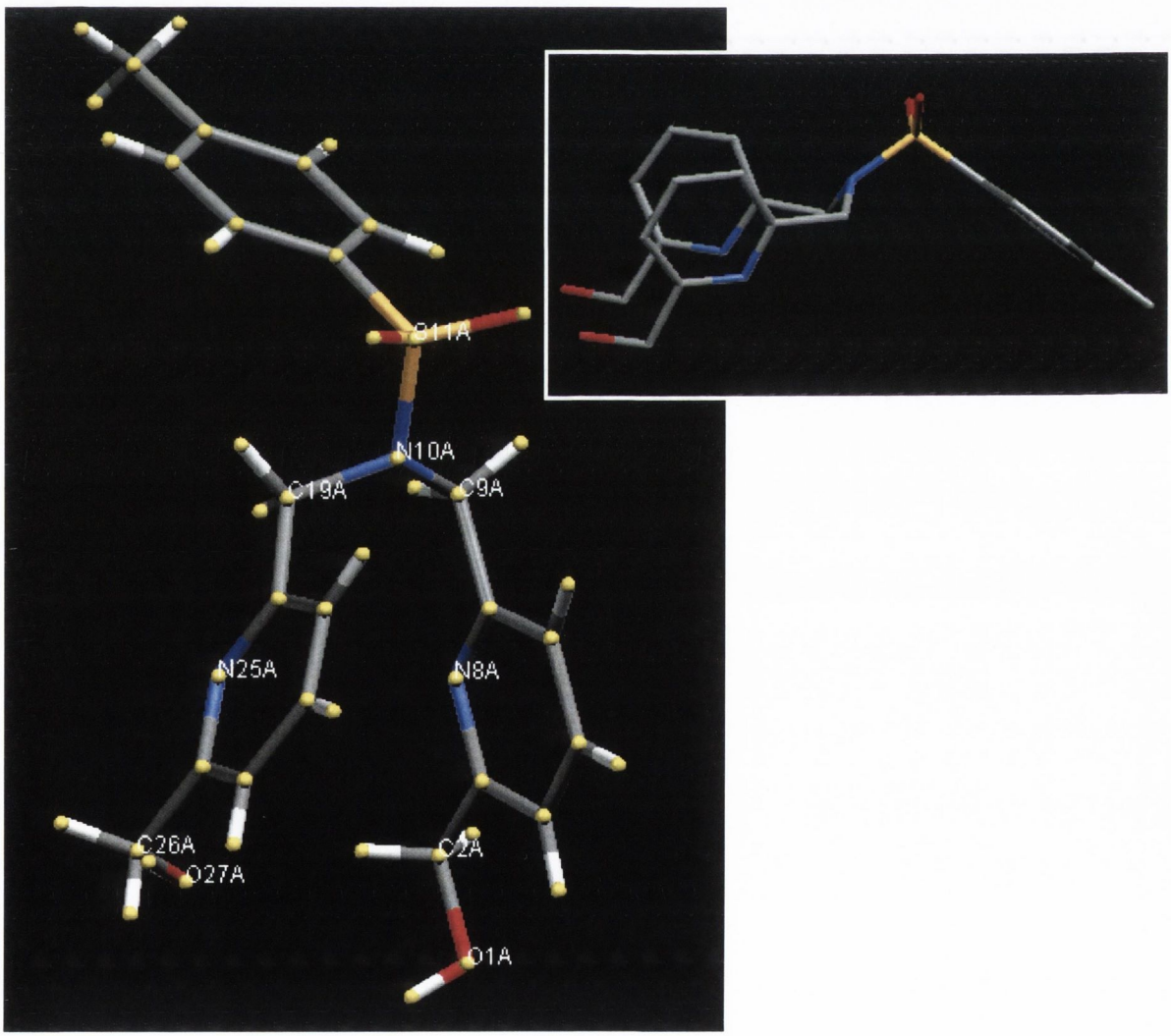

Fig. 3.4: Crystal structure of L. The inset demonstrates the backwards bending of the tosyl moiety from the pyridine groups.

The crystal structure of **L.Fe(II)** (Figure 3.5) is composed of $[\mathbf{L}.Fe(CH_3CN)_2](ClO_4)_2$. Fe(II) is coordinated to one ligand **L** and two CH_3CN molecules with CH_3CN in an axial position to **L**. The cations are hydrogen bonded to the anions via the oxygen of the hydroxy groups of **L**. There is a weak bond from the nitrogen of the tosylamide group and Fe(II). The metal is coordinated via the hydroxy group and the two nitrogen atoms on the pyridine moieties. This leaves a six-coordinated metal centre. It should be noted that the benzyl ring of the tosyl group is parallel to the two pyridine rings.

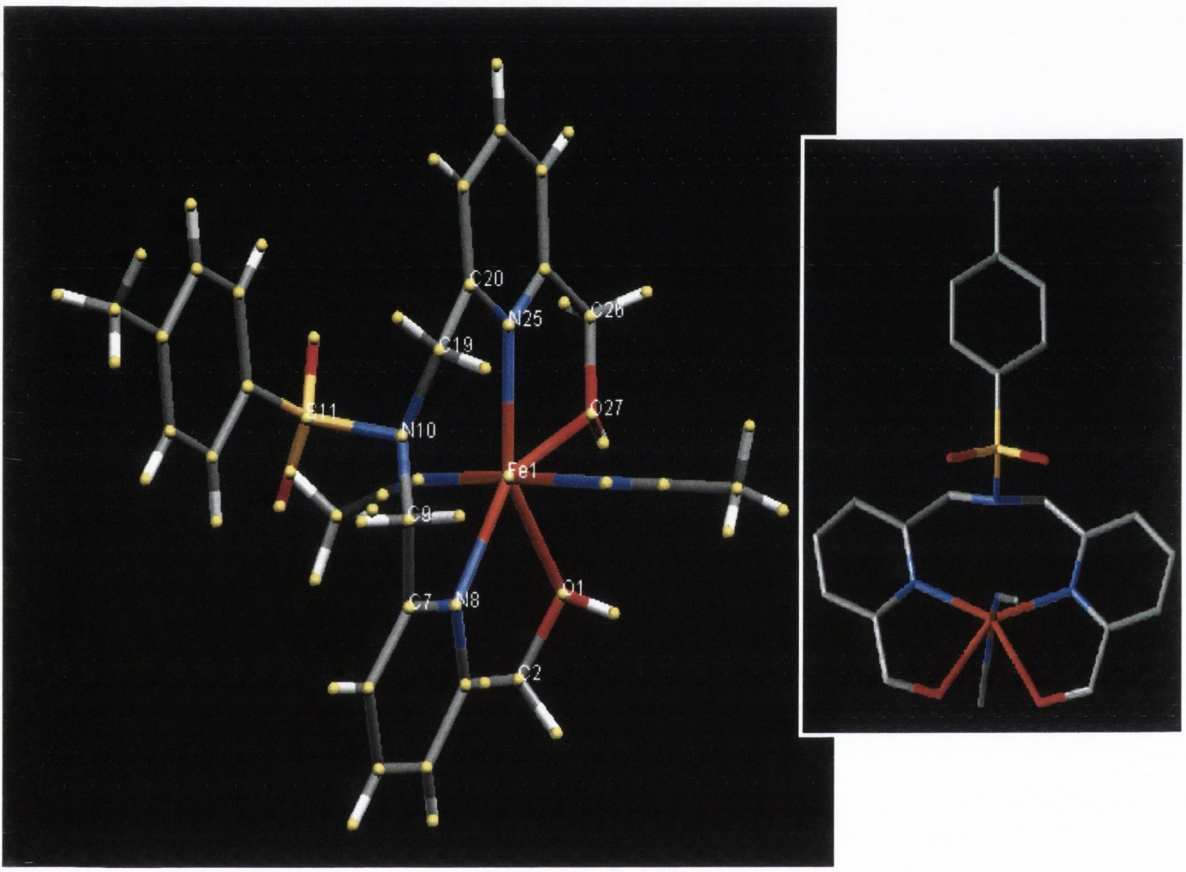

Fig. 3.5: Crystal structure of L.Fe(II) and numbering scheme. The dashed line shows the weak bond between N10 and Fe. The inset shows the complex from another angle with the hydrogens omitted for clarity. The inset shows the complex from another angle.

For **L.Fe(II)** and **L.Co(II)** the d_x^2-d_y^2 orbital of the metal is vacant resulting in a weak bond to the nitrogen on the tosylamide moiety. This nitrogen has a pyramidal conformation with the crystal structure of **L.Co(II)** (Figure 3.6) composed of $[\mathbf{L}.Co(CH_3CN)_2](ClO_4)$ with two solvate molecules, H_2O and two CH_3CN molecules that are coordinated in an axial position. The coordination environment around the Co(II) results in the benzyl ring of the tosyl moiety being parallel to the two pyridine rings. The metal is strongly coordinated to the two hydroxy groups and the two nitrogens of the pyridine rings. There is a weak bond between Co(II) and

the nitrogen of the tosylamide moiety lone pairs "directed" towards the metal. Co(II) is coordinated to one ligand molecule via the pyridine nitrogens and the hydroxy groups and to two MeCN solvent molecules.

The crystal structure of **L.Ni(II)** (Figure 3.7) is composed of [**L**.Ni(II)$(CH_3CN)_2$]$(ClO_4^-)_2$ where the cations are bound to the anions via the oxygen of the hydroxy group. The metal ion is coordinated to one ligand group in an equatorial position with two CH_3CN molecules coordinated in an axial position resulting in a distorted octahedral conformation. Again the metal is strongly coordinated to the two hydroxy groups and the nitrogens of the pyridine rings.

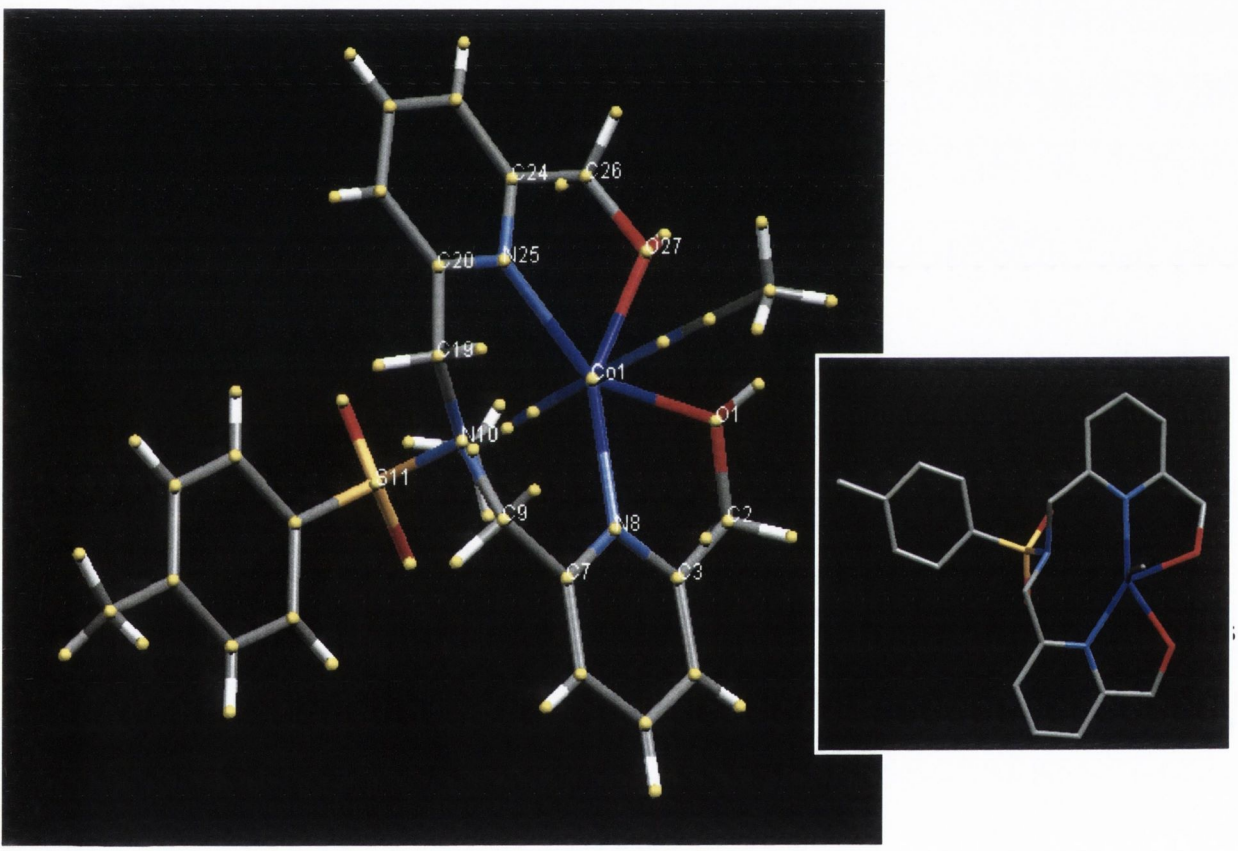

Fig. 3.6: Crystal structure of L.Co(II) and numbering scheme. The dashed line shows the weak bond between N10 and Co(II). The inset shows the complex from another angle with hydrogens omitted for clarity

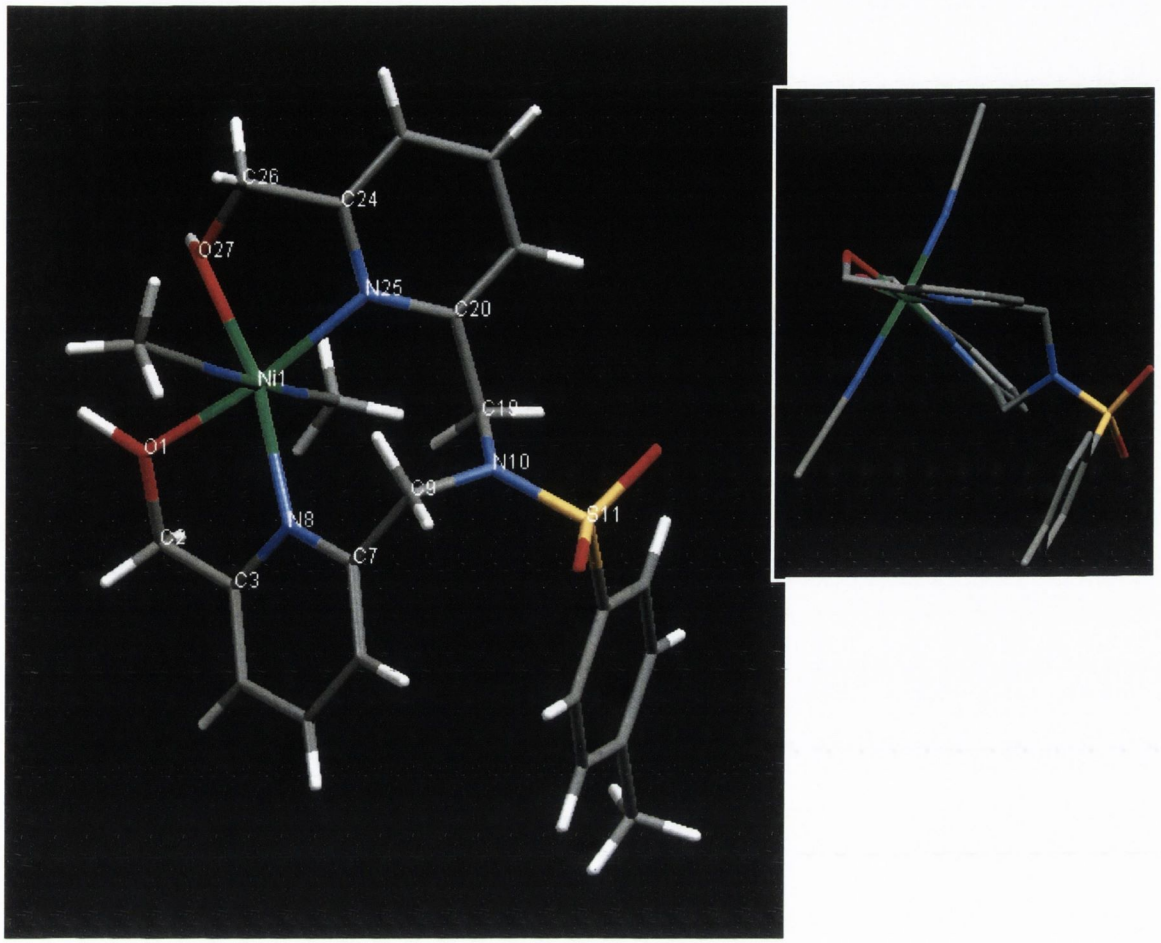

Fig. 3.7: Crystal structure of L.Ni(II) and numbering scheme. The inset shows the complex from another angle

It is significantly different to **L.Fe(II)** and **L.Co(II)** as the lone pair of the nitrogen on the tosylamide moiety is not directed towards the metal. Also the benzyl ring of the tosyl group is no longer parallel to the two pyridine rings, in fact they are almost orthogonal to each other resulting in the alteration of the cation packing. The cations are associated in layers via two types of π-π interaction: firstly via inter-tosylate moiety on the a axis and secondly inter-pyridine. The layers are packed in such a way that the methyl groups of CH_3CN are directed towards the pyridine rings.

The conformation of **L.Cu(II)** (Figure 3.8) can best be described as square-based pyramidal. It is a dimer of the form [$\mathbf{L}_2$Cu] with one of the hydroxyl groups deprotonated, which then acts as a bridging moiety. The Cu---Cu contact is 2.970Å. There are no associated solvent molecules. The "vacant" coordination sites are occupied by the N-SO_2 functionalities on the tosyl amide group with the lone pair on the nitrogen directed towards Cu---Cu. The inset

shown in figure 3.8 shows the complex from another angle and suggests the complex has a somewhat helical shape in its solid state.

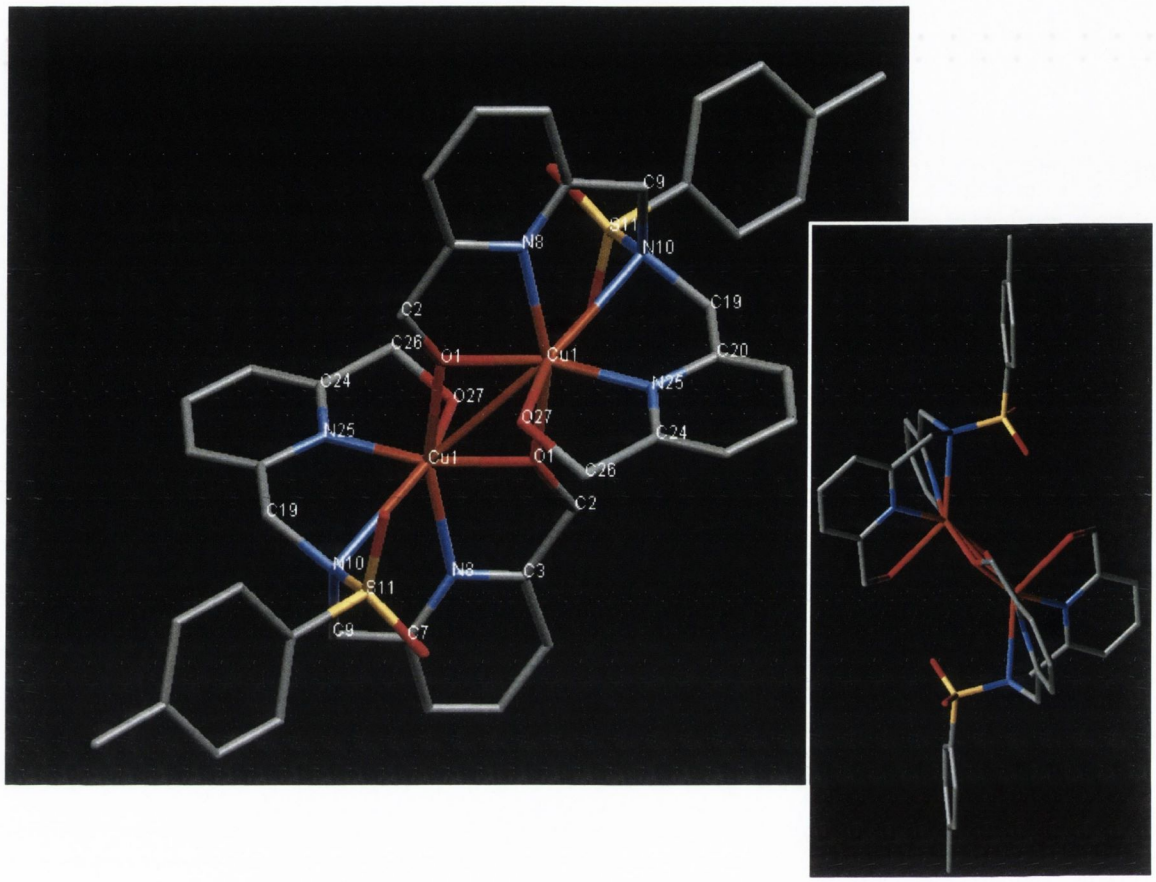

Fig. 3.8: Crystal structure of L.Cu(II) and numbering scheme. Hydrogens removed for clarity. The inset demonstrates the helical nature of the complex.

The crystal structure of **L.Zn(II)** (Figure 3.9) is best described as distorted trigonal bipyramidal with the apical atoms being the nitrogens of the pyridine moieties and oxygen of the associated water molecule. It has the form $[\mathbf{L}.Zn(CH_3CN)(H_2O)](ClO_4)_2$. It has a similar conformation to **L.Cu(II)** (Figure 3.7) by comparing the dihedral angle of the backbone at – 142.5° and 132.9° and the angle between the mean plane of the pyridine group of 101.5° and 81.5° for Zn and Cu respectively. The nitrogen of the tosylamide group is able to direct its lone pair to the metal with a bond length of 2.619Å.

Overall the crystal structures provide a number of interesting results. A comparison of the torsional angles of C7-C9-N10-C19 for all the metal complexes confirms the ligand, in four out of five complexes, has similar conformations except **L.Ni(II)**. In **L.Fe(II)**, **L.Co(II)**

and **L.Ni** the pyridine rings are essentially coplanar with the angles being 15°, 18° and 37° respectively.

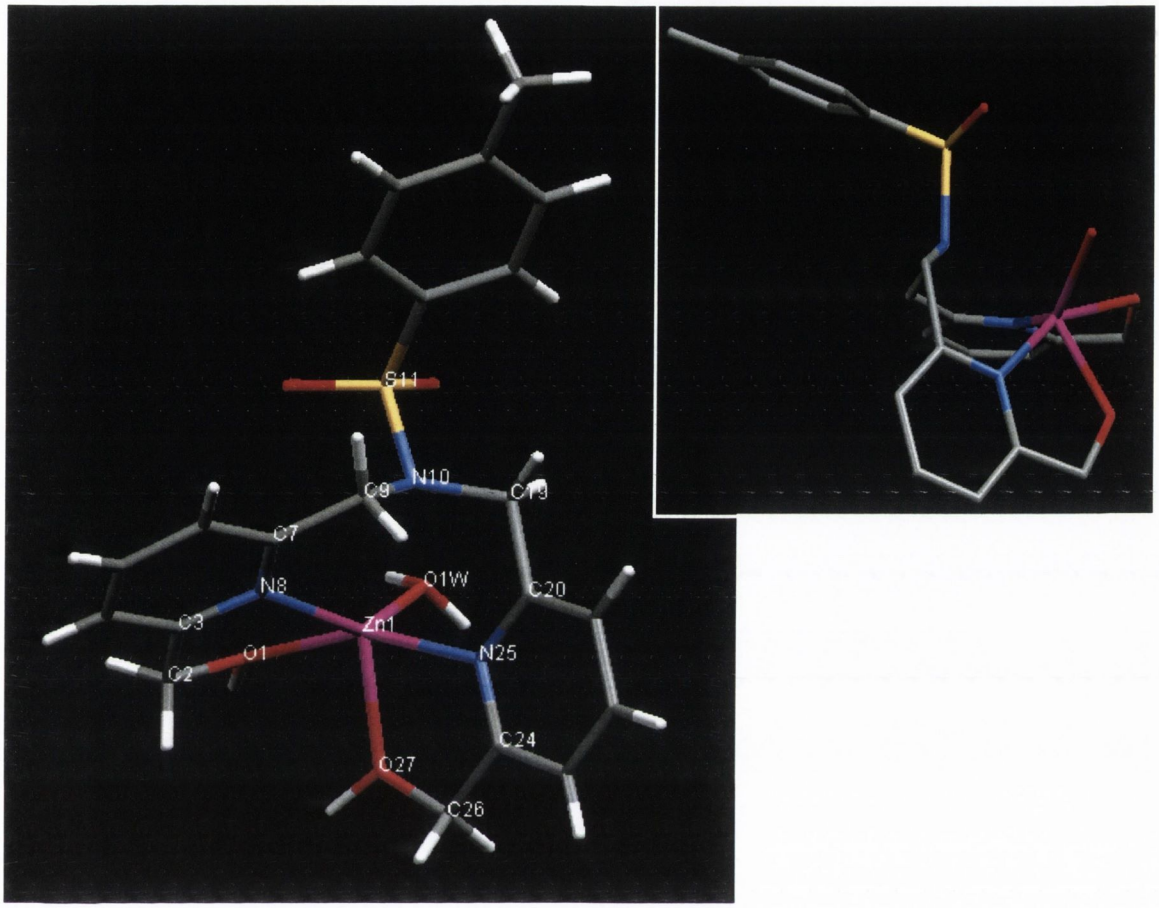

Fig. 3.9: Crystal structure of L.Zn(II) and numbering scheme. The inset shows the complex from another angle. Notice the tosyl group is bent away from the pyridyl groups.

For these complexes a comparison of the angle of the pyridine rings to the benzyl ring in the tosyl group is also useful as shown in Table 3.3. Table 3.4 shows some selected bond lengths and bond angles for the transition metal complexes.While the metal centres of these three complexes have a distorted octahedral conformation, the distortion on **L.Fe(II)** and **L.Co(II)** is more pronounced with a maximum deviation of 17-18° from 90° for O1-N8 and O27-N25 bite angles for **L.Fe(II)** and **L.Co(II)** compared to 13° and 10° for O1-N8 and O27-N25 bite angles in **L.Ni(II)**. The smaller bite angle for **L.Fe(II)** and **L.Co** may be due to an increased constraint on **L** because of weaker interaction between the metal and nitrogen on the tosylamide thus pulling **L** tighter to the metal. The ability of this nitrogen to interact with the metal depends on the d_x^2-d_y^2 orbital being unoccupied.

COMPLEX	TORSIONAL ANGLES		
	C7-C9-N10-C19	C3-C4-C5-C6-C7-N8	C20-C21-C22-C23-C24-N25
L.Cu(II)	**-133**	---	---
L.Zn(II)	-143°	---	---
L.Fe(II)	-153°	12°	3.4°
L.Co(II)	-150°	1.7°	9.3°
L.Ni (II)	66°	103°	73°

Table 3.3: Table showing some torsional angles for the various complexes.

The crystal structures of **L.Cu(II)** and **L.Zn(II)** suggest these complexes will be the best for RNA cleavage because their geometry favours phosphate ester binding. For **L.Cu(II)** the vacant coordination sites imply increased Lewis acid activation. For **L.Zn(II)** the bound water molecule could possibly activate the 2'-hydroxy group through nucleophilic activation. Conceivably the water molecule could be replaced by a negatively charged phosphate diester which can give rise to strong Lewis acid activation.

3.5 Spectroscopic Investigations into the Catalysts

UV, Fluorescence and NMR measurements were carried out on **L** using the metal salts (^{1}H NMR only run with Cu(I) and Zn(II)) to determine the binding constants and to see if the solution state complexes compare to the solid state of the crystal structures.

3.5.1 UV-Visible and Fluorescence Studies:

The UV and fluorescence studies were carried out on Cu(II), Zn(II), Co(II) and Ni(II) in MeCN and water at physiological pH with 0.1 M ionic strength and 0.1 M tris buffer, depending on solubility. Studies could not be run on Fe(II) due to solubility problems.

From the absorption spectra of **L** in MeCN two absorption bands at 231 and 267 nm with a shoulder at 274 nm were seen. Upon titration with $ZnClO_4$ changes were seen in the UV absorption spectra of **L** (Figure 3.10). The decrease in intensity seen at 267 nm was assigned to the pyridine moieties in **L** with a slightly blue shift to 265 nm upon titration with Zn(II). An isobestic point was seen at 256 nm indicating simple equilibrium. There was a slight red shift at 232 nm but this was only mildly affected by the titration of Zn(II). The changes in intensity in the fluorescence spectra upon titration of Zn(II) and excitation at 267 nm were more obvious as seen in Figure 3.10.

L·Fe(II)

Fe(1)-N(4S)	2.170(4)	N(4S)-Fe(1)-O(27)90.54(14)	
Fe(1)-O(27)	2.173(3)	N(4S)-Fe(1)-N(25)86.94(13)	
Fe(1)-N(25)	2.178(4)	O(27)-Fe(1)-N(25)71.94(15)	
Fe(1)-N(8)	2.180(4)	N(4S)-Fe(1)-N(8)90.71(13)	
Fe(1)-N(1S)	2.186(4)	O(27)-Fe(1)-N(8)146.12(15)	
Fe(1)-O(1)	2.216(3)	N(25)-Fe(1)-N(8)141.93(14)	
		N(4S)-Fe(1)-N(1S)173.89(14)	
		O(27)-Fe(1)-N(1S)86.34(14)	
		N(25)-Fe(1)-N(1S)97.06(13)	
		N(8)-Fe(1)-N(1S)88.97(14)	
		N(4S)-Fe(1)-O(1)90.69(13)	
		O(27)-Fe(1)-O(1)73.84(15)	
		N(25)-Fe(1)-O(1)145.66(15)	
		N(8)-Fe(1)-O(1)72.29(14)	
		N(1S)-Fe(1)-O(1)83.40(13)	

L·Ni(II)

Ni(1)-O(1)	2.036(3)	O(1)-Ni(1)-O(27)91.44(13)	
Ni(1)-O(27)	2.051(3)	O(1)-Ni(1)-N(1S)89.93(14)	
Ni(1)-N(1S)	2.073(4)	O(27)-Ni(1)-N(1S)84.91(14)	
Ni(1)-N(4S)	2.078(4)	O(1)-Ni(1)-N(4S)87.15(14)	
Ni(1)-N(25)	2.094(4)	O(27)-Ni(1)-N(4S)92.31(14)	
Ni(1)-N(8)	2.113(3)	N(1S)-Ni(1)-N(4S)175.92(15)	
		O(1)-Ni(1)-N(25)170.53(13)	
		O(27)-Ni(1)-N(25)79.85(13)	
		N(1S)-Ni(1)-N(25)92.96(14)	
		N(4S)-Ni(1)-N(25)89.48(14)	
		O(1)-Ni(1)-N(8)76.91(13)	
		O(27)-Ni(1)-N(8)166.95(13)	
		N(1S)-Ni(1)-N(8)89.17(14)	
		N(4S)-Ni(1)-N(8)92.94(14)	
		N(25)-Ni(1)-N(8)112.12(14)	

L·Co(II)

Co(1)-N(4S)	2.104(4)	N(4S)-Co(1)-N(1S)174.61(12)	
Co(1)-N(1S)	2.135(4)	N(4S)-Co(1)-N(25)94.27(13)	
Co(1)-N(25)	2.171(4)	N(1S)-Co(1)-N(25)88.02(13)	
Co(1)-N(8)	2.174(3)	N(4S)-Co(1)-N(8)92.61(13)	
Co(1)-O(27)	2.195(3)	N(1S)-Co(1)-N(8)88.53(13)	
Co(1)-O(1)	2.214(3)	N(25)-Co(1)-N(8)142.34(12)	
		N(4S)-Co(1)-O(27)86.62(12)	
		N(1S)-Co(1)-O(27)89.41(12)	
		N(25)-Co(1)-O(27)72.68(12)	
		N(8)-Co(1)-O(27)144.76(12)	
		N(4S)-Co(1)-O(1)83.70(12)	
		N(1S)-Co(1)-O(1)91.60(12)	
		N(25)-Co(1)-O(1)144.43(12)	
		N(8)-Co(1)-O(1)73.15(11)	
		O(27)-Co(1)-O(1)71.75(11)	

L.Cu(II)

Cu(1)-O(1)'	1.908(5)	O(1)'-Cu(1)-O(1)	78.4(2)
Cu(1)-O(1)	1.925(5)	O(1)'-Cu(1)-N(8)	157.6(2)
Cu(1)-N(8)	1.999(6)	O(1)-Cu(1)-N(8)	80.2(2)
Cu(1)-N(25)	2.027(6)	O(1)'-Cu(1)-N(25)	95.6(2)
Cu(1)-O(27)	2.419(6)	O(1)-Cu(1)-N(25)	162.4(3)
Cu(1)-Cu(1)'	2.970(2)	N(8)-Cu(1)-N(25)	106.8(3)
		O(1)'-Cu(1)-O(27)	92.4(2)
		O(1)-Cu(1)-O(27)	87.6(2)
		N(8)-Cu(1)-O(27)	93.4(2)
		N(25)-Cu(1)-O(27)	76.0(2)

L·Zn(II)

Zn(1)-O(1W)	2.003(2)	O(1W)-Zn(1)-N(8)	138.22(11)
Zn(1)-N(8)	2.038(3)	O(1W)-Zn(1)-N(25)	97.25(10)
Zn(1)-N(25)	2.092(3)	N(8)-Zn(1)-N(25)	110.77(11)
Zn(1)-O(27)	2.109(2)	O(1W)-Zn(1)-O(27)	100.40(10)
Zn(1)-O(1)	2.134(2)	N(8)-Zn(1)-O(27)	115.78(11)
		N(25)-Zn(1)-O(27)	75.87(10)
		O(1W)-Zn(1)-O(1)	90.09(10)
		N(8)-Zn(1)-O(1)	76.15(10)
		N(25)-Zn(1)-O(1)	157.05(11)
		O(27)-Zn(1)-O(1)	81.43(10)

Table 3.4: Selected bond lengths and bond angles for the transition metal complexes.

It is known that pyridine containing ligands, such as 1,10-phenanthroline and bipyridine, give rise to strong fluorescence changes in the presence of Zn(II) due to strong MLCT excited states[160,161,162]. No quenching effect was expected because the d^{10} shell of Zn(II) and its complexation to a ligand does not usually introduce low energy metal-centred excited states, therefore energy transfer and electron transfer processes cannot occur[163]. The d^{10} shell of Zn(II) is half-filled and is therefore not expected to donate an electron to quench

fluorescence because of this stability. Therefore it was not unexpected that a strong increase in emission was seen. The emission spectra of **L** in MeCN without the presence of Zn(II) consisted of a major emission band at 295 nm with a shoulder at 345 nm when excited at 267 nm.

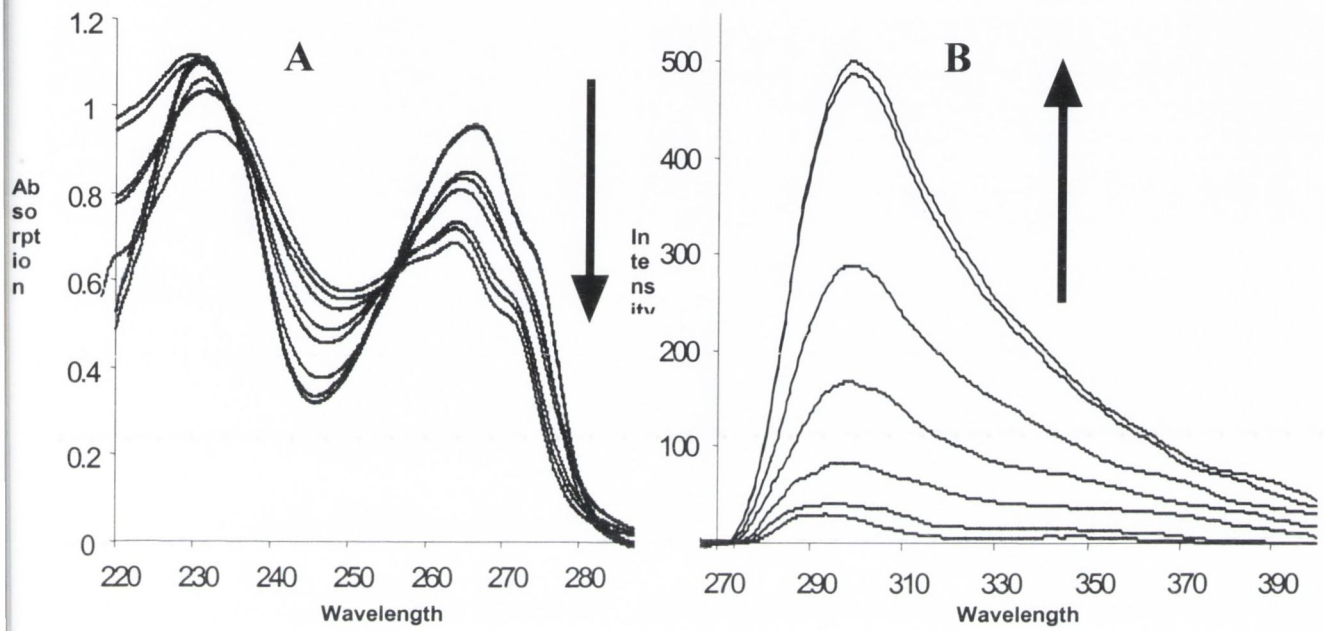

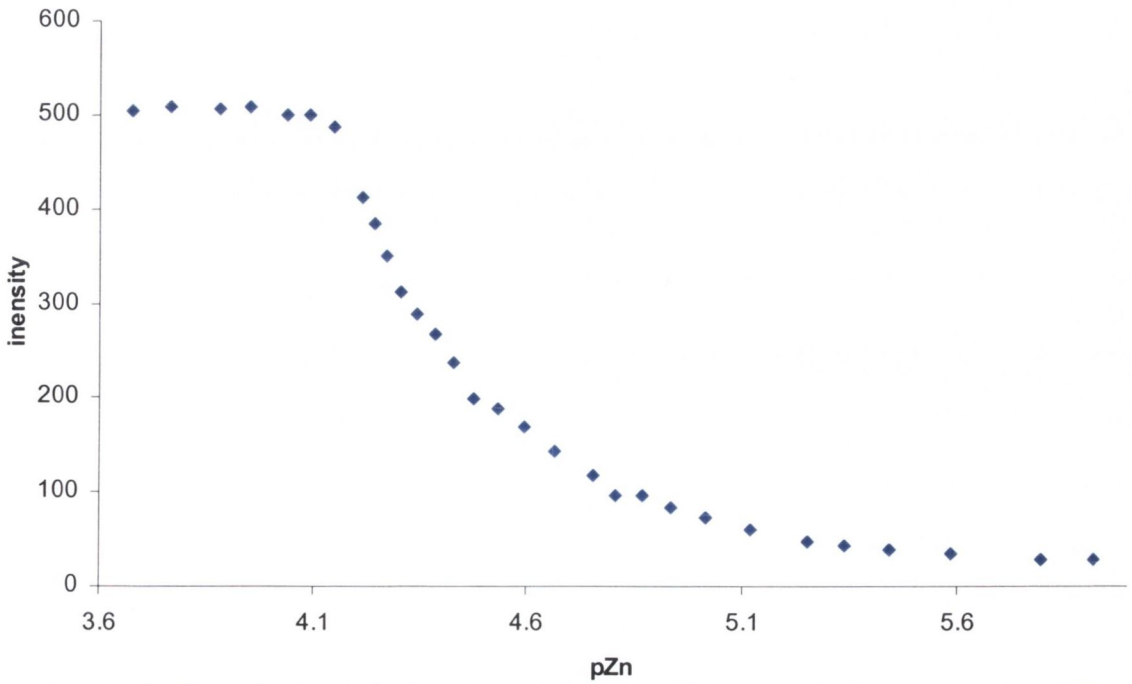

Fig. 3.11: Sigmoidal graph showing 1:1 binding of L to Zn(II) when excited at 267 nm.

Upon titration of **L** with Zn(II) ([Zn(II)] = 0→ 0.32 mM), the fluorescence intensity was increased giving a fluorescent enhancement of *ca.* 23 with an accompanying red shift from 295 nm to 300 nm as shown in Figure 3.10 B. Plotting the changes in intensity at 300 nm as a function of Zn(II) concentration gave a sigmoidal shaped curve indicating a 1:1 binding and simple equilibrium with log β = 4.4 (± 0.1)[∝] as shown in Figure 3.11[164].

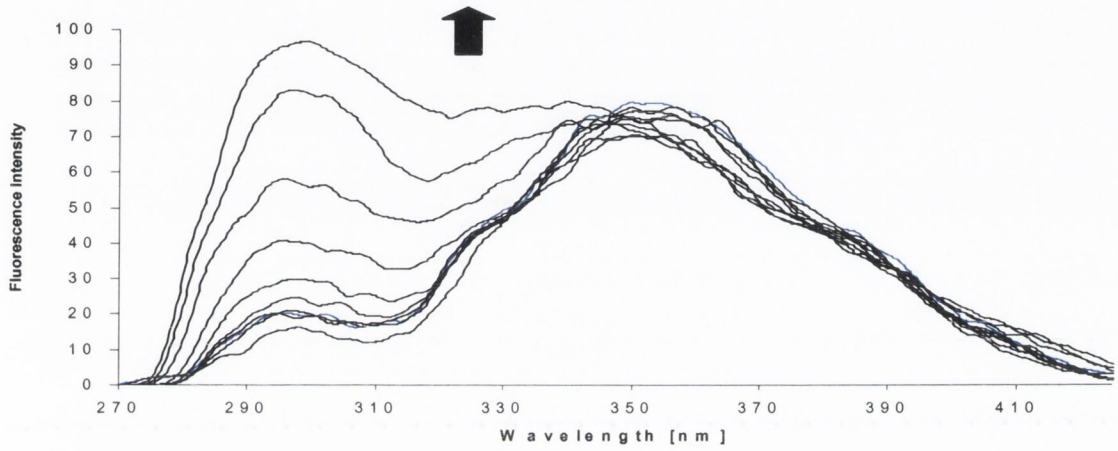

Fig. 3.12: Fluorescence spectrum of L upon titration of Cu(II) [0 -0.16mM].

In water at pH 7.4, the absorption and fluorescence spectra changes are less dramatic upon titration with Zn(II). The absorption spectra showed a slight increase in absorption at 265 nm. There was no shift at this wavelength. The corresponding fluorescence spectrum shows a major emission band at 352 nm with a shoulder at 295 nm. Upon titration with Zn(II) there was a slight increase in emission at 352 nm. The shoulder at 295 nm showed an increase in intensity of *ca.* 8 fold increase in intensity. Plotting the fluorescence intensity as a function of Zn(II) concentration gave a sigmoidal shaped curve where log β = 2.4 (± 0.1) with 1:1

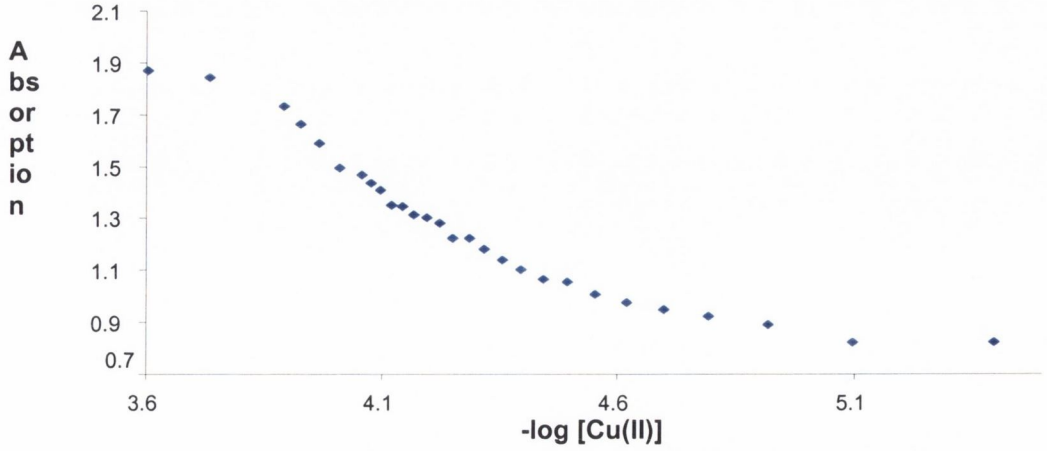

Fig. 3.13: Sigmoidal graph showing 1:1 binding for L with Cu(II)

[∝] Binding constant is found by plotting $[(I-I_{fmax})/(I_{fmin}-I)]$ versus $-\log(M^{n+})$

binding and simple equilibrium.

The titration of **L** with Cu(II) in CH_3CN gave significantly different results compared to those of Zn(II). Upon titration with Cu(II) the absorption spectrum of **L** in CH_3CN the peak at 274 nm increased slightly with no accompanying shift in wavelength. The peak at 235 nm increased in intensity from an absorption of 0.7 to 1.4 with a slight red shift to 230 nm. Plotting absorptions versus pCu gave a sigmoidal shaped curve with log β = 4.2 ($\pm$ 0.1)[164] (Figure 3.13). The sigmoidal curve was over two pCu units suggesting 1:1 binding and simple equilibrium. The fluorescence spectrum of **L** upon titration with Cu(II) leads to fluorescence quenching where the emission at 355 nm was fully quenched after the addition of 0.16 mM of Cu(II). This was expected because the Cu(II) was able to participate in electron transfer to the metal and subsequently quench fluorescence[160]. No measurements on **L** in water using Cu(II) were run due to solubility problems.

Upon addition of Ni(II) to **L** in CH_3CN gave rise to spectral changes. In the absorption spectra the peak at 265 nm was reduced with a slight red shift to 268 nm (Figure 3.14). Plotting the absorption changes *vs.* pNi resulted in a binding constant of log β = 4.5 ($\pm$ 0.1) (Figure 3.17). No major changes was seen in the fluorescence spectra of **L** upon titration with Ni(II) in MeCN. When the measurements were repeated in water at pH 7.4 with 0.1 mM TRIS

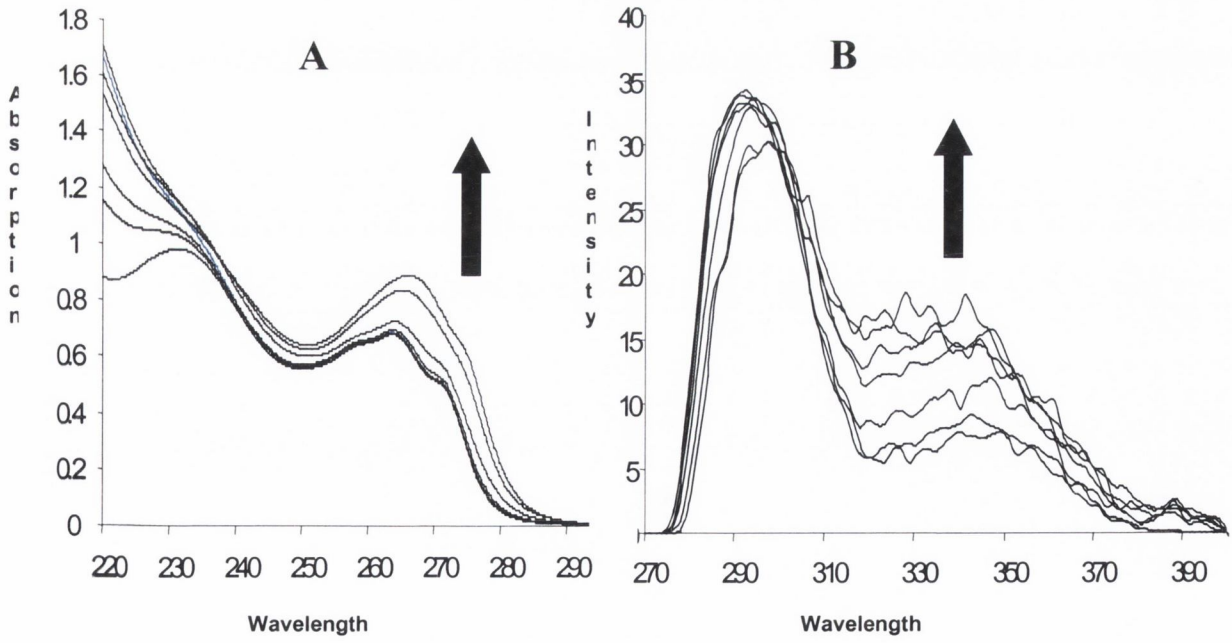

Fig 3.14: A: Absorption spectrum for titration of L with Ni(II); B: Fluorescent spectrum for titration of L with Ni(II) in MeCN.

buffer using tetramethylammonium chloride to maintain constant ionic strength the addition of Ni(II) yielded some changes were seen in the fluorescence spectra at high concentration but no changes were observed in the absorption spectra. No changes were seen in the fluorescence and absorption spectrum of **L** in water at pH 7.4 upon addition of Co(II). These measurements were not carried out in MeCN due to solubility problems.

The results of photophysical investigations suggest that L can selectively detect Zn(II) over Cu(II), Co(II) and Ni(II) in either water or CH_3CN. Therefore **L** can be considered as a fluorescent chemosensor for Zn(II). Zn(II) plays an important role in many cellular processes and any variation from normal concentration is normally associated with many neurological diseases such as Alzheimer's syndrome[160,162].

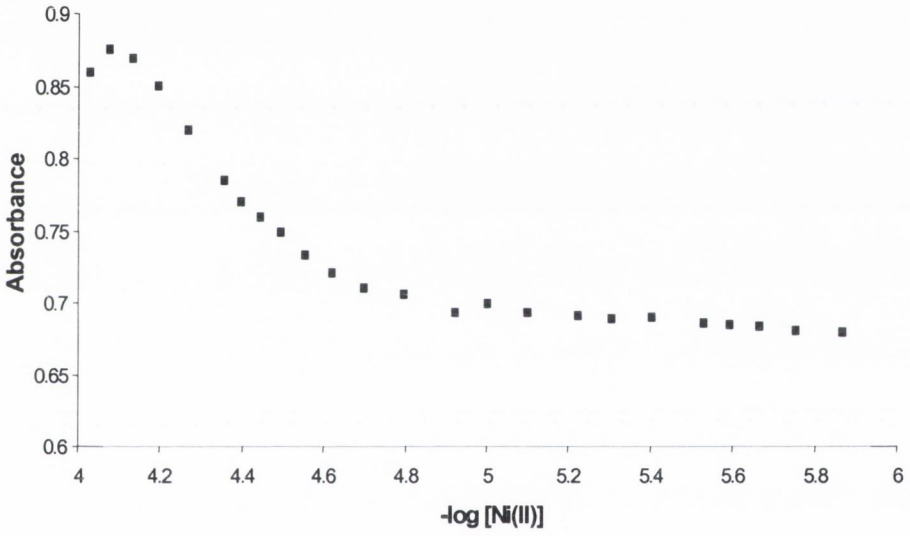

Fig. 3.15: Sigmoidal graph showing 1:1 binding for L with Ni(II) in MeCN upon excitation at 265 nm

Canary and co-workers suggest that many fluorescent chemosensors for Zn(II) suffer from interference by the binding of Cu(II) forming more stable complexes[165]. Burdette *et al* suggest that for efficient Zn(II) chemosensors the sensor must be selective for Zn(II) (especially over Cu(II)), have excitation wavelengths exceeding 340 nm and have emission wavelengths approaching 500 nm to avoid autofluorescence from fluorescing species present in the biological media[162]. Unfortunately **L** only achieves one of these criteria in that it is selective for Zn(II) over Cu(II). The excitation wavelength for **L** was 267 nm with an emission band at approximately 300 nm in MeCN.

Transition Metal	*Solvent*	*UV-Vis λ (nm)*	*Extinction coefficient*	*Emission λ (nm)*
Cu(II)	**MeCN**	265	6247	355
	H_2O	-----	-----	-----
Zn(II)	**MeCN**	266	2868	295
	H_2O	265	1885	352
Ni(II)	**MeCN**	263	2476.4	295, 345
	H_2O	265	1667	295
Co(II)	**MeCN**	-------	-------	-------
	H_2O	272.5	1884	345

Table 3.5: Luminescent data for all transition metal complexes. For L the UV spectra showed peaks at 231 and 267 nm. All excited at 267 nm. No measurements were run using Co(II)

3.5.1 ^{1}H NMR Investigations

The complexation of **L** with the diamagnetic ions Cu(I) and Zn(II) was observed using ^{1}H NMR spectra in CD_3CN, for Cu(II) and Zn(II), and DMSO- d_6 for Zn(II). Figure 3.16 shows changes in the ^{1}H NMR of **L** in CD_3CN upon titration with Cu(I). The free ligand showed two peaks at 4.55 and 4.59 ppm (numbered as *a* and *b* respectively in Figure 3.16) corresponding to the two $-CH_2-$ moieties in **L**. *b* was assigned to the CH_2 adjacent to the to the hydroxide group. In super-dry CD_3CN and DMSO-d_6 this signal was observed as a doublet coupled to the O-H, which appears at 3.58 ppm in Figure 3.16 (labelled as *c*). Therefore *a* can be assigned to the CH_2 beside the tosylamide. Upon addition of 0.5 and 1 equivalents of Cu(I) perchlorate, the *a* and *b* resonance shifted substantially; *a* was shifted downfield to 4.79 ppm and *b* upfield to 4.35 ppm after one equivalent of Cu(I) suggesting the formation of a new Cu(I)-**L** complex. The hydroxy signal at 3.58 ppm (*c*) disappeared indicating the direct participation of the hydroxy groups in metal ion coordination. Changes were also seen in the aromatic region. The triplet and two doublet signals assigned to the protons of the pyridine moieties with resonances at 7.62, 7.20 and 7.16 ppm respectively, were affected due to the direct coordination of the two nitrogen moieties to the Cu(I) centre. Upon further addition of Cu(I) the *a* and *b* resonances became even more shifted and after the addition of two equivalents of Cu(I) they had shifted to 4.90 and 4.28 ppm respectively. The aromatic region also had changed showing three sets of signals; a doublet at 7.30, a triplet at 7.56 and a multiplet at 7.87 ppm. No further changes were seen upon addition of further 5

equivalents of Cu(I). These results imply that **L.Cu(I)** is a dimer in solution state as well as solid state.

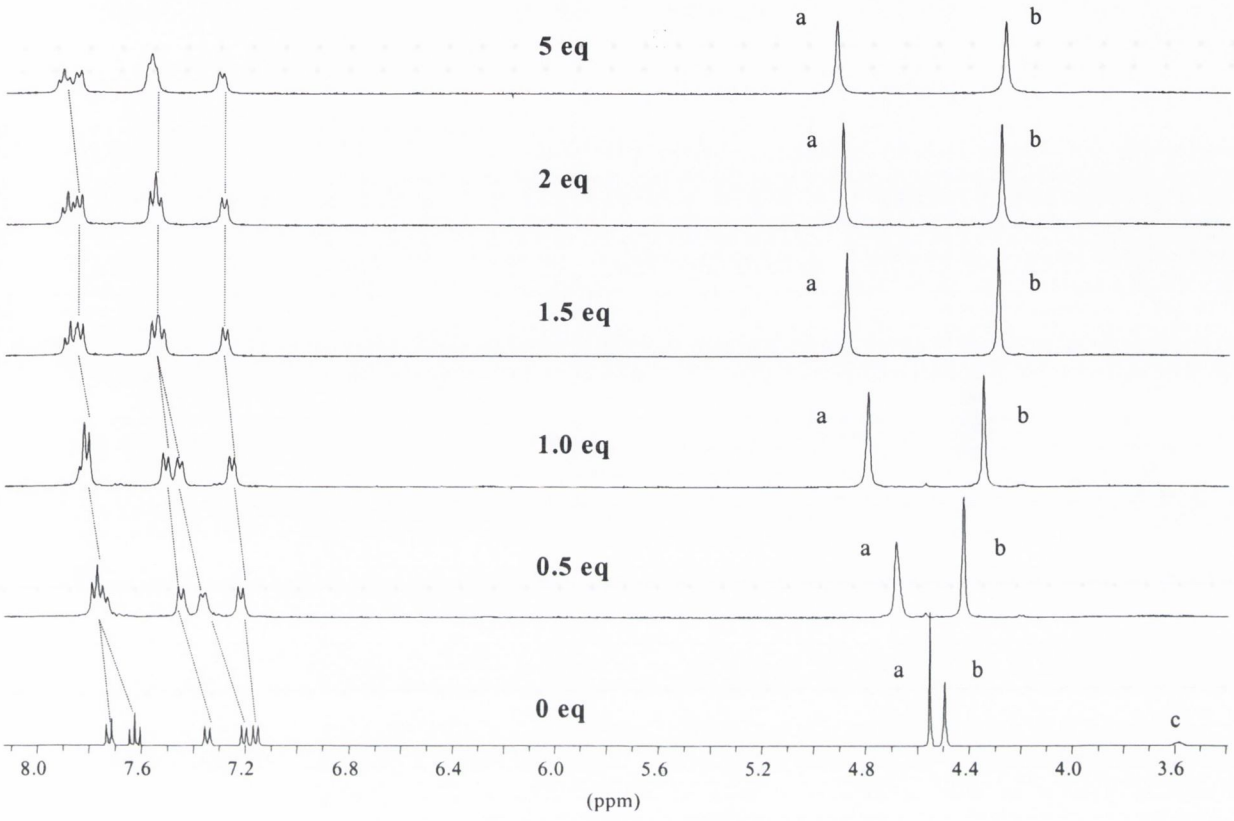

Fig. 3.16: ^{1}H NMR spectrum of L upon Cu(I) titration in MeCN.

The titration of **L** with Zn(II) in CD_3CN showed changes similar to those seen above (Figure 3.17). The only exception was that there were no clear shift in the resonances of *a* or *b* after the addition of two equivalents of Zn(II) with a corresponding broadening of the hydroxy signal. After the addition of a further five equivalents of Zn(II) the two CH2 groups had substantially shifted to 4.40 and 5.05 ppm for *b* and *a* respectively with a corresponding broadening of the signals. The hydroxy signal *c* was substantially shifted from 3.6 ppm in the free ligand to 5.01 ppm. Upon addition of a further two equivalents of Zn(II) there was a further broadening of the signals. Upon addition of a further three equivalents of Zn(II) there was a significant sharpening of the signals, with *a* and *b* appearing as clear singlets at 5.05 and 4.40 ppm respectively. The hydroxy signal appeared at 6.60 ppm although substantially broadened. The addition of Zn(II) also gave rise to substantial changes in the aromatic region. After twelve equivalents of Zn(II), a triplet, two doublets and a multiplet appeared at 8.14, 7.82, 7.64 and 7.52 ppm respectively indicating the formation of a new **L.Zn(II)** species.

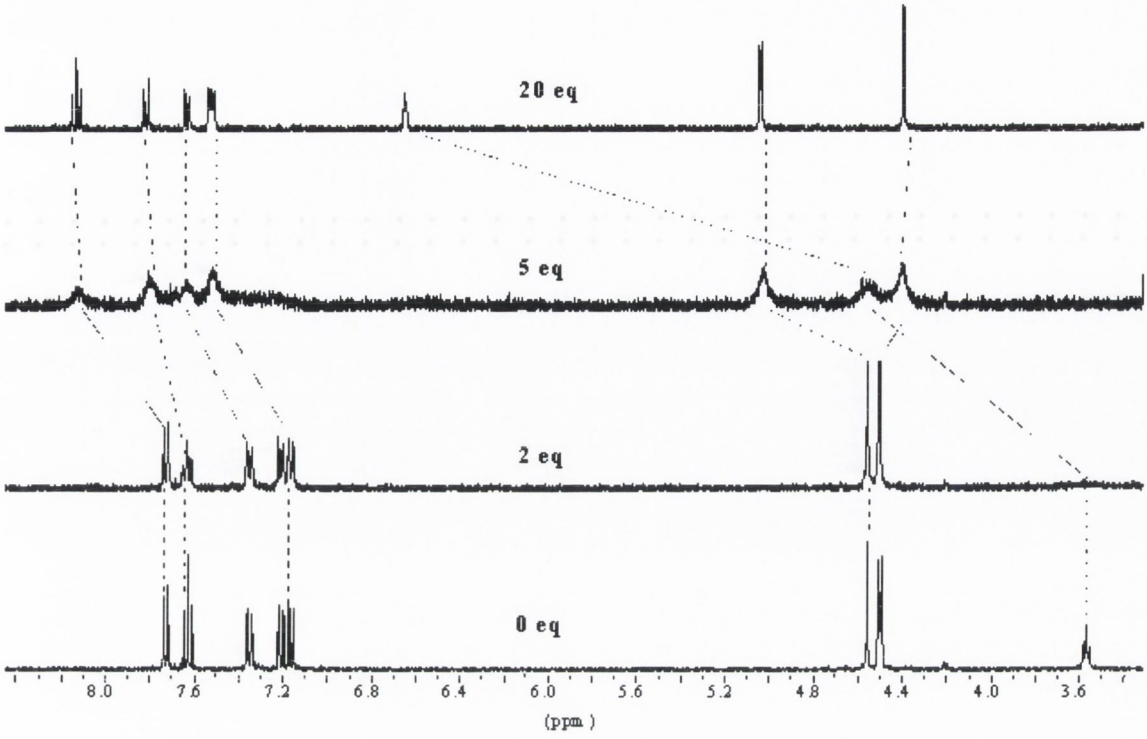

Fig. 3.17: ^{1}H NMR spectrum of L upon Zn(I) titration in MeCN.

The ^{1}H NMR spectrum of **L** in DMSO-d_6 showed two resonances at 4.49 and 4.38 ppm. The signal 4.38 ppm was a doublet and coupled to the hydroxy signal *c* at 5.3 ppm. Upon addition of one equivalent of Zn(II) there was no changes in the shift for *a* and *b* but a broadening of the hydroxy signal was seen. Further additions of Zn(II) showed no significant changes in shift of *a* and *b* or in the hydroxy signal. There were no changes seen in the aromatic region of the spectrum. These results suggest that the formation of the **L.Zn(II)** species was more difficult in DMSO-d_6. This may be due to the polar nature of the solvent making it difficult for Zn(II) to displace the solvent molecules around **L**.

3.4 Cleavage of the RNA-Mimic System 2-Hydroxypropyl-*p*-Nitrophenylphosphate (HPNP)

HPNP (2-hydroxypropyl *p*-nitrophenyl phosphate) is a RNA mimic compound (Figure 3.18) that is used to determine the kinetic ability of the various transition metal complexes **L.Fe(II)**, **L.Cu(II)**, **L.Co(II)**, **L.Zn(II)** and **L.Ni(II)** to cleave phosphodiester bonds under physiological conditions. HPNP is a RNA mimic because of the presence of a 2'-OH group, which is a nucleophile. The advantage of using HPNP is that it absorbs at 300 nm but upon hydrolysis by the transition metal complexes a new peak at 400 nm is seen corresponding to the *p*-nitrophenolate product as seen in Figure 3.18. A cyclic phosphate is also formed. The

which is a nucleophile. The advantage of using HPNP is that it absorbs at 300 nm but upon hydrolysis by the transition metal complexes a new peak at 400 nm is seen corresponding to the *p*-nitrophenolate product as seen in Figure 3.18. A cyclic phosphate is also formed. The changes in intensity of the absorption spectrum at 400 nm is used to determine the kinetic ability of the transition metal complexes **L.Fe(II)**, **L.Cu(II)**, **L.Co(II)**, **L.Zn(II)** and **L.Ni(II)** to cleave phosphodiester bonds as discussed earlier in section 3.1. The crystal structures of these complexes suggest that **L.Cu(II)** and **L.Zn(II)** provide the best prospect for phosphodieaster cleavage. **L.Zn(II)** has a metal-bound water molecule which, as discussed earlier, is advantageous and can aid hydrolysis by nucleophilic acid activation of the 2'-hydroxy group (scheme B in Figure 3.3).

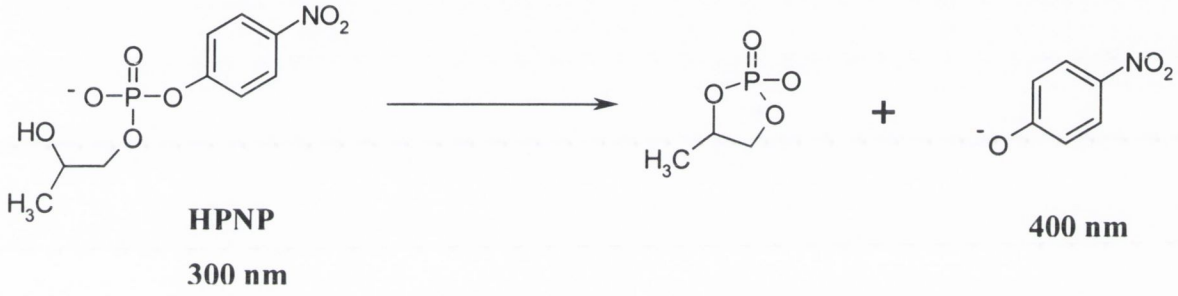

Fig 3.18: Hydrolysis of HPNP yielding a cyclic phosphate and *p*-nitrophenolate

Alternatively it has been shown that dinuclear Cu(II) complexes, such as **112**[125], were more efficient cleavers of RNA mimics than their mononuclear analogues. It was suggested by the authors that this was due to the synergistic action of the two metal centres. Other dinuclear Cu(II) complexes **114** and **115** developed by the Chin group found that both Cu(II) ions cooperate in the hydrolysis of the phosphodiesters by double Lewis acid coordination and the hydroxide groups then act as nucleophiles. The crystal structure of **L.Cu(II)** show a dinuclear dimer complex with a metal-bound O^- which suggests the effects on hydrolysis should be similar to these complexes. The crystal structure of **L.Fe(II)**, **L.Co(II)** and **L.Ni(II)** do not suggest that these complexes will have much catalytic ability. There is no associated water-bound water molecule and the hydroxy group on **L** is not bound to the metal, which would have aided catalytic ability. The experiments on HPNP were run on an *Agilent UV-Vis Photodiode Array Spectrometer* at pH 7.4 and 37°C in the presence of HEPES buffer, mimicking physiological conditions. The changes in intensity at 400 nm were used to determine the rate of hydrolysis of the complexes on HPNP with Figure 3.19 showing a typical spectrum seen over sixteen hours. Unfortunately the complexes absorb in the 300 nm

nitrophenolate. Table 3.6 shows the results of first order rate of hydrolysis obtained as an average of two or three runs.

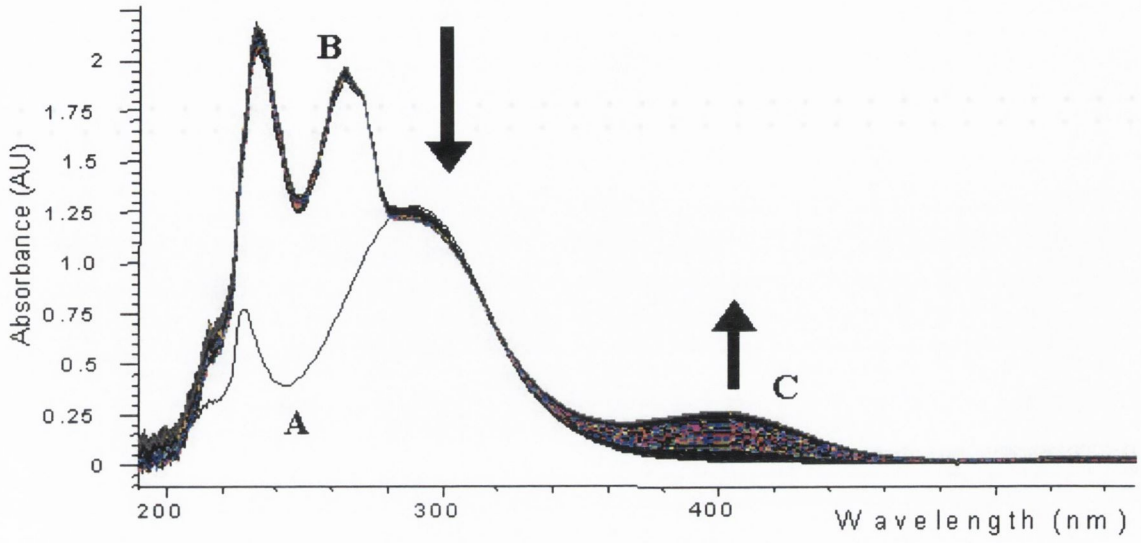

Fig. 3.19: The changes in the UV-Vis spectra of HPNP upon hydrolysis using L.Zn(II). Graph A is HPNP; B is the combined spectra of L.Zn(II) and C shows the growing in of the band at 400 nm, which is assigned to the formation of *p*-nitrophenolate.

The rate of hydrolysis *k* was determined by using first order rate kinetics using *Biochemical Analysis Software for Agilent ChemStation*. Unfortunately the results, whilst comparing favourably to literature, were not as dramatic as anticipated from the crystal structure data. **L.Cu(II)** gave the best rate of hydrolysis $k = 3.44 \times 10^{-4}\ s^{-1}$ resulting in a half-life of 5.6 hours and k_{obs} of 1005. These results favour comparably to the results obtained for **112**[125,126] and **114**[129] which had a rate of cleavage of $k = 2 \times 10^{4}\ hr^{-1}$. **L.Cu(II)** was an efficient catalyst for the cleavage of HPNP because of the presence of the two metal centres, which it has been suggested[125], are synergistically involved in catalysis by Lewis acid activation.

Complex	First Order Rate (s^{-1})	Half Life (hrs)	k_{obs}
L.Cu(II)	3.44×10^{-4}	5.60	1005
L.Zn(II)	2.86×10^{-4}	6.73	842
L.Co(II)	1.51×10^{-5}	12.72	444
L.Ni(II)	9.41×10^{-6}	20.46	275
L.Fe(II)	-------	------	-----

Table 3.6: Table showing the rates of cleavage for the complexes and the associated half-lives. These were all obtained as averages over 2-3 runs. $k_{obs} = k_{cat}/k_{uncat}$ where k_{uncat} is 0.00012 hr^{-1}

The presence of the metal-bound hydroxy group on **L** can aid nucleophilic activation. Surprisingly **L.Zn(II)** was not more efficient than **L.Cu(II)** for the hydrolysis of HPNP even though the crystal structure shows the presence of a metal-bound water molecule. The metal-bound water molecule is known to aid catalysis by nucleophilic acid activation and this may be due to the lack of two metal centres in **L.Zn(II)**, which may be more advantageous for HPNP cleavage. As expected **L.Fe(II)**, **L.Co(II)** and **L.Ni(II)** were poor catalysts for the cleavage of HPNP with **L.Co(II)** being half as effective as **L.Co(II)**. **L.Fe(II)** was totally ineffective and may have been unstable over the period of time for analysis.

3.6 Conclusion

Collating all the results obtained in this chapter it can be seen that several transition metal complexes have been synthesised from the ligand **L** [N,N-bis[[6-(hydroxymethyl)pyridne-2-yl]-*p*-tosylamide]] using Cu(II), Zn(II), Ni(II), Co(II) and Fe(II). These were fully analysed using ^{1}H NMR and ^{13}C NMR and where possible, ES-MS and IR spectroscopy. Suitable crystals of the complexes were grown and analysed using X-Ray crystallography analysis. The complexation of the transition metals to **L** were monitored by observing the changes in the ^{1}H NMR spectra of **L**, for Cu(I) and Zn(II), and in the absorption and fluorescence spectra of **L** upon complexation of the metal ions. It was found that **L** was a selective chemosensor for Zn(II) over the various other ions with a large fluorescent enhancement of *ca.* 23 but due to the short wavelengths of emission its application in biological systems is limited. The ability of these complexes to cleave the RNA-mimic HPNP was investigated. **L** was chosen as the ligand for these complexes because it is a simple ligand containing functional groups similar to those found in the active sites of natural ribonucleases. For all the complexes investigated, the metal ions were coordinated to the nitrogen moiety of the pyridyl unit and two hydroxy groups of the side arms. For **Co.L** and **Fe.L** the ions were also weakly coordinated to the nitrogen moiety of the tosylamide. Several of the complexes were moderate catalysts for the hydrolysis of HPNP but the rates of hydrolysis were smaller than expected. **L** was chosen because it has a relatively open structure, as seen in the crystal structure **L** (fig. 3.4), pending vacant coordination sites for occupation by solvent water molecules which would substantially increase the rate of hydrolysis of HPNP due to increased nucleophilic activation of the hydroxy group of the HPNP. Only **Zn.L** proved able to fulfil this criterion.

Chapter 4

A Novel PET Sensor for Lithium

4.1 Introduction:

With the advent of the discovery of the crown ethers by Pederson[5], supramolecular chemistry has developed into a highly developed and diverse field. One of the areas developed has been supramolecular photochemistry where the change in the photophysical properties of the receptor upon recognition of the guest can be utilised as light-converting systems, sensors, energy processing storage devices and photosensitive supramolecular catalysts as discussed in chapter 1. This chapter will discuss the synthesis and photophysical properties of a novel fluorescent Li^+ sensor giving a brief introduction into the history of fluorescence sensors and previous examples of Li^+ and amino acids sensors.

Sensors are tools, which are used to obtain information about an analyte of interest such as a cation, anion or a small neutral molecule. Sensors may be composed of a synthetically designed receptor that recognises the analyte and transmits this information to a chromophore or fluorophore leading to changes in the physical properties such as fluorescence intensity, emission wavelength and excited state lifetimes. There are many advantages in using fluorescence sensors. They are highly sensitive (10^{-12} to 10^{-11} M concentrations), with "on-off" switchability, resolution on a molecular level, toxicity can be kept to a minimum and they can be used in physiological media to provide "real-time" information as well as being cost efficient[166,167]. During the discovery of the crown ethers, Pederson noticed a change in the absorption spectrum of dibenzo-18-crown-6, which he put down to the complexation of K^+ in benzene. This inspired chemists to take advantage of these changes in the absorption or fluorescence spectra of the receptor to detect a guest of interest. Since then many different types of sensors have been developed employing many different methods to detect cations, anions and small organic molecules. Within the Gunnlaugsson group, sensors have been developed to detect pH[168], blood Na^+[169,170], anions[171,172] such as pyrophosphates[172], acetates[171], biscarboxylic acids[172] and halides[171]. Furthermore, lanthanide ion complexes have also been developed to detect a range of analytes such as aromatic carboxylic acids like salicylic acid[173]. Chemical sensors are thus a non-invasive and non-destructive technique, which has made them an important diagnostic tool in medicine and industry[174]. The vast range of sensor types necessitates the limiting of this introduction into discussing a type of sensor known as fluorescent photoinduced electron transfer (PET) sensors.

4.1.1 Properties of PET Sensors

There are three essential components of a PET sensor. The receptor detects the analyte of interest selectively, specifically and reversibly. The fluorophore reports this recognition by changes in fluorescent intensity, wavelength or lifetimes. The spacer covalently links the fluorophore and receptor close together whilst minimising any n-π and π–π orbital interactions.

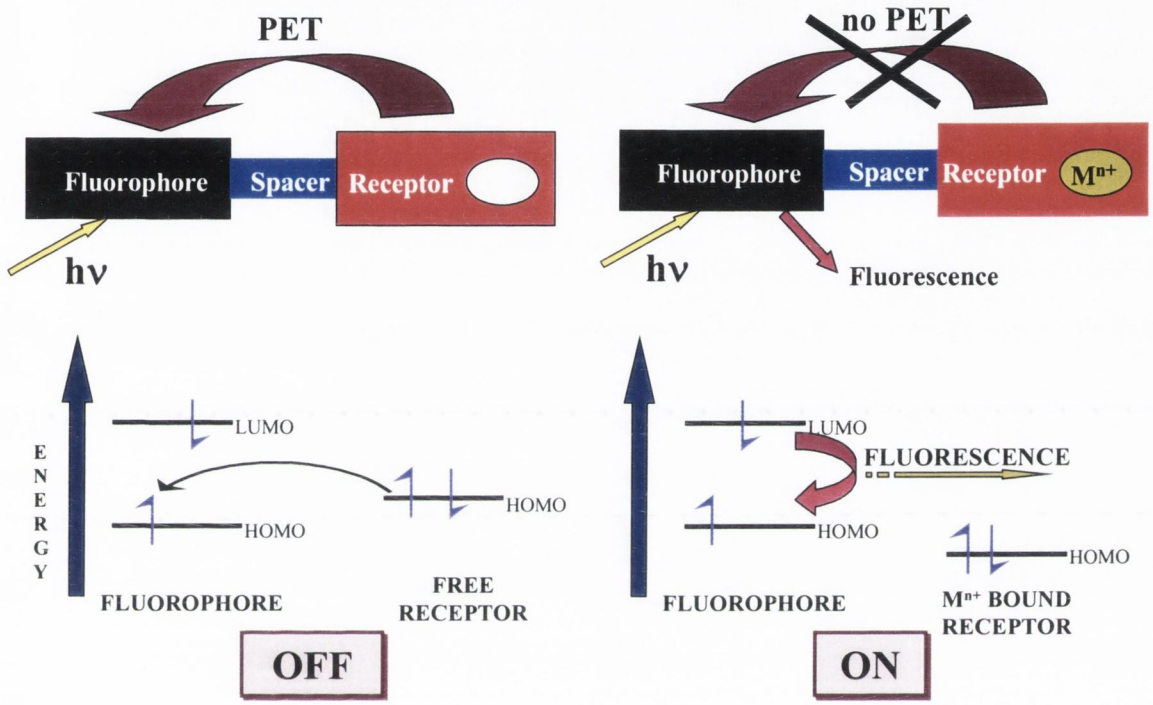

Fig. 4.1: Diagram showing the process of PET, above, and the associated frontier orbital diagrams. A: The fluorophore is excited. The excited state is quenched by PET from the receptor. B: When the receptor is bound to an analyte, PET cannot occur and the energy is released as fluorescence.

Hence, the only communication occurs *via* electron transfer. The efficiency of the electron transfer between the receptor and fluorophore depends on the spacer distance falling off as a function of $1/r^6$.[174] The smaller the spacer the faster the electron transfer, thus preventing any potential quenching from the solvent. The spacer ensures that the absorption spectrum of the fluorophore is independent of the analyte concentration and also ensures no internal charge transfer (ICT) processes can occur[174]. Figure 4.1 shows the process of PET highlighting "off-on" switching and the associated frontier orbital diagrams and is discussed fully below[175,176]. It must be mentioned that "on-off" switching can occur[177]. When the fluorophore is excited by the appropriate wavelength of light, an electron in the HOMO is promoted to the LUMO. The oxidation potential of the receptor is sufficient to donate an electron to the HOMO of the fluorophore. The electron in the LUMO of the fluorophore is

transferred to the HOMO the free receptor. Thus energy is dissipated throughout the molecule via vibrational energy loss. When the receptor is bound to an analyte of interest, the oxidation potential of the receptor is raised and reducing its ability to participate in PET. The energy is released as fluorescence and the change in fluorescence properties are used to gather information on the analyte of interest. The thermodynamic driving force for PET is the change in free energy of electron transfer (ΔG_{ET}) according to the Rehm-Weller equation[177]:

$$\Delta G_{ET} = - E_s - E_{red\ fluorophore} + E_{ox\ receptor} - e^2/\varepsilon r$$

where E_{ox} and E_{red} are the appropriate oxidation and reduction potentials for the receptor and fluorophore respectively and E_s is the singlet energy term. The term - $e^2/\varepsilon r$ is the attractive energy between a constant radical ion pair and is usually around 0.1 eV in acetonitrile. An increase in the oxidation potential of the receptor results in the E_{ox} term becoming more positive, making the free energy of electron transfer more positive and therefore the electron transfer from the receptor to the fluorophore thermodynamically unfavourable.

4.1.2 History of the Development of PET Sensors

De Silva *et al* were one of the first groups to exploit this elegant process. A number of papers by the de Silva group describe the history and development of PET sensors by their group and others in a number of reviews[175,178,179,180]. Some of the first sensors developed by de Silva *et al* were **146** and **147** and these developed as sensors for protons and sodium respectively[181]. For **146** the anthracene moiety was chosen as the fluorophore and the amine functionality was the receptor and a methyl group spacer separated both the fluorophore and receptor. In its free form (no protons bound) electron transfer took place from the nitrogen of the amine to the excited state of the anthracene moiety quenching fluorescence. In contrast, upon proton recognition the oxidation potential of the receptor was increased, causing the fluorescence to be switched on, as shown in Figure 4.1. This explains the processes involved for all the complexes discussed below.

The de Silva group proceeded to prepare a number of PET sensors by employing anthracene as a fluorophore with a crown ether receptor[178] such as **148** for sodium detection[182]. Later sensors such as **149** and **150** were prepared which were selective for protons and sodium respectively[183,184].

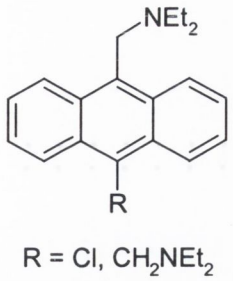

146

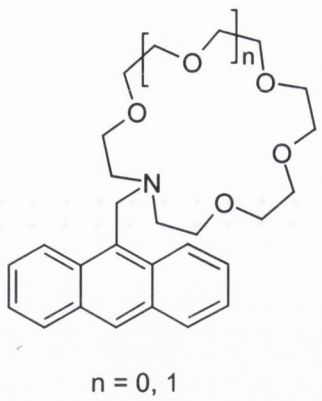

147

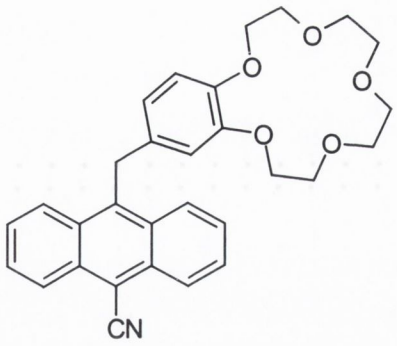

148

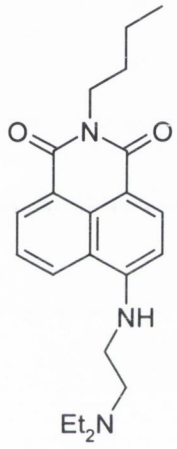

149

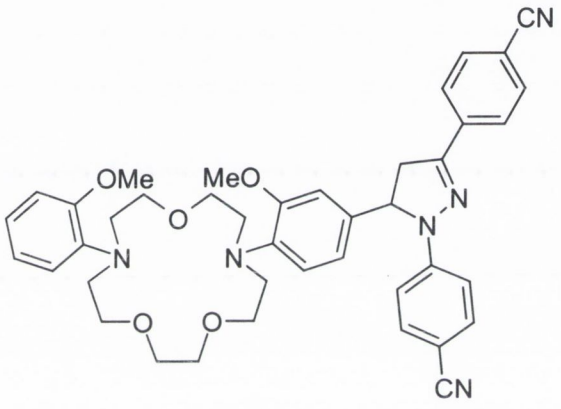

150

The Gunnlaugsson group developed neutral PET sensors for detecting the presence of anions using anthracene fluorophores **151** and **152** for the detection of fluoride and acetate, pyrophosphate and biscarboxylates respectively.

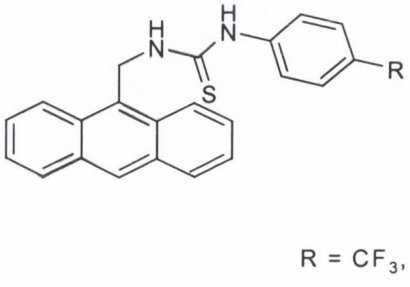

151

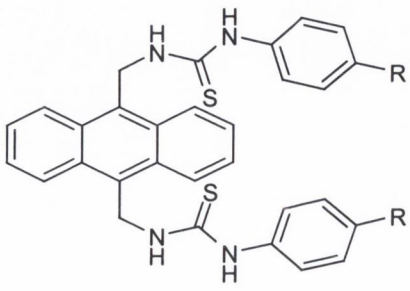

152

4.1.3: Why Analyse for Li^+ ?

Although PET sensors have been developed for a wide range of analytes, no Li^+ selective PET sensors have been reported in the literature. Li^+ is unusual in that it is one of the smallest and lightest solid elements and has important clinical, pharmacological and biochemical properties. It is found widely in nature. Its beauty lies in its simplicity in activating brain cells to regulate abnormal mood cycles for the treatment of mentally ill patients such as manic-depressives[185].

New uses of Li^+ include the treatment of skin diseases (such as dermatitis) and autoimmune and immunological diseases. Li^+ is administered orally as Li_2CO_3 at a total dose of up to 30 mM (approximately 2 g) per day for the treatment of mental health. The therapeutic index for Li^+ is narrow and should lie between 0.4 and 0.8 mM in serum 12 hours after the dose has been administered. If the serum concentration is too high (around 1.5 mM) shakes, dizziness, drowsiness, vomiting and diarrhoea occur in the patient indicating serious toxicity and are usually seen for four hours after the drug has been administered[185]. Long-term side effects include dermatological disorders, weight gain and some problems with kidney and thyroid functions. In medicine, Li^+ determination in blood samples was traditionally carried out using atomic absorption spectroscopy and flame emission spectroscopy. The impracticalities of measuring serum samples on site using these methods led to the development of ion-selective electrodes, which are more practical. They work by measuring the activity in solution of Li^+ and are active within the clinical range (0.4 – 0.8 mM serum). This technique gives immediate feedback without the long delays, high operation and instrumentation costs and bulkiness of instruments[186]. Determination of Li^+ levels in serum must also be monitored in the presence of 140 mM sodium, 4.3 mM potassium and 1.26 mM calcium. Therefore a major effort has been undertaken to create optical sensors that selectively detect Li^+ whilst being cost efficient, easy to use and give quick results[187].

4.1.4: Development of Ionophores for Li^+

Ionophores have been developed for selective determination of Li^+ over sodium for use in ion-selective electrodes[187]. Ionophores are molecules, which are used to transport metal ions from aqueous solution to organic solvents. Many have been based on crown ethers of different sizes with functional groups added to make the compound either more lipophilic or more selective for Li^+ . The Li^+ ion is exceptionally small with an ionic radius of 0.86Å compared to 1.12Å and 1.44Å for sodium and potassium respectively[186]. Li^+ has a large

hydration energy, which needs to be accounted for when designing a receptor for Li^+ recognition. Hori *et al* established that the cavity of 12-crown-4 is ideal for encapsulating the Li^+ ion but generally exhibits selectivity for sodium because it can form 2:1 ligand-to-metal complexes[188]. This is because the Li^+ ion is too heavily solvated to form 1:1 complexes. The aza-12-crown with sidearms containing one or two amine arms was deemed to have the best properties for Li^+ complexation[188]. Parker *et al* developed a family of 14-crown-4-ether ionophores containing strong σ-donors such as amides[189]. 14-crown-4-ethers have the optimum cavity size for incorporating Li^+ ions compared to 12-crown-4[190]. To ensure a six chelate ring was generated once Li^+ was bound to the receptor, a chiral methylene spacer was used between the ring and amide functionalities. The six chelate ring is known to ensure a preference for Li^+ over sodium and the chiral spacer was chosen to ensure the ionophores were selective for Li^+ over sodium[191]. Two crown ethers were developed **153** and **154** with various substituents. Only **153a**, **153e**, **153f** and **154a** were found to be selective for Li^+ in the therapeutic region using potentiometric methods. **153f** showed the best promise of selective Li^+ determination in the presence and absence of sodium, potassium and calcium. The Parker group concluded that the addition of other bulkier R groups (g → i) to **153** and **154** further enhanced the selectivity of Li^+ over other ions[192,193].

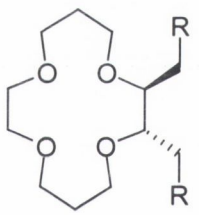

153

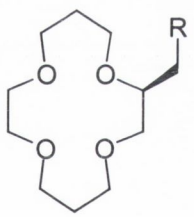

154

R = (a) OCH_2Ph
(b) OH
(c) OTs
(d) CN
(e) CO_2Me
(f) $CONBu_2$

(g) 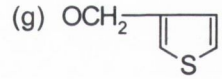

(h) OCH_2Ph
(i) $CON(iBu)_2$

It was also noticed that the addition of the sterically hindered axial position of the substituents suppressed 2:1 metal:ligand complex formation, which especially prevents interference from sodium and potassium. The ligands with the bulkiest substituents, namely **153a**, **153f** and **153i** were the best ionophores with **153i** showing selectivity close to ideal in blood plasma. The Parker group then went on to determine the effect of putting these sterically bulky substituents onto the middle of the trimethylene group producing **155** and **156**[194]. These molecules gave comparable results to **153i**. The Parker group and others continued this research into developing crown ethers with substituents that are able to undergo polymerisation for Li^+ electrodes[190,195,196].

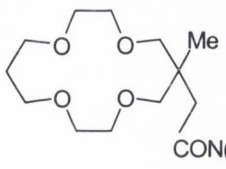

155

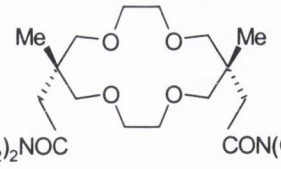

156a

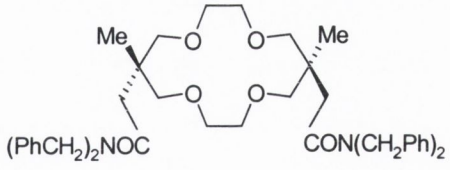

156b

Similar to the work by Parker *et al*, the Sachleben group developed other crown ether derivatives for Li^+ ion extraction[197]. The group found that bulky substituents at the dimethylene position of the crown ether formed a cylindrical cavity which selectively extracted Li^+ over Na^+, as shown in compounds **157** to **160** due to the bulky nature of the substituents. Compounds **157** and **158** were especially good at extracting Li^+ .

Crown Ether	% Extractability		
	Li^+	Na^+	K^+
161	~100	20	-----
162	81	5	3
163	11	1	1

Table 4.1: The % extractability of bulky crown ethers for metal picrate salts in a DCM-water system[198]

In a related work, Kobiro *et al* describes the ability of new crown ethers with bulky substituents to extract Li^+[198]. The compounds synthesised, **161** and **162,** showed remarkable selectivity for Li^+ when extracting lithiun picrate from water. The % extractability of these compounds is shown in Table 4.1.

Micheloni *et al* used cryptand molecules to extract Li^+ ions from aqueous solution. One of the first molecules they developed, **164**, showed that the small cavity of the cryptate was suited to allow the formation of a stable Li^+ complex in aqueous solution for selective lipophilic transportation across membranes[199]. Adapting this molecule by functionalisation at the X position yielded **164c** and **164d**, which were less selective for Li^+ compared to **164a**[200,201]. Varying the length of the inner chain for systematic studies on the cryptates indicated that the smaller chain length of **164a** was indeed the best binder of Li^+ [202,203]. The crystal structures also showed short Li-N bonds indicating a good match between cation radius and cavity size[204]. Other types of ionophores for Li^+ ion determination, including

phenanthroline-based receptors[205,206] and calixarene[207] receptors have been discussed extensively in a number of reviews[187].

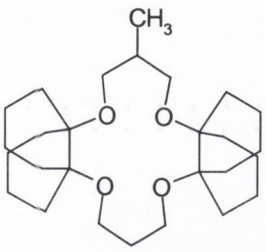

157

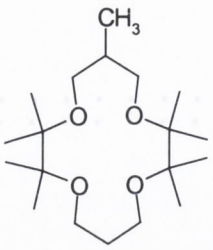

158

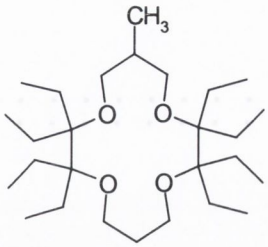

159

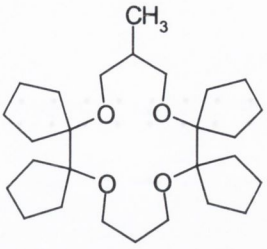

160

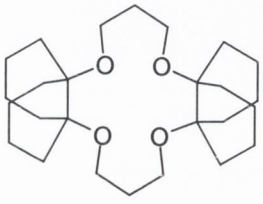

161

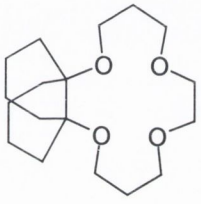

162

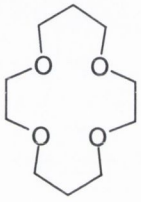

163

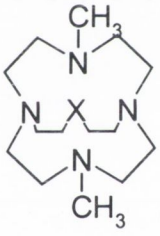

X = (a) N-Me
= (b) NH
= (c) O
= (d) S

164

4.1.5 Luminescent Sensors for Li^+

Early work on luminescent ionophores for Li^+ determination was centred on using crown ethers containing chromophore units. Pacey *et al* used acidity constants obtained from UV data to show that **165** was selective for Li^+ in blood and urine samples[208]. Comparisons of this method with the more usual atomic absorption techniques showed good agreement. Later studies by Pacey *et al* again focused on derivatives of **165** by varying the chain length of the crown ether producing compounds **166** and **167**[209]. The introduction of benzene into the crown, producing **168** to **170**, with a 2,4-dinitro-6-trifluorophenyl chromophore, provided another aspect to this study. Studies were carried out by comparing data in picrate ion-pairing extraction studies. For some of these compounds extraction ability depended on the solvent used. The paper found that the compounds **165** to **167** were more efficient extractors of Li^+ than the benzo-crowns **168** to **170**[209]. In 1987 the Kimura group used a fluorescent

naphthalimide 14-crown-4 derivative **171** for selective Li^+ ion extraction[210]. A new peak at 400 nm in the absorption spectrum was observed indicating Li^+ complexation. The fluorescence spectrum showed a decrease in intensity upon titration with Li^+ . The results suggest that **171** was 200 fold more selective for Li^+ over Na^+[210].

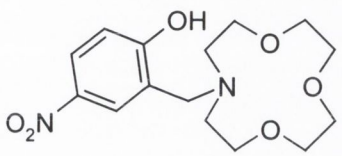

165

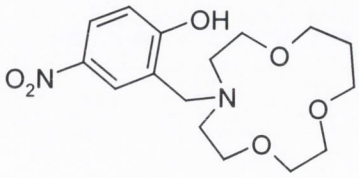

166

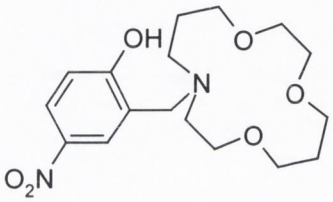

167

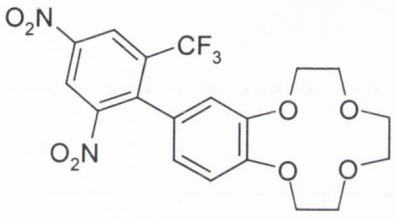

168

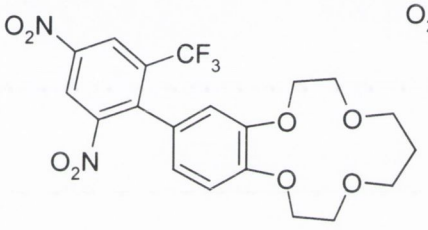

169

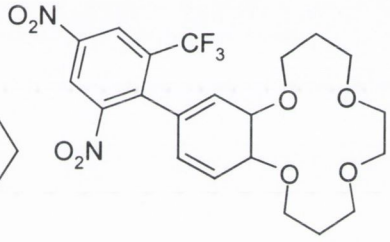

170

The Kirschke group developed Li^+ selective ionophores from 12-crown ethers containing a tryptophan-based chromophore[211]. A colour change was noticed in the presence of Li^+ from orange to purple for the (*E,E*) isomer **172a**. A dramatic increase in absorption at 550 nm was observed for **172a**. No effect was seen for **172b**. While the Li^+ selective ionophores, discussed above, focused on extracting Li^+ from aqueous solution only recently have luminescent Li^+ sensors been developed for the easy determination of Li^+ concentration in physiological media. The Blackburn group developed a 12-crown ether **173**, containing a coumarin fluorophore for Li^+ determination[212].

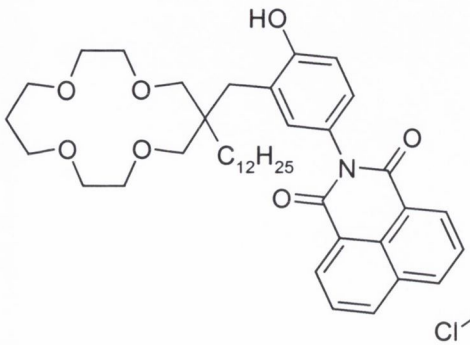

171

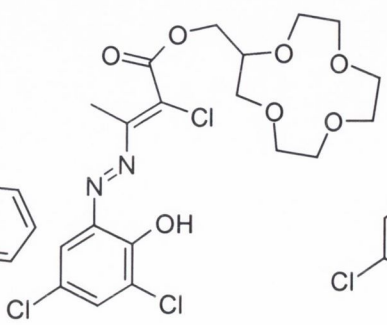

172a

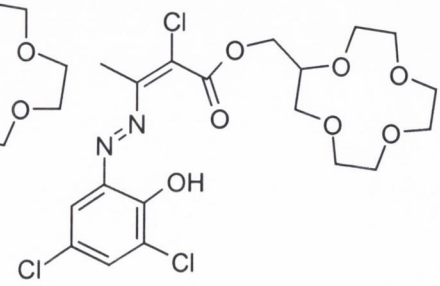

172b

In MeCN, **173** selectively detected Li^+ with a corresponding change in the absorption spectrum. When R = H no fluorescence changes were seen upon Li^+ complexation but when R = OMe a shift in the fluorescence wavelength was observed (from 485 nm to 462 nm) with a corresponding increase in fluorescent intensity. No changes were seen upon the addition of sodium. The Kim group developed an azacrown indoaniline-based sensor for Li^+ detection **174**[213]. Here the indoaniline dye was used as the chromophore, which is covalently attached to a monoaza 12-crown ether. The solvent was found to affect the complexation of **174** with the complex being more stable in a non-polar solvent such as MeCN. Photophysical studies show that while some changes are observed upon addition of sodium the overall effect is not as great as the changes observed on Li^+ addition as was suggested by molecular modelling studies.

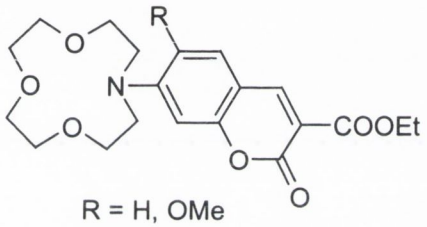

173

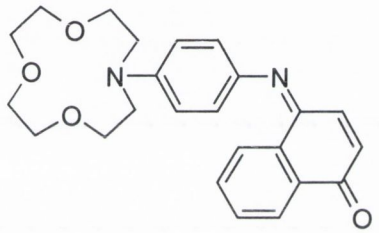

174

The Kimura group developed a spirobenzopyran azacrown derivative **175** for Li^+ determination in a micellar environment at high pH conditions[214]. An octadecyl group was added to the compound to aid the lipophilic nature of **175**. It was suggested that the complexation mechanism involved the breaking of the spirobenzene bond as shown in Figure 4.2. High lithium-selective changes in shift of the maximum wavelength were seen in the fluorescence spectra of the organic phase after liquid-liquid extraction.

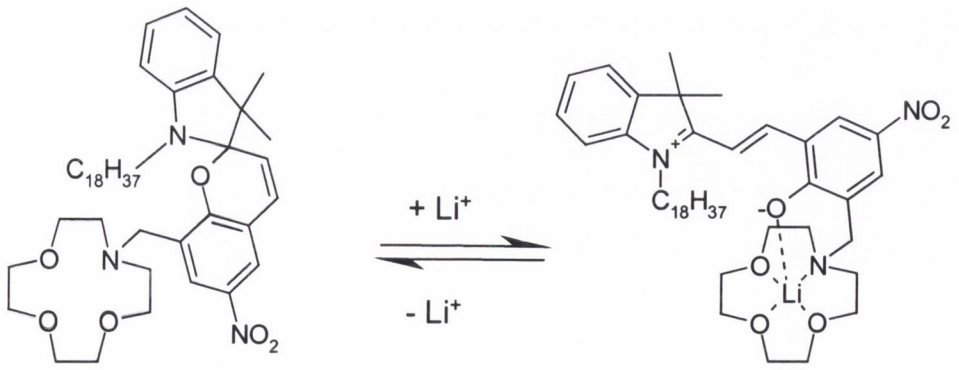

175

Fig 4.2: Suggested mechanism of Li^+ complexation of 175 as postulated by Kimura *et al*[214].

The Micheloni group developed aza-cages, containing an anthracene fluorophore, **176** to **178** for the recognition of Li^+ at physiological conditions. However the Li^+ detection was highly pH dependant, with luminescence only possible in basic solution[215]. The Murphy group used a 1,10-phenanthroline based ligand **179** for Li^+ ion determination and **180**[216,217].

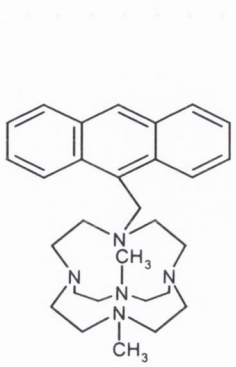

176

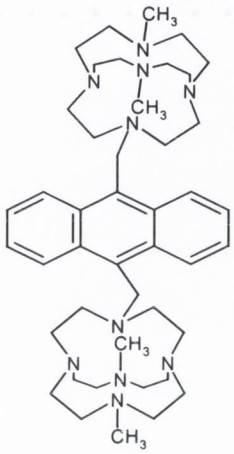

177

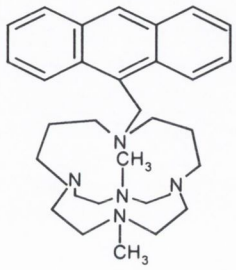

178

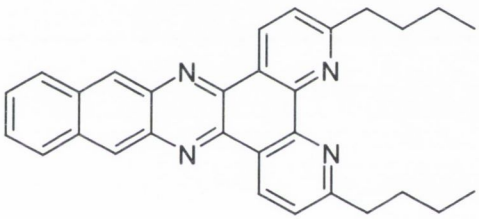

179

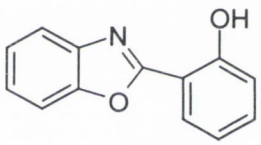

180

To summarize it can be concluded that the best type of receptor for Li^+ recognition should be based on a crown ether with a small cavity of 14-crown-4 or less with bulky substituents to allow selectivity of Li^+ over other alkali metals. A fluorophore is required that can emit in a wavelength region outside the physiological range *i.e.* greater than 330 nm to prevent autofluorescence. There has been a large variety of Li^+ selective sensors synthesised and characterised[215,216,217]. None so far have been based on the principle of PET. The next section will discuss the development, synthesis and photophysical evaluation of a novel Li^+ PET sensor[218].

4.2 Design of a Lithium PET Sensor 181

The elucidation of synthetic strategies and coordination properties to coordinate an organic molecule of Li^+ [186] should lead to a improved understanding of its biological activity to the design of better Li^+ sensors. Therefore a lithium-selective PET sensor **181** was designed based on a crown ether receptor with a naphthalene fluorophore. The introduction

section above has shown that 14-crown-4-ethers have the optimum cavity size for Li^+ selectivity especially if sterically bulky groups are added[190]. The receptor unit (shown in red) developed in this project is a small unit namely diaza-9-crown-3-ether containing an amide moiety at the *N*-positions. The small cavity size was chosen to ensure only Li^+ was complexed not within the cavity but just outside the cavity as speculated by molecular modelling studies. This would ensure that sodium would be discriminated against. The amide moieties were added to increase the bulkiness of the receptor thus increasing Li^+ selectivity as in the case of Parker *et al*[192]. The rate of electron transfer depends on the spacer distance according to $1/r^6$, where r equals the length of the spacer, thus the chiral methylene group (shown in black) was chosen as the spacer. It was hoped that the chiral nature of the spacer would also aid Li^+ detection by helping the receptor discriminate for Li^+ over other alkali metal ions. The fluorophore chosen was a naphthalene group (shown in blue), which is strongly fluorescent when excited at 280 nm with a corresponding quantum yield close to unity. These units should ensure the specificity and selectivity of the sensor for Li^+ within the therapeutic range of 0.4 to 0.8 mM ideally in physiological conditions.

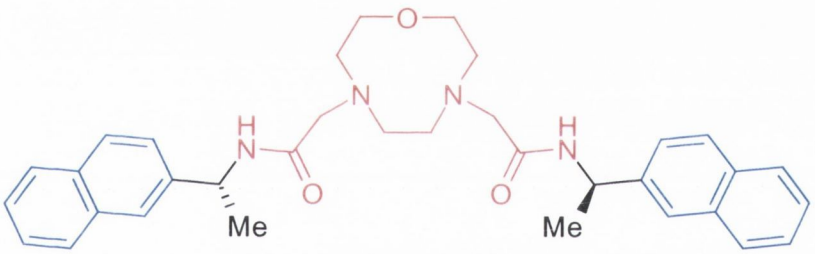

181

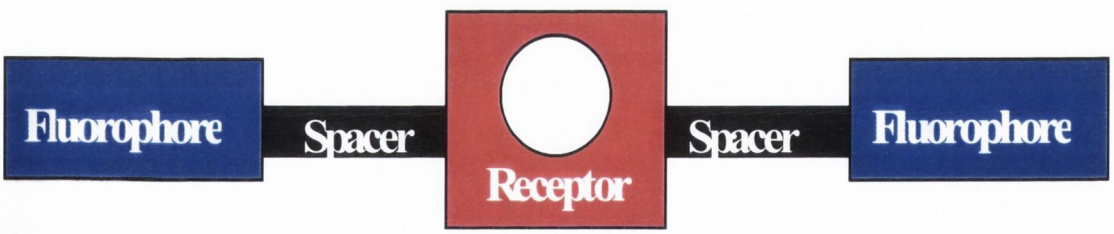

Fig. 4.3: The structure of the PET sensor 181 with the receptor, spacer and fluorophore highlighted

4.3 Synthesis of a Novel Lithium PET Sensor

The synthesis of **181** was achieved in two sequences each with a number of steps, which were all simple, high yielding reactions and all were characterised by conventional means. The first sequence was the synthesis of the diaza-9-crown-3-ether receptor **185**, which is a known compound[219]. The first step involved the addition of a tosyl group to diethylene glycol yielding diethylene glycol ditosylate **182** in 82 % yield as shown in scheme 4.1[219]. The OTs group is an excellent leaving group. Concurrently the *N,N*-ditosyl diaminoethane **183** was

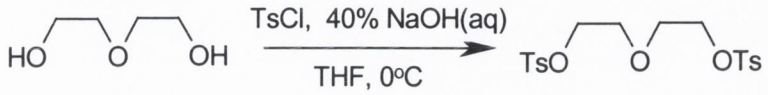

182

Scheme 4.1: Synthesis of diethylene glycol ditosylate.

synthesised in 60 % yield from the reaction of diaminoethane and tosyl chloride as seen in scheme 4.2[219]. For this reaction the tosyl group acts as a protecting group ensuring the monoalkylation of the two sulfonamide moieties[219]. The coupling of **182** to **183** yielded the tosyl-protected macrocycle *N,N'* ditosyl-1,4-diaza-9-crown ether **184** in 60 % yield. It was feared that the corresponding tetraza-18-crown-6-ether macrocycle could also be formed but

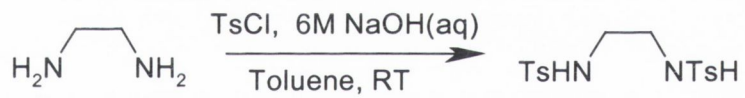

183

Scheme 4.2: Synthesis of N,N-ditosyl diaminoethane

by employing high dilution conditions only the 9-crown-3-ether was formed as shown in scheme 4.3[219]. The deprotected macrocycle 1,4-diaza-9-crown-3-ether was easily obtained by refluxing in 48% HBr-AcOH for four days yielding the HBr salt of **185** in 87 % yield. The macrocycle **185** has C_2 symmetry and thus its ^1H NMR spectrum shows two triplets at 3.98 and 3.45 ppm and a singlet at 3.70.

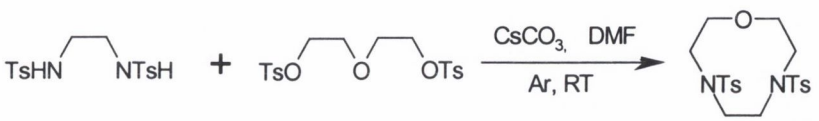

184

Scheme 4.3: Synthesis of *N,N'*-ditosyl-1,4-diaza-9-crown-3-ether

The second sequence involved the synthesis of the R- and S- isomers of the fluorophore and spacer 2-chloro-*N*-[-2-naphtyl]ethylethanamide **187** shown in scheme 4.5. This was simply made from the peptide coupling of chloroacetic acid with 1-[-1-naphtyl]ethylamine **186** using EDCI and HOBt as reactants in approximately 87% yield for both. This compound has

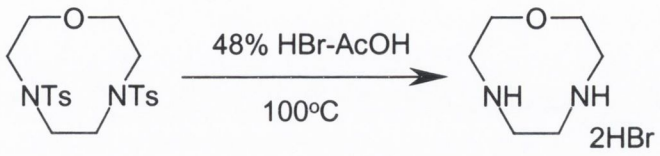

185

Scheme 4.4: Synthesis of 1,4-diaza-9-crown-3-ether

previously been synthesised by Parker *et al* using chloroacetic acid and **185** in approximately 67% yield under reflux[220]. The peptide coupling method proved to be a less harsh method with increased yields. There was no fear in losing chirality because the peptide coupling method is known to retain chirality. The final piece of the jigsaw was to couple the fluorophore and spacer **187** to the crown ether **185** as seen in scheme 4.6. This was done in MeCN at 80°C using standard condensation methods with approximately 65% yield. An increase in the reaction times did not increase yields nor prevent the one-armed system being formed. No advantage were achieved by refluxing the reaction in DMF, in fact this resulted in lower yields of 45% with increased yield of the one-armed side product.

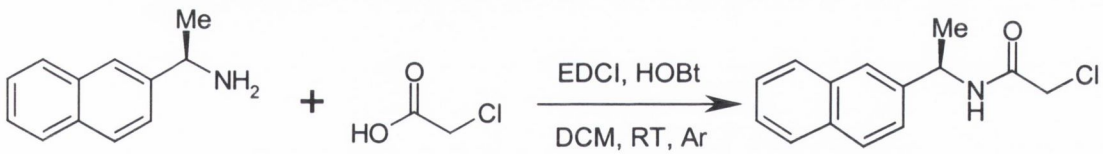

186 **187**

Scheme 4.5: Synthesis of R-2-chloro-*N*-[-2-naphtyl]ethylethanamide

187 **185** **181**

Scheme 4.6: Synthesis of the sensor 181

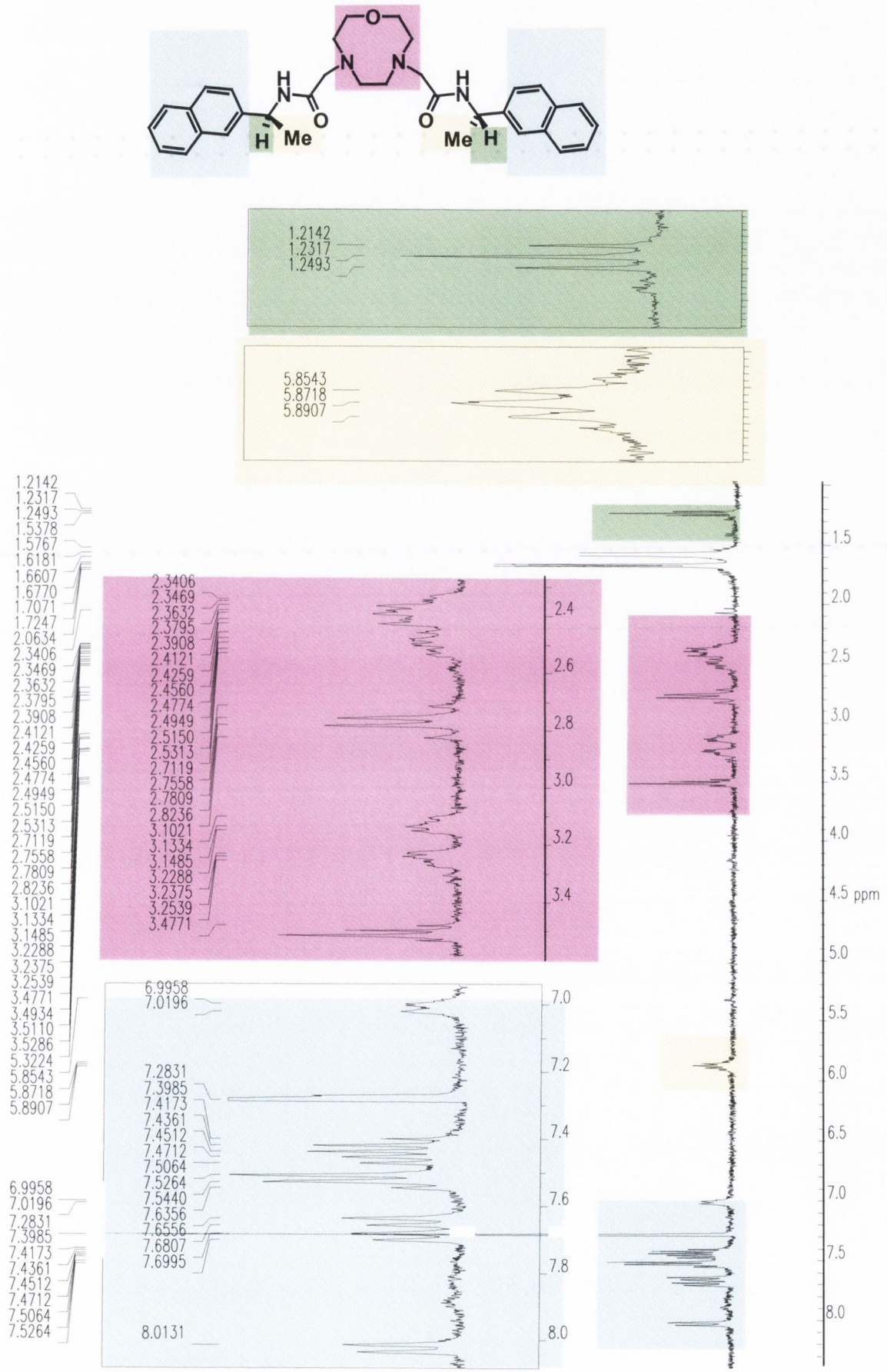

Fig. 4.4: ^{1}H NMR of the *S*–isomer of 141. The coloured areas on the ^{1}H NMR spectrum correspond to the coloured areas on the structure of 181

Both the *R*- and *S*- sensor **181** had to be purified using alumina chromatography using DCM and 0 to 1% MeOH as an eluent. When flash silica chromatography was used the sensor became protonated and it was necessary to treat the fractions with 1M NaOH to yield the free sensor. Both sensors were fully characterised by the conventional methods, ^1H and ^{13}C NMR, ES-MS, IR and CHN, and Figure 4.4 shows the NMR spectrum of the *S*- isomer of **181**. The molecule is diastereotopic. The axial and equatorial positions of the aza-crown ring are not equivalent, hence the serious of multiplets around 2.3 and 3.6 ppm. The diagnostic peak is a multiplet at 5.38 ppm representing the chiral methyl group of the spacer. It is expected that this peak would be a triplet but the fact that it is a multiplet suggests that the environment around the proton is non-equivalent.

The synthesis has shown that it is easy to prepare a novel PET sensor utilising known, reliable synthetic methods whilst acknowledging the prerequisites, discussed in section 4.2 above, of being simple, easy and quick to synthesise.

4.4 Photophysical Studies

The aim of this chapter was to prepare the *R* and *S* isomers of a novel PET sensor **181** for the selective determination of Li^+ at the therapeutic range (0.4 mM to 0.8 mM) under physiological conditions. The sensor must detect Li^+ selectivity over sodium, potassium and calcium. This will be analysed by fluorescence and ^1H NMR spectroscopy.

4.4.1 UV and Fluorescent Studies

The first measurements were carried out to determine the pKa of **181** because if the sensor was protonated at physiological pH it would not take up Li^+ due to electrostatic repulsion. Fluorescent spectra were measured at different pH starting from pH 12 to pH 2. The sensor was shown to be reversible when the pH was brought back up to 11 giving the same fluorescent intensity. No concurrent changes in absorption were observed suggesting a PET process was occurring. A graph of pH *vs.* fluorescent intensity at 338 nm showed a sigmoidal shaped curve over two pH units which is indicative of 1:1 binding and simple equilibrium as seen in Figure 4.5. This is indicative that the sensor is a pH PET sensor. From the graph it can be seen that the pKa was approximately 7.2 ± 0.1. This was disappointing because it suggests that in the physiological pH of 7.4 the sensor will be protonated thus affecting Li^+ complexation.

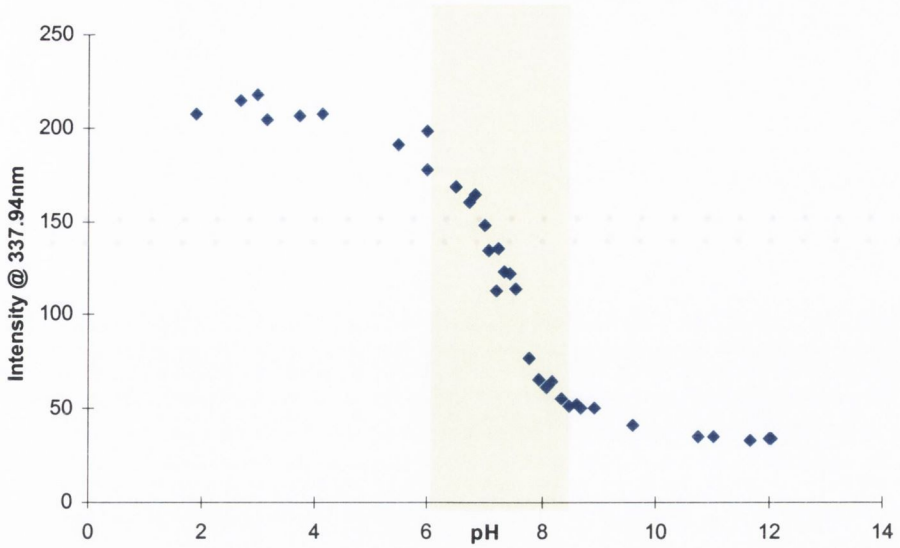

Fig. 4.5: Graph showing fluorescence intensity vs. pH. The yellow shading highlights the region for determining pKa.

This proved to be the case when measurements were carried out in buffered water solution at pH 7.4 using 0.1 M buffer and 0.1 M ionic strength. No fluorescence changes were seen upon titration with Li^+, Na^+ and K^+. Quenching was, however, seen in some cases. Upon further investigation it was established that the small halide ions were quenching fluorescence due to the heavy atom effect[221]. This is clearly demonstrated in Figure 4.6 which shows a graph of intensity versus Li^+ salt concentration. Significant quenching effects are observed with the spherical halide ions but not with the long chain acetate ions in the order $Br^->I^->^-OAc$.

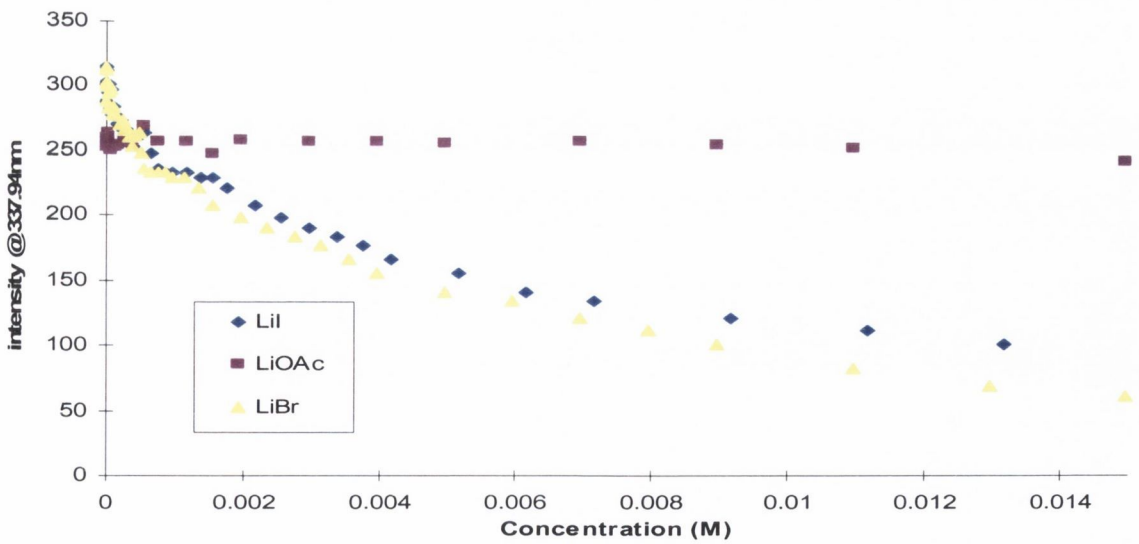

Fig. 4.6: Graph comparing the effect of quenching by various anions of Li^+ salts in the order $Br^->I^->^-OAc$.

Preliminary titrations on the α-chloronaphthalene ligand **187** were carried out using various Li^+ salts. They proved that the anion was quenching fluorescence due to the "heavy atom" effect even in the absence of the crown ether suggesting that the anion was not binding to the receptor. The heavy atom effect describes the interaction of small spherical anions acting as oscillators that result in vibrational energy competing with fluorescence to deactivate the excited state energy similar to the effect of hydroxy anions on lanthanide luminescence as discussed in chapter 1. Preliminary titrations were also run in water at pH 8.5 using a variety of Li^+ salts. From Figure 4.5 it is expected that the sensor **181** was fully deprotonated. No Li^+ recognition occurred but the results suggests that **181** was inefficient in removing the solvated water shell around the Li^+ ion. These results proved very disappointing as it showed that although **181** was capable of being a pH PET sensor it could not be used as a Li^+ PET sensor under physiological conditions.

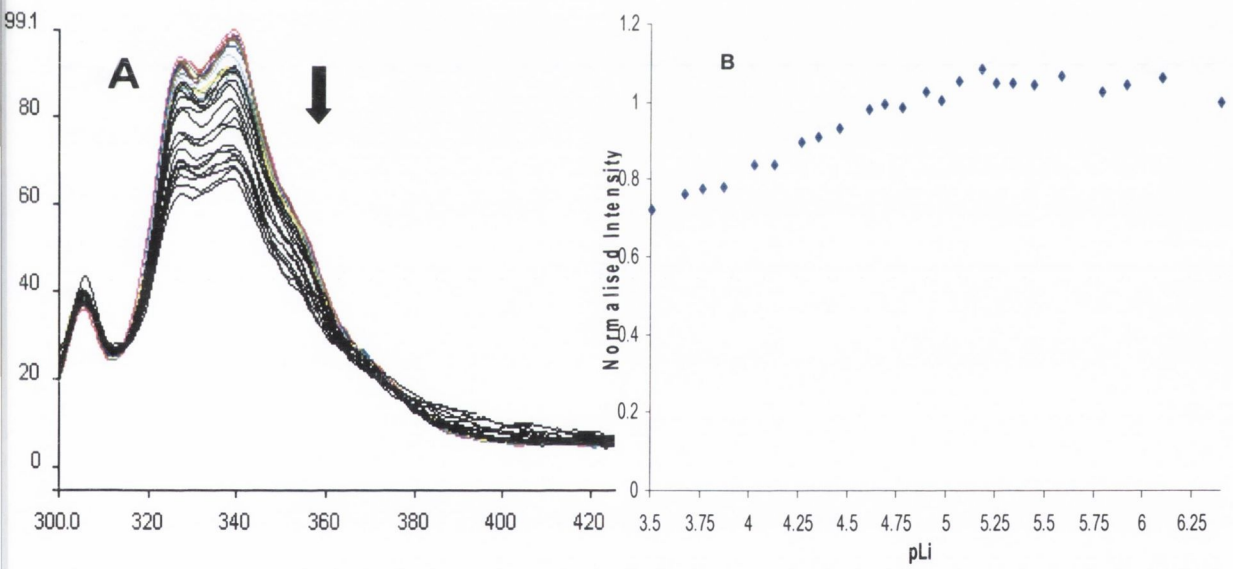

Fig. 4.7: A: Changes in fluorescence intensity upon titration of Li^+ acetate in MeOH. B: Graph showing ply (-log[Li^+]) versus fluorescence intensity in MeOH

Attempts were made to determine the Li^+ recognition ability of **181** in a range of solvents, MeOH, MeCN and in a mixture of both. In MeOH there were no significant changes in fluorescence when titrated with Lithium, sodium, potassium and calcium. This is highlighted in Figure 4.7. A slight decrease in fluorescence was also observed which was attributed to the heavy atom effect. Again, no changes were seen in 50:50 MeCN:MeOH. In

80:20 MeCN:MeOH a slight increase in fluorescence was seen but this was insignificant giving a 0.8 fold increase in fluorescence.

The titrations were repeated in MeCN using lithium acetate and lithium perchlorate salts. Unlike that previously discussed, the fluorescent emission at 337 nm was greatly enhanced upon titration with Li^+ leading to a 9-fold increase in fluorescent intensity. No changes were observed when titrated with sodium, potassium and calcium as is evident from Figure 4.8. The binding constant log β was found to be 5.4 using the formula[∝164]:

$$\mathbf{Log\ \beta = Log[(I_{max}-I)/(I-I_{min})]-Log[Li]}$$

where I is the fluorescent intensity, I_{max} is the maximum intensity observed and I_{min} is the minimum intensity observed.

The graph clearly shows that **181** is selective for Li^+ over all other metal alkali salts in MeCN. Even at high concentrations of sodium, potassium and calcium only slight changes in emission intensity were observed. It is clear that in MeCN it is easier for **181** to bind to Li^+ because in MeCN there is no hydration shell around the Li^+ ion. These results proved that the design of the sensor was appropriate for Li^+ recognition. It was a PET sensor (one of the first designed for Li^+) as the sigmoidal shaped curve was over two pM units, which as stated above is indicative of a simple equilibrium and 1:1 binding. No corresponding changes in the UV spectra were observed which is indicative of a PET sensor[175].

All the above photophysical investigations were run on the S-isomer of **181**. Investigations into the R-isomer showed that the R- isomer produced results almost identical to those of the S-isomer. Figure 4.9A displays the changes in intensity of the fluorescence spectrum upon Li^+ titration with the associated graph B showing the intensity versus –Log[Li]. The binding constant for the titration of **R-181** in MeCN with Li^+ was log β = 5.3. The quantum yield for the both isomers of the complexed sensor was found to be 0.11 whereas in the free sensor it was measured to be 0.022.

∝ See appendix 1 for derivation of this formula

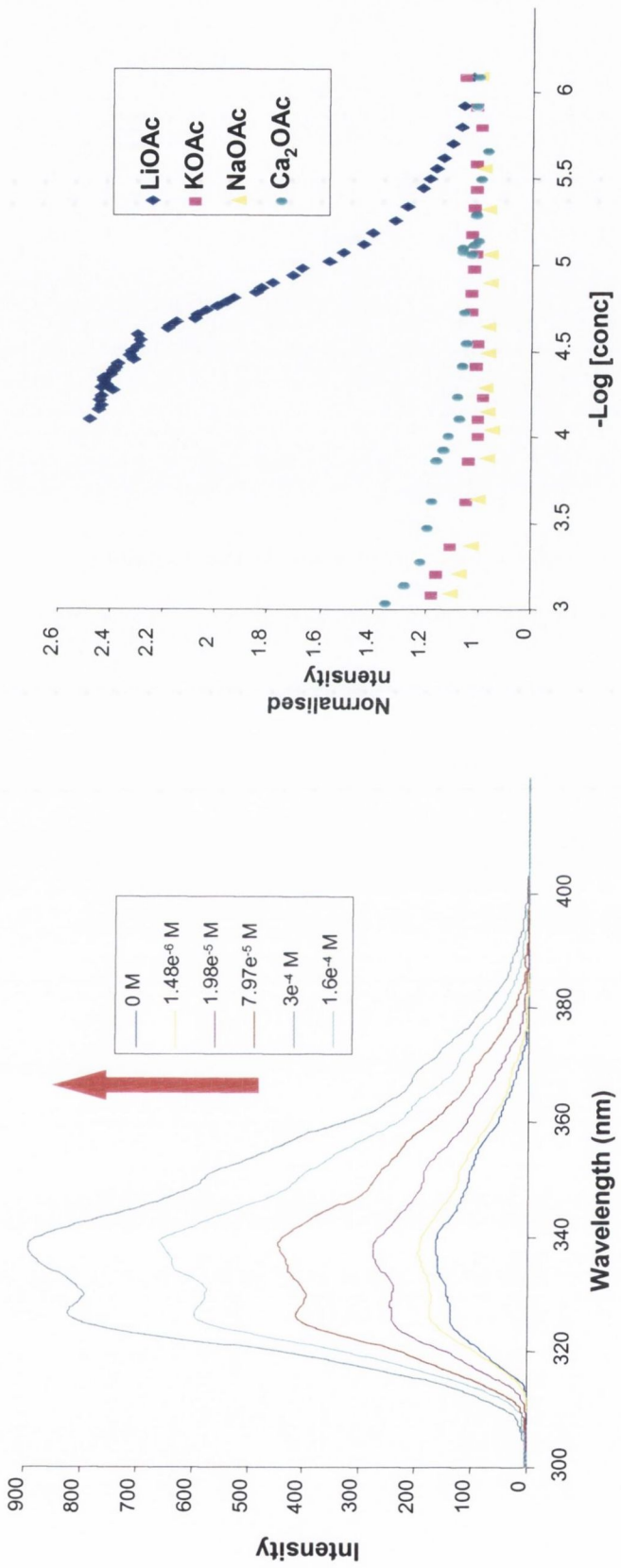

Figure 4.8: The fluorescence spectra of *S*-181 displaying changes in intensity upon titration with Li^+ in MeCN and the graph of intensity vs. -log[concentration]

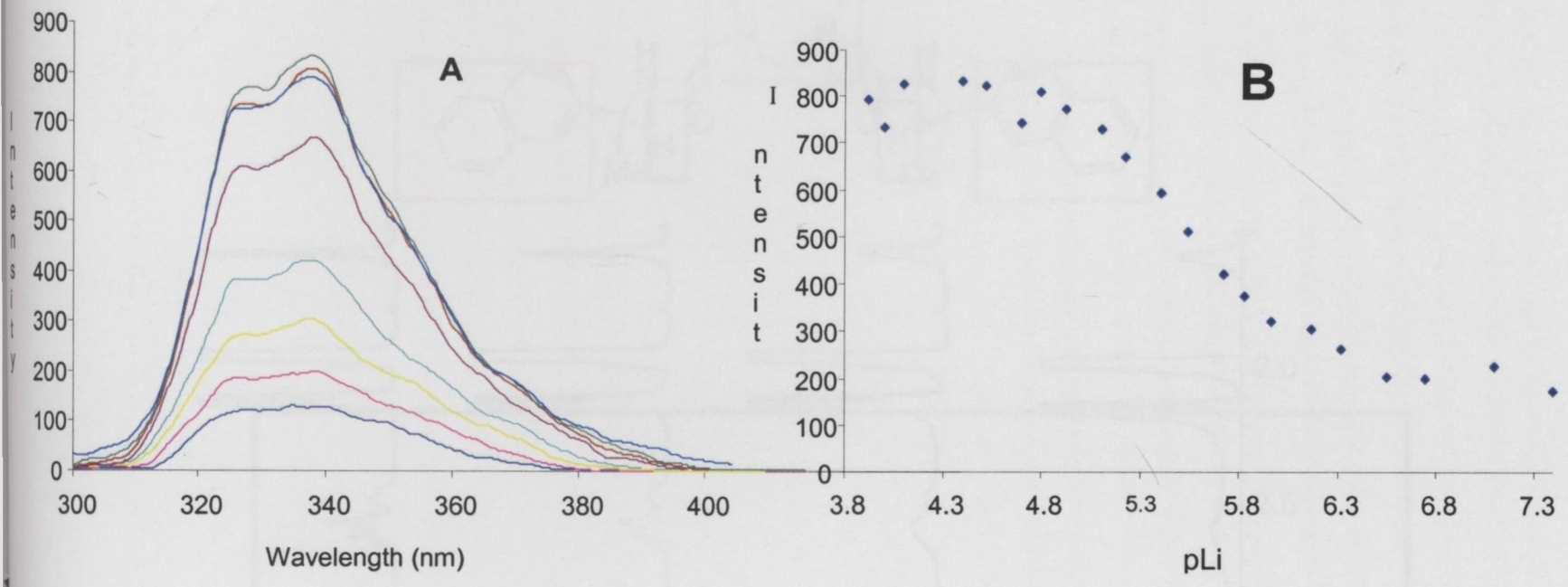

Fig. 4.9: Graphs showing the changes in intensity upon Li^+ titration for the R isomer of 181.

4.4.2 ^{1}H NMR Studies on **181**

^{1}H NMR studies were run to investigate if **181** undergoes conformational changes upon Li^+ recognition in d-MeCN. Figure 4.10 shows the ^{1}H NMR spectra of the S-isomer of **181** after the addition of 0, 1, 2 and 10 equivalents of Li^+. Minimal changes in resolution were observed in the aromatic region which is as expected because the naphthalene moiety does not participate directly in Li^+ binding. No changes in shift were seen for the diagnostic peak ($CH(CH_3)C$) but there was a loss of resolution due to perturbations in the conformation of **181**. The most dramatic changes in shift occurred in the crown ether region (2.25 to 3.5 ppm). In this region changes in shift and resolution were observed upon Li^+ titration. The peak at 3.04 ppm lost resolution from a multiplet to a broad singlet with a corresponding shift upfield to 3.5 ppm. The multiplet at 2.57 ppm transforms into a broad singlet with an upfield shift to approximately 3.0 ppm. The singlet at 3.04 ppm, corresponding to the CH_2, transformed into a broad singlet with a corresponding shift to 3.4 ppm. This was as expected as Li^+ The peak at 1.68 ppm, assigned to the CH_3 of the chiral methylene moiety, transformed from a doublet to a broad singlet with no change in shift. The ^{1}H NMR titrations support the data accumulated from the fluorescence titration studies. The data shows that the only changes in shift are seen in the crown ether region upon Li^+ recognition which is as expected as the crown ether needs to adapt its conformation in order to bind to Li^+ effectively. Minimal changes are seen in the other regions of the spectrum with only loss in resolution of peaks seen suggesting there is little or no change in conformation of **181** occurs upon Li^+ recognition.

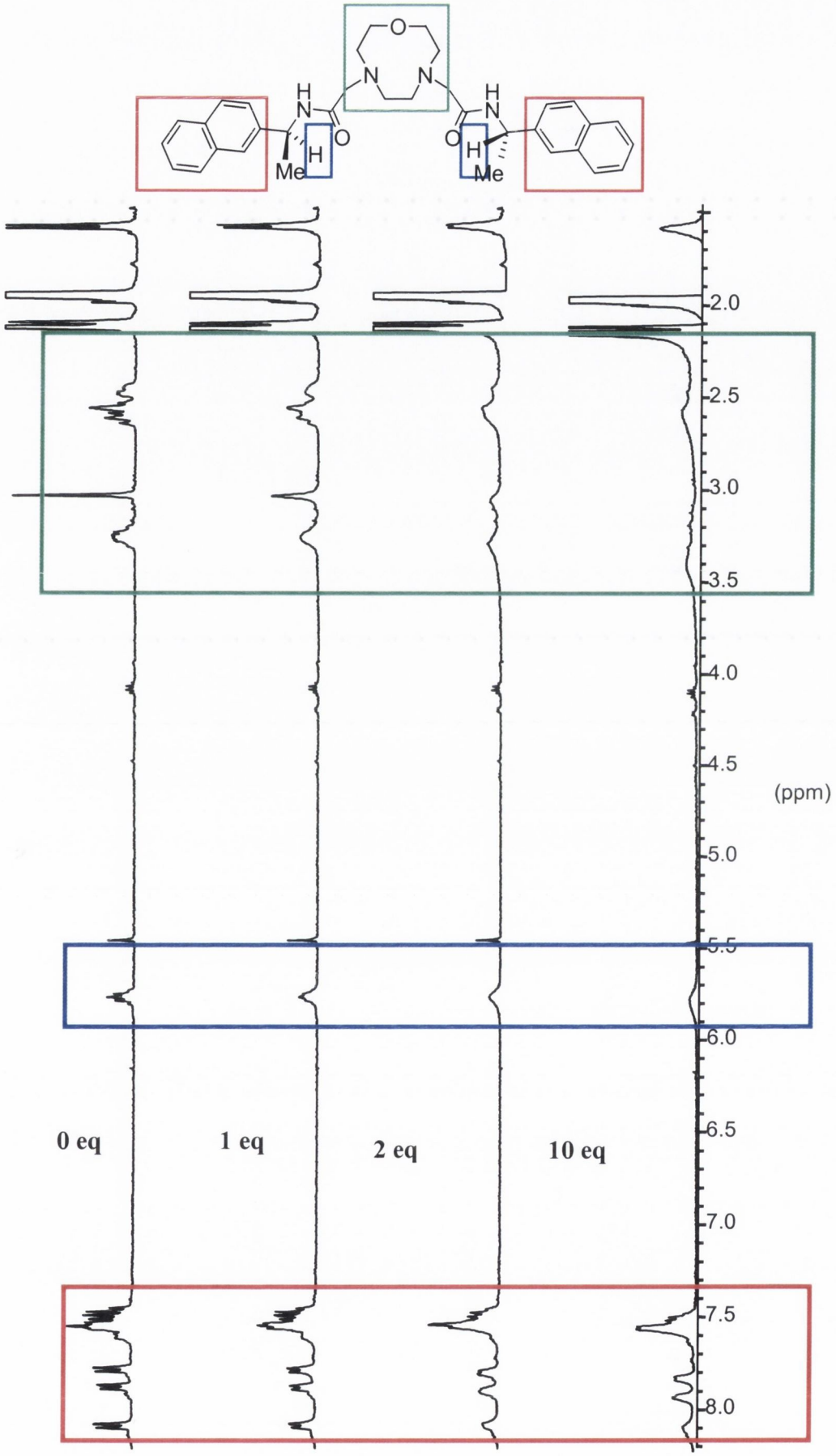

Fig. 4.10: Changes in the NMR spectroscopy upon Li^+ titration of *S*-181. The red section shows the aromatic changes; the blue section shows the changes of the diagnostic peak; the green section shows changes in the crown ether region.

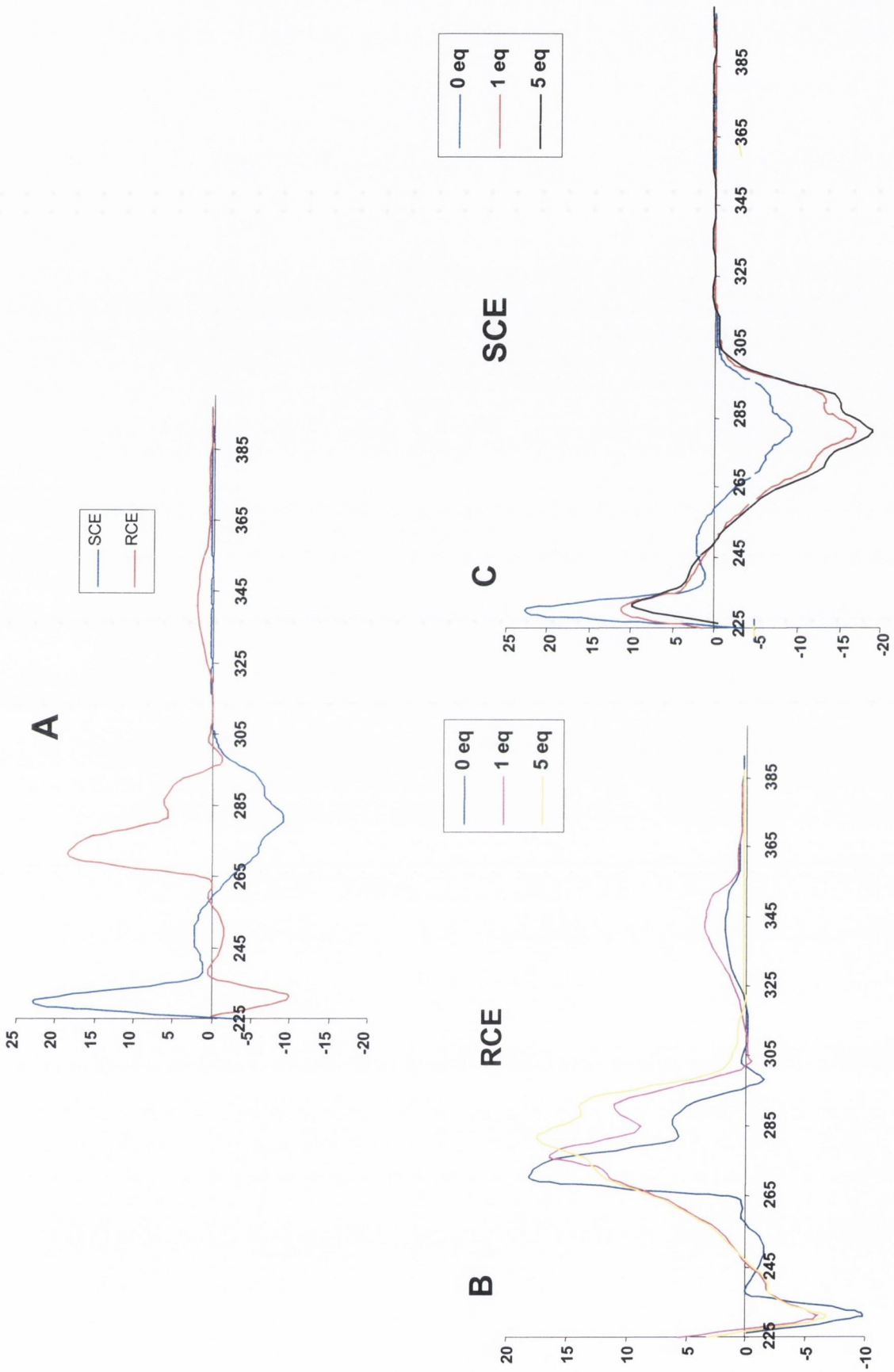

Fig. 4.11: A: CD spectra of the R- and S- isomers 181. Notice the opposite nature of the two curves indicating both compounds are isomers. B: CD spectra showing the effect on intensity of R-181 upon addition of one and five equivalents of Li^+. C: CD spectra showing the effect on intensity of S-181 upon addition of one and five equivalents of Li^+

4.4.3 CD Measurements

The chiral nature of **181** suggests that CD spectroscopy would be a useful tool to determine if a change in conformation occurs upon Li^+ recognition as shown in Figure 45.11. for both isomers of **181** the starting material for the chromophore was (+)-S-1-[-1-naphtyl]ethylamine or (-)-(R)-1-[-1-naphtyl]ethylamine. These compounds were coupled to chloroacetic acid using peptide-coupling methods, which are known to retain the chirality (*i.e.* opposite signs) of the starting materials. It is presumed that this chirality is retained during the synthesis of both isomers of **181**. Firstly, it was proved that both compounds were chiral, providing the proof that the synthesis of **181** (scheme 4.6) resulted in chiral compounds. When *S*-**181** was titrated with one and five equivalents of Li^+ an increase in intensity was observed with no corresponding change in shift. *R*-**181** showed no change in intensity but instead showed a change in shift from 270 nm to 280 nm

4.4.4 Conclusions

All these results gathered from the photophysical measurements on the *R*- and *S*-isomer of **181** with Li^+ and other alkali metal ions have shown that the sensor is a selective PET sensor for Li^+. It is also a pH PET sensor but the pKa is approximately 7. This suggests that the sensor is protonated in the physiological pH range. This was confirmed when the titrations were run in water at pH 7.4 but the sensor was inefficient at removing the solvated water molecules around Li^+.

4.5 Investigations into the Utilisation of 181 as Enantioselective Sensors for Amino Acids

Recently sensors for the enantioselective detection of amino acids have become of increasing importance. The ability of the receptor to discriminate between enantiomers could conceivably allow the separation of racemates *via* selective transport across a membrane. It was thought that the chiral nature of both isomers of **181** could allow the enantioselective discrimination of amino acids and their derivatives.

The Kilburn group used thiourea receptors **188** for the enantioselective recognition of amino acids and their derivatives[222]. These simple acyclic receptors are both sidechain selective and moderately enantioselective for a number of amino acids such as *N*-acetyl alanine, *N*-acetyl serine and *N*-acetyl tryptophan when analysed by ^1H NMR. The Pu group developed a fluorescent sensor **189** for the determination of the chiral α-hydroxycarboxylic acids, which are found to be the structural units of many natural products and drug molecules[223]. The fluorescence of *S,S* isomer of **189** was more enhanced in the presence of *S*-mandelic than *R*-

mandelic acid thus leading the authors to suggest that **189** was an enantioselective α-hydroxycarboxylic acid fluorescent sensor.

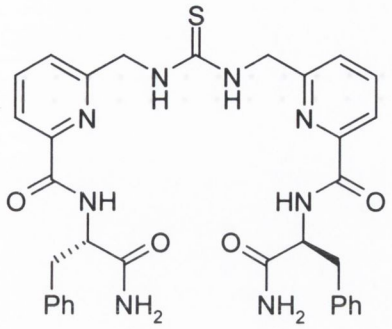

188

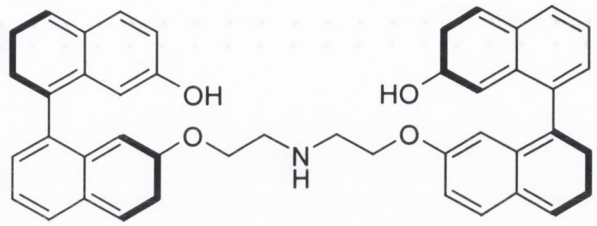

189

4.5.1 UV and Fluorescent Studies

These papers suggest that enantioselective determination can be achieved. To this end, it was decided to utilise **181** as an enantioselective fluorescent sensor for small chiral amino acids. The *R*- and *S*- isomers of **181** are chiral molecules containing a number of sites for hydrogen bonding. At pH 8 and 6 in 80:20 acetonitrile:water, no changes in fluorescence was seen upon titration with glycine, glycine methyl ester, glycine ethyl ester, D- and L-alanine and D- and L-alanine methyl ester

At pH 7.4 the S-isomer of **181** showed a substantial increase in fluorescence intensity upon titration with glycine in 80:20 acetonitrile:water as shown in Figure 4.12 with a log β of 5.45. This 5-fold increase in intensity was not seen for the R-isomer. The titrations were repeated using glycine methyl ester, D- and L-alanine and D- and L-alanine methyl ester. No enhancement of fluorescence was seen. This is shown in Figure 4.11. The fluorescence spectra show a change in shape suggesting that *S*-**181** undergoes a conformational change upon glycine recognition.

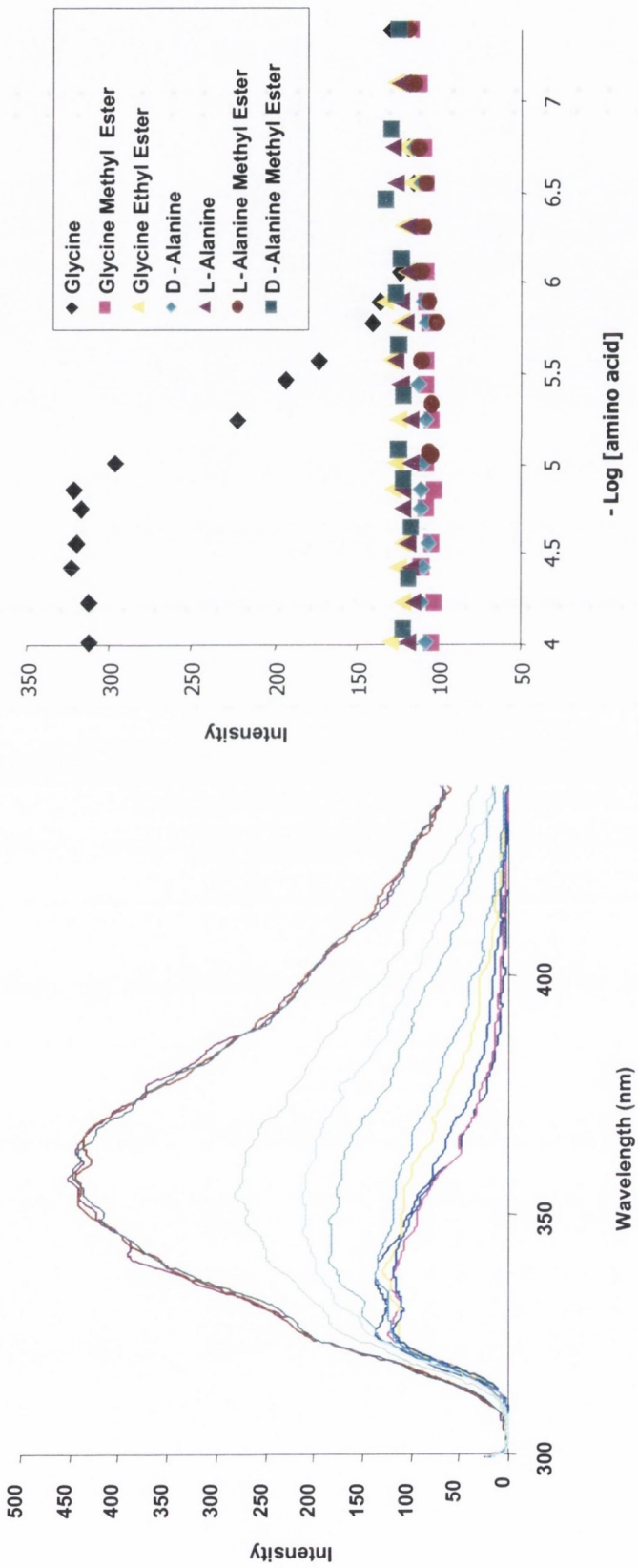

Fig. 4.12: Diagram displaying the selectivity of *S*-isomer of 181 for glycine over other amino acids.

Isomer of 181	*Analyte*	*Solvent*	*Excitation λ (nm)*	*Emission λ (nm)*	*Log β*	*Φ*
R	***Li^+***	MeCN	280	340	5.3	0.11
	Li^+	MeCN	280	343	5.4	0.11
S	***Glycine***	80:20 MeCN:H_2O	280	353	5.45	----

Table 4.2: Luminescent data for 181 with Li^+ and glycine.

4.6 Conclusion

In conclusion this chapter has discussed synthesis and photophysical evaluation of a pH and Li^+ PET sensor **181**. The design of the sensor was based on a small cavity crown ether. While 12-crown-4-ether is known to be an ideal fit for the Li^+ ion, 9-crown-3-ether has a smaller cavity and was chosen as the receptor to increase the discrimination of the small Li^+ over other physiologically important ions such as sodium and potassium. Amide arms were added to increase this discrimination and to aid the binding ability of the receptor. The spacer is a chiral methylene group as the shorter the spacer length the more efficient the electron transfer. The reporter group is a naphthalene fluorophore. The sensor is suitable as a pH sensor showing a pKa of 7.2. The sigmoidal shaped curve, Figure 4.5, is over two pH units, which is indicative of a PET sensor. Unfortunately this means that **181** is protonated at physiological pH. This was the case when titrations with Li^+ were run at pH 7.4 in aqueous solutions. Quenching was observed due to the heavy atom effect of the small spherical halides acting as oscillators. The titrations were repeated in MeCN. Dramatic changes in fluorescence intensity were observed upon Li^+ titration with both *S*- and *R*- **181**. A binding constant of log β 5.4 was observed with a quantum yield of 0.11 for the Li+ complexed sensor and 0.022 for the free sensor. These results suggest that **181** was a selective PET sensor for Li^+ in MeCN. Preliminary measurements were run to see if **181** could enantioselectively detect small amino acids. The *S*-**181** was selective for glycine in 80:20 acetonitrile:water with a 5-fold increase in fluorescence corresponding to a binding constant of log β 5.4. Glycine methyl ester, glycine ethyl ester, D and L-alanine and D, and L-alanine methyl ester showed no changes in fluorescent intensity. No changes were seen for the R-isomer **181.**

Chapter 5

Novel nitrogen-Based Ligands

5.1: Synthesis of Novel Supramolecular Compounds

The previous chapters have discussed the synthesis of a number of supramolecular ligands which have gone on to be utilised in a number of ways such as lanthanide luminescent complexes, catalysts for the hydrolysis of RNA and a lithium PET sensor. This chapter will discuss the design, synthesis and characterisation of a number of novel nitrogen-based pseudopeptide ligands which were subsequently complexed to Pt(II). Their anti-tumour activity was determined. It was attempted to use these ligands to synthesise novel macrocyclic ligands using Grubbs catalyst to create new C-C bonds. This was not achieved and instead **96** an intermediate in the synthesis of the pyridinophanes as discussed in chapter 2 was employed instead. From the basic architecture of **96** three intermediates in the synthesis of the macrocycles were obtained but they could not be further developed.

5.2 Novel Platinum Complexes As Cisplatin Analogues

Since the discovery of the anti-tumour activity of cisplatin (*cis*-$[Pt(NH_3)_2Cl_2]$) by Rosenberg in 1967, which is commonly used against ovarian and testicular cancer, research has been directed to the synthesis of cisplatin analogues to increase the anti-tumour activity whilst limiting side effects[224,225]. The side effects of cisplatin include nausea, vomiting and neurotoxicity. The anti-tumour activity of cisplatin arises from its binding to the major groove of DNA where the two chlorine atoms are replaced by the N7 atoms of the adjacent guanine base[226]. These cisplatin-DNA complexes bend and unwind the DNA duplex at the site of damage with its major groove being compressed and its minor groove widened[224]. Carboplatin is a closely related analogue of cisplatin and is one of the second generation of platinum complexes used for anti-tumour activity. It is less toxic but requires higher doses[224]. Cisplatin and carboplatin have two major shortcomings namely toxicity, which is thought to be related to protein binding of the Pt(II) complexes, and the development of resistance of a number of tumours to the first and second generation of drugs. Recently cisplatin analogues have been synthesised to improve the solubility and counteract the toxicity of cisplatin. Examples such as *cis*-$[Pt(DMSO)_2(CH_3)_2]$[227] **190** and JM-216 [*cis,trans,cis*-$PtCl_2(OAc)_2(NH_3)(C_6H_{11}NH_2)$] **191**, which is taken orally and is converted to Pt(II) in the stomach, have been synthesised which are more soluble than cisplatin and carboplatin with less of the toxic side effects such as nausea, vomiting and neurotoxicity[224,228]. Once a new complex has been synthesised its interactions with nucleic bases and oligionucleotides is tested to determine its anti-tumour activity.

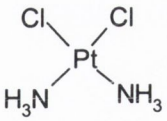

Cisplatin

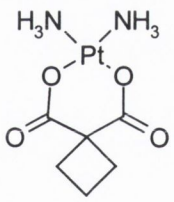

Carboplatin

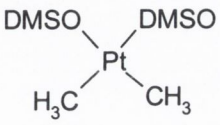

190

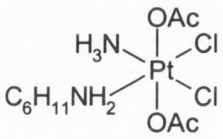

191

Recently a number of novel cisplatin analogues have been synthesised using platinum(II) complexed to pyrrolidines such as **192**[229,230], pyridine **193**[231], and benzimidazole **194**[231]. **193** and **194** were synthesised to increase the hydrophobicity around the platinum complex-DNA binding site thus preventing any interfering interactions.

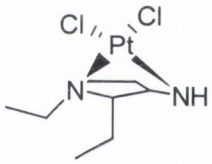

192

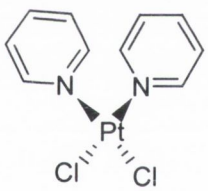

193

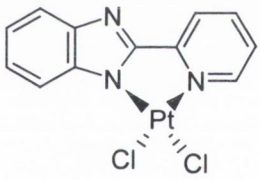

194

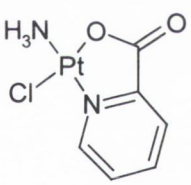

195

Structure-activity relationships have been developed for Pt complexes and they have shown that the *cis* geometry of amines and the presence of at least one NH group appear to be important for the complex to show some anti-cancer activity although some complexes have deviated from this classical model[232,233]. For example, Farrell *et al* have shown that while transplatin is inactive, the addition of a planar ligand dramatically enhances the *in vitro* cytotoxicity of the *trans* geometry[234]. They developed a complex containing an N,O chelating ligand *trans*-[PtCl(PyAc-*N,O*)(NH_3)] **195** to be more water-soluble than other *trans* platinum complexes[235], which was found to have similar activity to cisplatin *in vitro.* Nolan *et al* have developed several cisplatin analogues of ethylenediamine-derived ligands containing a number of substituents[237]. Similar complexes based on ethylenediamine ligands have been found to be less active than cisplatin[236], but the addition of $-CH_2CH_2OH$ substituents attached

to one or more of the nitrogen atoms, creating **196** and **197** respectively, helped stabilise the platinated DNA adduct by hydrogen bonding[237]. The anti-tumour activity of these complexes was better than those previously reported[236] but not as impressive as cisplatin[237]. The Nolan group developed these substituted diamines by adding an *N''*-methylacetamide group at the *N* position of diaminoethane to create 1,2-diaminoethane-*N,N,N'N'*-tetra(*N''*-methylacetamide) **198**[238]. When **198** was complexed to Pt(II) it was found that the complex was deprotonated at the amide position.

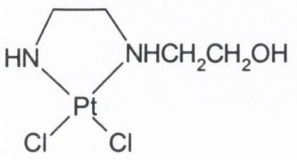

196

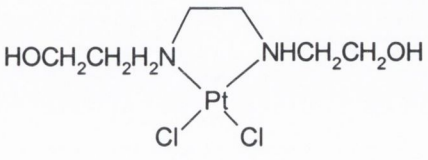

197

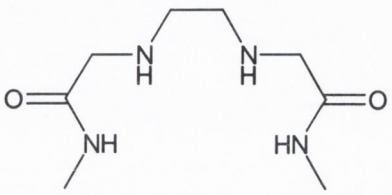

198

Reedjik *et al* developed a potentially active trimeric arginine-containing peptide complexed to Pt(II) **199** using solid phase synthesis[239]. The molecule **199** contains an arginine-glycine dipeptide tethered to an ethylenediamine moiety, which in turn serves as a platinum chelating ligand. They hoped to show that the presence of the peptide moiety would help prevent tumour resistance that has been seen in cisplatin and carboplatin.

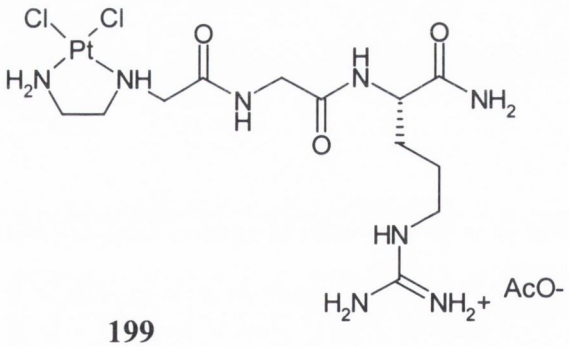

199

In conclusion, this brief introduction section has shown that novel platinum complexes are required to overcome the toxic effects of cisplatin and carboplatin whilst retaining similar activity to these. Structural-activity relationships have suggested that *cis* geometry is required and the presence of at least one NH group appear to be necessary for active anti-tumour agents. The Nolan group has shown that *N*-functionalised diaminoethane ligands readily form complexes with Pt(II) giving cisplatin analogues with excellent anti-tumour activity. The Reedjik group have also shown that large peptide groups can be attached to diaminoethane to

form stable complexes. To this end, novel pseudopeptide ligands were synthesised from diaminoethane and 1,2-trans-diaminocyclohexane, which were coupled, to L-alanine or L-proline producing the ligands **200, 201, 203** and **204**. These ligands were fully characterised and complexed to Pt(II) to produce cisplatin complexes.

5.2.1 Design of Novel Pseudopeptide Ligands for Platinum Complexation

Four pseudopeptide ligands were prepared for complexing to Pt(II) from the peptide coupling of an amino acid (L-proline or L-alanine) to a compound containing an amino moiety, in this case either diaminoethane or diaminocyclohexane. All the complexes were characterised using conventional methods. The Nolan group has already prepared Pt(II) ligands using diaminoethane, which have shown efficient anti-tumour activity so it was hoped that the addition of a chiral amino acid to the amino moiety via peptide coupling would add a new dimension to this series of molecules and help overcome tumour resistance to Pt(II) class of drugs.

5.2.2 Synthesis of Novel Platinum Complexes

The four pseudopeptide ligands **200** to **203** were prepared for complexing to Pt(II) from the peptide coupling of Boc-protected L-proline or L-alanine to a compound containing an amino moiety, in this case either diaminoethane or diaminocyclohexane. Peptide coupling was used to covalently link the amino acid to the amine-containing compound the synthesis requires mild reaction conditions, is quick and easy and retains chirality[240]. The four molecules synthesised for complexing to Pt(II) were *N,N'*-[Bis-(L-proline)]-*trans*-diaminocyclohexane **200**, *N,N'*-[Bis-(L-proline)]diaminoethane **201**, *N,N'*-[Bis-(L-alanine)]diaminoethane **202** and *N,N'*-[Bis-(L-alanine)]-*trans*-diaminocyclohexane **203**.

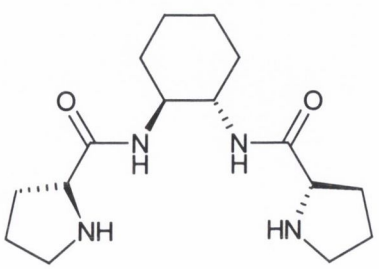

200

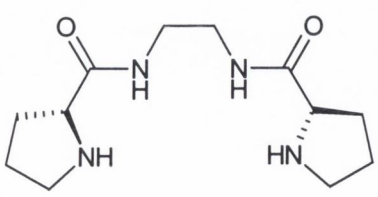

201

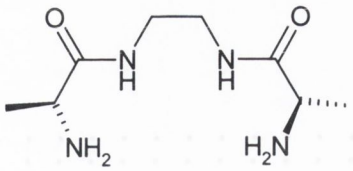

202

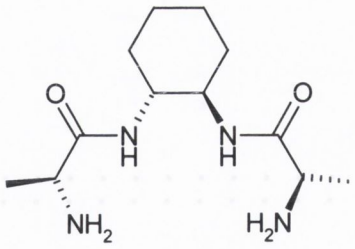

203

The first step in the synthesis of these ligands was the protection of the amine moiety in the amino acid to prevent self-coupling during the peptide coupling synthesis to produce *N*-Boc-L-alanine **204** and *N*-Boc-L-proline **205** from L-alanine and L-proline as shown in Scheme 5.1[240]. The synthesis involved the condensation of the amine moiety of the amino acid with $(Boc)_2O$ using basic conditions. The reaction proceeded well with yields of 61% and 64% for *N*-Boc-L-alanine and *N*-Boc-L-proline respectively.

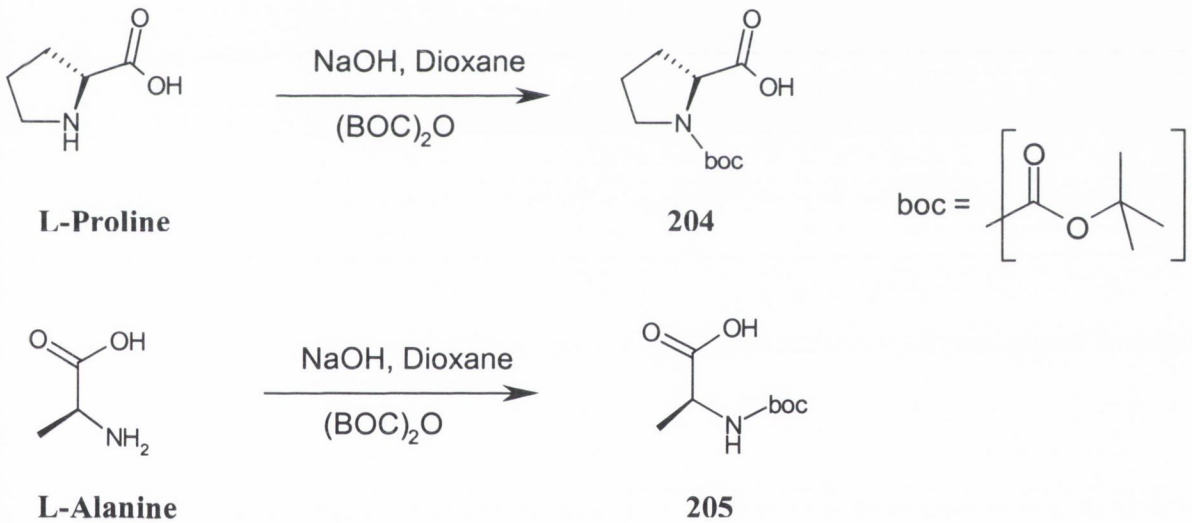

L-Proline **204**

L-Alanine **205**

Scheme 5.1 : Protection of the amine group using $(Boc)_2O$

The Boc-protected amino acids were then coupled to either diaminoethane or *trans*-1,2-diaminocyclohexane using standard peptide-coupling syntheses to give the Boc-protected pseudopeptides **206** to **209**[240]. The mechanism of the peptide coupling reaction involves the formation of an activated ester, using dicyclohexylcarbodiimide (DCC) or N-ethyl-N'-(dimethylamino)propylcarbodiimide (EDCI) shown below, on the amino acid and then the condensation of this activated ester with the amino-containing compound as shown in Scheme 5.2. HOBt is also used in the synthesis to increase the formation of the activated ester.

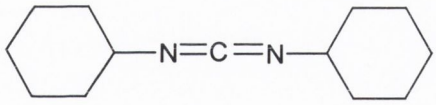

DCC

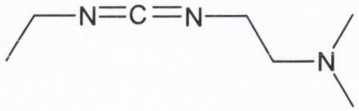

EDCI

The synthesis of *N,N'*-[bis(*N*-Boc-L-proline)]diaminoethane **206** was first attempted using dicyclohexylcarbodiimide (DCC). It was found that it was difficult to remove the DCC-urea by-product of the reaction by washing with base and brine since the urea was not water-soluble. The only effective way of removing the urea was by utilising column chromatography, which was not feasible in this case because of the difficulties of detecting the presence of **206**. It was found that replacing the coupling agent DCC with *N*-ethyl-*N*-dimethylcarbodiimide (EDCI), which has a urea by-product that is water-soluble and can be removed by washing with base and brine leaving the BOC-protected peptide. This coupling agent was used to synthesise the rest of the BOC-protected pseudopeptides **206** to **209**.

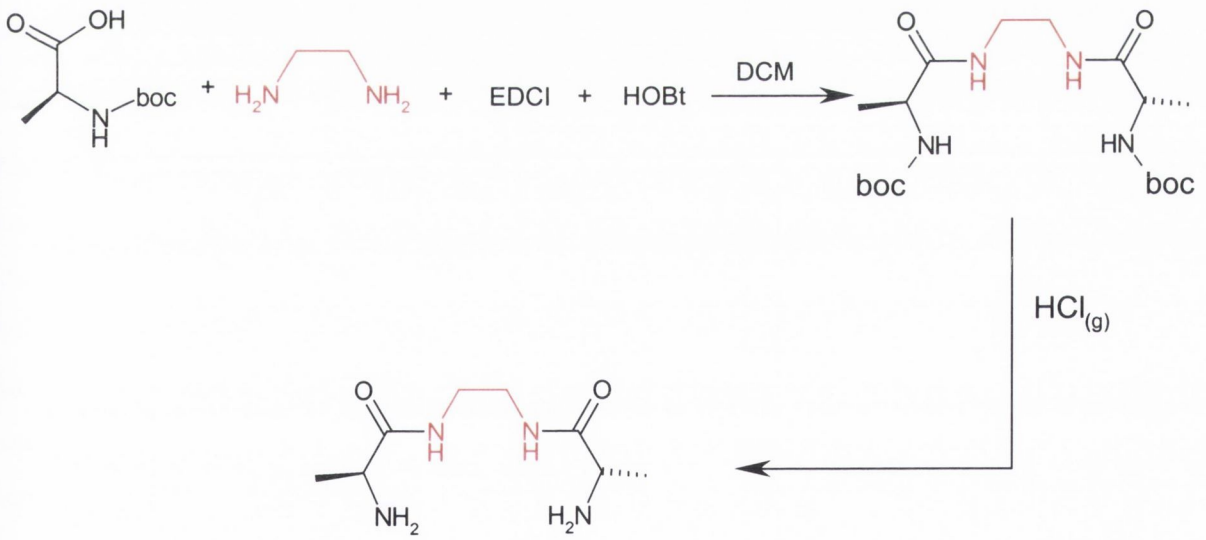

Scheme 5.2: Coupling of BOC-protected amino acid with amine-containing compounds and removal of the Boc protecting group.

The next stage in the synthesis of the pseudo peptides was to remove the Boc group to produce the free amine. The most common method of removing the Boc group is to stir the Boc-protected pseudopeptides in 10:90 TFA:DCM mixture[240]. However this method gave low

yields for **200**, **202** and **203** and degraded **201**. Another method employed to remove the Boc group was to stir the Boc-protected pseudopeptides in 4M HCl in dioxane[241]. This afforded the pseudopeptides in low yields.

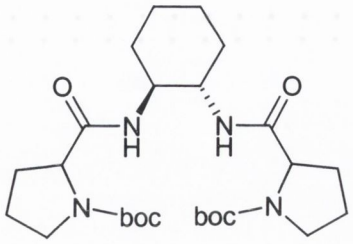

206

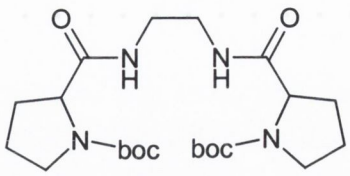

207

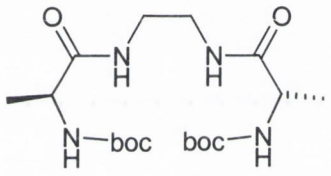

208

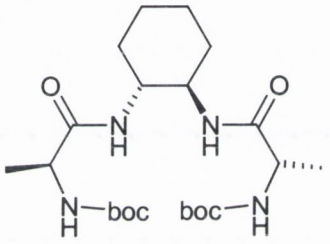

209

To increase the yields of the pseudopeptides, HCl gas was created *in situ* and bubbled through a solution of the Boc-protected pseudopeptide in ethanol. After stirring for four hours, ether was added and the product precipitated out of solution. The pseudopeptides were isolated by filtration as their hydrochloride salts in good yields, 35% for **201**, 92% for **200**, 96% for **202** and 93% for **203**. These compounds were very hydroscopic and had to be stored in a dessicator under P_2O_5. Characterisation of these complexes was achieved by the usual methods. As a result of the hygroscopic nature of these ligands, CHN data was not conclusive and accurate mass was used instead.

These pseudopeptide ligands were complexed to platinum using K_2PtCl_4 in water[242]. Originally the mixture was allowed to stir overnight at room temperature but the yields were very low[242]. The yields of the platinum complexes were increased by heating the reaction for four hours and the reaction was left to cool to room temperature. This resulted in a precipitate, which was collected by filtration[243,244]. All the complexes [**200**.$PtCl_2$], [**201**.$PtCl_2$], [**202**.$PtCl_2$] and [**203**.$PtCl_2$] (proposed structures based on literature information) were yellow in colour. Unfortunately it was not able to perform X-ray crystallography to determine the

precise nature of the complexes due to problems with solubility. The characterisation data, NMR, ES-MS, IR and CHN, suggests that the complexes were prepared. ES-MS data was not clear and suggests the complex broke down in solution when the column temperature was 100°C. The column temperature was cooled to 50°C and the Pt(II) complexes were analysed. For [**200**.$PtCl_2$] a peak at 622 was seen corresponding to [**200**.$PtCl_2$] with two sodium ions that were probably picked up during analysis. This shows the complex [**200**.$PtCl_2$] was present. Figure 5.2 shows a comparison of the ^{1}H NMR of **200** compared to its corresponding platinum complex [**200**.$PtCl_2$].

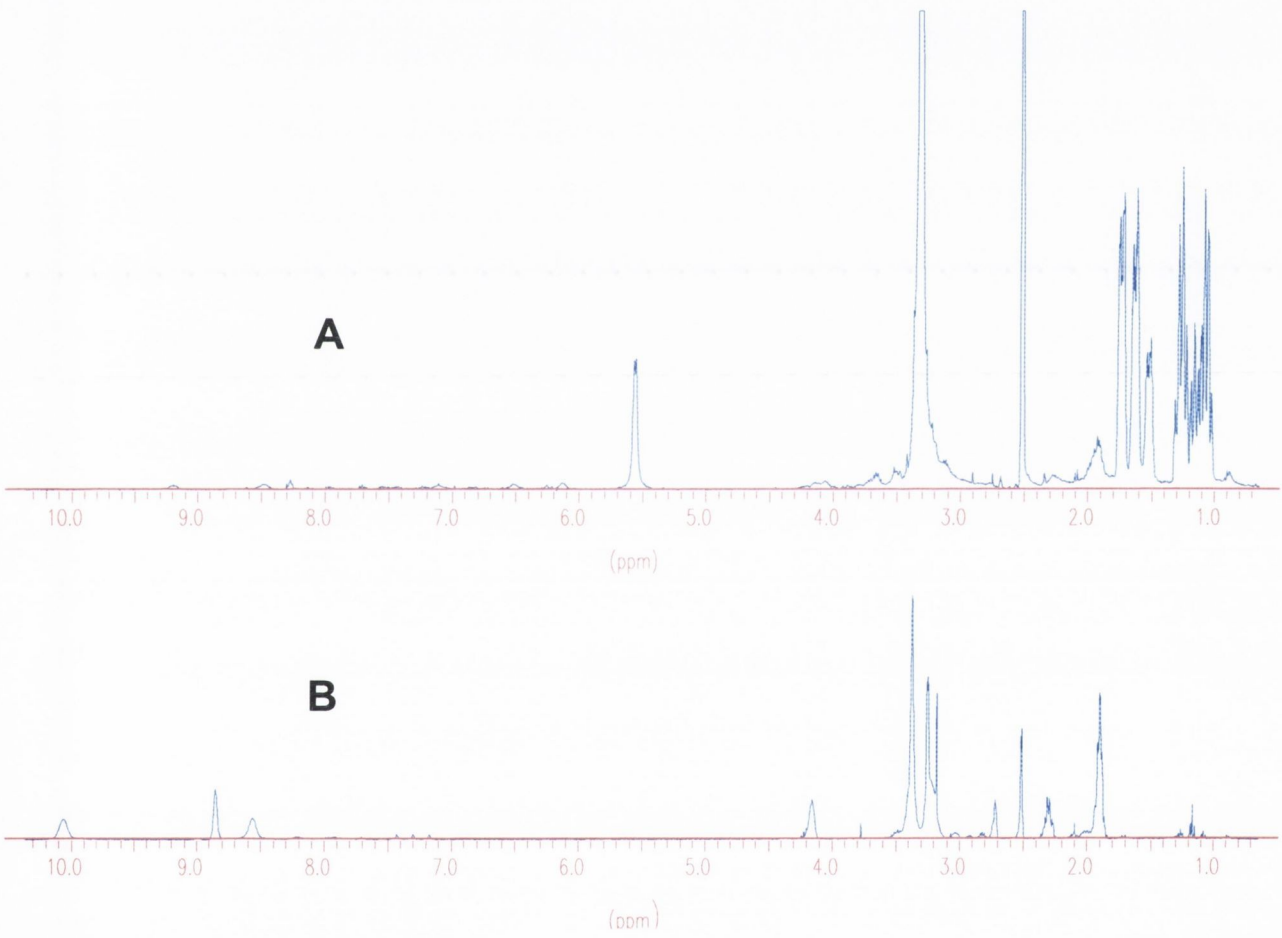

Fig. 5.2: comparison of the ^{1}H NMR of A: 200 compared to B: its corresponding platinum complex [200.$PtCl_2$].

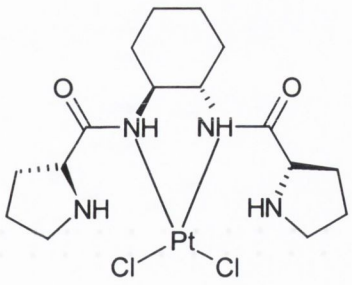

[**200**.$PtCl_2$]

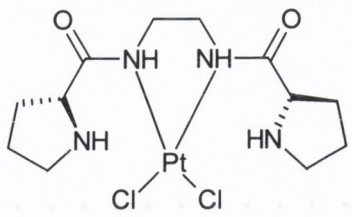

[**201**.$PtCl_2$]

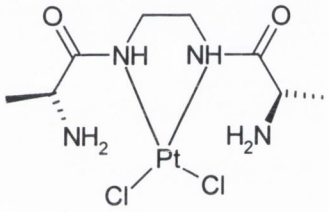

[**202**.$PtCl_2$]

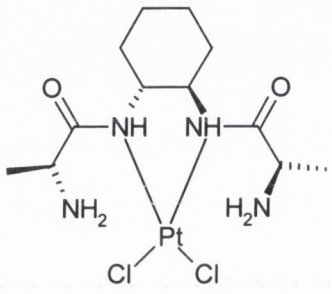

[**203**.$PtCl_2$]

These platinum complexes were then tested for anti-tumour activity in St. James hospital using HL-60 cells, which are general cancer cells used to determine a chemicals ability to induce cell death (apoptosis). The cytotoxicity effects of the Pt(II) complexes on HL-60 cells over 24 hours was determined by MTT assay. Table 5.1 shows each Pt(II) complex and its corresponding dose-response curve with HL-60 cells. These graphs show that the anti-tumour activity of the complexes was poor with only some cytotoxicity being achieved. The graph shows the complexes corresponding EC_{50} values. The EC_{50} value is the effective concentration at which 50% of cells are killed. For the complexes to be efficient at cell apoptosis an EC value of around one to five should be obtained to necessitate any further investigations into the complexes' anti-tumour ability. This data suggests that further functionalisation of the ligands should be utilised to increase the anti-tumour ability of the Pt(II) complexes.

Pt(II) Complex	Dose-Response Curve	EC_{50} Values
[**200**.$PtCl_2$]	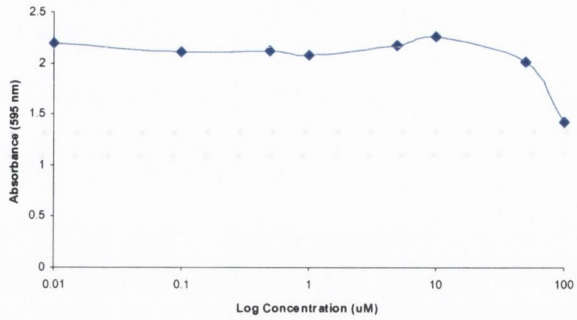	**76.82**
[**201**.$PtCl_2$]	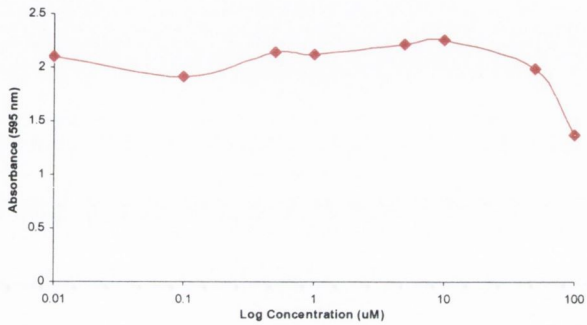	**78.45**
[**202**.$PtCl_2$]	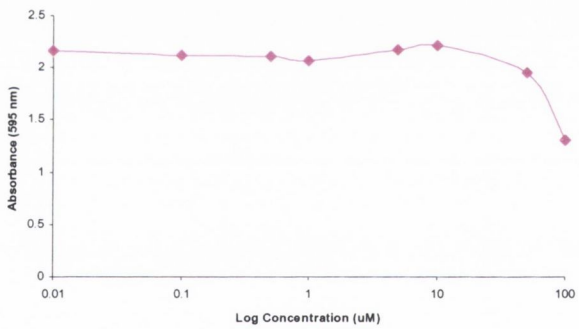	**64.36**
[**203**.$PtCl_2$]	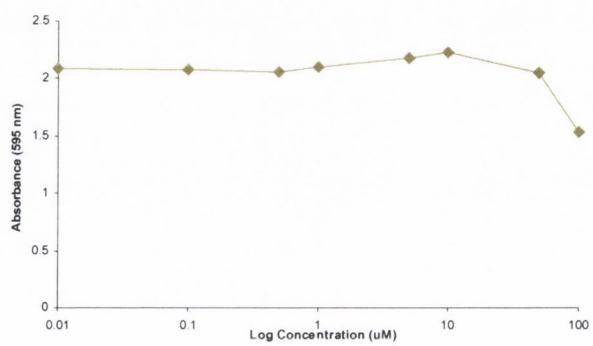	**109.1**

Table 5.1: The dose-response curve for the Pt(II) complexes with the corresponding EC_{50} value

5.2.3 Conclusion

This section has shown that the pseudopeptide ligands, **200**, **201**, **202** and **203**, are readily and easily synthesised using peptide-coupling techniques. Characterisation of these compounds was achieved using conventional methods. The Reedjik and Nolan groups have shown that Pt(II) complexes using peptides and a diaminoethane skeleton readily form complexes with Pt(II)[237,238,239]. This suggested that the pseudopeptides, **200**, **201**, **202** and **203**, would form complexes with Pt(II). Characterisation data show the complexes were synthesised cleanly and in good yields of 57%, 68%, 54% and 63% for **200**, **201**, **202** and **203** respectively. These pseudopeptides were then complexed to Pt(II) using K_2PtCl_4 to produce [**200**.$PtCl_2$], [**202**.$PtCl_2$], [**203**.$PtCl_2$] and [**204**.$PtCl_2$]. The complexes were synthesised in good yield as yellow solids. Characterisation data show the complexes were synthesised as a comparison of the ^1H NMRs of the free and Pt(II) complexed pseudopeptides show (Figure 5.2). Studies run in St. James hospital by Dr. Tony McElliott show that the complexes ability to induce cell apoptosis of HL-60 cells was poor giving EC_{50} values of around 75. This suggests that the complexes may have to undergo further functionalisation to increase their anti-tumour activity.

5.3: Synthesis of Novel Macrocycles:

Ring closing olefin metathesis (RCM) offers a versatile way to synthesise C-C bonds in otherwise inaccessible macrocycles with the use of catalysts[245]. State of the art ruthenium catalysts are not only highly active in forming new C-C bonds but are also compatible with most functional groups. The major ruthenium catalyst readily available to use is Grubbs catalyst as shown below developed by Grubbs and co-workers[246,247]. This catalyst has many applications including the synthesis of polymers, medium to large ring systems, fused ring systems and the synthesis of catenanes[248]. Unfortunately ruthenium catalysts are limited by their incompatibility with basic functional groups notably amines and nitriles. The mechanism of synthesis is that the diene is treated with the catalyst, a metal alkyldiene, to form an intermediate metal alkyldiene[249]. Two competing pathways are then available to the intermediate, RCM can occur to give cyclic products (**path A**) or an intermolecular reaction can occur to form polymer products (**path B**). This is shown in Figure 5.2 where limiting the amount of catalyst obtains the cyclic product over the polymers[250]. A number of reviews are available which discuss in detail the history, development, applications and mechanism of action of these catalysts[251,252,253].

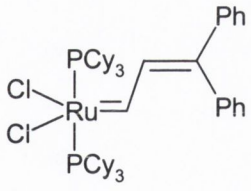

Grubbs Catalyst

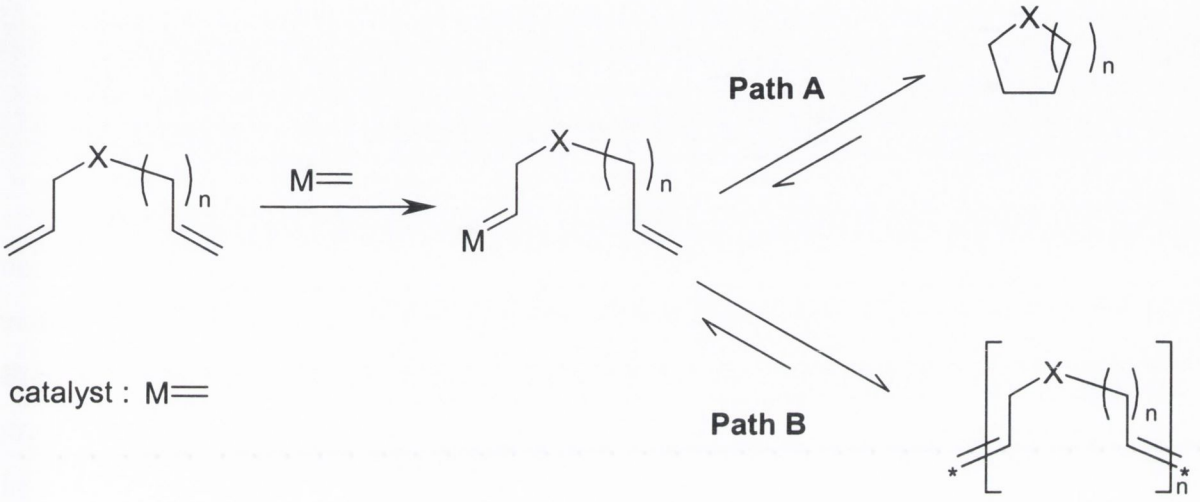

Fig. 5.2: Mechanism of action of Grubbs catalyst.

In this section the synthesis of novel macrocyclic ligands was attempted using RCM and Grubbs' catalyst. Using this catalyst it was hoped that novel, synthetically inaccessible, chiral macrocyclic compounds **210** to **213** could be synthesised from the pseudopeptides **200**, **201**, **202** and **203**. These would then be complexed to metals to synthesise novel complexes or to use the metal coordinated intermediates to synthesise catenanes. This was attempted firstly by synthesising an N-functionalised molecule **210** from **200** as an intermediate. **200** was added dropwise to a stirred solution of 5-bromopent-1-ene, Cs_2CO_3 and KI in DMF. After refluxing overnight, the precipitate was removed by filtration and the filtrate reduced under vacuum to give a brown oil. The brown oil was analysed and found to contain a number of products. Column chromatography was performed but unfortunately conventional means of detecting the relevant spots on TLC chromatography plates could not be achieved.

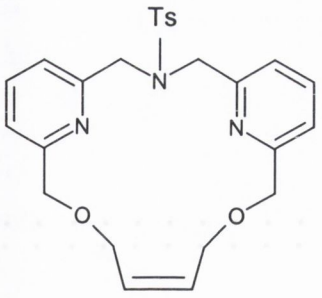

214

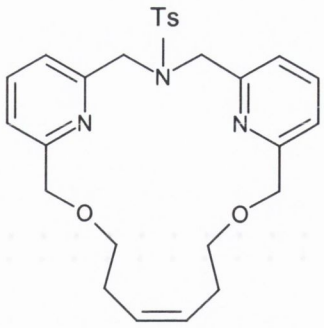

215

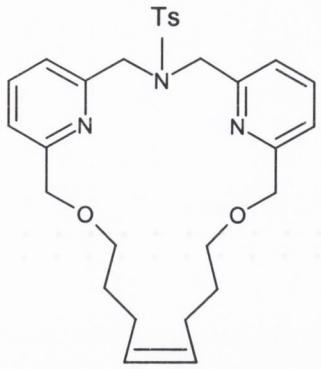

216

When this molecule could not be purified by conventional means three other macrocyclic ligands, **214**, **215** and **216** were attempted to be synthesised using the basic architecture of **96**. In chapter 3 the crystal structure of the Cu(II) complex of **96** was shown (Figure 3.4) to be a dimer structure. It was thought that RCM could provide a means of obtaining the catenane[248]. The synthesis of the intermediates and the attempted synthesis of the macrocyclic ligands will be discussed.

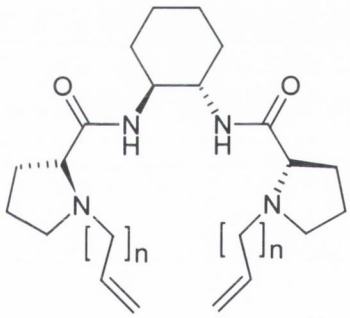

210

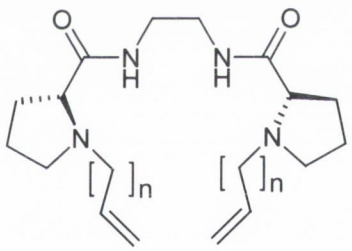

211

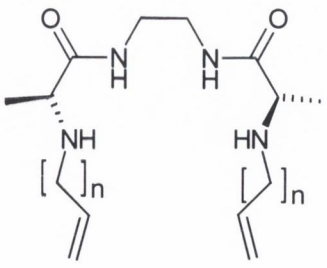

212

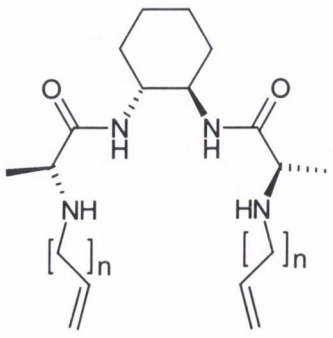

213

Where n = 0, 1 or 2

5.2.1: Attempted Synthesis of Novel Macrocyclic Compounds by RCM Using Grubbs' Catalyst:

Using **96**, an intermediate in the synthesis of the pyridinophane as discussed in chapter 2, three acyclic intermediates were prepared **217** (where n = 0, 1 or 2) from the reaction of **96** with an appropriate bromoalkene in the presence of NaH as shown in Scheme 5.3[254]. **96** was stirred in a solution of DMF at –10°C to which NaH was added. When the reaction turned red, the appropriate bromoalkene was added dropwise and the reaction brought to room temperature. After stirring for one hour, the reaction was quenched by pouring over ice and the product extracted into ethyl acetate. The reaction was quick and yielded the products in approximately 50 % yield after isolation by column chromatography to remove the mono-substituted products.

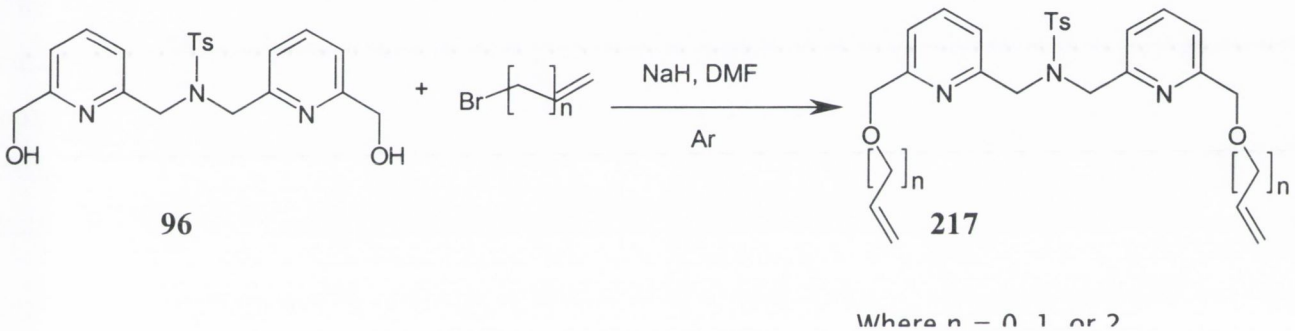

Scheme 5.3: Synthesis of the intermediate diene-type ligands 217

The RCM reaction was attempted on **217** (where n = 0) to synthesise **214**[249,255]. This was done by adding **217** to DCM in high dilution and degassing the solution. To this dry solution, a 20 % catalytic amount of Grubbs' catalyst was added and the solution was degassed again. The reaction was left to stir overnight at room temperature under inert atmosphere. The solvent was removed under vacuum leaving a black oily residue. Analysis showed a number of products were present and isolation of the product was attempted using column chromatography. Four extracts were collected and analysis showed them to contain starting material, catalyst and product. ES-MS of **214** showed a peak at 466 corresponding to the product **214** but it could not be isolated from the starting material. For the synthesis of **215** and **216** no product was isolated and the NMR and ES-MS data showed only the presence of the catalyst and starting material.

5.2.2: Conclusion:

The synthesis of a number of macrocyclic ligands was attempted using Grubbs catalyst to create new C-C bonds. At first it was attempted to synthesise novel macrocyclic ligands from the pseudo peptides **200** to **203**. The first synthesis involved the addition of an aliphatic alkene group onto the amine position of **200**. Unfortunately this peptide diene intermediate **210** could not be isolated from the starting materials and by-products.

Aliphatic diene chains were then added to the hydroxy position of **96**. This molecule was chosen because crystallographic data of the Cu(II) complex of **L.Cu(II)** shows a dimer structure which suggests a catenane complex could be formed upon reaction **L.Cu(II)** with Grubbs catalyst as suggested by Leigh *et al*[248]. Three intermediate diene molecules **217** were synthesised and isolated in average yield. It was disappointing to find that the products of the RCM synthesis could not either be synthesised for **215** and **216** or adequately isolated for **214**. The presence of the p-toluenesulfonamide group on the starting materials **217** may affect the catalyst in the RCM synthesis, as it is known that amines can hamper the catalyst[250]. Another possibility is that the starting materials may have sterically hindered the catalyst[249]. To overcome this the addition of a methyl or ethyl substituent at the end position of the diene can help overcome this problem[247,249].

Chapter 6
Experimental

Reagents (obtained from Aldrich and Lancaster) and solvents were purified using standard techniques[256]. Solvents were dried over the appropriate drying agent before use using standard procedures[256]. The ^{1}H (400.13 MHz) and ^{13}C (100.6 MHz) NMR spectra were recorded on a Bruker DPX 400 spectrometer in *d*-chloroform or d_3-acetonitrile unless otherwise stated and chemical shifts measured in ppm with *J* values given in Hz. Mass spectra and accurate masses were recorded on a Micromass LCT instrument with 50:50 MeCN:H_2O as carrier solvents unless otherwise stated. UV-Visible absorption spectra were recorded at 20-25°C using UNI-CAM (UV2) spectrometer and on a Shimadzu UV-2401PC spectrophotometer. Fluorescence emission spectra were recorded on a Perkin Elmer LS50B, and are uncorrected. Kinetic measurements were recorded on an Agilent UV-Vis photodiode array spectrometer fitted to a circulating temperature controlled water bath and water driven mechanical stirring. Melting points were recorded on a Gallencamp melting point apparatus and are uncorrected. IR spectra were measured using a Perkin Elmer FT-IR Paragon 100 spectrometer using KBr pellets. TLCs were carried out using Merck-Keiselgel 60 F_{254} or neutral alumina and were visualised by using a UV lamp and I_2. Flash column chromatography was carried out using Merck-Keiselgel silica 70-230 mesh. All solvents for chromatographic purpose were freshly distilled before use.

Throughout the titration experiments, the ligand and complex solutions were in the concentration range of 5-7 × 10^{-5} M. Aliquots of 3 ml were taken for absorption and luminescence measurements in standard quartz cuvettes with a 1 cm path length. The appropriate amount of the Zn(II), Cu(II) or Ni(II) (from freshly made stock solutions) was added using micropipettes. Determination of log β values was according to published procedure[164]. Crystal data were collected using a Bruker SMART diffractometer with graphite monochromated Mo-K_α radiation at *ca.* 150 K in a dinitrogen stream in by Dr. Mark Nieuwenhausen, Queens University, Belfast. Crystal stabilities were checked and there were no significant variations (< ± 1%). ω□phi scans were employed for data collection and Lorentz and polarisation corrections were applied. The structures were solved by direct methods and the non-hydrogen atoms were refined with anisotropic thermal parameters. Hydrogen-atom positions were added at idealised positions a riding model with fixed thermal parameters ($U_{iJ} = 1.2U_{eq}$ for the atom to which they are bonded (1.5 for Me)), was used for subsequent refinements. The function minimised was $\Sigma[\omega(|F_o|^2 - |F_c|^2)]$ with reflection weights $\omega^{-1} = [\sigma^2 |F_o|^2 + (g_1P)^2 + (g_2P)]$ where $P = [\max |F_o|^2 + 2|F_c|^2]/3$. The SAINT-NT[15] and SHELXTL[16] program packages were used for data reduction and structure solution

and refinement. Full structural data is available from the Cambridge Crystallographic Data Centre.

Chapter 2:

2,6-Methyl Pyridinedicarboxylate 87[257]:

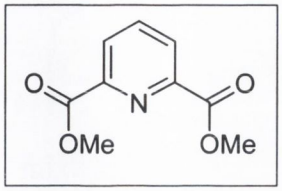

2,6-Pyridine dicarboxylic acid (50 g, 0.3 mol) was refluxed in thionyl chloride (200 mL) for twelve hours. The reaction was allowed to cool and thionyl chloride distilled off. The brown residue was brought to 0°C and methanol (200 mL) was added, *via* a pressure-equalised dropping funnel, over 30 minutes. The mixture was refluxed for one hour. The solvent was removed under reduced pressure and a yellow residue was collected by filtration and washed with cold methanol to give white crystals, (51.3 g. 87.6 % yield); ^{1}H NMR (400 MHz, $CDCl_3$): δ 8.34 (2 H, d, J = 7.56 Hz, Ar-CH), 8.06 (1 H, t, J = 7.52 Hz, Ar-CH), 4.05 (6 H, s, OCH_3); ^{13}C NMR (400 MHz, $CDCl_3$): δ 164.6 (C=O), 147.8 ($_qC$), 137.8 (Ar-CH), 127.5 (Ar-CH), 52.7 (OCH_3).

2,6-Bis(hydroxymethyl)pyridine 89[257]:

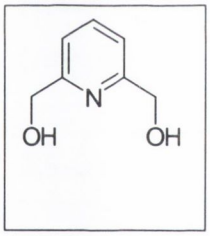

To a stirring solution of 2,6-methyl pyridinedicarboxylate (30 g, 0.15 mol) in ethanol (200 mL) at 0°C was added sodium borohydride (25 g, 0.67 mol). This was left to stir for one hour at 0°C, then stirred for three hours at room temperature and finally refluxed for twelve hours. The solvent was removed and acetone added to the resulting oily residue. The resulting mixture was refluxed for approximately one hour. The solvent was removed under reduced pressure and the residue taken up in aqueous K_2CO_3 (10 %) and refluxed for one hour. The solvent was removed once again and the resulting residue dissolved up in water. The latter was extracted with chloroform using a continuous extractor to give white crystals (16.67 g, 64.9 % yield); ^{1}H NMR (400 MHz, $CDCl_3$): δ 7.74 (1 H, t, J = 7.52 Hz), 7.23 (2 H, d, J = 8.04 Hz), 4.80 (4 H, s); ^{13}C NMR (400 MHz, $CDCl_3$): δ 158.0 ($_qC$), 137.0 (Ar-CH), 118.7 (Ar-CH), 63.9 (CH_2).

Attempted synthesis of 2,6-bis(bromomethyl)pyridine 90:

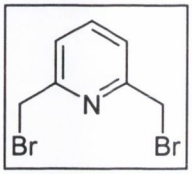

To a stirring solution of 2,6-lutidiene (10 g, 0.094 mol) and N-bromosuccinimide (26 g, 0.17 mol) in benzene (100 mL) was added peroxide (0.05 g, 0.009 mol). This was refluxed overnight. The reaction was quenched

in ice and washed with brine. The organic layer was collected, dried over MgSO4, filtered and evaporated to give a brown oil (1.53 g, 7 %).

2,6-Bis(bromomethyl)pyridine 90 and 2-bromomethyl-6-hydroxymethylpyridine 91[257]:

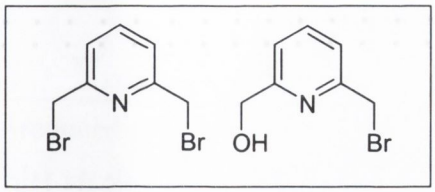

2,6-Bis(hydroxymethyl)pyridine (6 g, 0.043 mol) was refluxed in aqueous HBr (48 %, 60 mL) for five hours. The reaction was cooled to 0°C and neutralised with NaOH (40%). The precipitate was collected by filtration. The crude mixture was purified by flash silica column using DCM as eluent to isolate 2,6-bis(bromomethyl)pyridine (1.12g, 26.6 % yield). 1% methanol was added to isolate 2-bromomethyl-6-hydroxymethylpyridine (1.97 g, 40.6 % yield).

2,6-Bis(bromomethyl)pyridine: ^{1}H NMR (400 MHz, $CDCl_3$): δ 7.75 (1 H, t, J = 7.56 Hz, Ar-CH), 7.04 (2 H, d, J = 8.00 Hz, Ar-CH), 4.56 (4 H, s, CH_2); ^{13}C NMR (400 MHz, $CDCl_3$): δ 156.2 ($_qC$), 137.7 (Ar-CH), 122.3 (Ar-CH), 32.8 (CH_2).

2-bromomethyl-6-hydroxymethylpyridine: ^{1}H NMR (400 MHz, $CDCl_3$): δ 7.75 (1 H, t, J = 8.0 Hz, Ar-CH), 7.40 (1 H, d, J = 8.04 Hz, Ar-CH), 7.22 (1 H, d, J = 8.04 Hz, Ar-CH), 4.79 (2 H, s, CH_2), 4.59 (2 H, s, CH_2); ^{13}C NMR (400 MHz, $CDCl_3$): δ 158.5 ($_qC$), 139.5 ($_qC$), 137.5 (Ar-CH), 121.7 (Ar-CH), 119.4 (Ar-CH), 63.4 (CH_2-Br), 32.6 (CH_2-OH).

2,6-Bis(bromomethyl)pyridine 90[159]:

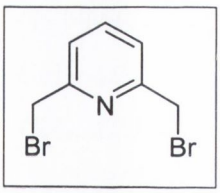

To a stirring solution of PBr_3 (3 mL, 0.014 mol) in dry $CHCl_3$ (50 mL) at 0°C was added 2,6-bis(hydroxymethyl)pyridine (2.0 g, 0.014 mmol) *via* a pressure-equalised dropping funnel, maintaining the temperature between –5 and 0°C. The mixture was left to stir at 0°C for one hour under inert atmosphere and then overnight at room temperature. The reaction was cooled in an ice-bath, neutralised with aqueous NaOH (40%) and then extracted with $CHCl_3$. The organic layer was dried over $MgSO_4$, filtered and evaporated to give a brown solid (3.05 g, 92% yield); ^{1}H NMR (400 MHz, $CDCl_3$): δ 7.74 (1 H, t, J = 7.56 Hz, Ar-CH), 7.06 (2 H, d, J = 8.00 Hz, Ar-CH), 4.55 (4 H, s, CH_2); ^{13}C NMR (400 MHz, $CDCl_3$): δ 156.2 ($_qC$), 137.6 (Ar-CH), 122.3 (Ar-CH), 32.9 (CH_2).

2,6-Bis(phthalimidemethyl)pyridine 93[159]:

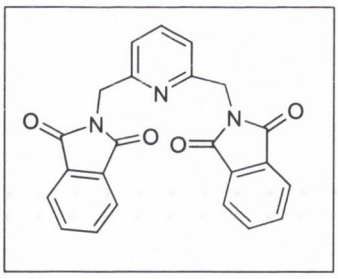

A solution of 2,6-bis(bromomethyl)pyridine (0.9 g, 3.8 mmol), potassium phthalimide (1.4 g, 7.6 mmol), K_2CO_3 (6.4 g, 0.046 mol) and KI (0.25 g, 1.5 mmol), in dry DMF (30 mL) under inert atmosphere, was refluxed overnight. The reaction was cooled and the resulting precipitate removed by filtration. The filtrate was reduced under vacuum and dried over P_2O_5 to give colourless crystals (1.18 g, 78.2 % yield); ^{1}H NMR (400 MHz, $CDCl_3$): δ 7.73 (8 H, m, Ar-CH(phthalimide)), 7.61 (1 H, t, J = 8.04 Hz, Ar-CH(pyridine)), 7.15 (2 H, d, J = 7.56 Hz, Ar-CH(pyridine)), 4.93 (4 H, s, CH_2); ^{13}C NMR (100 MHz, $CDCl_3$): δ 167.4 (C=O), 154.5 (C=O), 136.9 ($_qC$), 133.4 (Ar-CH), 131.6 (Ar-CH), 122.9 (Ar-CH), 119.4 (Ar-CH), 42.1(CH_2).

2,6-Bis(aminomethyl)pyridine dihydrochloride 94[159]:

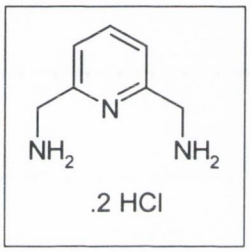

To a solution of 2,6-bis(phthalimidemethyl)pyridine (3.1 g, 7.8 mmol) in ethanol (50 ml) was slowly added hydrazine monohydrate (1 mL, 0.02 mol). The reaction was left to reflux for five hours and then allowed to cool. To this solution conc. HCl (5 mL) was added and the mixture was refluxed for a further two hours. The resulting precipitate was removed by filtration and washed with EtOH. The yellow filtrate was reduced under vacuum. The yellow residue was dissolved in hot H_2O and the insoluble material removed by hot filtration. The filtrate was evaporated under reduced pressure to give yellow crystals (1.61 g, 91.6 % yield); ^{1}H NMR (400 MHz, D_2O): δ 7.91 (1 H, t, J = 7.52 Hz, Ar-CH), 7.43 (2 H, d, J = 8.04 Hz, Ar-CH), 4.37 (4 H, s, CH_2); ^{13}C NMR (400 MHz, D_2O): δ. 151.0 ($_qC$), 138.5 (Ar-CH), 121.6 (Ar-CH), 42.1 (CH_2).

2,6-Bis[(*p*-tosylamino)methyl]pyridine 95[159]:

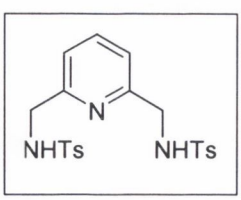

To a solution of K_2CO_3 (1.64 g, 0.012 mol) and 2,6-bis(aminomethyl)pyridine (0.66 g, 0.0048 mol) in water (40 mL) was added *p*-tosyl chloride (2.04g, 0.019 mol) in small portions over one hour. The mixture was refluxed overnight. The black precipitate was collected by filtration and washed with water (3 x 20 ml), methanol (3 x 20 ml) and diethyl ether (3 x 20 ml). The grey precipitate was collected and dried under vacuum (1.27 g, 65 % yield); ^{1}H NMR (400 MHz, $CDCl_3$): δ 7.75 (4 H, d, J = 8.03 Hz, Ar-CH(tosyl)), 7.55 (1 H, t, J = 7.59 Hz, Ar-CH(pyridine)), 7.26 (4 H, d, J = 8.04 Hz, Ar-CH(tosyl)), 7.10 (2 H, d, J = 8.03 Hz, Ar-CH(pyridine)), 5.80 (2 H, s, NH), 4.20 (4 H, s, CH_2), 2.41 (6 H, s, CH_3); ^{13}C NMR (100

MHz, $CDCl_3$): δ 154.2 ($_qC$), 143.0 ($_qC$), 137.65 (Ar-CH), 136.2 ($_qC$), 129.1 (Ar-CH), 126.7 (Ar-CH), 120.5 (Ar-CH), 46.6 (CH_2), 21.0 (CH_3). ES-MS: *m/z* 468 (M^{+Na}).

Attempted synthesis of 2,6-Bis[(*p*-tosylamino)methyl]pyridine 95[159]:

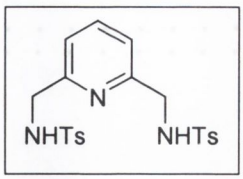

A solution of *p*-tosyl chloride (0.38 g, 2.0 mmol) and 2,6-bis(aminomethyl)pyridine (0.15 g, 0.7 mmol) in dioxane (30 mL) was stirred for thirty minutes. A 1M KOH solution (5 mL) was slowly added and the reaction was left to stir overnight. The solvent was evaporatd leaving a white residue, which was taken up in $CHCl_3$ and washed with water (3 x 25 mL). The organic layer was collected, dried over MgSO4, filteres and evaporated to give a yellow oil. ^{1}H NMR showed this to be starting material.

Attempted synthesis of 2,6-Bis[(*p*-tosylamino)methyl]pyridine 95[159]:

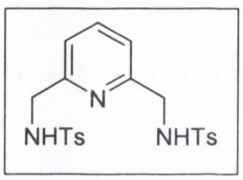

To a stirring solution of 2,6-bis(aminomethyl)pyridine (0.1 g, 4.9 mmol) and pyridine (10 mL) was added *p*-tosyl chloride (0.27 g, 10 mmol). This was refluxed overnight. The reaction was quenched in ice and the precipitate collected by filtration. This was dried and analysed and found by ^{1}H NMR and ES-MS to contain only the starting materials.

***N,N*-bis[(6-hydroxymethyl)pyridin-2-yl]-*p*-tosylamide 96[159]:**

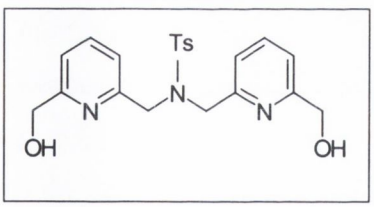

To a stirring solution of *p*-tosylamide (1.02 g, 0.006 mol), K_2CO_3 (5.01 g, 0.036 mol) and KI (0.1 g, 0.6 mmol) in dry acetone (25 mL) was added 2-bromomethyl-6-hydroxymethylpyridine (2.41 g, 0.012 mol) in acetone (25mL) *via* a pressure-equalised dropping funnel. The reaction was left to reflux for four days under inert atmosphere. The reaction was cooled and the insoluble material was removed by filtration and washed with $CHCl_3$. The filtrate was evaporated under reduced pressure. The brown residue was dissolved in $CHCl_3$ and washed with aqueous K_2CO_3 (10%). The organic layer was dried over $MgSO_4$, filtered and evaporated to give brown crystals (1.52 g, 62% yield); ^{1}H NMR (400 MHz, $CDCl_3$): δ 7.76 (2 H, d, *J* = 8.52 Hz, Ar-CH), 7.54 (2 H, t, *J* = 7.52 Hz, Ar-CH(tosyl)), 7.33 (2 H, d, *J* = 8.04 Hz, Ar-CH), 7.24 (2 H, d, *J* = 7.56 Hz, Ar-CH), 7.04 (2 H, d, *J* = 7.52 Hz, Ar-CH(tosyl)), 4.60 (4 H, s, CH_2-Br), 4.57 (4 H, s, CH_2-OH), 2.46 (3 H, s, CH_3); ^{13}C NMR (400 MHz, $CDCl_3$): δ 157.9 ($_qC$), 154.7 ($_qC$), 143.2 ($_qC$), 136.8 ($_qC$), 136.17 (Ar-CH), 129.2 (Ar-CH), 126.8 (Ar-CH), 121.2 (Ar-CH), 118.8 (Ar-CH), 63.4 (CH_2-Br), 53.1 (CH_2-OH), 21.0 (CH_3); ES-MS: *m/z* 414.2 (M^{+1}).

_N,N_-bis[(6-bromomethyl)pyridin-2-yl]-_p_-tosylamide 98[159]:

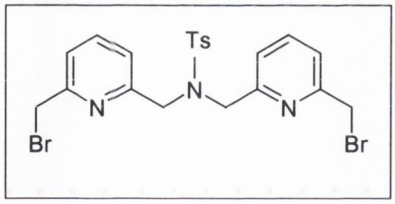

To a stirring solution of PBr_3 (0.5 mL) in dry $CHCl_3$ (10 mL) at 0°C was added *N,N*-bis[(6-hydroxymethyl)pyridin-2-yl]-*p*-tosylamide (0.2 g, 0.48 mmol) *via* a pressure-equalised dropping funnel, maintaining the temperature between –5 and 0°C. The mixture was left to stir at 0°C for one hour under inert atmosphere and then overnight at room temperature. The reaction was cooled in an ice-bath, neutralised with aqueous NaOH (40%) and then extracted with $CHCl_3$. The organic layer was dried over $MgSO_4$, filtered and evaporated to give a brown solid (0.25 g, 95% yield); ^{1}H NMR (400 MHz, $CDCl_3$): δ 7.75 (2 H, d, *J* = 8.52 Hz, Ar-CH(tosyl), 7.58 (2 H, t, *J* = 7.52 Hz, Ar-CH(tosyl)), 7.27 (6 H, m, Ar-CH(pyridine)), 4.59 (4 H, s, CH_2-Br), 4.37 (4 H, s, CH_2-N), 2.45 (3 H, s, CH_3); ES-MS: *m/z* 539.3 (M^+).

_N,N',N''_-Tri-_p_-tosyl-2,11,20-triaza[3.3.3](2,6)pyridinophane 99[159]:

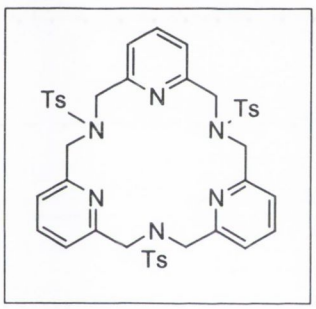

To a stirring solution of 2,6-bis(*p*-tosylaminomethyl)pyridine (0.02 g, 0.04 mmol), $CsCO_3$ (0.09 g, 0.2 mmol) and KI (0.01 g, 0.02 mmol) in dry MeCN (2 mL) at 0°C was added *N,N*-bis[[6-bromomethyl]pyridin-2-yl]-*p*-tosylamide (0.025 g, 0.05 mmol) in MeCN (1 mL), *via* a pressure-equalised dropping funnel. The mixture was left to stir for two days at room temperature under inert atmosphere and then at 75°C for one day. The resulting precipitate was filtered and evaporated to give a yellow oil which was recrystallised from $CHCl_3$ and diethyl ether (0.023 g, 65.1 % yield); ^{1}H NMR (400 MHz, $CDCl_3$): δ 7.68 (6 H, d, *J* = 8.04 Hz, Ar-CH(tosyl)), 7.44 (3 H, t, *J* = 7.52 Hz, Ar-CH(pyridine)), 7.29 (6 H, m), 7.14 (6 H, d, *J* = 7.52, ar-CH(pyridine)), 4.30 (12 H, s, CH_2), 2.44 (9 H, s, CH_3); ES-MS: *m/z* 822.7 (M^+).

2,11,20-triaza[3.3.3](2,6)pyridinophane 86[159]:

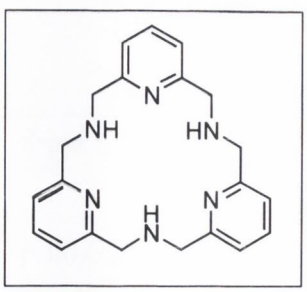

A solution of *N,N',N''*-tri-*p*-tosyl-2,11,20-triaza[3.3.3](2,6)pyridinophane (0.022 g, 0.06 mmol) in conc. H_2SO_4 (2 mL) was refluxed at 115°C for two hours. The reaction was quenched in ice and brought to pH 14 with aqueous NaOH (40%). The solution was extracted with $CHCl_3$, dried over $MgSO_4$, filtered and evaporated to give a white precipitate (0.008g, 83 % yield); ^{1}H NMR (400 MHz, $CDCl_3$): δ 7.57 (3 H, t, *J* = 7.56 Hz, Ar-CH), 7.12 (6 H, d, *J* = 7.52 Hz, Ar-CH), 3.97 (12 H, s, CH_2), 2.01 (3 H, s, b, NH); ES-MS: *m/z* 361.4 (M^+).

2,6-Pyridine Dicarbaldehyde 104[258]:

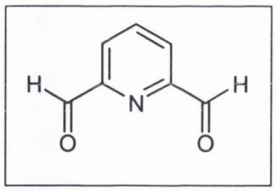

To a stirring solution of 2,6-bis(hydroxymethyl)pyridine (5 g, 0.036 mol) in dioxane (75 ml) was added SeO_2 (5 g, 0.04 mol). The mixture was left to reflux for four hours under inert atmosphere. The reaction was then allowed to cool and the precipitate removed by filtration through celite. The filtrate was evaporated to dryness to give pink crystals (3.723 g, 76.6 % yield); ^{1}H NMR (400 MHz, $CDCl_3$): δ 10.19 (s, 2 H, CHCHO), 8.21 (2 H, d, J = 7.50 Hz, Ar-CH), 8.11 (1 H, t, J = 7.52 Hz, Ar-CH); ^{13}C NMR (400 MHz, $CDCl_3$): δ 191.9 (C=O), 152.5 ($_qC$), 138.0 (Ar-CH), 124.9 (Ar-CH).

Synthesis of [48.Sm]:

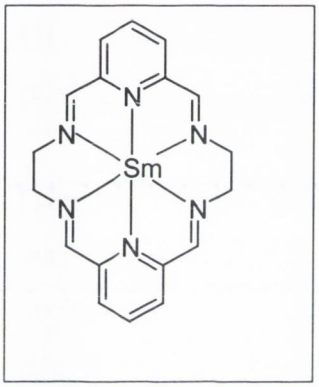

To a stirring solution of 2,6-dicarbaldehyde pyridine (0.10g, 0.9 mmol) in dry methanol (10 mL) was added $Sm(NO_3)_3$ (0.21 g, 0.45 mmol). The mixture was left to stir for 20 minutes under inert atmosphere. Diaminoethane (0.06 g, 9.5 mmol) in dry methanol (10 mL) was added and the reaction was left to reflux for four hours. The reaction was cooled and the precipitate was collected by filtration, washed with diethyl ether and dried under vacuum, (0.036 g). Mp 174°C. ^{1}H NMR (400 MHz, DMSO-d_6): δ 8.6 (d,d), 7.7 (s), 7.3 (s), 3.5 (s), 2.7 (s); ν/cm^{-1} (KBr discs) 3380 (lattice and coordinated water), 1659 (C=N), 1591 (pyridine), 1384 (NO_3)

General Synthesis of [100.Ln(III)]:

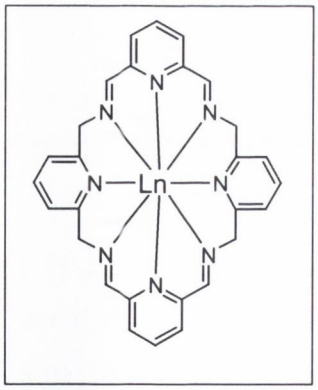

To a stirring solution of 2,6-dicarbaldehyde pyridine (2 eq) in dry solvent (10 mL) was added the appropriate lanthanide metal salt (1 eq). The mixture was left to stir for 20 minutes under inert atmosphere. 2,6-Di(aminomethyl)pyridine (2 eq) in dry solvent (10 mL) was added and the reaction was left to reflux for four hours. The solvent was concentrated and diethyl ether was added. The precipitate was collected by filtration, washed with diethyl ether and dried under vacuum.

[**100**.Sm(NO_3)]: Procedure as described above in MeOH using $Sm(NO_3)_3.6H_2O$. The product was isolated as brown crystals (0.012 g); Mp 156°C. Calculated for $C_{28}H_{32}N_8Sm.(NO_3)_3$: C, 41.17; H, 3.95; N, 18.86. Found: C; 51.56; H, 4.21; N, 23.37; ν/cm^{-1} (KBr) 3386 (lattice and coordinated water), 1645 (C=N), 1589 (pyridine), 1452 (NO_3).

[**100**.Sm(NO_3)]: Procedure as described above in MeOH using Sm(NO_3)$_3$.6H_2O. The reaction was cooled to 0°C and $NaBH_4$ aded *in situ*. The solvent was removed by evaporation. The product was isolated as a yellow solid, (0.024 g). Mp 175°C. Calculated for $C_{28}H_{32}N_8Sm.(NO_3)_3$: C, 41.17; H, 3.95; N, 18.86. Found: C; 47.62; H, 4.04; N, 19.00; 1H NMR (400 MHz, DMSO-d_6): δ 8.1 (b,m), 7.1 (t), 1.3 (s); ν/cm^{-1} (KBr) 3396 (lattice and coordinated water), 1569 (pyridine), 1452, 1384 (NO_3)

[**100**.Pr(NO_3)]: Procedure as described above in MeOH using Pr(NO_3)$_3$.H_2O. The product was isolated as an orange solid (0.23 g). Mp >200°C. Calculated for $C_{28}H_{32}N_8Pr.(NO_3)_3$: C, 41.65; H, 3.99; N, 19.08. Found: C; 36.50; H, 3.27; N, 14.17; ^{1}H NMR (400 MHz, DMSO-d_6): δ 8.6 (s), 7.9 (s), 7.2 (s), 4.2 (s), 3.2 (s); ν/cm^{-1} (KBr) 3370(lattice and coordinated water), 1620 (C=N), 1458 (NO_3)

[**100**.Gd(NO_3)]: Procedure as described above in MeOH using Gd(NO_3)$_3$.H_2O. The product was isolated as a brown solid (0.24 g). Mp 188°C. Calculated for $C_{28}H_{32}N_8Gd.(NO_3)_3$: C, 40.92; H, 3.91; N, 18.70. Found: C; 38.42; H, 3.42; N, 13.99; ^{1}H NMR (400 MHz, DMSO-d_6): δ 8.4 (m); ν/cm^{-1} (KBr) 3385 (lattice and coordinated water), 1618 (C=N), 1560 (pyridine), 1457 (NO_3)

[**100**.Gd(trif)]: Procedure as described above in MeCN using Gd(trif)$_3$.H_2O. The product was isolated as an orange solid (0.27 g). Mp 198°C. Calculated for $C_{28}H_{32}N_8Gd.(trif)_3$: C, 34.32; H, 2.97; N, 10.33. Found: C; 28.19; H, 3.21; N, 12.05; ^{1}H NMR (400 MHz, DMSO-d_6): δ 9.3 (s), 8.6 (s), 8.1 (s), 5.6 (s), 4.9 (s); ν/cm^{-1} (KBr) 3380 (lattice and coordinated water), 1620 (C=N), 1277, 1164 (trif)

[**100**.Pr(trif)]: Procedure as described above in MeCN using Pr(trif)$_3$.H_2O. The product was isolated as a brown solid (0.26 g). Mp 167°C. Calculated for $C_{28}H_{32}N_8Pr.(trif)_3$: C, 34.84; H, 3.02; N, 10.48. Found: C; 28.15; H, 2.81; N, 12.89; ^{1}H NMR (400 MHz, DMSO-d_6): δ 8.6 (s), 7.5 (s), 7.3 (s), 4.2 (s), 4.0 (s,b); ν/cm^{-1} (KBr) 3124 (lattice and coordinated water), 1617 (C=N), 1454 (pyridine) 1276, 1164 (trif)

[**100**.La(trif)]: Procedure as described above in MeCN using La(trif)$_3$.H_2O. The product was isolated as a brown solid (0.38 g). Mp 176°C. Calculated for $C_{28}H_{32}N_8La.(trif)_3$: C, 34.91; H,

3.02; N, 10.50. Found: C; 28.48; H, 2.73; N, 9.65; ^{1}H NMR (400 MHz, DMSO-d_6): δ 8.6 (s), 7.9 (s), 7.3 (s), 4.2 (s), 2.9 (d), 2.1 (s); ν/cm^{-1} (KBr) 3067 (lattice and coordinated water), 1618 (C=N), 1459 (pyridine) 1277, 1163 (trif)

[**100**.Yb(trif)]: Procedure as described above in MeCN using Yb(trif)$_3$.H_2O. The product was isolated as a brown solid (0.26 g). Mp >200°C. Calculated for $C_{28}H_{32}N_8$Yb.(trif)$_3$: C, 33.82; H, 2.93; N, 10.48. Found: C; 25.88; H, 2.64; N, 12.17; ^{1}H NMR (400 MHz, DMSO-d_6): δ 8.5 (s), 7.9 (s), 7.5 (s), 4.3 (s), 3.9 (s,b); ν/cm^{-1} (KBr) 3390 (lattice and coordinated water), 1631 (C=N), 1457 (pyridine) 1250, 1169 (trif)

[**100**.Tb(trif)]: Procedure as described above in MeCN using Tb(trif)$_3$.H_2O. The product was isolated as a brown solid (0.13 g). Mp >200°C. Calculated for $C_{28}H_{32}N_8$Tb.(trif)$_3$: C, 34.26; H, 2.97; N, 10.31. Found: C; 25.33; H, 2.46; N, 10.13; ^{1}H NMR (400 MHz, DMSO-d_6): δ 8.9 (s), 4.7 (m); ν/cm^{-1} (KBr) 3334 (lattice and coordinated water), 1635 (C=N), 1592, 1457 (pyridine) 1246, 1166 (trif)

[**100**.Eu(trif)]: Procedure as described above in MeCN using Eu(trif)$_3$.H_2O. The product was isolated as a brown solid (0.15 g). Mp 182°C. Calculated for $C_{28}H_{32}N_8$Eu.(trif)$_3$: C, 34.48; H, 2.99; N, 10.38. Found: C; 26.66; H, 2.75; N, 11.98; ^{1}H NMR (400 MHz, DMSO-d_6): δ 8.6 (s), 7.9 (m); ν/cm^{-1} (KBr) 3367 (lattice and coordinated water), 1618 (C=N), 1458 (pyridine) 1243, 1165 (trif)

[**100**.Eu(trif)a]: Procedure as described above in MeCN using Eu(trif)$_3$.H_2O. The product was isolated as a green solid (0.021 g). Mp 176°C; ν/cm^{-1} (KBr) 3398 (lattice and coordinated water), 1623 (C=N), 1446 (pyridine) 1280, 1174 (trif)

[**100**.Eu(CH_3COO^-)]: Procedure as described above in MeOH using Eu(CH_3COO^-)$_3$.H_2O. The product was isolated as a yellow solid (0.068 g). Mp 178°C. Calculated for $C_{28}H_{32}N_8$Eu.(CH_3COO^-)$_3$: C, 50.43; H, 5.10; N, 13.80. Found: C; 44.40; H, 3.90; N, 18.88; ^{1}H NMR (400 MHz, DMSO-d_6): δ 7.2 (t); ν/cm^{-1} (KBr) 3395 (lattice and coordinated water), 1620 (C=N), 1459 (pyridine) 1566, 1402 (CH_3COO^-)

[**100**.Tb(CH_3COO^-)]: Procedure as described above in MeOH using Tb(CH_3COO^-)$_3$.H_2O. The product was isolated as a yellow solid (0.074 g). Mp >200°C. Calculated for

$C_{28}H_{32}N_8Tb(CH_3COO^-)_3$: C, 50.00; H, 5.06; N, 13.72. Found: C; 40.52; H, 3.21; N, 16.96; ^1H NMR (400 MHz, DMSO-d_6): δ 7.2 (t); ν/cm^{-1} (KBr) 3406 (lattice and coordinated water), 1618(C=N), 1459 (pyridine) 1560, 1441 (CH_3COO^-)

General Procedure for the synthesis of [101.Ln(III)]:

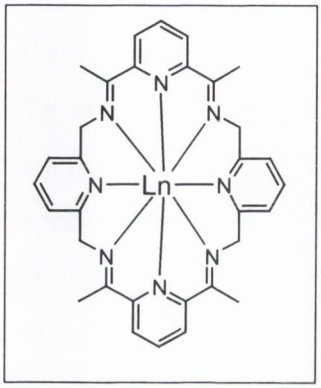

To a stirring solution of 2,6-diacetylpyridine (2 equiv.) in 10 mls dry solvent was added the appropriate lanthanide metal salt (1 equiv.). This was left to stir for 20 minutes under inert atmosphere. 2,6-di(aminomethyl)pyridine (2 equiv.) in 10 mls dry solvent was added and the reaction was left to reflux for four hours. The solvent was concentrated and diethyl ether was added. The precipitate was collected by filtration, washed with diethyl ether and dried under vacuum.

[**101**.Eu(trif)]: Procedure as described above in MeCN using Eu(trif)$_3$.H_2O. The product was isolated as a yellow solid (0.22 g). Mp >200°C. Calculated for $C_{32}H_{40}N_8Eu.(trif)_3$: C, 37.01; H, 3.55; N, 9.80. Found: C; 26.70; H, 3.28; N, 10.63; ^1H NMR (400 MHz, DMSO-d_6): δ 8.6 (s), 7.9 (s), 7.5(s), 7.2 (t), 4.2 (s); ν/cm^{-1} (KBr) 3369 (lattice and coordinated water), 1617 (C=N), 1461 (pyridine) 1246, 1164 (trif)

[**101**.Tb(trif)]: Procedure as described above in MeCN using Tb(trif)$_3$.H_2O. The product was isolated as a yellow solid (0.19 g). Mp >200°C. Calculated for $C_{32}H_{40}N_8Tb.(trif)_3$: C, 36.78; H, 3.53; N, 9.80. Found: C; 27.73; H, 3.63; N, 12.26; ^1H NMR (400 MHz, DMSO-d_6): δ 9.4 (s), 8.7 (m), 4.9 (s); ν/cm^{-1} (KBr) 3376 (lattice and coordinated water), 1617 (C=N), 1463 (pyridine) 1277, 1162 (trif)

[**101**.Yb(trif)]: Procedure as described above in MeCN using Yb(trif)$_3$.H_2O. The product was isolated as a brown solid (0.30 g). Mp >200°C. Calculated for $C_{32}H_{40}N_8Tb.(trif)_3$: C, 36.34; H, 3.48; N, 9.69. Found: C; 26.67; H, 2.84; N, 9.69; ^1H NMR (400 MHz, DMSO-d_6): δ 91.0 s, 65.6 (s), 42.6 (s), 37.2 (s), 24.2 (s), 3.4 (s), -3.7 (s), -5.8 (s), -13.6 (s), -19.4 (s); ν/cm^{-1} (KBr) 3375 (lattice and coordinated water), 1616 (C=N), 1462 (pyridine) 1272, 1169 (trif)

[**101**.La(trif)]: Procedure as described above in MeCN using La(trif)$_3$.H_2O. The product was isolated as a brown solid (0.33 g). Mp >200°C. Calculated for $C_{32}H_{40}N_8Tb.(trif)_3$: C, 37.44; H, 3.59; N, 9.69. Found: C; 25.71; H, 3.01; N, 12.97; ^1H NMR (400 MHz, DMSO-d_6): δ 8.6

(s), 7.9 (s), 7.5(s), 7.2 (t), 4.2 (s); ν/cm^{-1} (KBr) 3371 (lattice and coordinated water), 1618 (C=N), 1461 (pyridine) 1277, 1163 (trif)

Chapter 3:

General procedure for complex synthesis:

To a solution of **L** (0.05 g, 0.12 mmol) in dry acetonitrile (10 mL) was added equimolar equivalents of the appropriate metal perchlorate salt. After standing at room temperature for approximately 2 days, under a diethyl ether atmosphere, crystals were observed. These were collected by filtration, washed with cold acetonitrile and dried under vacuum in the presence of P_2O_5.

[L.Cu(II)]: Procedure as described above, using $[Cu(I)(ClO_4)](MeCN)_4$ (0.12 mmol). The white crystals were left in the open air to oxidise to the Cu(II) complex. Complex was collected as green crystals (85% yield); mp 221.6°C; Calculated for $C_{42}H_{44}Cl_2N_6O_{16}S_2Cu_2.H_2O$: C, 43.15; H, 3.97; N, 7.19. Found: C; 43.04; H, 3.74; N, 6.53; ^1H NMR (400 MHz, CD_3CN, recorded freshly in the presence of 10 equivalents of Cu(I)): δ 7.91 (2 H, bs, Ar-H), 7.85 .2 H, d, Ar-H, J = 6.5 Hz), 7.57 (4 H, bs, Ar-H), 7.30 (2 H, d, Ar-H, J = 6.5 Hz), 4.95 (4 H, s, HOCH_2), 4.27 (4 H, s, ArCH_2NH), 2.25 (3 H, s, CH_3); ES-MS: *m/z* 477.08 (M+1); λ_{max}/nm (CH_3CN) 225 ($\varepsilon/dm^3\ mol^{-1}\ cm^{-1}$ 8023.7) 265 (6247); ν/cm^{-1} (KBr) 3486m (OH), 2924 (SN), 1609, 1585, 1435 (C=C) (C=N), 1353, 1164 (S=O), 1091 (ClO_4).

[L.Zn(II)]: Procedure as described above, using $[Zn(ClO_4)](H_2O)_6$ (0.12 mmol). The complex was collected as white crystals (75% yield); mp 191.5°C; Calculated for $C_{23}H_{30}Cl_2N_4O_{14}SCZn$: C, 36.60; H, 4.01; N, 7.42. Found: C; 35.83; H, 3.46; N, 5.70; ^1H NMR (400 MHz, CD_3CN, recorded freshly in the presence of 40 equivalents of Zn(II)): δ 8.14 (2 H, t, Ar-H, J = 7.8 Hz), 7.83 (2 H, d, J = 8.3 Hz, Ar-H), 7.65 (2 H, d, , Ar-H, J = 8.04 Hz), 7.53 (2 H, d, Ar-H, J = 4.0 Hz), 7.51 (2 H, d, Ar-H, J = 4.0 Hz,), 6.65 (2 H, bs, O*H*), 5.04 (4 H, d, HOCH_2, J = 3.54 Hz), 4.39 (4 H, s, ArCH_2NH), 2.57 (3 H, s, CH_3); ^{13}C NMR (100 MHz, CD_3CN): 158.7, 155.4, 147.5, 143.4, 132.9, 130.2, 129.4, 125.8, 122.4, 62.8, 54.0, 22.1; ES-MS: *m/z* 557 (M^+). λ_{max}/nm (CH_3CN) 223 ($\varepsilon/dm^3\ mol^{-1}\ cm^{-1}$ 6421.6) 266 (2868); ν/cm^{-1} (KBr) 3412 (OH) (SN), 1610, 1588, 1439 (C=C) (C=N), 1354 (S=O), 1089.

[L.Ni(II)]: Procedure as described above, using $[Ni(ClO_4)](H_2O)_6$ (0.121 mmol). Complex was collected as blue crystals (70% yield); mp 193.2°C; Calculated for $C_{23}H_{30}Cl_2N_4O_{14}SCZn$: C, 39.87; H, 3.88; N, 9.30. Found: C; 39.87; H, 3.81; N, 9.06; ES-MS: *m/z* 570; λ_{max}/nm (CH_3CN) 229 (ε/dm^3 mol^{-1} cm^{-1} 3481) 263 (2476.4); ν/cm^{-1} (KBr) 3422 (OH) (SN), 1609, 1586, 1449 (C=C) (C=N), 1329 (S=O), 1090 (ClO_4^-)

[L.Co(II)]: Procedure as described above, using $[Co(ClO_4)](H_2O)_6$ (1.21 x 10^{-4} mol) except solution was placed in a butyl ether atmosphere. Complex was collected as pink crystals (55% yield); mp 182.4°C; Calculated for $C_{23}H_{30}Cl_2N_4O_{14}SCZn$: C, 39.91; H, 4.22; N, 10.34. Found: C; 38.91; H, 3.88; N, 9.12; ES-MS: *m/z* 472.49; λ_{max}/nm (CH_3CN) 223.5 (ε/dm^3 mol^{-1} cm^{-1} 6509) 272.5 (1884.4); ν/cm^{-1} (KBr) 3386 (OH) (SN), 1610, 1580, 1440 (C=C) (C=N), 1353 (S=O), 1089 (ClO_4^-)

[L.Fe(II)]: Procedure as described above, using $[Fe(ClO_4)](H_2O)_6$ (0.121 mmol). Complex was collected as brown crystals (73% yield); mp 190.7°C; Calculated for $C_{25}H_{29}Cl_2N_5O_{12}SCFe$: C, 40.02; H, 3.90; N, 9.33. Found: C; 39.95; H, 3.65; N, 9.04; ES-MS: *m/z* 466.43; λ_{max}/nm (CH_3CN) 267.3 (ε/dm^3 mol^{-1} cm^{-1} 2271) 230.8 (6084); ν/cm^{-1} (KBr) 3421 (OH), 2923 (SN), 1610, 1581, 1447 (C=C), 1345 (S=O), 1161, 1098 (ClO_4^-).

Chapter 4:

_N,N_-bis(tosyl)diaminoethane 183[219]:

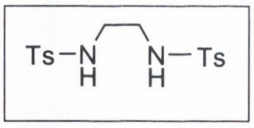

A solution of diaminoethane (10 g, 0.16 mol) and NaOH (14 g, 0.50 mol) in toluene (200 mL) and water (60 mL) was stirred at 0°C. Tosyl chloride (65 g, 0.35 mol) in toluene (100 mL) was then slowly added over twenty minutes. The mixture was warmed to room temperature and stirred overnight. The resulting precipitate was collected by filtration and washed with ethanol. (35.5 g, 57.9% yield); ^{1}H NMR (400 MHz, $CDCl_3$): δ 7.74 (4 H, d), 7.35 (4 H, d), 4.77 (2 H, s, br), 3.09 (4 H, t), 2.46 (6 H, s); ^{13}C NMR (100 MHz, $CDCl_3$): δ 143.7 ($_qC$), 136.1 ($_qC$), 124.6 (Ar-CH), 122.0 (Ar-CH), 42.9 (CH_2), 22.2 (CH_3)

Diethyleneglycol ditosylate 182[219]:

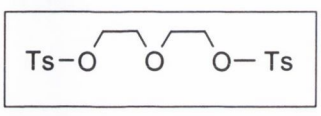

To a stirring solution of NaOH (40 g, 1 mol) in water (50 mL) was added diethyleneglycol (55 g, 0.36 mol) in THF (200 mL) and water

(50 mL) whilst maintaining the temperature below 0°C. Tosyl chloride (145 g, 0.80 mol) in THF (200 mL) was slowly added over four hours maintaining the temperature between 0 to 5°C. This was stirred for a further 4 hours. The reaction mixture was poured into a beaker of ice water and toluene (200 mL) was added and stirred for twenty minutes. The resulting precipitate was collected by filtration, washed with water and dried over P_2O_5. (134 g, 81.8 % yield); ^{1}H NMR (400 MHz, $CDCl_3$): δ 7.82 (4 H, d), 7.37 (4 H, d) 4.17 (4 H, d), 3.68 (4 H, d), 3.55 (4 H, s), 2.47 (6 H, s); ^{13}C NMR (100 MHz, $CDCl_3$): δ 144.5 ($_qC$), 132.3 ($_qC$), 129.3 (Ar-H), 127.4 (Ar-H), 68.6 (CH_2), 68.3 (CH_2), 21.2 (CH_3).

_N,N'_ ditosyl-1,4-diaza-9-crown ether 184[219]:

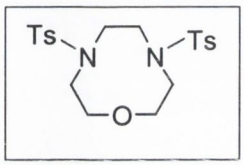

To a stirring solution of diethyleneglycol ditosylate (5 g, 0.012 mol) and $CsCO_3$ (8.26 g, 0.042 mol) in DMF (200 mL) was added *N,N'*-ditosyl diaminoethane (4.44 g, 0.012 mol) in DMF (200 mL) over 5 hours. The yellow solution was left to stir overnight under inert atmosphere. The reaction mixture was evaporated to dryness under reduced pressure, the residue dissolved in DCM and washed with water. The organic layer was dried over $MgSO_4$, filtered and evaporated to give colourless crystals, which were recrystallised, from the minimum amount of hot toluene (3.13 g, 59.2% yield); ^{1}H NMR (400 MHz, $CDCl_3$): δ 7.73 (4 H, d, J = 8.03 Hz), 7.35 (4 H, d, J = 8.53 Hz), 3.92 (4 H, t, J = 4.51 Hz), 3.49 (4 H, s), 3.28 (4 H, t, J = 4.52 Hz), 2.45 (6 H, s); ^{13}C NMR (100 MHz, $CDCl_3$): δ 143.2 (ar-C_q), 135.25 ($_qC$), 129.4 (Ar-H), 126.9 (Ar-H), 71.5 (CH_2), 51.67 (CH_2), 50.1 (CH_2), 21.1 (CH_3)

1,4-Diaza-9-crown ether hydrobromic acid salt 185[219]:

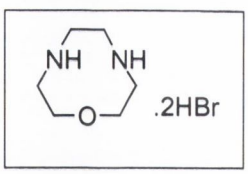

A mixture of *N,N'*-ditosyl-1,4-diaza-9-crown ether (2.0 g, 4.4 mmol), phenol (0.94 g, 10 mmol), and 48% HBr-acetic acid (40 mL) were refluxed at 100°C for twenty hours with a gas outlet.The reaction was cooled to 0°C, diethyl ether added and the mixture was left to stir for two hours. The resulting precipitate was collected by filtration and washed with diethyl ether and acetone (1.78 g, 87% yield); ^{1}H NMR (400 MHz, D_2O): δ 3.98 (4 H, t), 3.70 (4 H, s), 3.45 (4 H, t); ^{13}C NMR (100 MHz, D_2O): δ 43.6 (CH_2), 45.7 (CH_2), 65.4 (CH_2)

General synthesis of 2-chloro-*N*-(-2-naphtyl)ethylethanamide 187:

1-(-1-Naphtyl)ethylamine (1 g, 0.63 mmol) and HOBt (0.8 g, 0.63 mmol), chloroacetic acid (0.6 g, 0.63 mmol) were stirred in DCM (25 mL) at –10°C for twenty minutes under inert

atmosphere. EDCl (1.2 g, 0.63 mmol) was then added and the reaction stirred overnight at room temperature under inert atmosphere. The solution was washed with 1M $NaHCO_3$ and brine. The organic layer was collected, dried over $MgSO_4$, filtered and evaporated to give a white solid.

2-Chloro-*N*-[(*S*)-2-naphtyl]ethylethanamide ***S*-187**: (0.58 g, 86.9% yield); mp 140°C; Calculated for

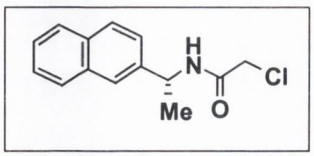

$C_{14}H_{14}NOCl$: C 67.88; H, 5.70; N, 5.65. Found C 67.63, H 5.77, N 5.86; ^{1}H NMR (400 MHz, CD_3CN): δ 8.16 (1 H, d, Ar-H, J = 8.52 Hz), 7.96 (1H, d, Ar-H, J = 7.52 Hz), 7.87 (1 H, d, Ar-H, J = 7.52 Hz), 7.59 (1 H, m, Ar-H), 7.25 (1 H, sb, Ar-H,), 5.83 (1 H, m, J = 7.04 Hz), 4.04 (2 H, s), 1.63 (3 H, d, J = 7.04 Hz); ^{13}C NMR (100 MHz, CD_3CN): 164.8, 138.8, 133.4, 130.2, 128.31, 127.3, 125.0, 125.3, 125.0, 122.6, 122.1, 42.2, 20.1. ES-MS: *m/z* 247.9 (M+); ν/cm^{-1} (KBr) 3295 (N-H), 1648 (C=O), 1541 (C=C), 780 (C-Cl).

2-chloro-N-[-(*R*)-2-naphtyl]ethylethanamide ***R*-187**: (0.60 g, 87.3% yield); mp 140°C; Calculated for $C_{14}H_{14}NOCl$:

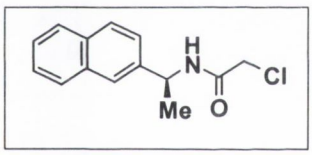

C, 67.88; H, 5.70; N, 14.31. Found: C; 67.67; H, 5.81; N, 5.83; ^{1}H NMR (400 MHz, $CDCl_3$): δ 8.11 (1 H, d, J = 8.52 Hz), 7.92 (1 H, d, J = 8.56 Hz), 7.86 (1 H, d, J = 7.56 Hz), 7.56 (4 H, m), 6.81 (1 H, s, N-*H*), 4.15 (2 H, q), 1.74 (3 H, d, J = 7.00 Hz); ^{13}C NMR (100 MHz, $CDCl_3$): 164.4($_q$C), 137.0 ($_q$C), 133.5 ($_q$C), 130.5 ($_q$C), 128.5 (Ar-H), 128.2 (Ar-H), 126.2 (Ar-H), 125.5 (Ar-H), 124.8 (Ar-H), 122.6 (Ar-H), 122.1 (Ar-H), 44.8 (C*H*$_2$), 42.2 (C*H*$_2$), 20.4 (C*H*$_3$); ES-MS: *m/z* 247.9 (M^+); ν/cm^{-1} (KBr) 3290 (N-H), 1652 (C=O), 1540 (C=C), 782 (C-Cl).

General synthesis of the Sensor 181:

1,4-Diaza-9-crown-3-ether (1 eq), Cs_2CO_3 (6 eq) and KI (0.1 eq) were stirred in MeCN under inert atmosphere. The appropriate chromophore (2.1 eq) in MeCN was added *via* a pressure equalised dropping funnel. The mixture was left to reflux at 80°C overnight under inert atmosphere. The reaction was filtered and the solvent evaporated. The yellow residue was dissolved in $CHCl_3$ and washed with 10% K_2CO_3 (3 x 20mls). The organic layer was collected, dried over $MgSO_4$, filtered and evaporated to give a white solid. After purification by alumina chromatography with DCM: 0→ 5% MeOH, the product was recrystallised from diethyl ether to yield a white solid.

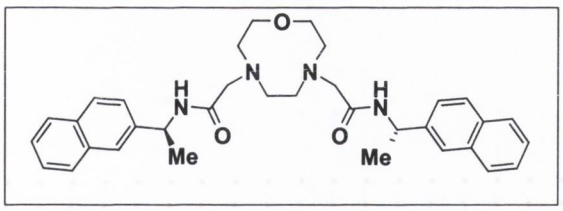

S-181: (0.22 g, 32.7 % yield); mp 107°C; Calculated for $C_{34}H_{40}N_4O_3$: C 73.88; H, 7.29; N, 10.14. Found C 73.39, H 7.14, N 9.66; ^{1}H NMR (400 MHz, CD_3CN): δ 8.12 (2 H, d, Ar-H, J = 8.52 Hz), 7.91 (2 H, d, Ar-H, J = 7.52 Hz), 7.81 (2 H, d, Ar-H, J = 8 Hz), 7.53 (8 H, m, J = 8 Hz), 5.80 (2 H, m, J = 7.04 Hz), 3.24 (4 H, m), 3.05 (4 H, s), 2.57 (8 H, m), 1.68 (6 H, d, J = 7.04 Hz); ^{13}C NMR (100 MHz, CD_3CN): 139.2 133.4, 130.5, 128.2, 127.2, 125.8, 125.3, 124.9, 122.8, 122.2, 71.7, 60.2, 56.3, 55.1, 43.7, 19.8. ES-MS: *m/z* 553.5 (M^+); λ_{max}/nm (CH_3CN) 260.8 (ε/dm^3 mol^{-1} cm^{-1} 10427) 281.6 (11801) 293.2 (6801.5); ν/cm^{-1} (KBr) 3287 (N-H); 2525, 2554 (ar C=H); 1650 (C=O amide); 1602, 1511 (ar C=C); 1450 (C-N amide); 1357 (C-N crown ether); 1126 (C-O-C crown ether).

R-181: (0.18 g, 30.1% yield), mp 107°C. Accurate mass: Calculated for $C_{34}H_{40}N_4O_3$: found $C_{34}H_{41}N_4O_3$

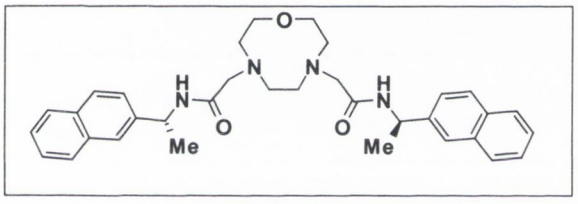

^{1}H NMR (400 MHz, $CDCl_3$): δ 8.02 (2 ArH, d, J = 8.36 Hz), 7.67 (5 ArH, d,d, J = 8.04 Hz), 7.53 (4 H, d, Ar-H, J = 8 Hz), 7.03 (2 H, d, N-H), 5.59 (2 H, d, C*H*(CH_3)NH), 3.22 (4 H, m), 2.77 (4 H, q), 2.40 (8 H, m), 1.67 (6 H, d, J = 6.52 Hz, CH(C*H*$_3$)NH); ^{13}C NMR (100 MHz, CD_3CN): 169.8 (C=O), 137.7 (Ar-H), 133.4 (Ar-H), 130.9 (Ar-H), 128.3 (Ar-H), 128.0 (Ar-H), 126.1 (Ar-H), 125.5 (Ar-H), 124.7 (Ar-H), 123.1 (Ar-H), 122.3 (Ar-H), 71.6, 60.2, 56.0, 54.8, 43.5, 19.7 (CH(*C*H$_3$); ES-MS: *m/z* 552.9 (M^+); λ_{max}/nm (CH_3CN) 260.7 (ε/dm^3 mol^{-1} cm^{-1} 10399) 281.6 (11750) 293.2 (6889.5); ν/cm^{-1} (KBr) 3272 (N-H); 2499, 2554 (ar C=H); 1656 (C=O amide); 1607, 1528 (ar C=C); 1468 (C-N amide); 1357 (C-N crown ether); 1132 (C-O-C crown ether).

Chapter 5:

General synthesis for the protection of amino acids using $(Boc)_2O$[259]:

A stirring solution of amino acid in a 1: 1 ratio of dioxane and 1M $NaOH_{aq}$ was left to stir in an ice-bath for 30 minutes and $(Boc)_2O$ (0.5 equiv.) was added. The reaction was left to stir overnight. The solvent was concentrated to 30 mls, acidified to pH 3 using 10 % $KHSO_4$ and extracted with EtOAc (3 x 100 mls). The organic layer was collected, dried over $MgSO_4$, filtered and evaporated to give colourless crystals.

N-Boc-L-Alanine 205

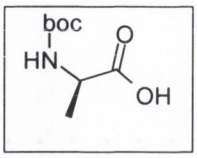

Procedure as described above. (13.45 g, 63.4% yield); ^{1}H NMR (400 MHz, CD_3CN): δ 7.06 (1 H, s, b, NH), 3.92 (1 H, m, CH), 1.38 (9 H, s, BOC), 1.23 (3 H, d, CH_3); ^{13}C NMR (100 MHz, d_6-DMSO): 175.0, 155.5, 78.3, 49.2, 28.6, 17.4.

N-Boc-L-Proline 204

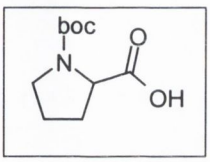

Procedure as described above. (22.9 g, 61.4% yield); ^{1}H NMR (400 MHz, CD_3CN): δ 4.19 (1 H, m), 3.37 (2 H, m), 2.03 (2 H, m), 1.89 (2 H, m); ^{13}C NMR (100 MHz, d_6-DMSO): 174.3, 153.4, 78.8, 58.4, 46.3, 30.3, 29.4, 28.1, 23.9, 28.1.

General Synthesis for Peptides[259]:

To a stirring solution of diamine (1 eq) in dry DCM was added EDCI (2 eq) and Boc-amino acid (2 eq). The reaction was left to stir under inert atmosphere at 0°C for 30 minutes and HOBt (2 eq) was added in one portion. The reaction was left to stir for 2 hours at 0°C and then overnight at room temperature. The reaction was washed with 10% $NaHCO_3$ (3 x 25 mls), water (3 x 25mls) and brine (3 x 25 mls). The organic layer was collected, dried over $MgSO_4$, filtered and evaporated to give colourless crystals.

***N,N'*-[Bis(N-Boc-L-proline)]diaminoethane 207**

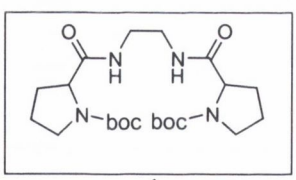

Procedure as described above. Crystallised from methanol/water yielding white crystals. (2.06 g, 88.67% yield), Mp 163°C. Calculated for $C_{22}H_{38}N_4O_6$: C, 58.13; H, 8.43; N, 12.92. Found: C; 57.95; H, 8.36; N, 12.31; ^{1}H NMR (400 MHz, CD_3CN): δ 6.92 (2 H, s, (N*H*)), 4.06 (2 H, s, *H*CNBoc), 3.40 (4 H, m, BocNC*H*$_2$), 3.25 (4 H, s, HNC*H*$_2$), 2.21 (4 H, m, BocNCH$_2$C*H*$_2$), 1.90 (4 H, m, NCHC*H*$_2$), 1.56 (9 H, s); ^{13}C NMR (100 MHz, CD_3CN): 173.0 (C=O), 153.6 (C=O), 78.7 ($_q$C), 60.5 (H*C*NBoc), 46.49 (BocN*C*H$_2$), 38.6 (HN*C*H$_2$), 30.6 (BocNCH$_2$*C*H$_2$), 27.2 (C(*C*H$_3$)$_3$), 23.7 (NCH*C*H$_2$). ES-MS: *m/z* 455.0 (M^+). ν/cm^{-1} (KBr) 3301, 2987, 2898, 1704, 1656, 1541, 1389, 1172.

N,N'-[Bis(N-Boc-L-proline)]-*trans*-diaminocyclohexane 206

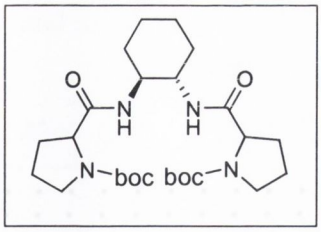

Procedure as described above; (2.45 g, 92.5% yield); Mp 130°C. Calculated for $3[C_{26}H_{44}N_4O_6].2H_2O$: C, 59.89; H, 8.78; N, 10.76. Found: C; 59.80; H, 8.36; N, 10.66; ^{1}H NMR (400 MHz, CD_3CN): δ 6.76 (2 H, s,b), 4.05 (2 H, m), 3.55 (2 H, m), 3.38 (4 H, m), 1.96 (12 H, m), 1.45 (18 H, s, Boc), 1.31 (4 H, m); ^{13}C NMR (100 MHz, CD_3CN): 172.5, 154.1, 78.8, 59.7, 52.9, 46.3 ,33.0, 31.4, 30.5, 27.2, 23.9 , ES-MS: *m/z* 509.0 (M^+). ν/cm^{-1} (KBr) 3312, 2980, 2937, 1699, 1658, 1549, 1397, 1256, 11170, 1153.

N,N'-[Bis(N-Boc-L-alanine)]diaminoethane 208

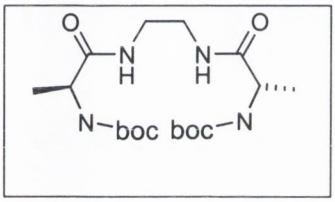

Procedure as described. Crystallised form EtOAc/Hexane. (1.18 g, 56.47% yield); Mp 161°C; Calculated for $C_{18}H_{34}N_4O_6$: C, 53.72; H, 8.51; N, 13.92. Found: C; 53.44; H, 8.34; N, 14.14; ^{1}H NMR (400 MHz, d_6-DMSO): δ 7.80 (2 H, s,b, H_2CNH), 6.84 (2 H, sb, Boc-N*H*), 3.89 (2 H, m, H_3CCHNH), 3.10 (4 H, m, CH_2NH), 1.37 (18 H, s, Boc), 1.16 (6 H, d, CH_3CH); ^{13}C NMR (100 MHz, d_6-DMSO): 172.8 (C=O), 155.0 (C=O), 78.0 ($_qC$), 49.7 (H_3CCH-NH), 38.3 (CH_2NH), 24.2 (($CH_3)_3C$), 18.3 (CH_3CH); ES-MS: *m/z* 403.0 (M^+); ν/cm^{-1} (KBr) 3344, 2983, 2942, 1685, 1525, 1453, 1369, 1324, 1254, 1172, 1070.

N,N'-[Bis(N-Boc-L-alanine)]-*trans*-diaminocyclohexane 209

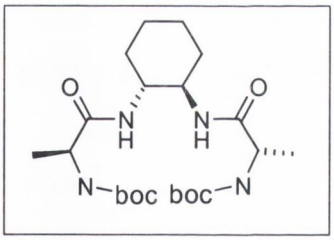

Procedure as described above. (1.62 g, 45.3% yield); Mp >200°C; Calculated for $2[C_{22}H_{40}N_4O_6]H_2O$: C, 56.75; H, 8.88; N, 12.03. Found: C; 56.99; H, 8.72; N, 12.20; ^{1}H NMR (400 MHz, d_6-DMSO): δ 6.73 (2 H, s,b, H_2C-N*H*), 5.61 (2 H, s,b, Boc-N*H*), 3.96 (2 H, m, H_3CCHNH), 3.56 (2 H, m, CH_2NH), 1.73 (4 H, m, CH_2), 1.64 (4 H, m, CH_2) 1.44 (18 H, s, Boc), 1.26 (6 H, m, H_3CCHNH); ^{13}C NMR (100 MHz, D_6-DMSO): 172.5 (C=O), 154.9 (C=O), 78.07 ($C(CH_3)_3$), 52.0 (H_3CCH-NH), 50.0 (CH_2NH), 32.0 (CH_2), 28.2 (($CH_3)_3C$), 24.4 (CH_2), 18.7 (CH_3CH); ES-MS: *m/z* 457.0 (M^+); ν/cm^{-1} (KBr) 3323, 2981, 1938, 2861, 1718, 1661, 1546, 1368, 1254, 1117, 1069.

General Procedure For The Removal Of The Boc Protecting Group:

The Boc protected pseudopeptide was dissolved in the appropriate amount of ethanol. HCl gas (prepared *in situ*) was diffused into the sample for approximately one hour and the reaction was left to stir overnight. The sample was concentrated and diethyl ether added until

a precipitate was seen. The precipitate was collected by filtration, washed with diethyl ether and dried under vacuum.

_N,N'_-[Bis(L-proline)]diaminoethane 201

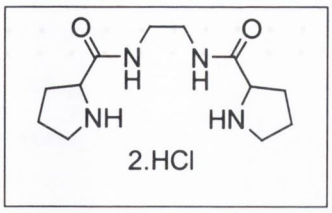

(0.30 g, 34.7 % yield); mp 58.1°C; Accurate Mass: calculated for 254.3347: Found 255.1821; ^{1}H NMR (400 MHz, DMSO): δ 8.85 (2 H, s, N*H*), 5.57 (2 H, s, N*H*), 4.19 (2 H, m), 3.36 (4 H, m), 3.29 (4 H, m, CH_2(ethane)), 2.32 (4 H, m), 1.88 (4 H, m); ^{13}C NMR (100 MHz, CD_3CN): 168.2 ($_q$C), 59.0 (*C*H), 45.4 (*C*H_2), 38.4 (*C*H_2), 29.3 (*C*H_2), 23.6 (*C*H_2); ES-MS: *m/z* 255.04 (M^+); ν/cm^{-1} (KBr) 3332, 3087, 2935, 1678, 1629, 1578, 1450, 1313, 1246, 1091.

_N,N'_-[Bis(L-proline)]diaminocyclohexane 200

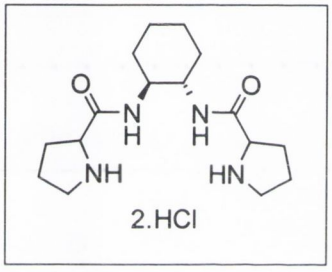

(0.94 g, 92 % yield), mp 67.0°C; Calculated for 2[$C_{16}H_{30}N_4O_2Cl_2$]H_2O: C, 49.23; H, 8.00; N, 14.35. Found: C; 49.25; H, 7.75; N, 14.21; ^{1}H NMR (400 MHz, d_6-DMSO): δ 8.55 (2 H, s, N*H*), 4.08 (2 H, s), 3.56 (2 H, s), 3.17 (4 H, s), 2.22 (2 H, s), 1.85 (4 H, s), 1.73 (2 H, s), 1.26 (4 H, s); ^{13}C NMR (100 MHz, d_6-DMSO): 23.6, 24.2, 29.6, 31.8, 45.6, 52.0, 58.7, 167.5; ES-MS: *m/z* 308.8 (M^+); ν/cm^{-1} (KBr) 3451, 3211, 3072, 2931, 2764, 2562, 1673, 1571, 1450, 1398, 1315,1046.

_N,N'_-[Bis(L-alanine)]diaminoethane 202

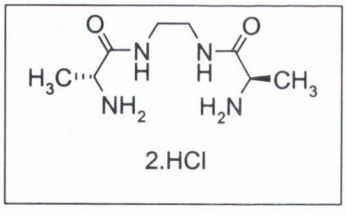

(0.82 g, 96% yield); mp 59.7°C; Accurate Mass: calculated for 202.1508: Found 203.1508; ^{1}H NMR (400 MHz, DMSO-d_6): δ 8.64 (2 H, s, N*H*), 8.25 (4 H, s, N*H*), 3.96 (2 H, m), 3.21 (4 H, s), 1.02 (6 H, m); ^{13}C NMR (100 MHz, DMSO-d_6): 169.5 ($_q$C), 48.4 (*C*H), 38.2 (*C*H_2), 16.9 (*C*H_3); ES-MS: *m/z* 203.01 (M^+); ν/cm^{-1} (KBr) 3285, 1690, 1573, 1503, 1266, 1217, 1121, 1003.

_N,N'_-[Bis(L-alanine)]diaminocyclohexane 203

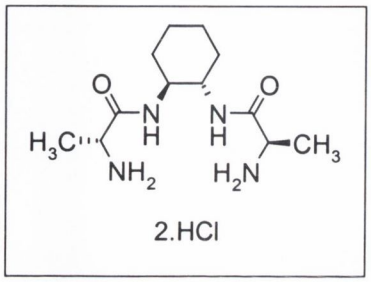

(1.01 g, 93% yield); mp 179.4°C; Accurate Mass: calculated for 257.1978: Found 256.3507; ^{1}H NMR (400 MHz, d_6-DMSO): δ 3.42 (m, 10 H), 1.76 (m, 4 H), 1.25 (m, 4 H); ^{13}C NMR (100 MHz, d_6-DMSO): 165.7 (C=O), 52.7, 40.3, 31.6, 24.5; ES-MS:

m/z 256.96 (M^+); ν/cm^{-1} (KBr) 3454, 3956, 3091, 2943, 1678, 1567, 1499, 1123.

General Synthesis of the Platinum Complexes:

To a solution of pseudopeptide (1 eq) in water (5 mL) was added a solution of K_2PtCl_4 (1 eq) in water (5 mL). The red solution was heated to 80°C for four hours and stirred at room temperature overnight. The yellow solution was left to stand until a yellow precipitae was seen, collected by filtration and dried under P_2O_5.

Platinum complex of *N,N'*-[Bis(L-proline)]diaminoethane [201.$PtCl_2$]

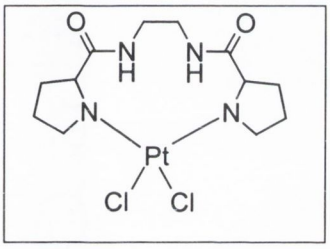

(0.05 g, 67.9% yield); mp >200°C; ^{1}H NMR (400 MHz, DMSO): δ 5.56 (2 H, s), 1.93 (2 H, m), 1.70 (6 H, m), 1.51 (2 H, m), 1.21 (6 H, m), 1.04 (6 H, m); ^{13}C NMR (100 MHz, CD_3CN): 156.6, 47.5, 44.4, 33.3, 25.3, 24.4; ν/cm^{-1} (KBr) 3328, 2932, 2851, 1627, 1578, 1439, 1313, 1246, 1091, 642.

Platinum complex of *N,N'*-[Bis(L-proline)]diaminocyclohexane [200.$PtCl_2$]

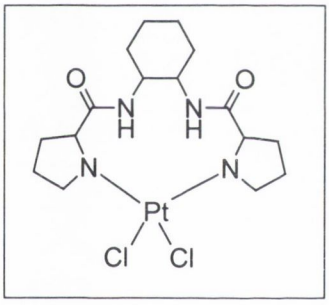

(0.04 g, 56.8% yield), mp >200°C; Calculated for $C_{16}H_{26}N_4O_2PtCl_2$: C, 33.34; H, 5.25; N, 9.72. Found: C; 22.79; H, 3.00; N, 5.92; ^{1}H NMR (400 MHz, d_6-DMSO): δ 8.42 (2 H, m), 7.94 (2 H, m), 6.26 (2 H, s), 4.74 (2H, m), 4.07 (2 H, m), 3.58 (2 H, m), 1.93 (2 H, m), 1.56 (2 H, m), 1.08 (2 H, m); ^{13}C NMR (100 MHz, CD_3CN): 167.5, 63.6, 60.3, 58.9, 54.1, 52.0, 45.7, 31.9, 29.5, 25.2, 23.7; ν/cm^{-1} (KBr) 3321, 2967, 2867, 1631, 1581, 1428, 1378, 1224, 1087, 644.

Platinum complex of *N,N'*-[Bis(L-alanine)]diaminoethane [202.$PtCl_2$]

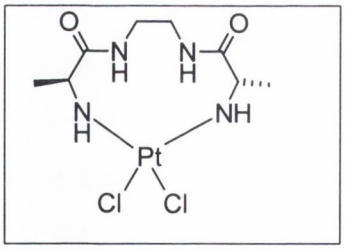

(0.02 g, 54.2% yield); mp >200°C; ^{1}H NMR (400 MHz, DMSO-d_6): δ ; 8.42 (2 H, m), 7.94 (2 H, m), 6.26 (2 H, s), 4.74 (2H, m), 4.07 (2 H, m), 3.58 (2 H, m), 1.93 (2 H, m), 1.56 (2 H, m), 1.08 (2 H, m); ν/cm^{-1} (KBr) 3452, 3269, 3182, 2937, 1616, 1569, 1450, 1097

Platinum complex of *N,N'*-[Bis(L-alanine)]diaminocyclohexane [203.$PtCl_2$]

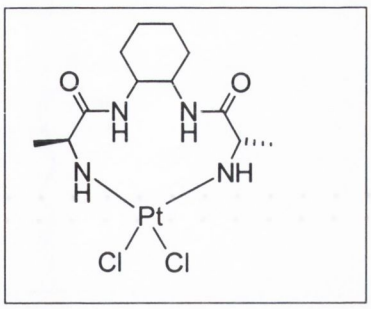

(0.02 g, 63.1% yield); mp >200°C; Calculated for $C_{12}H_{22}N_4O_2Cl_2Pt$: C, 27.70; H, 4.26; N, 10.77. Found: C; 19.79; H, 2.86; N, 8.44; ^{1}H NMR (400 MHz, d_6-DMSO): δ 8.05 (2 H, m), 4.69 (1 H, m), 4.12, (1 H), 3.47, (2 H, s), 3.17 (2 H, m) 1.78 (2 H, m), 1.34 (2 H, m), 1.14 (1 H, m); ν/cm^{-1} (KBr) 3460, 3271, 3195, 2933, 2866, 1655, 1560, 1450, 1211, 1161, 758.

Attempted Synthesis of *N,N'*-[Bis(*N'',N'''*-pent-5-ene-L-proline-)]diaminocyclohexane 210

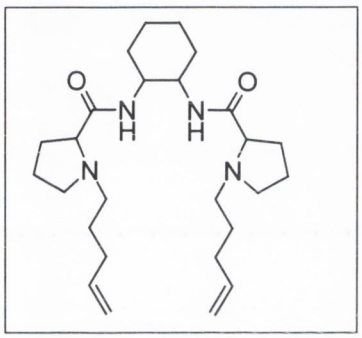

To a stirring solution of 5-bromopent-1-ene (0.16 g, 1.1 mmol), Cs_2CO_3 (1.026 g, 3.1 mmol) and KI (0.02 g, 0.1 mmol) in DMF (15 ml) was slowly added *N,N'*-[Bis(L-proline-)]diaminocyclohexane (0.2 g, 0.5 mmol). The reaction was refluxed overnight under inert atmosphere. The precipitate was removed by filtration and the solvent removed under vacuum to yield a brown oil

***N,N'*-Bis-(6-Pent-4-enyloxymethyl-pyridin-2-ylmethyl)-*p*-tosylamide 217a**

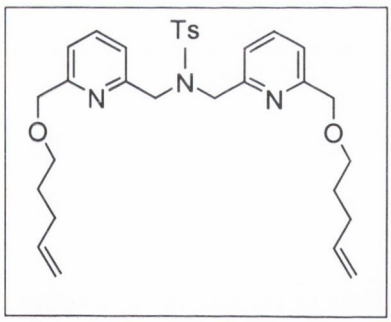

To a stirring solution of *N,N*-bis[[6-hydroxymethyl]pyridin-2-yl]-*p*-tosylamide (0.1 g, 0.24 mmol) in DMF (5 mL) at 0°C was added NaH (0.017 g, 0.73 mmol). The reaction was left to stir for 30 minutes under inert atmosphere where it turned a red colour. To this 5-bromopent-1-ene (0.24 g, 0.48 mmol) was slowly added and stirred for 1 hour maintaining temperature at 0°C. The yellow solution was slowly warmed to room temperature and quenched with water. The reaction was extracted with EtOAc (3 x 25 mls). The organic extracts were collected and washed with brine (3 x 25 mls). The organic layer was collected, dried over Na_2SO_4, filtered and evaporated to give a yellow oil. The product was isolated by flash chromatography on silica with 98:2 EtOAc:Hexane. (0.07 g, 50.0 % yield), mp 68°C. Accurate Mass: calculated for 549.7382: Found 550.2740; ^{1}H NMR (400 MHz, CD_3CN) 7.81 (2 H, d, J = 8.0 Hz), 7.70 (2H, d, J = 8.0 Hz), 7.56 (2 H, t, J = 8.04 Hz), 7.38 (2 H, d, J = 7.52 Hz), 7.25 (2 H, d, J = 7.52 Hz), 5.90 (2 H, m), 5.10 (4H, m), 4.53 (4 H, s), 4.47 (4 H, s), 3.52 (4 H, m), 2.41 (3 H, s), 1.71 (4 H, m); ^{13}C NMR (100 MHz, CD_3CN): 157.9, 155.3, 137.7, 136.9, 120.5, 119.5, 115.9, 114.6, 114.2, 73.0, 69.9, 53.6, 29.8, 29.2, 28.5, 21.4, 13.6; ES-MS: *m/z* 550.1 (M^+)

_N,N_-Bis-(6-But-3-enyloxymethyl-pyridin-2-ylmethyl)-_p_-tosylamide 217b

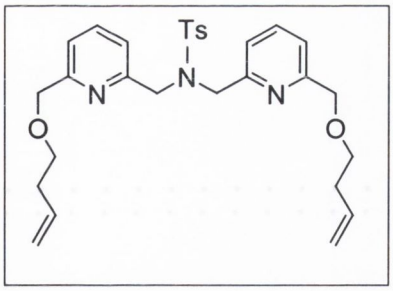

A solution of NaH (0.017 g, 0.73 mol) and _N,N_-bis[[6-hydroxymethyl]pyridin-2-yl]-_p_-tosylamide (0.10 g, 0.24 mmol) in DMF (10 mL) was stirred at 0°C under inert atmosphere until a red colour was seen. 4-Bromobut-1-ene (0.097 g, 0.73 mmol) in DMF (5 mL) was added maintaining the temperature at 0°C. The reaction was left to stir for one hour. The yellow solution was quenched in water (20 mls) and extracted with water (3 x 25 mls). The organic extracts were collected and washed with brine (3 x 25 mls). The organic layer was collected, dried over Na_2SO_4, filtered and evaporated to give a brown oil. The product was isolated by flash chromatography on silica with 80:20 EtOAc:Hexane. (0.07g, 49.1% yield), mp 75°C. Accurate Mass: calculated for 521.6840: Found 522.2427; ^{1}H NMR (400 MHz, CD_3CN) 7.63 (2 H, d, J = 8.0 Hz), 7.50 (2H, d, J = 8.0 Hz), 7.35 (2 H, t, J = 8.04 Hz), 7.29 (2 H, d, J = 7.52 Hz), 7.22 (2 H, d, J = 7.52 Hz), 5.67 (2 H, m), 4.72 (4H, m), 4.55 (4 H, s), 4.43 (4 H, s), 3.64 (4 H, m), 2.46 (3 H, s), 2.32 (4 H, m); ^{13}C NMR (100 MHz, CD_3CN): 155.9, 154.1, 137.9, 137.2, 122.8, 119.0, 116.4, 114.1, 113.8, 73.4, 69.3, 52.6, 29.7, 29.2, 22.4, 12.9; ES-MS: *m/z* 522.3 (M^+)

_N,N_-Bis-(6-allyloxymethyl-pyridin-2-ylmethyl)-_p_-tosylamide 217c

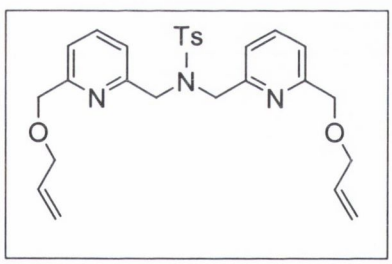

A solution of _N,N_-bis[[6-hydroxymethyl]pyridin-2-yl]-_p_-tosylamide (0.1 g, 2,4 x 10^{-4} mol) and NaH (0.017 g, 7.3 x 10^{-4} mol) in DMF (15 ml) was stirred at 0°C for 30 minutes under inert atmosphere until a red colour was seen. To this allyl bromide (0.087 g, 7.3 x 10^{-4} mol) was added maintaining the temperature at 0°C. This was left to stir for one hour under inert atmosphere at 0oC. The yellow reaction mixture was quenched in water (20 ml) and extracted with EtOAc (3 x 20 ml). The organic extracts were combined and washed with brine (3 x 15 ml). The organic layer was collected, dried over Na_2SO_4, filtered and evaporated to give a brown oil. The product was isolated by flash silica chromatography using 50:50 EtOAc:Hexane solvent system. (0.06 g, 54.1% yield), mp 79°C. Accurate Mass: calculated for 493.6298: Found 494.2114; ^{1}H NMR (400 MHz, CD_3CN) 7.69 (2 H, d, J = 8.0 Hz), 7.63 (2H, d, J = 8.0 Hz), 7.34 (2 H, t, J = 8.04 Hz), 7.26 (2 H, d, J = 7.52 Hz), 7.20 (2 H, d, J = 7.52 Hz), 5.98 (2 H, m), 5.35 (4H, m), 4.54 (4 H, s), 4.40 (4 H, s), 2.43 (3 H, s); ^{13}C NMR (100 MHz, CD_3CN): 158.8, 156.1, 139.4, 136.8, 123.4, 119.9, 116.9, 114.6, 113.8, 74.6, 69.9, 55.2, 27.2, 23.9, 13.5; ES-MS: *m/z* 494.7 (M^+)

Attempted Synthesis of the macrocycle 214

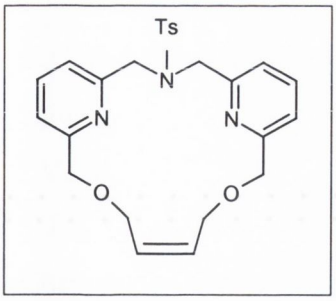

To a stirring solution of *N,N*-Bis-(6-allyloxymethyl-pyridin-2-ylmethyl)-*p*-tosylamide (0.2 g, 0.3 mmol) in DCM (80 ml) was added Grubbs catalyst (0.006 g, 0.06 mmol). The solution was degassed and left to stir overnight under inert atmosphere. The solvent was removed under vacuum leaving a brown oily residue.

[1] J.W. Steed and J.L. Atwood. *Supramolecular Chemistry: A Concise Introduction*, 1999, John Wiley and sons Ltd

[2] V. Balzani and F. Scandola. *Supramolecular Photochemistry*, 1991, Ellis Horwood Ltd.

[3] JM Lehn. *Supramolecular Chemistry: Concepts and Perspectives; a Personal Account*, Chap. 1, 1995, VCH

[4] D. Cram. *Angew. Chem. Intl. Ed.*, 1986, **25**, 1039-1057

[5] D. Cram and CJ Pederson. *Angew. Chem. Int. Ed.*, 1988, **27**, 1009-1020

[6] J.M. Lehn. *Angew. Chem. Int. Ed.*, 1988, **27**, 89-112

[7] G. Stochel, A. Wanat, E. Kuliś and Z. Stasicka. *Coord. Chem. Rev.*, 1998, **171**, 203-220

[8] Z. Kontos, P. Huszthy, J.S. Bradshaw and R.M. Izatt. *Tetrahedron: Assym*, 1999, **10**, 2087-2099

[9] R.M. Izatt, J.S. Bradshaw, R.L. Bruening, B.J. Tarbet and M.L. Bruening. *Pure Appl. Chem*, 1995, **7**, 1069-1074

[10] Ed. A.E. Merbach and E. Toth. *The Chemistry of Contrast Agents in Medicinal Magnetic Resonance Imaging*, 2001, Wiley and Sons.

[11] L. Thunus and R. Lejeune. *Coord. Chem. Rev.*, 1999, **184**, 125-155

[12] N. Sabbatin and E. Guardini. *Coord. Chem. Rev.*, 1993, **123**, 201-228

[13] JM Lehn. *Supramolecular Chemistry: Concepts and Perspectives; a Personal Account*, Chap. 8, 1995,VCH

[14] B. Alpha, R. Ballardini, V. Balazani, J.M. Lehn, S. Perathoner and N. Sabbatini. *Photochem. Photobio.*, 1990, **52**, 299-306

[15] G. Stein and E. Würzbeg. *J. Chem. Phys.*, 1975, **1**, 208-213

[16] W. Dee Horrocks and D.R. Sudnik. *Acc. Chem. Res*, 1981, **4**, 384-392

[17] F.S. Richardson. *Chem. Rev.*, 1982, **82**, 541-552

[18] a: M. Elbanowski and B. Makowska. *J. Photochem. Photobio. A: Chemistry*, 1996, **99**, 85-92; b: B. Alpha, J.M. Lehn and G. Mathis. *Angew. Chem. Int. Ed.*, 1987, **3**, 266-267

[19] F.S. Richardson and A. Das Gupta. *J. Am. Chem. Soc.*, 1981, **103,** 5716-5725

[20] J.C.G. Bünzli. *Inorg. Chim. Acta.*, 1987, **139**, 219-222

[21] J. Georges. *Analyst*, 1993, **118**, 1481-1486

[22] D.S. Hubbard, M.P. Houlne, G.E. Kiefer, K. McMillan and D.J. Bornhop. *Bioimaging*, 1998, **6**, 63-70

[23] C.O. Paul-Roth, J-M. Lehn, J. Guilhem and C. Pascard. *Helv. Chim. Acta*, 1995, **78**, 1895-1903

[24] E.F. Gudgin Dickson, A. Pollack and E.P. Diamondis. *J. Photochem. Photobio. B: Biology*, 1995, **27**, 3-19

[25] F. Benetollo, G. Bombieri, A.M. Adeyga, K.K. Fonda, W.A. Gootee, K.M. Samaria and L.M. Vallarino. *Polyhed.*, 2002, **21**, 425-433

[26] P.G. Sammes and G. Yahioglu. *Natl. Prodt. Reports*, 1996, 1-28

[27] V.M. Mukhala and J.J. Kinkare. *Helv. Chim. Acta*, 1992, **75**, 1578-1592

[28] M. Pietraszkiewicz, J. Karpiuk and O. Pietraszkiewicz. *Spectrochim. Acta Part A*, 1998, **54**, 2229-2236

[29] N. Sato, M. Gato, S. Matsumoto and S. Shinkai. *Tetrahedron Lett.*, 1993, **34**, 4847-4850

[30] F.J. Steemers, W. Verboom, D.N. Reinhoudt, E.B. van der Tol and J.W. Verhoeven. *J. Am. Chem. Soc.*, 1995, **117**, 9408-9412

[31] F.J. Steemers, W. Verboom, D.N. Reinhoudt, E.B. van der Tol and J.W. Verhoeven. *J. Photochem. Photobio. A: Chemistry*, 1998, **113**, 141-144

[32] E.B. van der Tol, H.J. van Ramesdonk, J.W. Verhoeven, F.J. Steemers, E.G. Kerver, W. Verboom and D.N. Reinhoudt. *Chem. Eur. J.*, 1998, **11**, 2315-2323

[33] B.H. Bakker, M. Goes, N. Hoes, H.J van Ramesdonk, J.W. Verhoeven, M.H.V. Werts and J.W. Hofstraat. *Coord. Chem. Reviews*, 2000, **208**, 3-16

[34] M.H.V. Werts, R.H. Woudenberg, P.G. Emmerink, R. van Gassel, J.W. Hofstraat and J.W. Verhoeven. *Angew. Chem. Int. Ed.*, 2000, **24**, 4542-4544

[35] M.P.O. Woulbers, F.C.J.M. van Veggel, B.H.M. Snellink-Ruel, J.W. Hofstraat, F.A.J. Guerts and D.N. Reinhoudt. *J. Chem. Soc., Perkin Trans 2*, 1998, 2141-2150

[36] C. Galaup, J.M. Couchet, C Picard and P. Tisnes. *Tetrahedron Lett.*, 2001, **42**, 6275-6278

[37] C. Galaup, M.C. Carrie, J. Azema and C. Picard. *Tetrahedron Lett*, 1998, **39**, 1573-1576

[38] C. Galaup, M.C. Carrie, P. Tisnes and C. Picard. *Eur. J. Org. Chem.*, 2001, 2165-2175

[39] C. Galaup, C. Picard, B. Cathala, L. Cazaux, P. Tisnes, H. Autiero and D. Aspe. *Helv. Chim. Acta*, 1999, **82**, 543-560

[40] M. Wang, L. Jin and J-C. G. Bünzli. *Polyhed.* 1999, **18**, 1853-1861

[41] Ed.: N.V. Gerbeleu, V.B. Arion and J. Burgess. *Template Synthesis of Macrocyclic Compounds*, Chap. 3, S.M. Nelson, 1998, Wiley-VCH

[42] V. Alexander. *Chem. Rev.*, 1995, **95**, 273-342

[43] D.E. Fenton, R. Bastida and P.A. Vigato. *Chem. Soc. Rev.*, 1988, **17**, 69-90

[44] J.D.J Backer-Dirks, C.J. Gray, F.A. Hart, M.B. Hurtsthouse and B.C. Schoop. *J. Chem Soc., Chem. Commun*, 1979, 774-775

[45] K.K. Abid, D.E. Fenton, R. Bastida, U. Castellato, P.A. Vigato and R. Graziani. *J. Chem. Soc., Dalton Trans.*, 1984, 351-354

[46] A.M. Arif, J.D. J Backer-Dirks, C.J. Gray, F.A. Hart and M.B. Hursthouse. *J. Chem. Soc., Dalton Trans.*, 1987, 1665-1673

[47] M.G.B. Drew, J. Nelson, F. Esho, V. McKee and S.M. Nelson. *J. Chem. Soc., Dalton Trans.*, 1982, 1837-1843

[48] F. Benetollo, G. Bombieri, W.A. Gootee, K.K. Fonda, K.M. Samaria and L.M. Vallarino. *Polyhed.*, 1998, **20**, 3633-3642

[49] J. Lisowski and P. Starynowicz. *Polyhed.*, 2000, **19**, 465-469

[50] F. Benetollo, G. Bombieri, K.K. Fonda, A. Polo, J.R. Qualiano and L.M. Vallarino. *Inorg. Chem.*, 1991, **30**, 1345-1353

[51] V. Arul Joseph Aruna and V. Alexander. *Inorg. Chim. Acta,* 1996, **249**, 93-100

[52] V. Alexander. *J. Chem. Soc., Dalton Trans.,* 1996, 1867-1873

[53] D.S. Kumar and V. Alexander. *Inorg. Chim. Acta,* 1995, **238**, 63-71

[54] D.S. Kumar and V. Alexander. *Polyhed.*, 1999, **18**, 1561-1568

[55] V. Alexander. *J. Chem. Soc., Dalton Trans.,* 1999, 1773-1777

[56] D.S. Kumar, V. Arul Joseph Aruna and V. Alexander. *Polyhed.*, 1999, **18**, 3123-3128

[57] U. Casellato, S. Tamburini, P. Tomasin, P.A. Vigato, S. Aime and M. Botta. *Inorg. Chem.*, 1999, **38**, 2906-2916

[58] N. Brianese, U. Castellato, S. Tamburini, P. Tomasin and P.A. Vigato. *Inorg. Chim. Acta*, 1999, **293**, 178-194

[59] R. Bastida, A. de Blas, P. Castro, D.E. Fenton, R. Bastida, A. Macias, R. Rial, A. Rodriguez and T. Rodriguez-Blas. J. *Chem. Soc., Dalton Trans.*, 1996, 1493-1497

[60] S.R. Collinson, D.E. Fenton and R. Bastida. *Coord. Chem. Rev.*, 1996, **148**, 19-40

[61] L. Valencia, R. Bastida, A. de Blas, D.E. Fenton and Bastida, A. Macias, A. Rodriguez, T. Rodriguez-Blas and A. Castineiras. *Inorg. Chim. Acta*, 1998, **282**, 42-49

[62] C. Platas, R. Bastida, A. de Blas, D.E. Fenton, R. Bastida, A. Macias, A. Rodriguez and T. Rodriguez-Blas. *Polyhed.* 1998, **10**, 1759-1765

[63] C. Lodeiro, R. Bastida, A. de Blas, D.E. Fenton, A. Macias, A. Rodriguez and T. Rodriguez-Blas. *Inorg. Chim. Acta*, 1998, **267**, 55-62

[64] M. Vincente, C. Lodeiro, H. Adams, R. Bastida, A. de Blas, D.E. Fenton, A. Macias, A. Rodriguez and T. Rodriguez-Blas. *Eur. J. Inorg. Chem*, 2000, 1015-1024

[65] F. Benetollo, G. Bombieri, A.M. Adeyga, K.K. Fonda, W.A. Gootee, K.M. Samaria and L.M. Vallarino. *Polyhed.*, 2002, **21**, 425-433

[66] S. Amin, J.R. Morrow, C.H. Lake and M.R. Churchill. *Angew. Chem. Int. Ed. Engl.,* 1994, **33**, 773-775 ; S. Amin, D.A. Voss, W .De W. Horrocks, C.H. Lake, M.R. Churchill and J.R. Morrow. *Inorg. Chem.*, 1995, **34**, 3294-3300; J.R. Morrow, K. Aures and D. Epstein. *J. Chem. Soc. Chem. Comm.,* 1995, 2431-2432

[67] D. Parker and J.A.G. Williams. *J. Chem. Soc., Perkin Trans. 2*, 1995, 1305-1314

[68] D. Parker and J.A.G. Williams. *J. Chem. Soc., Perkin Trans. 2*, 1996, 1581-1586

[69] D. Parker, P.K. Senanayake and J.A.G. Williams. *J. Chem. Soc., Perkin Trans. 2*, 1998, 2129-2139

[70] D. Parker. *Coord. Chem. Rev.*, 2000, **205**, 109-130

[71] T. Gunnlaugsson and D. Parker. *J. Chem. Soc., Chem. Comm.*, 1998, 511-512

[72] M.P. Lowe and D. Parker. *J. Chem. Soc., Chem. Comm.*, 2000, 707-708

[73] M.P. Lowe and D. Parker. *Inorg. Chim. Acta.,* 2001, **317**, 163-173

[74] T. Gunnlaugsson. *Tetrahedron. Lett.,* 2001, **42**, 8901-8905

[75] C. Bazzicalupi, A. Bencini, E. Berni, A. Bianchi, C. Giorgi, V. Fusi, B. Valtanicoli, C. Lodeiro, A. Roque and F. Pina. *Inorg. Chem.*, 2001, **40**, 6172-6179

[76] A. Beeby and S. Faulkner. *Chem. Phys. Lett.,* 1997, **266**, 116-122

[77] S. Faulkner, A. Beeby, M.C. Carrie, A. Dadabhoy, A.M. Kenwright and P.G. Sammes. *Inorg. Chem. Comm,* 2001, 187-190

[78] O. Reaney, T. Gunnlaugsson and D. Parker. *J. Chem. Soc., Perkin Trans. 2,* 2000, 1819-1831

[79] O. Reaney, T. Gunnlaugsson and D. Parker. *J. Chem. Soc., Chem. Comm.,* 2000, 473-474

[80] G. Kaptein. *J. Org. Chem.,* 1990, **55**, 811-812

[81] G. Lee, Y. Miyahara and T. Inazu. *Chem. Lett.,* 1996, 873-874

[82] G. Lee, M. Oka, M. Takemura, Y. Miyahara, N. Shimizu, T. Inazu. *J. Org. Chem.,* 1996, **61**, 8304-8306

[83] M. Newcomb, J. Timoko, D. Walba and D.J. Cram. *J. Am. Chem. Soc.,* 1977, **99**, 1875-1879

[84] W. Rabjohn. *Organic Synthesis Collective,* 1963, **4**, 921-923

[85] E. Buhleier, W. Wehner and F. Vogtle. *J. Liebs. Annal. Chem.,* 1978, **4**, 537-544

[86] Ed: D. Parker. *Macrocyclic Synthesis- A Practical Approach,* 1996, Oxford University Press

[87] M.W. Hosseini, J. Camarmond and J.M. Lehn. *Helv.Chim. Acta,* 1989, **72**, 1066-1077

[88] C-M Che. *Polyhed.,* 1994, **13**, 771-776

[89] Ed.: N.V. Gerbeleu, V.B. Arion and J. Burgess. *Template Synthesis of Macrocyclic Compounds*, Chap. 3, S.M. Nelson, 1998, Wiley-VCH

[90] V. Alexander. *Chem. Rev.*, 1995, **95**, 273-342

[91] D.E. Fenton, R. Bastida and P.A. Vigato. *Chem. Soc. Rev.*, 1988, **17**, 69-90

[92] N.W. Alcock, R.G. Kingston, P. Moore and C. Pierpoint. *J. Chem. Soc., Dalton Trans.*, 1984, 1937-1943

[93] E.P. Papadopoulos, A. Jarrar and C.H. Issidorides. *J. Org. Chem.*, 1966, **31**, 272-273

[94] K.K. Abid, D.E. Fenton, R. Bastida, U. Castellato, P.A. Vigato, R. Graziani. *J. Chem. Soc., Dalton Trans.*, 1984, 351-354

[95] A.M. Arif, J.D. J Backer-Dirks, C.J. Gray, F.A. Hart, M.B. Hursthouse. *J. Chem. Soc., Dalton Trans.*, 1987, 1665-1673

[96] M.G.B. Drew, J. Nelson, F. Esho, V. McKee, S.M. Nelson. *J. Chem. Soc., Dalton Trans.*, 1982, 1837-1843

[97] P.A. Vigato, D.E Fenton. *Inorg.Chim. Acta,* 1987, **139**, 39-48

[98] K.K. Abid, D.E. Fenton. *Inorg. Chim. Acta,* 1984, **95**, 119-123

[99] K.K. Abid, D.E. Fenton. *Inorg. Chim. Acta,* 2001, **317**, 147-156

[100] M.W. Hosseini, J. Camarmond, J.M. Lehn. *Helv. Chim. Acta,* 1989, **72**, 1066-1077

[101] Ed. IUPAC Commission on Photochemistry. *Pure Appl. Chem., 1988, **60**, 1108-1114*

[102] T. Gunnlaugsson, M. Nieuwenhuyzen and C. Nolan. *J. Chem. Soc., Dalton Trans.*, Submitted for publication

[103] F.H. Westheimer, *Science,* 1987, **235**, 1173-1178

[104] R.G. Kuimelis and L.W. McLaughlin. *Chem. Rev.*, 1998, **98**, 1027-1044

[105] A. Blasko and T.C. Bruice. *Acc. Chem. Res.*, 1999, **32**, 475-484

[106] J.Chin. *Curr. Op. Chem. Bio.*, 1997, **1**, 514-521

[107] R. Haner, J. Hall, A. Pfutzer and R. Husken. *Pure App. Chem.*, 1998, **70**, 111-116

[108] D.M. Perreault and E.V. Anslyn, *Angew. Chem. Int. Ed. Engl.*, 1997, **36**, 432-450

[109] N.H. Williams and P. Wyman. *J. Chem. Soc., Perkin 2,* 2001, 2068-2073

[110] N.H. Williams, B. Taskaski, M. Wall and J. Chin. *Acc. Chem. Res.*, 1999, **32**, 485

[111] B.N. Trawick, A.T. Daniher and J.K. Bashkin. *Chem. Rev.*, 1998, **98**, 939-960

[112] R. Breslow and M. Labelle, *J. Am. Chem. Soc.*, 1986, **108**, 2655-2659

[113] R. Breslow and E. Anslyn, *J. Am. Chem. Soc.*, 1989, **111**, 4473-4482

[114] R. Breslow and D-L. Huang, *J. Am. Chem. Soc.*, 1990, **112**, 9621-9623

[115] J.K. Bashkin, J.K. Gard and A.S. Modak. *J. Org. Chem.*, 1990, **55**, 5125-5132

[116] J.J. Butzow and G.L. Eichhorn, *Nature*, 1975, **254**, 358-359

[117] R. Breslow, D.L. Huang and E. Anslyn. *Proc. Natl. Acad. Sci. USA,* 1989, **86**, 1746-1750

[118] R. Breslow and D.L. Huang. *Proc. Natl. Acad. Sci. USA,* 1991, **88**, 4080-4083

[119] J.H. Kim and J. Chin. *J. Am. Chem. Soc.,* 1992, **114** 9792-9795

[120] J.A. Connelly, M. Banaszczyk, R.C. Hynes and J. Chin. *Inorg. Chem.,* 1994, **33**, 665-669

[121] N.H. Williams, W. Cheung and J. Chin. *J. Am. Chem. Soc.,* 1998, **120**, 8079-8087

[122] M. Komiyama, Y. Matsumoto, H. Takahashi, T. Shiiba, H. Tsuzuki, H. Yajima, M. Yashiro and J. Sumaoka, *J. Chem. Soc. Perkin 2,* 1998, 691-695

[123] R. Hettich and H-J. Schneider, *J. Am. Chem. Soc.*, 1997, **119**, 5638-5647

[124] P. Molenveld, S. Kapsabelis, J.F.J. Engberson and D.N. Reinhoudt. *J. Am. Chem. Soc.,* 1997, **119**, 2948-2949

[125] P. Molenveld, J.F.J. Engberson, H. Kooijman, A.L. Spek and D.N. Reinhoudt. *J. Am. Chem. Soc.,* 1998, **120**, 6726-6737

[126] P. Molenveld, J.F.J. Engberson and D.N. Reinhoudt. *Angew. Chem. Int. Ed. Engl.,* 1999, **38**, 3189-3192

[127] P. Molenveld, J.F.J. Engberson and D.N. Reinhoudt. *J. Org. Chem.,* 1999, **64**, 6337-6341

[128] P. Molenveld, J.F.J. Engbersen and D.N. Reinhoudt, *J. Chem. Soc., Chem. Soc. Rev.*, 2000, **29**, 75-86

[129] M. Wall, R.C. Hynes and J. Chin, *Angew. Chem. Int. Ed.,* 1993, **32**, 1633-1639

[130] M.J. Young and J. Chin, *J. Am. Chem. Soc.*, 1995, **117**, 10577-10578

[131] A. Hamilton, Z. Luo and S. Liu, *Angew. Chem. Int. Ed.*, 1997, **36**, 2678-2680

[132] A. Hamilton and S. Liu, *Tetrahedron. Lett.*, 1997, **7**, 1107-1110

[133] A. Hamilton and S. Liu, *J. Chem. Soc., Chem. Comm.*, 1999, 587-588

[134] M. Yashiro, A. Ishikubo and M. Komiyama. *J. Chem. Soc., Chem. Comm.*, 1995, 1793-1794

[135] S. Matsudo, A. Ishikubo, A. Kuzuya, M. Yahiro and M. Komiyama. *Angew. Chem. Int. Ed. Engl.,* 1998, **37**, 3284-3286

[136] M. Irisawa, N. Takeda and M. Komiyama. *J. Chem. Soc., Chem. Comm.,* 1995, 1793-1794

[137] M. Yasturo, A. Ishikybo and M. Komiyama, *J. Chem. Soc., Chem. Comm.,* 1997, 83-84

[138] J. Sumaoka, K. Koawata and M. Komiyama. *Chem. Lett.,* 1999, 439-440

[139] G. Park, J. Shao, F.H. Lu, R.D. Rogers, N.D. Chasteen, M. Brechbiel and R.P. Planalp. *Inorg. Chem.,* 2001, **40**, 4167-4175

[140] K.A. Deal, G. Park, J. Shao, N.D. Chasteen, M. Brechbiel and R.P. Planalp. *Inorg. Chem.,* 2001, **40**, 4176-4182

[141] T. Clifford, A.M. Danby, P. Lightfoot, D.T. Richens and R.W. Hay. *J. Chem. Soc., Dalton,* 2001, 240-246

[142] H-J. Schneider. *Tetrahedron Lett.*, 2002, **43**, 411-414

[143] S. Amin, J.R. Morrow, C.H. Lake and M.R. Churchill. *Angew. Chem. Int. Ed. Engl.,* 1994, **33**, 773-775

[144] S. Amin, D.A. Voss, W.De W. Horrocks, C.H. Lake, M.R. Churchill and J.R. Morrow. *Inorg. Chem.*, 1995, **34**, 3294-3300

[145] J.R. Morrow, K. Aures and D. Epstein, *J. Chem. Soc. Chem. Comm.,* 1995, 2431-2432

[146] J. Sumaoka, M. Yashiro and M. Komiyama, *J. Chem. Soc., Chem. Comm.*, 1992, 1707-1708

[147] M. Komiyama, T. Shiiba, T. Kodama, N. Takeda, J. Sumaoka and M. Yashiro. *Chem. Lett.*, 1994, 1028-1028

[148] N. Takeda, M. Irisawa and M. Komiyama, *J. Chem. Soc., Chem. Comm.*, 1994, 2773-2774

[149] N. Hayashi, N. Takeda, T. Shiiba, M. Yashiro, K. Watanbe and M. Komiyama, *Inorg. Chem.,* 1993, **32**, 5899-5900

[150] H.J. Schneider, J. Rammo and R. Hettich. *Angew. Chem. Int. Ed. Engl.,* 1993, **32**, 1716-1719

[151] K.G. Ragunathan and H.J. Schneider. *Angew. Chem. Int. Ed. Engl.,* 1996, **35**, 1219-1221

[152] J. Rammo, R. Hettich, A. Roigk and H.J. Schneider. *J. Chem. Soc., Chem. Comm.,* 1996, 105-106

[153] S. Jin Oh, C.W. Yoon and J.W. Park, *J. Chem. Soc., Perkin 2*, 1996, 329-331

[154] S. Jin Oh, K.H. Soon and J.W. Park, *J. Chem. Soc., Chem. Comm*, 1995, 575-576

[155] Jin Oh, K.H. Song, D. Whang, K. Kim, T.H. Yorn, H. Moon and J.W. Park. *Inorg. Chem.,* 1996, **35**, 3780-3785

[156] S. Jin Oh, Y.S. Choi, S. Hwangbo, S.C. Bae, J.K. Ku and J.W. Park. *J. Chem. Soc., Chem. Comm.,* 1998, 2189-2190

[157] J. Hall, D. Husken and R. Haner. *Nucleic Acid Res.,* 1996, **24**, 3522-3626

[158] R. Haner, J. Hall and G. Rihs. *Helv. Chim. Acta*, 1997, **80**, 487-494

[159] G. Lee, M. Oka, M. Takemura, Y. Miyahara, N. Shimizu, T. Inazu. *J. Org. Chem.,* 1996, **61**, 8304-8306

[160] A. Bencicni, M.A. Bernado, A. Bianchi, V. Fusi, C. Giorgi, F. Pina and B. Valtancoli. *Eur. J. Inorg. Chem.*, 1999, 1911-1918

[161] E.C. Constable. *Metals and Ligand Reactivity – An Introduction to the Organic Chemistry of Metal complexes*, 1996, VCH

[162] S.C. Burdette, G.K. Walkup, B. Spingler, R.Y. Tsien and S.J. Lippard. *J. Am. Chem. Soc.*, 2001, **123**, 7831-7841

[163] C. Bargossi, M.C. Fioini, M. Montalti, L. Prodi and N. Zaccheroni. *Coord. Chem. Rev.*, 2000, **208**, 17-32

[164] K.A. Connors. *Binding Constants – The Measurement of Molecular Complex Stability*, 1987, Wiley and Sons

[165] Z. Dai, X. Xu and J.W. Canary. *J. Chem. Soc., Chem. Comm.*, 2002, 1414-1415

[166] A.W. Czarnik. *Fluorescent Chemosensors of Ion and Molecule Recognition*, Ed. ACS Symp. Ser. 538, ACS books. Washington DC, 1993

[167] J. Slavik. *Fluorescent Probes in Cellular and Molecular Biology*. CRC Press, 1994

[168] T. Gunnlaugsson. *Tetrahedron Lett.*, 2001, **42**, 8901-8905

[169] T. Gunnlaugsson, M. Nieuwenhuyzen, L. Richard and V. Thoss. *Tetrahedron Lett.*, 2001, **42**, 4725-4728

[170] T. Gunnlaugsson, M. Nieuwenhuyzen, L. Richard and V. Thoss. *J. Chem. Soc., Perkin Trans.*, 2002, 141-150

[171] T. Gunnlaugsson, A.P. Davis and M. Glynn. *J. Chem. Soc., Chem. Comm.*, 2001, 2556-2557

[172] T. Gunnlaugsson, A.P. Davis, M. Glynn and J.E. O'Brien. *Org. Lett.*, 2002, **4**, 2449-2452

[173] T. Gunnlaugsson, A.J. Harte, J.P. Leonard, and M. Nieuwenhuyzen. *J. Chem. Soc., Chem,. Comm.*, In Press

[174] H-F. Ji, R. Dabestani, G.M. Brown and R.L. Hettich. *Photochem and Photobio.*, 1999, **69**, 513-516

[175] A.P. de Silva, H.Q.N. Gunaratne, T. Gunnlaugsson, A.J. Huxely, C.P. McCoy, J.T. Pademacher and T.E. Rice. *Chem. Rev.*, 1997, **97**, 1515-1566.

[176] B. Valeur, and I. Leary. *Coord. Chem. Rev.*, 2000, **205**, 3-40

[177] V. Balzani and F. Scandola. *Supramolecular Photochemistry*, 1991, Ellis Horwood Ltd.

[178] R.A. Bissell, A.P. de Silva, H.Q.N. Gunaratne, P.L.M. Lynch, G.E.M. Maguire, C.P. McCoy and K.R.A.S. Sandanayake. *Top. Curr. Chem.*, 1993, **168**, 224-264

[179] A.P. de Silva, T. Gunnlaugsson and T.E. Rice. *Analyst*, 1996, **121**, 1759-1762

[180] A.P. de Silva, D.B. Fox, A.J.M. Huxley and T.S. Moody. *Coord. Chem. Rev.*,2000, **205**, 41-57

[181] A.P. de Silva and S.A. de Silva. *J. Chem. Soc., Chem. Comm.*, 1986, 1709-1710

[182] A.P. de Silva and R.A.D.D. Rupashinge. *J. Chem. Soc., Chem. Comm.*, 1985, 1669-1671

[183] A.P. de Silva, H.Q.N. Gunaratne, T. Gunnlaugsson and M. Nieuwenhuizen. *J. Chem. Soc., Chem. Comm.,* 1996, 1967-1968

[184] T. Gunnlaugsson. PhD Dissertation. 1996. Queens University Belfast.

[185] N.J Birch. *Chem. Rev.,* 1999, **99**, 2659-2682

[186] L.F. Lindoy. *The Chemistry of Macrocyclic Ligand Complexes.* 1989, Cambridge University Press

[187] G.D. Christian. *J. Pharma. Biomed. Analysis,* 1996, **14**, 899-908

[188] K. Hori and H. Tsukbe. *J. Inclusion Phenom. Mol. Recognit. Chem.*, 1998, **32**, 311-329

[189] R. Kataky, P.E. Nicholson and D. Parker. *Tetrahedron Lett.,* 1989, **30**, 4559-4562

[190] K. Kobiro. *Coord. Chem. Rev.,* 1996, **148**, 135-149

[191] R.D. Hancock. *Pure Appl. Chem.,* 1986, **58**, 1445-1448

[192] R. Kataky, P.E. Nicholson and D. Parker. *J. Chem. Soc., Perkin Trans. 2.* 1990, 321-327

[193] R. Kataky, P.E. Nicholson, D. Parker and A.K. Covington. *Analyst*, 1991, **116**, 135-140

[194] S. Faulkner, R. Kataky, D. Parker and A. Teasdale. *J. Chem Soc., Perkin Trans. 2,* 1995, 1761-1769

[195] L. Collie, J.E. Denness, D. Parker, F. O'Carroll and C. Tachon. *J. Chem. Soc,. Perkin Trans. 2*, 1993, **10**, 1747-1758; J.E. Denness, D. Parker and H.S.A. Hubbard. *J. Chem. Soc., Perkin Trans. 2*, 1994, 1445-1453

[196] A. Bencini, V. Fusi, C. Giorgi, M. Micheloni, N. Nardi and B. Valtancoli. *J. Chem. Soc., Perkin Trans. 2*, 1996, 2297-2302

[197] R.A. Sachleben, M.C. Davis, J.J. Bruce, E.S. Ripple, J.L. Driver and B.A. Meyer. *Tetrahedron Lett.,* 1993, **34**, 5373-5376

[198] K. Kobiro. *Coord. Chem. Rev.,* 1996, **148**, 135-149

[199] A. Bencini, A. Bianchi, A. Borselli, M. Ciampolini, E.G. Espana, P. Dapporto, M. Micheloni, P. Paoli, J.A. Ramirez and B. Valtancoli. *Inorg. Chem.,* 1989, **28**, 4279-4284

[200] A. Bencini, A. Bianchi, A. Borselli, S. Chimichi, M. Ciampolini, P. Dapporto, M. Micheloni, N. Nardi, P. Paoli and B. Valtancoli. *Inorg. Chem.,* 1990, **29**, 3282-3286

[201] A. Bencini, A. Bianchi, A. Borselli, M. Ciampolini, M. Micheloni, N. Nardi, P. Paoli, B. Valtancoli, S Chimichi and P. Dapporto. *J. Chem. Soc., Chem. Comm.,* 1990, 174-175

[202] A. Bencini, A. Bianchi, S. Chimichi, M. Ciampolini, P. Dapporto, E.G. Espana, M. Micheloni, N. Nardi, P. Paoli and B. Valtancoli. *Inorg. Chem.,* 1990, **30**, 3687-3691

[203] A. Bencini, V. Fusi, C. Giorgi, M. Micheloni, N. Nardi and B. Valtancoli. *J. Chem. Soc., Perkin Trans. 2,* 1996, 2297-2302

[204] M. Formica, V. Fusi, M. Micheloni, R. Pontelli and P. Romani. *Coord. Chem. Rev.,* 1999, **184**, 347-363

[205] H. Sugihara and K. Hiratani. *Coord. Chem. Rev.,* 1996, **148**, 285-299

[206] P.D. Beer, J.P. Danks, M.G.B. Drew and J.F. McAleer. *J. Organomet. Chem.,* 1994, **476**, 63-72

[207] M.McCarrick, B. Wu, S.J. Harris, D. Diamond, G. Barrett and M.A. McKervey. *J. Chem. Soc., Perkin Trans. 2,* 1993, 1963-1968

[208] K. Saski and G. Pacey. *Anal. Chim. Acta,* 1985, **174**, 141-149

[209] K. Wilcox and G.E. Pacey. *Talanta*, 1991, **38**, 1315-1324

[210] K. Kimura, S.I. Iketani and T. Shono. *Anal. Chim. Acta.* 1987, **203**, 85-89

[211] K. Kirschke, H. Baumann, B. Costisella and M. Ramm. *Liebigs Ann. Chem.,* 1994, 265-268

[212] C. Balckburn, M. Bai, K.A. Le Compte and M.E. Langmuir. *Tetrahedron Lett.,* 1994, **35**, 7915-7918

[213] S.H. Kim, J.W. Kim, J.H. Kim, K.N. Koh and S.W. Kang. *Dyes and Pigments,* 2000, **46**, 49-53

[214] H. Sakamoto, M. Tanaka and K. Kimura. *Chem. Lett.,* 2000, 928-929

[215] M. Ciampolini, M. Formica, V. Fusi, A. Saint-Mauricec, M. Micheloni, N. Nardi, R. Pontellini, F. Pina, P. Romani, A.M. Sabatini and B. Valtancoli. *Eur. J. Inorg. Chem.,* 1999, 2261-2268

[216] S.O. Obare and C.J. Murphy. *New J. Chem.*, 2001, **25**, 1600-1604

[217] S.O. Obare and C.J. Murphy. *Inorg. Chem.,* 2001, **40**, 6080-6082

[218] T. Gunnlaugsson, B. Bichell and C. Nolan. *Tetrahedron Lett.,* 2002, **43**, 4989-4992

[219] Ed. David Parker. *Macrocyclic Synthesis – A Practical Approach,* 1996, Oxford University Press

[220] J.M. Lehn. *Supramolecular Chemistry – Concepts and Perspectives: a Personal Account*, Chap. 8, 1995, VCH

[221] N.J. Turro. *Modern Molecular Photochemistry*, 1991, University Science Books

[222] G.M. Kyne, M.E. Light, M.B. Hursthouse, J. de Mendoza and J.D. Kilburn. *J. Chem. Soc., Perkin trans. 1,* 2001, 12558-1263

[223] J. Lin, Q-S. Hu, M-H. Xu and L. Pu. *J. Am. Chem. Soc.,* 2002, **124**, 2088-2089

[224] B. Lippert. *Cisplatin. Chemistry and Biochemistry of a Leading Anticancer Drug,* 1999, Wiley-VCH, Weinheim

[225] S.J. Lippard. *Coord. Chem. Rev.,* 1991, **59**, 731

[226] J. Reedijk. *Chem. Rev.,* 1999, **99**, 2499-2510

[227] D. Minniti and M.F. Parisi. *Inorg. Chim. Acta,* 1991, **188**, 127

[228] S.E. Sherman and S.J. Lippard. *Chem. Rev.,* 1987, **87**, 1153-1181

[229] V. Morena, G. Cervantes, G.B. Onoa, F. Sampero, P. Santalo, X. Solans and M. Font-Bardia. *Polyhed.,* 1997, **16**, 4297-430

[230] M. Vives, R. Gargallo, R. Tauler and V. Moreno. *J. Inorg. Biochem.,* 2001, **85**, 279-290

[231] C. Mock, I. Puscasu, M.J. Rauterkus, G. Tallen, J.E.A. Wolff and B. Krebs. *Inorg. Chim. Acta,* 2001, **319**, 109-116

[232] J. Reedijk. *Chem. Comm.,* 1996, 801-802

[233] J. Reedijk. *Inorg. Chim. Acta,* 1992, **198-200**, 873-876

[234] M. Van Beusichen and N. Farrell. *Inorg. Chem.,* 1997, **36**, 3657-3662

[235] U. Bierbach, M. Sabat and N. Farrell. *Inorg. Chem.,* 2000, **39**, 1882-1900

[236] M. Coluccia, M. Corraele, D. Giordano, M.A. Mariggio, S. Moscelli, F.P. Fanizzi, G. Natile and L. Maresca. *Inorg. Chim, Acta,* 1986, **123**, 225-228

[237] J.N. Jolley, A.I. Yanovsky, L.R. Kelland and K.B. Nolan. *J. Inorg. Biochem.,* 2001, **83**, 91-100

[238] C.J. Campbell, A. Castineiras and K.B. Nolan. *Inorg. Chim. Acta,* 1996, **245**, 257-263

[239] M.S. Robillard, A.R.P. Valentijn, N.J. Meeuwenoord, G.A. van der Marel, J.H. van Boom and J. Reedjik. *Angew. Chem. Int. Ed.,* 2000, **39**, 3096-3099

[240] M. Bodansky and A. Bodansky. *The Practice of Peptide Synthesis.* 2nd Ed., Springer Laboratory Manual, 1997

[241] G.L. Stahl. *J. Org. Chem.,* 1978, **43**, 2285-2289

[242] V.Y. Kukushkin, A. Oskarsson, L.I. Elding and N. Farrell. *Transition metal complexes and precursors,* 1999, Chapter 3, Oxford University Press

[243] M. Van Beusichem and N. Farrell. *Inorg. Chem.,* 1992, **31**, 634-639

[244] R.I. Haines, D.R. Hutchings and T.M. McCormack. *J. Inorg. Biochem., 2001, **85**, 1-7*

[245] S.T. Nguyen, L.K. Johnson, R.H. Grubbs and J.W. Ziller. *J. Am. Chem. Soc.,* 1992, **114**, 3974-3975

[246] S.T. Nguyen, L.K. Johnson, R.H. Grubbs and J.W. Ziller. *J. Am. Chem. Soc.,* 1992, **114**, 3974-3975

[247] G.C. Fu, S.T. Nguyen and R.H. Grubbs. *J. Am. Chem. Soc.,* 1993, **115**, 9856-9857

[248] D.A. Leigh, P.J. Lusby, S.J. Trent, A.J. Wilson and J.K.Y. Wong. *Angew. Int. Ed.,* 2001, **40**, 1538-1543

[249] M.S. Sandford, J.A. Love and R.H. Grubbs. *J. Am. Chem. Soc.,* 2001, **123**, 6543-6554

[250] J. Tsuji and S. Hashiguchi. *Tetrahedron Lett.,* 1980, **21,** 2955-2958

[251] R.H. Grubbs, S.J. Miller and G.C. Fu. *Acc. Chem. Res.,* 1995, **28**, 446-452

[252] T.N. Trnka and R.H. Grubbs. *Acc. Chem. Res.,* 2001, **34**, 18-29

[253] A. Furstner. *Angew. Chem. Int. Ed.,* 2000, **39**, 3012-3043

[254] M. Arisawa, X. Kato, M. Kaneka, A. Nishida and M. Nakagawa. *J. Chem. Soc., Perkin Trans 1,* 2000, 1873-1876

[255] F.P.J.T. Rutjes and H.E. Schoemaker. *Tetrahedron Lett.,* 1997, **38**, 677-680

[256] B.S. Furniss, A.J. Hannaford, P.W.G Smith, A.R. Tatchell. VOGEL's Textbook of Practical Organic Chemistry 5th Edition. Longman Scientific and Technical

[257] M. Newcomb, J. Timoko, D. Walba and D.J. Cram. *J. Am. Chem. Soc.,* 1977, **99**, 1875-1879

[258] N.W. Alcock, R. G. Kingston, P.Moore, C.Pierpoint. *J. Chem.,. Soc. Dalton Trans.,* 1984, 1937-1943

[259] M. Bodansky and A. Bodansky. *The Practice of Peptide Synthesis.* 2nd Edition, 1997, Springer Laboratory Manual

On the assumption of 1:1 binding between the receptor (**L**) and the cation (**M+**) can be measured bvy changes in either the changes in the absorption or fluorescence spectra. The equilibrium can be written as:

$$M^+ + L \overset{\beta}{\rightleftharpoons} ML^+$$

The binding constant β is given by (I):

$$\beta = \frac{[ML^+]}{[M^+][L]} \qquad \text{(I)}$$

The total cation free concentration in the solution, $[M+]_{total}$, can be expressed yb the conservation equation (II):

$$[M^+]_{total} = [M^+] + [ML^+] \qquad \text{(II)}$$

where [M+] is the free cation concentration in the solution and [ML+] is the bound cation concentration in solution. In the same way the total concentration of the receptor $[L]_{total}$ can be expressed as (III):

$$[L]_{total} = [L] + [ML^+] \qquad \text{(III)}$$

where [L] is the free receptor concentration in the solution and [ML+] is the bound receptor concentration in solution. The fluorescent intensity I_f (or alternatively the absorption) is proportional to the concentration of the chromophore and can be expressed by equations (IV) to (VI):

$$I_F = k[ML^+] + k'[L]_{total} \qquad \text{(IV)}$$

$$I_{Fmin} = k'[L]_{total} \qquad \text{(V)}$$

$$I_{Fmax} = k[ML+]_{max} = k[L]_{total} \qquad \text{(VI)}$$

Where I_{Fmin} is the fluorescence inte nsity when the receptor is not bound and I_{Fmax} is the maximum fluorescent intensity. k and k' are proportionality constants. By substituting for $[L]_{total}$ and [ML+] in equation (III) and with some rearrangements (VII) is obtained. Thus the binding constant is obtained:

$$I_{Fmax} - I_F = (k - k')[L] \qquad \text{(VII)}$$

By substituting for k and k' using equations (IV) and (V) equation (IX) can be obtained:

$$\frac{(I_{Fmax} - I_F)}{(I_F - I_{min})} = 1 + \frac{[ML^+]}{[L]} \qquad \text{(VIII)}$$

Finally, taking the log of both side of the equation the binding constant can be obtained form equation (IX). Note this equation takes the form of a straight line with the slope equivalent to log β.

$$\mathbf{Log\ \beta = Log[(I_{Fmax}-I_F)/(I_F-I_{Fmin})]-Log[M^+]}$$